

---

# B

---

## Base-Isolated Systems, Reliability-Based Characterization of

Hector A. Jensen and D. S. Kusanovic  
Department of Civil Engineering, Santa Maria  
University, Casilla, Valparaiso, Chile

### Synonyms

Advanced simulation techniques; First excursion probability; Isolation systems; Rubber bearings; Stochastic excitation

### Introduction

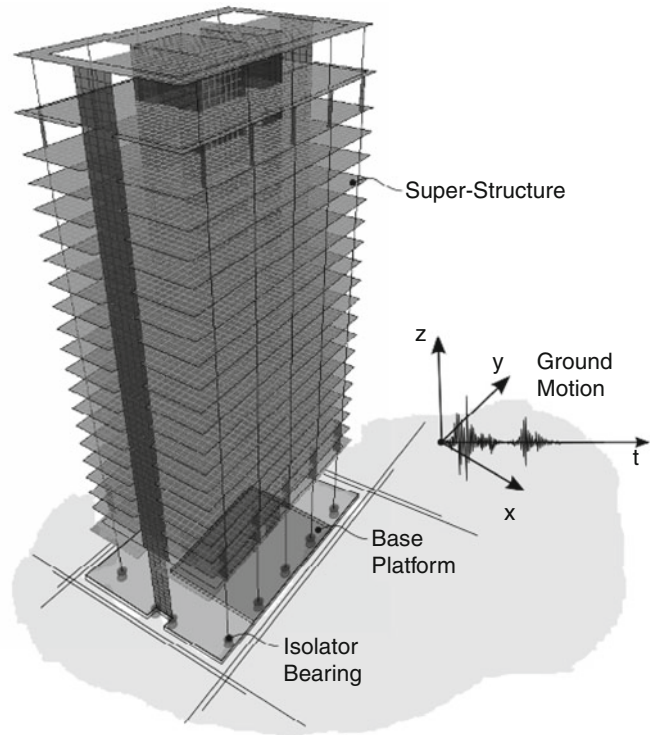
The recent improvements in isolation system products have led to the design and construction of an increasing number of seismically isolated buildings worldwide (Ceccoli et al. 1999; Chopra 2001; Kelly 1986; Zou et al. 2010). Similarly, seismic isolation has been extensively used for seismic retrofitting of existing buildings (De Luca et al. 2001; Mokha et al. 1996). In addition, base isolation concepts are utilized for the protection from shock and vibration of sensitive components of critical facilities such as hospitals, nuclear reactors, and industrial and data center facilities. One of the difficulties in the analysis and design of base-isolated systems has been the explicit consideration of the nonlinear behavior of the isolators. Another challenge has

been the efficient prediction of the dynamic response under future ground motions considering their potential variability as well as competing objectives related to the protection of the superstructure and the minimization of base displacement. The objective of this work is to characterize the performance of base-isolated systems from a reliability point of view. In particular, the case of large-scale building models is considered here. Isolation systems composed by rubber bearings are used in the present formulation. The nonlinear behavior of these devices is characterized by a biaxial hysteretic model which is calibrated with experimental data (Yamamoto et al. 2009). First excursion probabilities are used as measures of the system reliability. In this setting, reliability is quantified as the probability that the response quantities of interest (base displacement and superstructure response) will not exceed acceptable performance bounds within a particular reference period (Lutes and Sarkani 2004). Such probabilities are estimated by a stochastic simulation method (Au and Beck 2001). The variability of future excitations is addressed by adopting a probabilistic approach which belongs to the class of point-source models (Boore 2003).

The organization of this entry is as follows: Section “[Structural Model](#)” introduces the structural model for the superstructure and base platform. The characterization of the isolation system is presented in section “[Isolation Model](#).” Section “[Excitation Model](#)” deals with the

### Base-Isolated Systems, Reliability-Based Characterization of,

**Fig. 1** Schematic representation of a base-isolated finite element building model



stochastic model for the excitation. The reliability assessment and the structural response of base-isolated buildings are discussed in sections “[Reliability Measures](#)” and “[System Response](#),” respectively. In section “[Application Problem](#),” the proposed characterization is illustrated by means of a based-isolated finite element building model. The entry closes with some final remarks.

### Structural Model

Finite element building models with a relatively large number of degrees of freedom are considered for modeling the superstructure, i.e., the structure above the isolation system. For illustration purposes a schematic representation of a base-isolated finite element building model under ground motion is shown in Fig. 1. In general, base-isolated buildings are designed such that the superstructure remains elastic. Hence, the superstructure is modeled as a

three-dimensional linear elastic system, while the base is assumed to be rigid in plane and it is modeled using 3 degrees of freedom. Let  $x_s(t)$  be the  $n$ th dimensional vector of relative displacements of the superstructure with respect to the base and  $M_s$ ,  $C_s$ ,  $K_s$  be the corresponding mass, damping, and stiffness matrices. Also, let  $x_b(t)$  be the vector of base displacements with three components and  $G_s$  be the matrix of earthquake influence coefficients of dimension  $n \times 3$ , that is, the matrix that couples the excitation components of the vector  $\ddot{x}_g(t)$  to the degrees of freedom of the superstructure. The equation of motion of the superstructure is expressed in the form

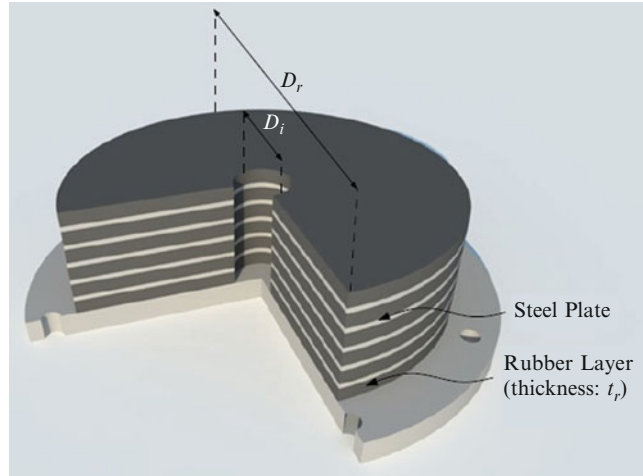
$$M_s \ddot{x}_s(t) + C_s \dot{x}_s(t) + K_s x_s(t) = -M_s G_s [\ddot{x}_b(t) + \ddot{x}_g(t)] \quad (1)$$

where  $\ddot{x}_b(t)$  is the vector of base accelerations relative to the ground. To complete the formulation of the combined model, the equation of motion for the base platform is written as

### Base-Isolated Systems, Reliability-Based

### Characterization of,

**Fig. 2** Schematic representation of a rubber bearing



B

$$\begin{aligned} & (\mathbf{G}_s^T \mathbf{M}_s \mathbf{G}_s + \mathbf{M}_b) (\ddot{\mathbf{x}}_b(t) + \ddot{\mathbf{x}}_g(t)) + \mathbf{G}_s^T \mathbf{M}_s \ddot{\mathbf{x}}_s(t) \\ & + \mathbf{C}_b \dot{\mathbf{x}}_b(t) + \mathbf{K}_b \mathbf{x}_b(t) + \mathbf{f}_{is}(t) = 0 \end{aligned} \quad (2)$$

where  $\mathbf{M}_b$  is the mass matrix of the rigid base,  $\mathbf{C}_b$  is the resultant damping matrix of viscous isolation components,  $\mathbf{K}_b$  is the resultant stiffness

matrix of linear elastic isolation components, and  $\mathbf{f}_{is}(t)$  is the vector containing the nonlinear isolation elements forces.

Rewriting the previous equations, the combined equation of motion of the base-isolated structural system can be formulated in the form

$$\begin{aligned} & \begin{bmatrix} \mathbf{M}_s & \mathbf{M}_s \mathbf{G}_s \\ \mathbf{G}_s^T \mathbf{M}_s & \mathbf{M}_b + \mathbf{G}_s^T \mathbf{M}_s \mathbf{G}_s \end{bmatrix} \begin{Bmatrix} \ddot{\mathbf{x}}_s(t) \\ \ddot{\mathbf{x}}_b(t) \end{Bmatrix} + \begin{bmatrix} \mathbf{C}_s & \mathbf{O} \\ \mathbf{O} & \mathbf{C}_b \end{bmatrix} \begin{Bmatrix} \dot{\mathbf{x}}_s(t) \\ \dot{\mathbf{x}}_b(t) \end{Bmatrix} + \\ & \begin{bmatrix} \mathbf{K}_s & \mathbf{O} \\ \mathbf{O} & \mathbf{K}_b \end{bmatrix} \begin{Bmatrix} \mathbf{x}_s(t) \\ \mathbf{x}_b(t) \end{Bmatrix} = - \begin{bmatrix} \mathbf{M}_s \mathbf{G}_s \\ \mathbf{M}_b + \mathbf{G}_s^T \mathbf{M}_s \mathbf{G}_s \end{bmatrix} \ddot{\mathbf{x}}_g(t) - \begin{Bmatrix} \mathbf{0} \\ \mathbf{f}_{is}(t) \end{Bmatrix} \end{aligned} \quad (3)$$

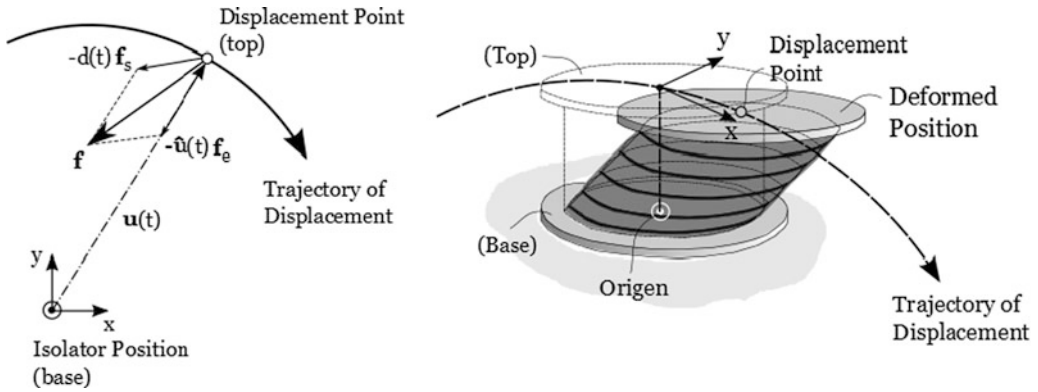
The above formulation can be extended to other cases as well, for example, the consideration of nonlinear models for the superstructure.

### Isolation Model

Rubber bearings are considered for modeling the isolation system. Such devices have been used over many years in a number of seismically isolated buildings worldwide (Kelly 1986; Su et al. 1990; Makris and Chang 1998). They require minimal initial cost and maintenance compared to other passive, semi-active, and active energy absorption devices. A rubber bearing consists of layers of rubber and steel, with the

rubber being vulcanized to the steel plates. Rubber bearing systems are able, in principle, to support the superstructure vertically, to provide the horizontal flexibility together with the restoring force, and to supply the required hysteretic damping. Figure 2 shows a schematic representation of a rubber bearing, where  $D_r$  represents the external diameter of the isolator,  $D_i$  indicates the internal diameter, and  $H_r = t_r n_r$  is the total height of rubber in the device, where  $t_r$  is the layer thickness and  $n_r$  is the number of rubber layers.

An analytical model that simulates measured restoring forces under bidirectional loadings is used in the present formulation. The model is based on a series of experimental tests conducted for real-size rubber bearings (Yamamoto



**Base-Isolated Systems, Reliability-Based Characterization of, Fig. 3** Schematic representation of the decomposition of the restoring force

et al. 2009; Minewaki et al. 2009). The loading tests of seven full-scale isolators were carried out using the Caltrans Seismic Response Modification Device Test Facility at the University of California, San Diego. The specimens used in the tests were made with high damping rubber compounds. In particular, horizontal bidirectional loading tests for isolators with a diameter of 0.7 m and 1.3 m were conducted. On the basis of the test results, the model assumes that the restoring force on the rubber bearing is composed of a force directed to the origin of the isolator and another force approximately opposite to the direction of the movement of the isolator. Such decomposition of the restoring force is shown schematically in Fig. 3.

According to the model, the direction of the movement of the isolator  $d(t)$  is defined in terms of the components in the  $x$  and  $y$  direction of the base displacement vector  $x_b(t)$  by means of the nonlinear differential equation

$$\begin{aligned} \dot{d}(t) &= \frac{1}{\alpha} \|\dot{u}(t)\| \left[ \hat{u}(t) - \|\dot{d}(t)\|^\beta \hat{d}(t) \right], \quad (4) \\ u(0) &= 0, \quad d(0) = 0 \end{aligned}$$

where the components of the vector  $u(t)$  correspond to the components in the  $x$  and  $y$  direction

of the base displacement vector  $x_b(t)$ ;  $\dot{u}(t)$  is the velocity vector;  $\hat{u}(t)$  and  $\hat{d}(t)$  are the unit directional vectors of  $\dot{u}(t)$  and  $\dot{d}(t)$ , respectively; and  $\|\cdot\|$  indicates the Euclidean norm. The parameters  $\alpha = 0.2H_r$  and  $\beta = 0.7$  are positive constants that relate to the yield displacement and smoothness of yielding, respectively. Once the vector  $d(t)$  has been derived, the restoring force  $f(t)$  on the isolator (in the  $x$  and  $y$  direction) is expressed in terms of the unit directional vector  $\hat{u}(t)$  and the vector  $d(t)$  as  $f(t) = -\hat{u}(t)f_e(t) - d(t)f_s(t)$ , where  $f_e(t)$  is the nonlinear elastic component and  $f_s(t)$  is the elastoplastic component. The previous decomposition of the restoring force to elastic and dissipative components simplifies the restoring force characteristics and results in a simple and accurate model. These two forces have different appearance mechanisms and different influencing factors. For example, the dependency of these forces on factors such as temperature, vertical pressure, and maximum experienced shear strain would differ. Therefore, the previous decomposition has the potential for more general modeling of other dependencies. Based on experimental results, the components of the restoring force on the rubber bearing can be approximated as

$$f_e(t) = \begin{cases} 0.35\gamma(t)A & \text{if } 0 \leq \gamma(t) \leq 1.8 \\ \left(0.35\gamma(t) + 0.2(\gamma(t) - 1.8)^2\right)A & \text{if } \gamma(t) \geq 1.8 \end{cases} \quad (5)$$

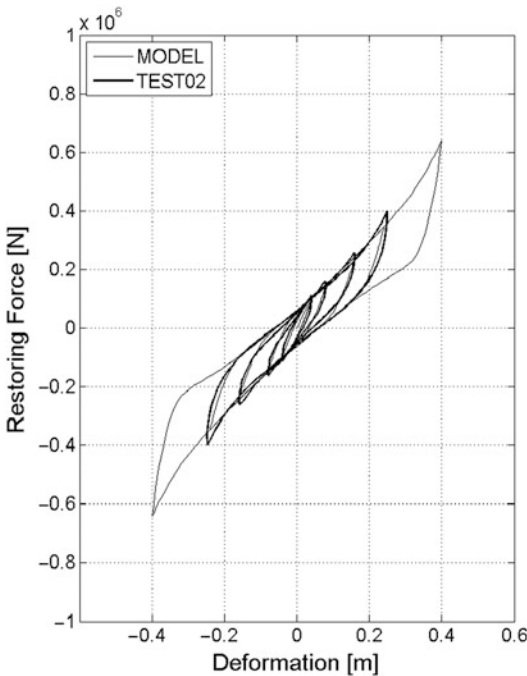


and

$$f_s(t) = \left( 0.125 + 0.015\gamma(t) + 0.012\gamma(t)^3 \right) A \tag{6}$$

where  $A$  is the cross-sectional area of the rubber and  $\gamma(t) = \|u(t)\|/H_r$  is the average shear strain. Validation calculations have shown that the analytical model is able to accurately simulate the test results for both bidirectional and unidirectional loading. The reader is referred to Yamamoto et al. (2009) and Minewaki et al. (2009) for a detailed description of the analytical model presented in this section.

Using the previous calibration of the analytical model by means of bidirectional loading tests, the restoring forces and those calculated by the model under unidirectional loading are compared in Fig. 4 for a medium-size rubber bearing. The test results were conducted for a maximum average shear strain of 150 %.



**Base-Isolated Systems, Reliability-Based Characterization of, Fig. 4** Comparison of analytical and experimental hysteresis loops for a medium-size rubber bearing.  $D_r = 0.8$  m,  $H_r = 0.16$  m,  $D_i = 0.15$  m

It is observed that the analytical model simulates the test results very well. Additional validation calculations have shown that the analytical model is also able to accurately simulate the test results for bidirectional loadings.

### Excitation Model

The uncertain earthquake excitation is modeled as a non-stationary stochastic process. In particular, a point source model characterized by the moment magnitude  $M$  and epicentral distance  $r$  is considered in this work (Boore 2003; Atkinson and Silva 2000). The time history for a specific event magnitude  $M$  and epicentral distance  $r$  is obtained by first generating a discrete white noise sequence  $z^T = \langle \sqrt{2\pi/\Delta t} z_j, j = 1, \dots, n_T \rangle$ , where  $z_j, j = 1, \dots, n_T$ , are independent, identically distributed standard Gaussian random variables,  $\Delta t$  is the sampling interval, and  $n_T$  is the number of time instants equal to the duration of the excitation  $T$  divided by the sampling interval. The white noise sequence is then modulated by an envelope function  $h(t, M, r)$  at the discrete time instants. Discrete Fourier transform is applied to the modulated white noise sequence. The resulting spectrum is normalized by the square root of the mean square of the amplitude spectrum. Finally, the normalized spectrum is multiplied by a ground motion spectrum  $S(f, M, r)$  after which discrete inverse Fourier transform is applied to transform the sequence back to the time domain to yield the desired ground acceleration time history. The envelope function is represented by

$$h(t, M, r) = a_1 \left( \frac{t}{t_n} \right)^{a_2} e^{-a_3 \left( \frac{t}{t_n} \right)} \tag{7}$$

where

$$a_1 = \left( \frac{e}{0.2} \right)^{a_2}, a_2 = \frac{-0.2 \ln(0.05)}{1 + 0.2(\ln(0.2) - 1)}, a_3 = \frac{a_2}{0.2} \tag{8}$$

On the other hand, the total spectrum of the motion at a site  $S(f, M, r)$  is expressed as the

product of the contribution from the earthquake source  $E(f, M)$ , path  $P(f, r)$ , site  $G(f)$ , and type of motion  $I(f)$ , i.e.,  $S(f, M, r) = E(f, M) P(f, r) G(f) I(f)$ .

The source component is given by  $E(f, M) = C M_0(M) S_a(f, M)$ , where  $C$  is a constant,  $M_0(M) = 10^{1.5M + 10.7}$  is the seismic moment, and the factor  $S_a$  is the displacement source spectrum given by

$$S_a(f, M) = \frac{1 - \varepsilon}{1 + \left(\frac{f}{f_a}\right)^2} + \frac{\varepsilon}{1 + \left(\frac{f}{f_b}\right)^2} \quad (9)$$

where the corner frequencies  $f_a$  and  $f_b$ , and the weighting parameter  $\varepsilon$  are defined, respectively, as  $\log(f_a) = 2.181 - 0.496 M$ ,  $\log(f_b) = 2.41 - 0.408 M$ , and  $\log(\varepsilon) = 0.605 - 0.255 M$ . The constant  $C$  is given by  $C = UR_\Phi VF / 4\pi\rho_s\beta_s^3R_0$ , where  $U$  is a unit-dependent factor ( $10^{-20}$ ),  $R_\Phi$  is the radiation pattern,  $V$  represents the partition of total shear-wave energy into horizontal components,  $F$  is the effect of the free surface amplification,  $\rho_s$  and  $\beta_s$  are the density and shear-wave velocity in the vicinity of the source, and  $R_0$  is a reference distance.

The path effect  $P(f, r)$  which is another component of the process that affects the spectrum of motion at a particular site is represented by functions that account for geometrical spreading and attenuation  $P(f, r) = Z(R(r)) e^{-\pi f R(r)/Q(f)\beta_s}$ , where  $R(r)$  is the radial distance from the hypocenter to the site given by  $R(r) = \sqrt{r^2 + h^2}$ , where  $\log(h) = 0.15 M - 0.05$ . The attenuation quantity  $Q(f)$  is taken as  $Q(f) = 180f^{0.45}$ , and the geometrical spreading function is selected as  $Z(R(r)) = 1/R(r)$  if  $R(r) < 70.0$  km and  $Z(R(r)) = 1/70.0$  otherwise.

The modification of seismic waves by local conditions, site effect  $G(f)$ , is expressed by the multiplication of a diminution function  $D(f)$  and an amplification function  $A(f)$ . The diminution function accounts for the path-independent loss of high frequency in the ground motions and can be accounted for a simple filter of the form  $D(f) = e^{-0.03\pi f}$ . The amplification function  $A(f)$  is based on empirical curves given for

**Base-Isolated Systems, Reliability-Based Characterization of, Table 1** Parameters for the stochastic ground acceleration model

Parameter	Numerical value	Parameter	Numerical value
$\rho_s$ (gm/cc)	2.8	$\beta_s$ (km/s)	3.5
$V$	$1/\sqrt{2}$	$R_\Phi$	0.55
$F$	2.0	$R_0$ (km)	1.0

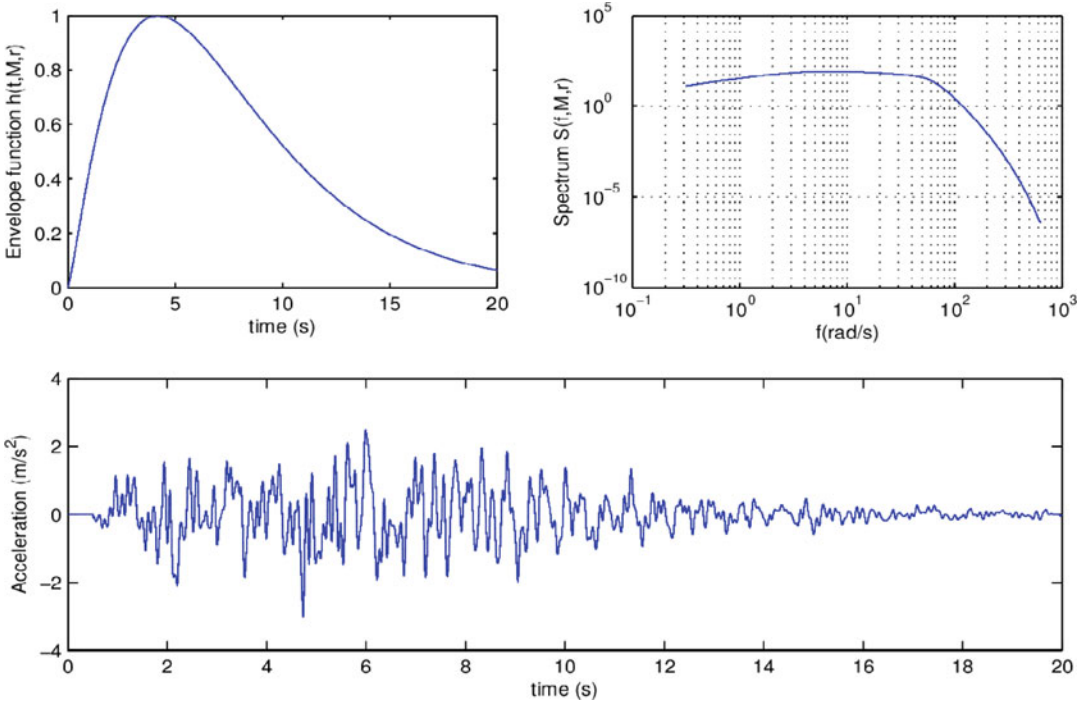
generic rock sites. An average constant value equal to 2.0 is considered.

Finally, the filter that controls the type of ground motion  $I(f)$  is chosen as  $I(f) = (2\pi f)^2$  for ground acceleration. The particular values of the different parameters of the stochastic ground acceleration model used in this work are given in Table 1. For a detailed discussion of the point-source model, the reader is referred to Anderson and Hough (1984), Boore et al. (1997), Atkinson and Silva (2000), and Boore (2003).

The previous excitation model is complemented by considering the moment magnitude  $M$  and epicentral distance  $r$  as uncertain. The uncertainty in moment magnitude is modeled by the Gutenberg-Richter relationship truncated on the interval [6.0, 8.0], which leads to the probability density function  $p(M) = b e^{-bM} / (e^{-6.0b} - e^{-8.0b})$  where  $b = 1.8$  is a seismicity factor (Kramer 2003). For the uncertainty in the epicentral distance  $r$ , a lognormal distribution with mean value of 20 km and coefficient of variation equal to 35 % is considered. For illustration purposes Fig. 5 shows a typical envelope function, a ground motion spectrum, and a corresponding sample of ground motion.

## Reliability Measures

The performance of base-isolated structural systems is characterized by means of a set of response functions  $h_i(t, y, \theta)$ ,  $i \in I_h$ ,  $t \in [0, T]$ , where  $y$  is the vector of controllable system parameters;  $\theta$  is the vector of uncertain variables that characterizes the stochastic excitation model, i.e., the white noise sequence  $z$  and the



**Base-Isolated Systems, Reliability-Based Characterization of, Fig. 5** Envelope function, ground motion spectrum, and a sample ground motion

seismological parameters  $M$  and  $r$ ; and  $I_h$  is a set of indices. The controllable system parameters are taken as the external diameter and the total height of rubber of the isolators, that is,  $y^T = \langle D_r, H_r \rangle$ . The probability that performance conditions are satisfied within a particular reference period  $T$  is used as a reliability measure. In this context a failure event  $F$  is defined in terms of a performance function  $g(y, \theta)$  as  $F(y, \theta) = g(y, \theta) \leq 0$ , where

$$g(y, \theta) = 1 - \max_{i \in I_h} \left( \max_{t \in [0, T]} \frac{|h_i(t, y, \theta)|}{h_i^*} \right) \quad (10)$$

and  $h_i^*$ ,  $i \in I_n$  are the corresponding acceptable response levels. In particular, the probability of failure events associated with the base drift and superstructure absolute acceleration are considered in the present formulation. The probability of failure  $P_F(y)$  evaluated at some particular value of the isolation system parameters  $y$  can be expressed in terms of the probability integral

$$P_F(y) = \int_{g(y, \theta) \leq 0} p(\theta) d(\theta) \quad (11)$$

where  $p(\theta)$  is the multidimensional probability density function that characterizes the parameters involved in the excitation model. For systems under stochastic excitation, the probability integral involves in general a large number of uncertain parameters. Thus, the reliability estimation constitutes a high-dimensional problem. This problem is solved by applying an advanced simulation technique called subset simulation (Au and Beck 2001). In the approach, the failure probabilities are expressed as a product of conditional probabilities of some chosen intermediate failure events, the evaluation of which only requires simulation of more frequent events. Therefore, a rare event simulation problem is converted into a sequence of more frequent event simulation problems. Validation calculations have shown that subset simulation can be applied efficiently to first excursion response problems for a wide range of dynamical systems.

Details of this simulation procedure from the theoretical and numerical viewpoint can be found in Au and Beck (2001), Ching et al. (2005), and Zuev et al. (2011).

## System Response

The response of base-isolated structural systems is obtained from the solution of the equation of motion that characterizes the combined system, that is, isolation system and superstructure (Eq. 3). The solution of this equation is obtained in an iterative manner due to the nonlinearity of the isolators forces. The solution scheme is implemented as follows:

- (i) At the beginning of the iteration ( $l = 0$ ) within the time interval  $[t, t + \Delta t]$ , it is assumed that  $d_j^{(l)}(t + \Delta t) = d_j(t)$  and  $u_j^{(l)}(t + \Delta t) = u_j(t)$ ,  $j = 1, \dots, n_I$  where  $d_j(t)$  and  $u_j(t)$  represent the direction of the movement and displacement vector of isolator number  $j$ , respectively, and  $n_I$  is the total number of isolators in the isolation system.
- (ii) The previous information and the characterization of the restoring force given in section “[Isolation Model](#),” allow the characterization of the vector containing all nonlinear isolators forces  $f_{is}^{(l)}(t + \Delta t)$  (in the right-hand side of Eq. 3) is obtained.
- (iii) The solution of Eq. 3 is obtained by any suitable step-by-step integration scheme. Such solution gives the base responses  $\ddot{x}_b^{(l+1)}(t + \Delta t)$  and  $\dot{x}_b^{(l+1)}(t + \Delta t)$ . From these quantities the isolator displacement and velocity vectors  $u_j^{(l+1)}(t + \Delta t)$  and  $\dot{u}_j^{(l+1)}(t + \Delta t)$ ,  $j = 1, \dots, n_I$ , respectively, are computed.
- (iv) The nonlinear differential Eq. 4 is integrated to obtain a new estimate for  $d_j(t + \Delta t)$ ,  $j = 1, \dots, n_I$ , i.e.,  $d_j^{(l+1)}(t + \Delta t)$ , and the nonlinear forces in the isolation system  $f_{is}(t + \Delta t)$  (in the right-hand side in Eq. 3). The solution of the equation for the evolution of the set of variables  $d_j(t)$ ,  $j = 1, \dots, n_I$  is obtained by

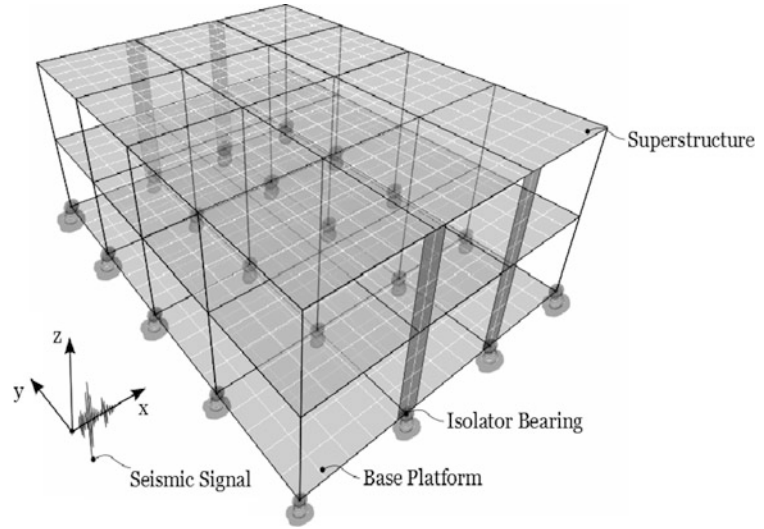
a proper integration scheme such as the Crank-Nicolson method (Burden and Faires 2011).

- (v) The iteration starting with solving Eq. 3 needs to be repeated until the variation of the quantities  $d_j(t + \Delta t)$ ,  $j = 1, \dots, n_I$  is sufficiently small between two consecutive iterations (Jensen and Sepulveda 2011).

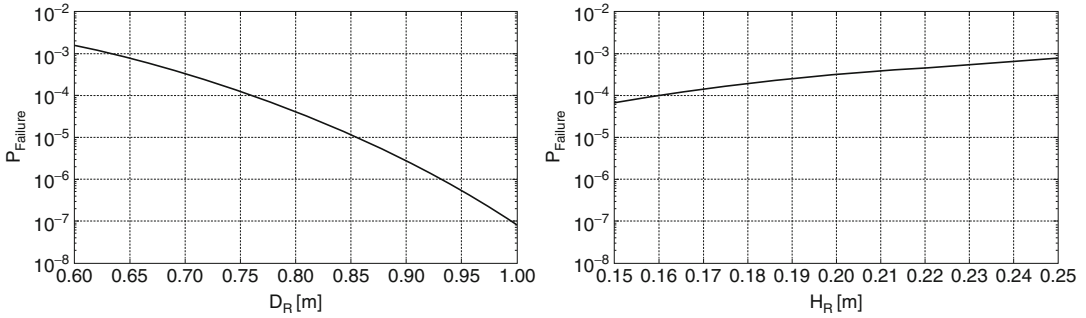
## Application Problem

The objective of the application problem is to evaluate the effect of basic design isolator characteristics such as the rubber diameter ( $D_r$ ) and the height of rubber ( $H_r$ ) on the reliability of a base-isolated structural system. To this end, a three-dimensional reinforced concrete building model with more than 7000 degrees of freedom is considered for the analysis. The isometric view of the finite element model is shown in Fig. 6. Material properties of the reinforced concrete structure have been assumed as follows: Young’s modulus  $E = 2.5 \times 10^{10}$  N/m<sup>2</sup>; and Poisson ratio  $\nu = 0.2$ . The total mass of the first and second floor is  $7.0 \times 10^5$  kg and  $6.0 \times 10^5$  kg, respectively. On the other hand, the total mass of the platform is equal to  $6.0 \times 10^5$  kg. The height of each floor is 3.5 m, and the floors are modeled with shell elements with a thickness of 0.25 m. Additionally, beam and column elements are used in the model. A 5% of critical damping is added to the structural system. For anti-seismic design purposes, the structure is equipped with a total number of 20 rubber bearings in its isolation system. The structural system is excited by a ground acceleration in the  $x$  direction and modeled as described in section “[Excitation Model](#).” The sampling interval and the duration of the excitation are taken equal to  $\Delta t = 0.01$  s and  $T = 30$  s, respectively. Thus, the generation of synthetic ground motions involved more than 3000 random variables in this case. The reliability of the base-isolated system is evaluated in terms of the probability of failure events associated with the base drift and superstructure absolute acceleration. The failure event related to the base drift is defined as

**Base-Isolated Systems, Reliability-Based Characterization of, Fig. 6** Building model with base isolation system



B



**Base-Isolated Systems, Reliability-Based Characterization of, Fig. 7** Probability of the failure event related to the base drift as a function of the isolation system parameters

$$F_{\text{drift}}(y, \theta) = 1 - \max_{t \in [0, T]} \frac{|x_{bx}(t, y, \theta)|}{x_{bx}^*} \quad (12)$$

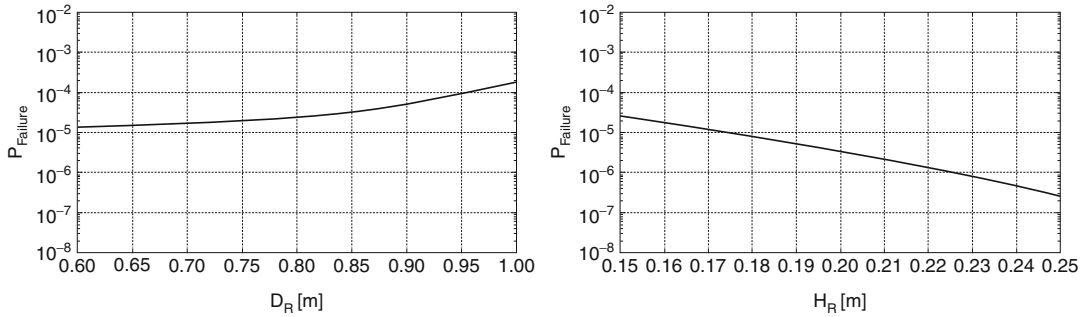
where  $x_{bx}(t, y, \theta)$  represents the base displacement in the  $x$  direction,  $x_{bx}^*$  is the critical threshold level equal to 0.25 m, and  $\theta^T = \langle z_1, z_2, \dots, z_{3001}, M, r \rangle$  is the vector of random variables that characterizes the excitation.

On the other hand, the failure event associated with the superstructure absolute acceleration is given by

$$F_{\text{acceleration}}(y, \theta) = 1 - \max_{i \in I} \left( \max_{t \in [0, T]} \frac{|\ddot{x}_{sxi}^{(\text{absolute})}(t, y, \theta)|}{\ddot{x}^*} \right) \quad (13)$$

where  $\ddot{x}_{sxi}^{(\text{absolute})}(t, y, \theta), i \in I$  represent the absolute acceleration of the degrees of freedom of the superstructure in the  $x$  direction and  $\ddot{x}^*$  is the acceptable level of response equal to  $3.94 \text{ m/s}^2$ .

Figure 7 shows the probability of failure in terms of the base drift response as a function of the isolation system parameters. In this figure the nominal values of the isolation parameters are set equal to  $D_r = 0.75 \text{ m}$ ,  $H_r = 0.168 \text{ m}$ , and  $D_i = 0.10 \text{ m}$ . It is seen that there is a decrease in the probability of failure as the rubber diameter is increased. This is reasonable since the base isolation system becomes stiffer in this case. On the other hand, the probability of failure increases as the height of the rubber



**Base-Isolated Systems, Reliability-Based Characterization of, Fig. 8** Probability of the failure event related to the superstructure absolute acceleration as a function of the isolation system parameters

increases. In this case the isolation system becomes more flexible.

The effects of the isolation system parameters on the superstructure absolute acceleration are shown in Fig. 8. In this figure the probability of failure in terms of the absolute acceleration of the superstructure is presented. The probability of failure increases as the rubber diameter increases. In contrast, as the height of the rubber increases, the probability of failure is decreased. Clearly these effects are opposite to the effects of the isolation system parameters on the base response. For example, the introduction of additional stiffness in the isolation system makes the structural response ineffective. In other words, this additional stiffness which controls the base displacement makes the superstructure more vulnerable. This in turn affects the primary objective of the isolation system, namely, the reduction of the superstructure response. The previous results and observations show that the protection of the superstructure and the control of the base displacement are conflicting objectives.

## Summary

A reliability-based characterization of base-isolated systems under stochastic excitation has been proposed. The characterization allows to evaluate the effect of important design isolator

characteristics on the reliability of such systems. The results of the example problem indicate that the minimization of the superstructure absolute acceleration and the minimization of the base displacement are conflicting goals. For example, the provision of additional stiffness to the isolation system decreases the superstructure reliability. Contrarily, the flexibility of the isolators has a positive impact on the reliability of the superstructure. However, this flexibility may induce undesirable effects on the base isolation system. Therefore, the performance of the superstructure as well as the response of the base isolation system should be considered simultaneously for a proper characterization of base-isolated systems. It is noted that additional considerations such as the evaluation of the superstructure reliability in terms of interstory drifts can also be taken into account. This could lead to important results and conclusions. Similarly, the explicit consideration of near-field ground motions may have important implications for flexible structures such as base-isolated systems. For these systems near-field ground motions may lead to excessive base deformations and superstructure deformations with important implications for the reliability of the combined structural system (isolation system and superstructure). In summary, the proposed reliability-based characterization of base-isolated systems under stochastic excitation provides a valuable basic tool for the analyst and designer.



## Cross References

- ▶ [Code-Based Design: Seismic Isolation of Buildings](#)
- ▶ [Earthquake Mechanisms and Stress Field](#)
- ▶ [Engineering Characterization of Earthquake Ground Motions](#)
- ▶ [Integrated Earthquake Simulation](#)
- ▶ [Lead-Rubber Bearings with Emphasis on Their Implementation to Structural Design](#)
- ▶ [Nonlinear Dynamic Seismic Analysis](#)
- ▶ [Nonlinear Finite Element Analysis](#)
- ▶ [Probabilistic Seismic Hazard Models](#)
- ▶ [Random Process as Earthquake Motions](#)
- ▶ [Reliability Estimation and Analysis](#)
- ▶ [Robust Control of Building Structures Under Uncertain Conditions](#)
- ▶ [Seismic Reliability Assessment, Alternative Methods for](#)
- ▶ [Sensitivity of First-Excursion Probabilities for Nonlinear Stochastic Dynamical Systems](#)
- ▶ [Stochastic Ground Motion Simulation](#)
- ▶ [Structural Reliability Estimation for Seismic Loading](#)
- ▶ [Structural Seismic Reliability Analysis](#)
- ▶ [Subset Simulation Method for Rare Event Estimation: An Introduction](#)

## References

- Anderson JG, Hough SE (1984) A model for the shape of the Fourier amplitude spectrum of acceleration at high frequencies. *Bull Seismol Soc Am* 74(5):1969–1993
- Atkinson GM, Silva W (2000) Stochastic modeling of California ground motions. *Bull Seismol Soc Am* 90(2):255–274
- Au SK, Beck JL (2001) Estimation of small failure probabilities in high dimensions by subset simulation. *Probabilist Eng Mech* 16(4):263–277
- Boore DM (2003) Simulation of ground motion using the stochastic method. *Pure Appl Geophys* 160(3–4):635–676
- Boore DM, Joyner WB, Fumal TE (1997) Equations for estimating horizontal response spectra and peak acceleration from western North American earthquakes: a summary of recent work. *Seismol Res Lett* 68(1):128–153
- Burden RL, Faires JD (2011) Numerical analysis. Brooks Cole, Pacific Grove, Boston, MA 02210, USA
- Ceccoli C, Mazzotti C, Savoia M (1999) Non-linear seismic analysis of base-isolated RC frame structures. *Earthq Eng Struct Dyn* 28(6):633–653
- Ching J, Au SK, Beck JL (2005) Reliability estimation for dynamical systems subject to stochastic excitation using subset simulation with splitting. *Comput Method Appl Mech Eng* 194(12–16):1557–1579
- Chopra AK (2001) Dynamics of structures: theory and applications to earthquake engineering. Prentice Hall, Englewood Cliffs, Upper Saddle River, NJ 07458, USA
- De Luca A, Mele E, Molina J, Verzeletti G, Pinto AV (2001) Base isolation for retrofitting historic buildings: evaluation of seismic performance through experimental investigation. *Earthq Eng Struct Dyn* 30(8):1125–1145
- Jensen HA, Sepulveda JC (2011) On the effects of vibration control devices in the reliability-based design of stochastic dynamical systems. In: Proceedings of the 8th international conference on structural dynamics (EURODYN 2011), Leuven, 4–6 July 2011
- Kelly JM (1986) Aseismic base isolation: review and bibliography. *Soil Dyn Earthq Eng* 5(4):202–216
- Kramer SL (2003) Geotechnical earthquake engineering. Prentice Hall, Upper Saddle River, Englewood Cliffs, New Jersey, NJ, USA
- Lutes L, Sarkani S (2004) Random vibrations: analysis of structural and mechanical systems. Elsevier Butterworth-Heinemann, Burlington
- Makris N, Chang S (1998) Effects of damping mechanisms on the response of seismically isolated structures. PEER report 1998/06. Pacific Earthquake Engineering Research Center. College of Engineering, University of California, Berkeley
- Minewaki S, Yamamoto M, Higashino M, Hamaguchi H, Kyuke H, Sone T, Yoneda H (2009) Performance tests of full size isolators for super high-rise isolated buildings. *J Struct Eng AIJ* 55(B):469–477
- Mokha AS, Amin N, Constantinou MC, Zayas V (1996) Seismic isolation retrofit of large historic building. *J Struct Eng* 122(3):298–308
- Su L, Ahmadi G, Tadjbakhsh JG (1990) A comparative study of performances of various base isolation systems, part II: sensitivity analysis. *Earthq Eng Struct Dyn* 19:21–33
- Yamamoto M, Minewaki S, Higashino M, Hamaguchi H, Kyuke H, Sone T, Yoneda H (2009) Performance tests of fully size rubber bearings for isolated superhigh-rise buildings. In: International symposium on seismic response controlled buildings for sustainable society, S1-4, Tokyo
- Zou X-K, Wang Q, Li G, Chan C-M (2010) Integrated reliability-based seismic drift design optimization of base-isolated concrete buildings. *J Struct Eng* 136(10):1282–1295
- Zuev K, Beck JL, Au SK, Katafygiotis L (2011) Bayesian post-processor and other enhancements of Subset Simulation for estimating failure probabilities in high dimensions. *Comput Struct* 5:599–607



---

## Bayesian Operational Modal Analysis

Siu-Kui Au

Institute for Risk & Uncertainty and Centre for Engineering Dynamics, Liverpool, UK

### Synonyms

Ambient modal identification; Bayes' theorem; Modal identification; Operational modal analysis; Signal-to-noise ratio; System identification; Uncertainty law

### Introduction

Operational modal analysis, or ambient modal identification, aims at identifying the modal properties (natural frequency, damping ratio, mode shape, etc.) of an instrumented structure using only the (output) vibration response (acceleration, velocity, etc.). The input excitation to the structure is not measured but is assumed to be broadband random, often referred to as “ambient.” This allows vibration data to be collected when the structure is in its working or “operating” condition without much intervention, therefore implying significant economy over free-vibration (initially excited but no input afterwards) or forced-vibration tests (known input). The broadband random assumption essentially requires that the spectral characteristics (shape) of the measured response reflect the properties of the modes rather than those of the excitation, which is assumed to be constant in the vicinity of the natural frequencies.

In the absence of input loading, the uncertainties associated with the identified modal properties are often significantly higher than those identified from free-vibration tests or forced-vibration tests. The situation is aggravated by the presence of “modeling errors” that can be significant in field tests, i.e., the structure may not obey the modeling assumptions used in identifying the modal properties.

A Bayesian system identification approach provides a fundamental mathematical framework for quantifying the uncertainties and their effects on the identification results. This article describes the basics of Bayesian operational modal analysis, covering issues on formulation, efficient computations, interpretation of results, the quantification of identification uncertainties, and their management.

The methods presented in this article make use of the FFT (Fast Fourier transform) of measured acceleration data on a selected frequency band around the modes of interest. The modes are assumed to be classically damped.

In theory, ambient modal identification can be performed in either the time domain or the frequency domain. In practice, however, a frequency domain approach is preferable because it allows a natural partitioning of information in the data for identifying the modes of interest. It significantly simplifies the identification model because it only needs to model the modes in the selected band. For well-separated modes, one can select the band to cover one mode only, so that it can be identified independently of other modes. In general, the number of modes in the identification model only needs to be equal to the number of closely spaced modes, which rarely exceeds three. In the Bayesian formulation, this does not require any band-pass filtering because it can be done by simply omitting the FFT data of the excluded bands from the likelihood function.

Using only the FFT data within a selected band also significantly reduces modeling error risk because the identification results are invariant to complexities in the excluded bands containing other modes not of interest or even dynamics that are difficult to model. The mechanical response, excitation, and channel noise are assumed to have a flat spectrum within the selected frequency band only, rather than over the whole sampling band from zero to the Nyquist frequency (half of the sampling frequency). The latter is inevitable in time-domain identification approaches.

As a literature note, operational modal analysis was first formulated using a Bayesian approach in the Master's Thesis of Yuen (1999).

This led to the time-domain formulation in Yuen and Katafygiotis (2001a), a spectral density formulation in Yuen and Katafygiotis (2001b) and later an FFT formulation in Yuen and Katafygiotis (2003). As mentioned before, the time-domain formulation is not preferred for its assumption on the prediction error and modal force. The spectral density formulation involves statistical averaging and may not make full use of the information contained in the data. The Bayesian formulation based on FFT is therefore the preferred choice. The above formulations are only computationally feasible for a small number of measured degrees of freedom (dofs). This partly explains why the formulations did not flourish and there were no applications for a number of years after the formulations first appeared. Based on the FFT formulation, fast but equivalent formulations that allow mathematical analysis and feasible implementation in general were developed in Au (2011) (see also Zhang and Au 2013) for well-separated modes, Au (2011, 2012a) for multiple (possibly close) modes, and Au and Zhang (2012a) and Zhang et al. (2015) for well-separated modes but multiple setups. Application to field or experimental data can be found in Au et al. (2012a, b), Au and To (2012), Au and Zhang (2012b), and Fan et al. (2012). See also Yuen and Kuok (2010a, b) for application of the Bayesian spectral density approach. Asymptotic uncertainty laws that provide insights on the achievable limits operational modal analysis have been developed in Au (2014a, b). Recent overviews can be found in Yuen and Kuok (2011) and Au et al. (2013).

**Context**

The primary objective of ambient modal identification is to identify the natural frequencies, damping ratios, and mode shapes of a constructed structure using (output) vibration response measurement at a number of measured degrees of freedom (dofs) under “ambient conditions.” The latter is a notion relative to the mode of interest. It refers specifically to the situation

where it is justified to assume that the modal (not physical) force has a constant power spectral density in the vicinity of the resonance band dominated by the mode.

Following a Bayesian approach in the frequency domain, use is made of the (scaled) FFT of the measured acceleration response at a number of dofs on the structure, denoted by  $\{\hat{\mathbf{x}}_j \in R^n : j = 0, \dots, N - 1\}$  and abbreviated as  $\{\hat{\mathbf{x}}_j\}$ , where  $n$  is the number of measured dofs. The (scaled) FFT of  $\{\hat{\mathbf{x}}_j\}$  is the complex-valued sequence  $\{F_k \in C^n : k = 0, \dots, N - 1\}$  where

$$F_k = \sqrt{\frac{2\Delta t}{N}} \sum_{j=0}^{N-1} \hat{\mathbf{x}}_j \exp(-2\pi i j k / N) \quad (1)$$

$$k = 0, \dots, N - 1$$

and  $i^2 = -1$  and  $\Delta t$  is the sampling interval. For a given  $k$ , the FFT  $F_k$  corresponds to frequency

$$f_k = k / N \Delta t \quad k = 0, \dots, \text{int}[N/2] \quad (2)$$

where  $\text{int}[N/2]$  is the integer part of  $N/2$  and is the index corresponding to the Nyquist frequency.

The FFT  $F_k$  has been scaled so that  $F_k F_k^* \in C^{n \times n}$  gives the one-sided sample spectral density (periodogram) matrix. Summing the  $i$ -th diagonal element of  $F_k F_k^*$  over  $k = 0, \dots, N - 1$  and multiplying by the frequency resolution  $\Delta f = 1 / N \Delta t$  gives twice the mean square value of the  $i$ -th measured dof (Parseval equality).

For the purpose of identifying the modes of interest, it is sufficient and preferable to make use of the FFT data only on a selected frequency band around the mode(s). This is because in reality, the data contains a variety of dynamic (colored) activities over its sampling spectrum (up to the Nyquist frequency), most of which are irrelevant to identifying the mode(s) or are difficult to model.

Suppose there are  $m$  modes within the selected frequency band and let  $\{F_k\}$  denote the collection of FFT data within the band. It is modeled as a sum of contributions from the structural vibration (the target to be measured) and a prediction error

(noise) that accounts for the difference between the theoretical and measured response:

$$F_k = \sum_{i=1}^m \Phi_i \ddot{\eta}_{ik} + \epsilon_k \quad (3)$$

where  $\Phi_i \in R^n$  ( $i = 1, \dots, m$ ) is the mode shape of the  $i$ -th mode in the selected frequency band;  $\ddot{\eta}_{ik} \in C$  is the FFT at frequency  $f_k$  of the  $i$ -th modal acceleration response; and  $\epsilon_k \in C^n$  is the FFT of the prediction error, which may arise due to measure (channel) noise and modeling error (e.g., unaccounted dynamics). Assuming classically damped modes, the time-domain counterpart of  $\eta_{ik}$  satisfies the uncoupled equation of motion:

$$\ddot{\eta}_i(t) + 2\zeta_i \omega_i \dot{\eta}_i(t) + \omega_i^2 \eta_i(t) = p_i(t) \quad (4)$$

where  $\omega_i = 2\pi f_i$ ;  $f_i$ ,  $\zeta_i$ , and  $p_i(t)$  are, respectively, the natural frequency (in Hz), damping ratio, and modal force.

In the above context, the set of modal parameters to be identified from the FFT data  $\{F_k\}$ , denoted by  $\theta$ , consists of the parameters:

- (1) Natural frequencies  $f_1, \dots, f_m \in R^+$
- (2) Damping ratios  $\zeta_1, \dots, \zeta_m \in (0, 1)$
- (3) Mode shapes  $\Phi_1, \dots, \Phi_m \in R^n$
- (4) PSD matrix of modal forces  $S \in C^{n \times n}$  (assumed constant within the band)
- (5) PSD of prediction error  $S_e \in R^+$  (assumed constant within the band)

Each mode shape  $\Phi_i = [\Phi_{1i}, \Phi_{2i}, \dots, \Phi_{ni}]^T$  is subjected to a unit norm constraint, i.e.,

$$\|\Phi_i\|^2 = \Phi_i^T \Phi_i = \sum_{j=1}^n \Phi_{ji}^2 = 1 \quad i = 1, \dots, m \quad (5)$$

## Formulation from First Principle

In a Bayesian context, the information about the set of modal parameters  $\theta$  that can be inferred from the FFT data  $\{F_k\}$  is encapsulated in the “posterior probability density function” (PDF) of

$\theta$ , denoted by  $p(\theta|\{F_k\})$ . Using Bayes’ theorem, it is given by

$$p(\theta|\{F_k\}) = p(\{F_k\})^{-1} p(\{F_k\}|\theta) p(\theta) \quad (6)$$

The first term on the RHS does not depend on  $\theta$ . As far as the identification of  $\theta$  is concerned, it can be ignored. The middle-term  $p(\{F_k\}|\theta)$  is called the “likelihood function.” It is derived based on modeling assumptions that relate the response of the theoretical model for a given  $\theta$  to the FFT data. The middle-term  $p(\theta)$  is the “prior distribution” that reflects one’s knowledge about  $\theta$  in the absence of data. In modal identification problems with sufficient data, it can be taken as a constant because it is slowly varying compared to the likelihood function. As a result, it is sufficient for modal identification problems to use

$$p(\theta|\{F_k\}) \propto p(\{F_k\}|\theta) \quad (7)$$

Deriving the likelihood function requires deriving the joint PDF of  $\{F_k\}$  for a given  $\theta$ . This PDF is generally complicated, but it turns out to admit an asymptotic closed form when the number of data points  $N$  is large (Brillinger 1981). In particular, as  $N \rightarrow \infty$ ,  $\{F_k\}$  at different  $k$ ’s are asymptotically independent. For a given  $k$ , the real and imaginary parts of  $F_k$  are jointly Gaussian with zero mean. Thus,

$$p(\theta|\{F_k\}) \propto p(\{F_k\}|\theta) = (2\pi)^{-nN_f} \left[ \prod_k \det C_k \right]^{-1/2} \exp \left\{ -\frac{1}{2} \sum_k \begin{bmatrix} \text{Re} F_k \\ \text{Im} F_k \end{bmatrix}^T C_k^{-1} \begin{bmatrix} \text{Re} F_k \\ \text{Im} F_k \end{bmatrix} \right\} \quad (8)$$

where the sum is overall frequency ordinates in the selected band, whose number is equal to  $N_f$ ;  $C_k \in R^{2n \times 2n}$  is the covariance matrix of the augmented vector  $[\text{Re} F_k; \text{Im} F_k] \in R^{2n}$ ; and  $\det(\cdot)$  denotes the determinant of the argument matrix. For high sampling rate, it can be shown using random-vibration theory (Lutes and Sarkani 1997) that asymptotically

$$\mathbf{C}_k = \frac{1}{2} \begin{bmatrix} \Phi(\text{Re}\mathbf{H}_k)\Phi^T & -\Phi(\text{Im}\mathbf{H}_k)\Phi^T \\ \Phi(\text{Im}\mathbf{H}_k)\Phi^T & \Phi(\text{Re}\mathbf{H}_k)\Phi^T \end{bmatrix} + \frac{S_e}{2} \mathbf{I}_{2n} \quad (9)$$

where  $\Phi = [\Phi_1, \dots, \Phi_m] \in R^{n \times m}$  is the mode shape matrix and  $\mathbf{H}_k \in C^{m \times m}$  is the modal transfer matrix whose  $(i, j)$  entry is given by

$$\mathbf{H}_k(i, j) = S_{ij} h_{ik} h_{jk}^* \quad (10)$$

$$h_{ik} = [(\beta_{ik}^2 - 1) + (2\zeta_i \beta_{ik})\mathbf{i}]^{-1} \quad (11)$$

$$\beta_{ik} = f_i / f_k \quad (12)$$

and  $S_{ij}$  is the  $(i, j)$  entry of the PSD matrix of modal force,  $\mathbf{S} \in C^{m \times m}$ . Note that  $\mathbf{H}_k$  and  $\mathbf{S}$  are Hermitian (i.e., equal to its conjugate transpose);  $\mathbf{C}_k$  is real symmetric.

### Posterior Most Probable Value and Covariance Matrix

For convenience in analysis or computation, the posterior PDF is written in terms of the NLLF (negative log-likelihood function):

$$L(\boldsymbol{\theta}) = \frac{1}{2} \sum_k \text{Indet} \mathbf{C}_k + \frac{1}{2} \sum_k \begin{bmatrix} \text{Re}F_k \\ \text{Im}F_k \end{bmatrix}^T \mathbf{C}_k^{-1} \begin{bmatrix} \text{Re}F_k \\ \text{Im}F_k \end{bmatrix} \quad (13)$$

so that

$$p(\boldsymbol{\theta}|\{F_k\}) \propto \exp(-L(\boldsymbol{\theta})) \quad (14)$$

Note that the constant  $nN_f \ln(2\pi)$  has been omitted from the NLLF.

With sufficient data often encountered in practice, the posterior PDF has a single peak in the parameter space of  $\boldsymbol{\theta}$ , which is the most probable value (MPV) of the modal parameters given the data. Equivalently, the NLLF has a unique minimum at the MPV. Approximating the NLLF by a second-order Taylor expansion about the MPV leads to a Gaussian approximation of the posterior PDF. The resulting Gaussian distribution has a mean at the MPV, and its covariance matrix, called the ‘‘posterior covariance matrix,’’ reflects the remaining uncertainties of the modal parameters

in the presence of the data. Mathematically, the posterior covariance matrix is equal to the inverse of the Hessian of the NLLF at the MPV.

The above results can be reasoned as follows. Given the data, let the MPV of the modal parameters be denoted by the vector  $\hat{\boldsymbol{\theta}}$ . Approximating the NLLF by a second-order Taylor expansion about  $\hat{\boldsymbol{\theta}}$ ,

$$L(\boldsymbol{\theta}) \approx L(\hat{\boldsymbol{\theta}}) + \nabla L(\hat{\boldsymbol{\theta}}) (\boldsymbol{\theta} - \hat{\boldsymbol{\theta}}) + \frac{1}{2} (\boldsymbol{\theta} - \hat{\boldsymbol{\theta}})^T \nabla^2 L(\hat{\boldsymbol{\theta}}) (\boldsymbol{\theta} - \hat{\boldsymbol{\theta}}) \quad (15)$$

where  $\nabla L(\hat{\boldsymbol{\theta}})$  and  $\nabla^2 L(\hat{\boldsymbol{\theta}})$  denote, respectively, the gradient (row) vector and Hessian matrix of the NLLF at  $\hat{\boldsymbol{\theta}}$ . Since the NLLF is minimized at  $\hat{\boldsymbol{\theta}}$ ,  $\nabla L(\hat{\boldsymbol{\theta}}) = \mathbf{0}$  (a zero vector) and  $\nabla^2 L(\hat{\boldsymbol{\theta}})$  are positive definite matrix. Applying this on Eq. 15 and then substituting into Eq. 14 gives

$$\begin{aligned} p(\boldsymbol{\theta}|\{F_k\}) &\propto \exp \left[ -L(\hat{\boldsymbol{\theta}}) - \frac{1}{2} (\boldsymbol{\theta} - \hat{\boldsymbol{\theta}})^T \nabla^2 L(\hat{\boldsymbol{\theta}}) (\boldsymbol{\theta} - \hat{\boldsymbol{\theta}}) \right] \\ &\propto \exp \left[ -\frac{1}{2} (\boldsymbol{\theta} - \hat{\boldsymbol{\theta}})^T \nabla^2 L(\hat{\boldsymbol{\theta}}) (\boldsymbol{\theta} - \hat{\boldsymbol{\theta}}) \right] \\ &\propto \exp \left[ -\frac{1}{2} (\boldsymbol{\theta} - \hat{\boldsymbol{\theta}})^T \hat{\mathbf{C}}^{-1} (\boldsymbol{\theta} - \hat{\boldsymbol{\theta}}) \right] \end{aligned} \quad (16)$$

where

$$\hat{\mathbf{C}} = \nabla^2 L(\hat{\boldsymbol{\theta}})^{-1} \quad (17)$$

is a positive definite matrix. Eq. 16 is just the variable part of a joint Gaussian PDF with zero mean and covariance matrix equal to  $\hat{\mathbf{C}}$ . The proportionality constant of the equation is  $(2\pi)^{-n_0/2} (\det \hat{\mathbf{C}})^{-1/2}$  ( $n_0$  is the number of modal parameters), which can be obtained by integration or by probability reasoning. Thus,

$$\begin{aligned} p(\boldsymbol{\theta}|\{F_k\}) &= (2\pi)^{-n_0/2} (\det \hat{\mathbf{C}})^{-1/2} \\ &\exp \left[ -\frac{1}{2} (\boldsymbol{\theta} - \hat{\boldsymbol{\theta}})^T \hat{\mathbf{C}}^{-1} (\boldsymbol{\theta} - \hat{\boldsymbol{\theta}}) \right] \end{aligned} \quad (18)$$

### Computational Problems

The MPV of modal parameters cannot be obtained analytically because the relationship

between the NLLF and the modal parameters is complicated. Brute-force numerical minimization of the NLLF with respect to the modal parameters is prohibitive or not convergent, primarily because the number of modal parameters is typically large. The latter arises primarily from the number of measured dofs and secondarily from the number of modes. Taking into account the Hermitian nature of the PSD matrix of modal force, the number of modal parameters in  $\boldsymbol{\theta}$  is equal to

$$n_{\theta} = (m + 1)^2 + nm \quad (19)$$

For example, a setup with 18 measured dofs and a band with  $m = 2$  modes result in  $(2 + 1)^2 + (18)(2) = 45$  parameters.

Adding to the difficulty is the ill-conditioned nature of the matrix  $\mathbf{C}_k$  in Eq. 9. For good quality data, it is close to being rank deficient since it is then dominated by the first term, which has a rank of at most  $2m$  and is often less than  $2n$  (the number of modes  $m$  is often less than the number of measured dofs  $n$ ).

### Fast Equivalent Formulation

Using linear algebra techniques, it is possible to rewrite the NLLF in a form that facilitates analysis and computations. In particular, the NLLF can be written as a quadratic form of the mode shape, thereby allowing the most probable mode shape to be determined efficiently when the remaining parameters are given. Based on this, the MPV of all modal parameters can be obtained by optimizing different groups of parameters in turn, iterating until convergence.

Using the equivalent forms, analytical expressions for the Hessian of the NLLF can also be derived effectively. This allows the posterior covariance matrix to be evaluated efficiently and accurately, without resorting to finite difference method.

### Single Mode

When there is only one mode in the selected band, the set of modal parameters reduces to

$$\boldsymbol{\theta} = \{f, \zeta, S, S_e, \boldsymbol{\Phi}\} \quad (20)$$

where mode index has been dropped for simplicity;  $S \in R^+$  is the PSD of modal force;  $\boldsymbol{\Phi} \in R^n$  is the mode shape.

It can be shown that the NLLF in Eq. 13 can be rewritten as

$$\begin{aligned} L(\boldsymbol{\theta}) = & -nN_f \ln 2 + (n - 1)N_f \ln S_e \\ & + \sum_k \ln(SD_k + S_e) \\ & + S_e^{-1} (d - \boldsymbol{\Phi}^T \mathbf{A} \boldsymbol{\Phi}) \end{aligned} \quad (21)$$

where

$$\mathbf{A} = \sum_k \left(1 + \frac{S_e}{SD_k}\right)^{-1} (\text{Re}F_k \text{Re}F_k^T + \text{Im}F_k \text{Im}F_k^T) \in R^{n \times n} \quad (22)$$

$$D_k = \left[ (\beta_k^2 - 1)^2 + (2\zeta\beta_k)^2 \right]^{-1} \beta_k = f/f_k \quad (23)$$

$$d = \text{Re}F_k^T \text{Re}F_k + \text{Im}F_k^T \text{Im}F_k \quad (24)$$

Note that  $\mathbf{A}$  depends on  $f, \zeta, S, S_e$ ;  $D_k$  depends on  $f, \zeta$ . The significance of Eq. 21 in comparison to Eq. 13 is that it no longer involves the inverse of ill-conditioned matrix. More importantly, the mode shape  $\boldsymbol{\Phi}$  only appears in the quadratic form. Given the remaining parameters  $\{f, \zeta, S, S_e\}$ , minimizing the NLLF with respect to  $\boldsymbol{\Phi}$  subjected to the norm constraint  $\boldsymbol{\Phi}^T \boldsymbol{\Phi} = 1$  gives the most probable shape as the eigenvector of  $\mathbf{A}$  with the largest eigenvalue. This effectively reduces the dimension of the optimization problem for MPV to only four ( $f, \zeta, S, S_e$ ), which can be readily performed numerically (Au 2011).

### Multiple Modes

When there is more than one mode in the selected band, the set of modal parameters  $\boldsymbol{\theta}$  is given by that stated in section Context, which is repeated here:

- (1) Natural frequencies  $f_1, \dots, f_m \in R^+$
- (2) Damping ratios  $\zeta_1, \dots, \zeta_m \in (0, 1)$
- (3) Mode shapes  $\Phi_1, \dots, \Phi_m \in R^n$
- (4) PSD matrix of modal forces  $\mathbf{S} \in C^{n \times n}$   
(assumed constant within the band)
- (5) PSD of prediction error  $S_e \in R^+$  (assumed constant within the band)

Each mode shape  $\Phi_i = [\Phi_{1i}, \Phi_{2i}, \dots, \Phi_{ni}]^T$  is subjected to a unit norm constraint, i.e.,

$$\|\Phi_i\|^2 = \Phi_i^T \Phi_i = \sum_{j=1}^n \Phi_{ji}^2 = 1 \quad i = 1, \dots, m \quad (25)$$

In this case the most probable mode shape cannot be obtained directly by solving a standard eigenvalue problem. The mathematical structure of the optimization problem is more complex because the mode shapes are not necessarily orthogonal to each other. However, it is possible to reduce the complexity by representing the mode shape via a set of orthonormal basis and noting that the dimension of the subspace spanned by such basis does not exceed the number of modes. The mode shape matrix  $\Phi = [\Phi_1, \dots, \Phi_m] \in R^{n \times m}$  is represented as

$$\Phi = \mathbf{B}' \alpha \quad (26)$$

where

$$\mathbf{B}' = [\mathbf{B}'_1, \dots, \mathbf{B}'_{m'}] \in R^{n \times m'} \quad (27)$$

contains in its columns a set of orthonormal “mode shape basis”  $\{\mathbf{B}'_i \in R^n : i = 1, \dots, m'\}$  spanning the “mode shape subspace;”  $\alpha \in R^{m' \times m}$  contains in its columns the coordinates of each mode shape with respect to the mode shape basis;  $m' \leq \min(n, m)$  is the dimension of the mode shape subspace, which can be determined with the help of a singular-value spectrum. The MPVs of  $\mathbf{B}'$  and  $\alpha$  need to be determined in the identification process.

Based on Eq. 26, it can be shown that the NLLF can be rewritten as

$$\begin{aligned} L(\theta) = & -nN_f \ln 2 + (n - m')N_f \ln S_e \\ & + S_e^{-1}d + \sum_k \ln |\det \mathbf{E}'_k| \\ & - S_e^{-1} \sum_k F_k^* \mathbf{B}' (\mathbf{I}_{m'} - S_e \mathbf{E}'_k^{-1}) \mathbf{B}'^T F_k \end{aligned} \quad (28)$$

where  $d$  is given by Eq. 24 as in the case of single mode, and

$$\mathbf{E}'_k = \alpha \mathbf{H}_k \alpha^T + S_e \mathbf{I}_{m'} \quad (29)$$

is an  $m'$ -by- $m'$  Hermitian matrix. The significance of Eq. 28 is that the mode shape basis  $\mathbf{B}$  has been segregated out in the last term, which is quadratic in nature. The most probable basis should therefore minimize the quadratic form under orthonormal constraints. This does not lead to a standard eigenvalue problem, but procedures have been developed that allow the most probable basis to be determined efficiently by Newton iteration. This resolves the potentially high-dimensional optimization with respect to the mode shape. Based on this, a strategy has been developed for determining the MPV of different groups of parameters, iterating until convergence (Au 2012a).

## Modal Signal-to-Noise Ratio

The term “signal-to-noise ratio” (s/n ratio) is often used to describe the quality of data to indicate the contribution of the signal targeted to be measured compared to the contribution of “noise,” which inevitably arises from sensor, cables transmitting the signal (especially for analog signals), digitizing hardware, etc. The actual quantitative definition differs depending on the particular application, however. In ambient modal identification, the s/n ratio that affects the identification results is related to the spectral contribution of the modal response compared to the spectral contribution of the noise in the vicinity of the resonance frequency band. In the case of well-separated modes, a definition of the s/n ratio that is found to govern fundamentally the



characteristics of the identification results is the PSD of the theoretical acceleration response at resonance ( $SD_k = S/4\zeta^2$ ) divided by the PSD of the prediction error ( $S_e$ ):

$$\gamma = \frac{S}{4S_e\zeta^2} \quad (30)$$

### Governing Factors

The modal s/n ratio in Eq. 30 depends on the following factors:

- (1) The prediction error PSD  $S_e$ . This includes contributions from the channel noise as well as modeling errors, e.g., due to unaccounted modes and colored nature of modal force.
- (2) The damping ratio  $\zeta$ . The smaller the damping, the higher the modal s/n ratio, as a result of higher modal response PSD at resonance.
- (3) The modal force PSD  $S$ . This in turn depends on the intensity of environmental excitation and (less trivially) on the measured dofs. Specifically, let  $\xi$  denote the “full” mode shape of the structure containing all (possibly an infinite number of) dofs, and it is scaled to have unit norm, i.e.,  $\xi^T \xi = 1$ . Then it can be reasoned that

$$S = S_p \left( \sum_i \xi_i^2 \right) \quad (31)$$

where the sum is over the measured dofs, and

$$S_p = \frac{\xi^T \mathbf{S}_F \xi}{(\xi^T \mathbf{M} \xi)^2} \quad (32)$$

is the modal force PSD consistent with the scaling of the global mode shape  $\xi$ ;  $\mathbf{M}$  is the mass matrix of the structure. Note that in reality, the full mode shape  $\xi$  and the mass matrix  $\mathbf{M}$  can hardly be identified and so is  $S_p$ . Instead, the measured mode shape  $\Phi$  and the modal force PSD  $S$  consistent with the scaling  $\Phi^T \Phi = 1$  is identified. Eq. 31 shows that the modal force PSD  $S$  always increases with the number of measured dofs, although the rate depends on the mode shape of the dof incrementally added to the existing set of measured dofs. As a result, the

modal s/n ratio in Eq. 30 always increases with the number of measured dofs.

### High s/n Asymptotics

It turns out that the Bayesian modal identification results in terms of the MPV and posterior covariance matrix reduce to intuitive forms when the modal s/n ratio is large (theoretically infinity). This is referred to as “high s/n asymptotics.”

Asymptotically for large modal s/n ratio, the terms in the NLLF can be separated into two terms: one quadratic term depending only on the mode shape (and the prediction error PSD in a multiplicative manner) and the other term depending only on the remaining parameters (natural frequency, damping ratio, modal force PSD, prediction error PSD). The mode shapes are therefore asymptotically uncoupled from the remaining parameters. This has important implications on the behavior of the MPV and the posterior covariance matrix. The former provides a sound basis for setting initial guess and designing fast algorithms for determining the MPV of modal parameters. The latter leads to remarkably simple closed-form formulas for the posterior variance of the modal parameters. These are collectively known as “uncertainty laws,” which govern the achievable limits of operational modal analysis.

The asymptotic behavior of the most probable mode shape is discussed in sections [Single Mode](#) and [Multiple Modes](#) for a single mode and multiple modes in the selected frequency band, respectively. The posterior covariance matrix is discussed in the context of uncertainty laws in section [Uncertainty Laws](#).

#### Single Mode

For a single mode in the selected band, asymptotically the most probable mode shape  $\Phi$  is equal to the eigenvector with the largest eigenvalue of the following matrix:

$$\mathbf{A}_0 = \sum_k (\text{Re}F_k \text{Re}F_k^T + \text{Im}F_k \text{Im}F_k^T) \quad (33)$$

This matrix depends only on the data, and so the most probable mode shape can be calculated explicitly without optimization.



The above result can be reasoned as follows. Asymptotically the matrix  $\mathbf{A}$  in the NLLF Eq. 21 becomes  $\mathbf{A}_0$  in Eq. 33, and so the NLLF becomes

$$\begin{aligned} L(\boldsymbol{\theta}) &\sim -nN_f \ln 2 + (n-1)N_f \ln S_e \\ &\quad + \sum_k \ln(SD_k + S_e) + S_e^{-1}d \\ &\quad - S_e^{-1} \boldsymbol{\Phi}^T \mathbf{A}_0 \boldsymbol{\Phi} \end{aligned} \quad (34)$$

In the above expression, only the last term depends on  $\boldsymbol{\Phi}$ , which is a quadratic form with a constant coefficient matrix  $\mathbf{A}_0$ . Minimizing it with respect to  $\boldsymbol{\Phi}$  and subjected to the norm constraint  $\boldsymbol{\Phi}^T \boldsymbol{\Phi} = 1$  gives the most probable mode shape as the eigenvector of  $\mathbf{A}_0$  with the largest eigenvalue.

### Multiple Modes

When there is more than one mode in the selected band, asymptotically the most probable mode shape basis is given by the eigenvectors of  $\mathbf{A}_0$  in Eq. 33 corresponding to the first  $m'$  largest eigenvalues. Note that this does not give directly the most probable mode shapes because the MPV of the coordinates with respect to the basis, i.e.,  $\boldsymbol{\alpha}$  in Eq. 26, is not known but its determination is still nontrivial.

The above can be reasoned as follows. Asymptotically, the term  $(\mathbf{I}_{m'} - S_e \mathbf{E}'_k)$  in the quadratic term of the NLLF in Eq. 28 becomes the identity matrix  $\mathbf{I}_{m'}$  and so

$$\begin{aligned} L(\boldsymbol{\theta}) &\sim -nN_f \ln 2 + (n-m')N_f \ln S_e \\ &\quad + S_e^{-1}d + \sum_k \ln |\det \mathbf{E}'_k| \\ &\quad - S_e^{-1} \sum_k F_k^* \mathbf{B}' \mathbf{B}'^T F_k \end{aligned} \quad (35)$$

This expression depends on the mode shape basis  $\mathbf{B}'$  only through the sum in the last term, which is quadratic in nature. Substituting  $\mathbf{B}' = [\mathbf{B}'_1, \dots, \mathbf{B}'_{m'}]$ , the sum can be rewritten as

$$\begin{aligned} \sum_k F_k^* \mathbf{B}' \mathbf{B}'^T F_k &= \sum_{i=1}^{m'} \mathbf{B}'_i{}^T \left( \sum_k F_k F_k^* \right) \mathbf{B}'_i \\ &= \sum_{i=1}^{m'} \mathbf{B}'_i{}^T \mathbf{A}_0 \mathbf{B}'_i \end{aligned} \quad (36)$$

Minimizing the NLLF is equivalent to maximizing the sum on the rightmost. Since it contains no cross terms between  $\mathbf{B}'_i$  and  $\mathbf{B}'_j$  ( $i \neq j$ ), maximizing it gives the most probable basis as the eigenvectors of  $\mathbf{A}_0$  corresponding to the first  $m'$  largest eigenvalues.

## Quantification of Identification Uncertainty

### Mode Shape Uncertainty

For scalar-valued modal parameters such as the natural frequency and damping ratio, the posterior uncertainty can be conveniently described in terms of the posterior standard deviation or in a nondimensional manner the posterior coefficient of variation (c.o.v.), equal to the posterior standard deviation divided by the MPV. The posterior standard deviation is equal to the square root of the posterior variance, which can be obtained from the corresponding diagonal entry of the posterior covariance matrix.

The above quantification cannot be applied to the mode shape because it is vector valued and is subject to the norm constraint. One way to quantify the uncertainty of the mode shape is through the Expected modal assurance criterion (MAC), defined analogously as in the deterministic case. According to the posterior distribution, which is approximated by a Gaussian distribution, given the measured data, the mode shape is a Gaussian vector with mean vector equal to the most probable mode shape and a covariance matrix  $\mathbf{C}_\Phi \in R^{n \times n}$ . The latter is given by the corresponding  $n \times n$  partition of the full covariance matrix (containing all modal parameters). The Expected MAC is defined as the expected value of the cosine of the hyper angle between the random mode shape vector and the most probable mode shape vector. This value ranges between 0 and 1; the higher the value, the smaller the mode shape uncertainty. An exact closed-form expression for the Expected MAC has not been developed, but an asymptotic expression is available, which is adequate for practical purposes. It can be shown that asymptotically

$$\text{Expected MAC} = \left( 1 + \sum_{i=2}^n \kappa_i^2 \right)^{-1/2} \quad (37)$$

where  $\{\kappa_i : i = 1, \dots, n\}$  are the eigenvalues (principal variances) of the posterior covariance matrix of the mode shape,  $\mathbf{C}_\Phi$ . This formula is asymptotically correct for small  $\{\kappa_i\}$  or large  $n$ . The sum does not contain  $\kappa_1$  because it is theoretically equal to zero, resulting from the norm constraint on the mode shape Au 2011.

In well-controlled ambient tests, the Expected MAC is often close to 1. A complementary measure of the mode shape uncertainty is the expected value of the hyper angle between the random mode shape vector and the most probable mode shape vector. It can be shown that under the same asymptotic conditions in Eq. 37, the expected value of the hyper angle is given by

$$\delta_\Phi = \left( \sum_{i=2}^n \kappa_i^2 \right)^{1/2} \quad (38)$$

and it is related to the Expected MAC by

$$\text{Expected MAC} = 1 - \frac{1}{2} \delta_\Phi^2 \quad (39)$$

## Bayesian Versus Non-Bayesian Measure

### Bayesian Measure

In the context of Bayesian system identification, the spread of the posterior PDF is a direct fundamental quantification of the remaining uncertainty associated with the modal parameters for a given assumed identification model and in the presence of the measured data. Since the posterior PDF is typically unimodal and it can be approximated by a joint Gaussian PDF, the uncertainty of the modal parameters can be quantified by the covariance matrix, which is called the “posterior covariance matrix.” The posterior covariance matrix is the inverse of the Hessian matrix of the NLLF, and it can be calculated for a given set of data. Clearly it depends on the particular set of data.

### Non-Bayesian Measure

In non-Bayesian identification methods, the identification results are often given in terms of the “best” or “optimal” value calculated from an accepted algorithm. This is analogous to the MPV calculated in a Bayesian identification method. In a non-Bayesian context, one conventional quantification of the uncertainty of the identified parameters is through the ensemble variance (or more generally, the ensemble covariance matrix) of the modal parameters. This can be understood as the variance among the identified (i.e., best) values calculated from a large (theoretically infinite) number of repeated experiments. This is a “frequentist” measure of the uncertainty of the identified parameters. Unlike the posterior variance that is defined for a given set of data, the ensemble variance requires (at least conceptually) the notion of repeated experiments. Because of its ensemble nature, it does not depend on a particular data set. If there were no modeling error, i.e., the data in the repeated experiments indeed results from a process obeying the identification model assumed, the variability of the identified values among repeated experiments reflects the quality of the identification algorithm and the amount of data used. Otherwise, it reflects also the variability due to other factors such as the changes in system properties among the experiments and modeling errors.

### Connection

Due to their different definitions, the Bayesian and frequentist measure of the identification uncertainty of modal parameters need not coincide, although intuition suggests that they should be of similar order of magnitude when there is no modeling error. It can be shown that when there is no modeling error then in a weighted sense, the expectation of the posterior covariance matrix (Bayesian) is equal to the ensemble variance of the most probable value among repeated experiments (Au 2012b). In reality where modeling error can exist and conditions can change among the repeated experiments, the Bayesian and frequentist measure can differ significantly.

The Bayesian and frequentist measure of identification uncertainty has different roles. The Bayesian measure reflects fundamentally the remaining uncertainty associated with the parameters for a given identification model and a given set of data. It does not reflect what the identification results would be if the experiment is repeated, because modeling error can exist and conditions of the next experiment can change. It does not describe ensemble variability. On the other hand, the frequentist measure is an aggregate effect of identification uncertainty, modeling error, and system changes over the repeated experiments.

### Uncertainty Laws

Under the Bayesian framework, the posterior uncertainty of the modal parameters can be calculated in terms of the posterior covariance for a given set of measured data. This process is computational and implicit in nature. It does not yield much insight about how the identification uncertainty depends on test configurations.

In the case of a single mode in the selected band, it has been possible to derive closed-form analytical expressions for the posterior covariance matrix under asymptotic conditions, namely, small damping and long data duration, which are typically met in applications. The expressions are collectively referred as “uncertainty laws” (Au 2014a, b). They provide insights on the scientific nature of the ambient modal identification problem and its fundamental limits on identification uncertainty. The uncertainty laws can also be used for drafting specifications for ambient vibration tests.

### Context

The uncertainty laws have been derived under the following context:

- (1) The damping ratio is small,  $\zeta \rightarrow 0$ .
- (2) The spectral information for identifying the mode is large, in the sense that  $N_f = 2\kappa\zeta N_c \rightarrow \infty$  where  $N_c = T_d/T$ ,  $T_d$  is

the data duration, and  $T$  is the natural period of the target mode. Note that  $N_f \rightarrow \infty$  and  $\zeta \rightarrow 0$  imply that  $N_c \rightarrow \infty$  as well.

- (3) The selected frequency band is assumed to be  $f(1 \pm \kappa\zeta)$ , where  $\kappa$  is called the “bandwidth factor.” The bandwidth factor is a trade-off between identification information (the larger, the better) and modeling error risk (the smaller, the better). Typically it ranges between 3 and 10.
- (4) The FFT data  $\{F_k\}$  in the selected band is assumed to indeed result from a process obeying the identification model, i.e., no modeling error. Note that prediction error is still present because it is part of the identification model.

The selected frequency bandwidth is assumed to be proportional to the damping ratio because the width of the resonance band around the natural frequency does, e.g., the half power band is  $f(1 \pm \zeta)$ , corresponding to  $\kappa = 1$ . An asymptotically small damping ratio implies that the modal s/n ratio  $\gamma = S/4S_e\zeta^2$  in Eq. 30 is asymptotically high. It is therefore implied in the uncertainty laws that the modal s/n ratio is high.

### Main Results

The asymptotic expressions of the posterior coefficient of variation of the modal parameters are summarized in Table 1. In terms of correlation, except for that between the damping ratio  $\zeta$  and the modal force PSD  $S$ , the correlation between any pair of the modal parameters among  $\{f, \zeta, S, S_e, \Phi\}$  is asymptotically small, at most  $O(\zeta)$ . The correlation between  $\zeta$  and  $S$  is  $O(\kappa^{-1/2})$ .

### Implications

The following implications can be drawn from the uncertainty laws:

- (1) For small damping ratio, the posterior uncertainties of the natural frequency and mode shape are significantly smaller than those of the damping ratio and the modal force PSD. The former are  $O(\zeta^{1/2})$  and the latter are  $O(\zeta^{-1/2})$ .

**Bayesian Operational Modal Analysis, Table 1** Summary of uncertainty laws

Parameter	Uncertainty law	Bandwidth factor
Frequency $f$	Squared posterior c.o.v. $\delta_f^2 = \frac{\zeta}{2\pi N_e B_f(\kappa)}$	$B_f(\kappa) = \frac{2}{\pi} \left( \tan^{-1}\kappa - \frac{\kappa}{\kappa^2+1} \right)$
Damping $\zeta$	Squared posterior c.o.v. $\delta_\zeta^2 = \frac{1}{2\pi\zeta N_e B_\zeta(\kappa)}$	$B_\zeta(\kappa) = \frac{2}{\pi} \left[ \tan^{-1}\kappa + \frac{\kappa}{\kappa^2+1} - \frac{2(\tan^{-1}\kappa)^2}{\kappa} \right]$
Modal force PSD $S$	Squared posterior c.o.v. $\delta_S^2 = \frac{1}{N_f B_S(\kappa)}$	$B_S(\kappa) = 1 - \frac{2}{\kappa} (\tan^{-1}\kappa)^2 \left( \tan^{-1}\kappa + \frac{\kappa}{\kappa^2+1} \right)^{-1}$
Prediction error PSD $S_e$	Squared posterior c.o.v. $\delta_{S_e}^2 = \frac{1}{(n-1)N_f}$	–
Mode shape $\Phi$	Covariance matrix $\mathbf{C}_\Phi = \frac{v_\zeta^2}{N_e B_\Phi(\kappa)} (\mathbf{I}_n - \Phi\Phi^T)$ Expected hyper angle (squared) $\delta_\Phi^2 = \frac{(n-1)v_\zeta^2}{N_e \tan^{-1}\kappa}$	$B_\Phi(\kappa) = \tan^{-1}\kappa$

- (2) The damping ratio has the greatest uncertainty in terms of posterior c.o.v. and is therefore expected to govern the accuracy requirement in ambient vibration tests.
- (3) The mode shape is the only modal property whose leading order uncertainty is affected by the modal s/n ratio. Its posterior uncertainty is typically small. This implies that in reality the quality of the mode shape is likely to be governed by other sources such as sensor alignment error.
- (4) When the modal s/n ratio is high, reducing the channel noise level (e.g., with better equipment) or increasing the measured dofs has little or no effect on reducing the posterior c.o.v.s of modal parameters. It is because these factors influence only the modal s/n ratio, but the latter has no role in the uncertainty laws.
- (5) Assuming a damping ratio of 1 % and a bandwidth factor of 6, the minimum data duration to achieve a posterior of c.o.v. of 30 % in the damping ratio is 300 natural periods.

## Summary

A Bayesian approach for modal identification provides a fundamental means for processing the information contained in the data to make inference on the modal parameters consistent

with probability logic and modeling assumptions. This is especially relevant for ambient modal identification where the input excitation is not measured and where significant uncertainty can exist in the identified modal parameters even in the presence of data. A frequency domain approach is preferred over a time-domain approach because it significantly relaxes the broadband assumption on the modal force and prediction error. By making inference using the FFT on a selected frequency band around the mode of interest, the modal force and prediction error only need to have a flat spectrum within the band. The likelihood function can be formulated from first principles using random-vibration theory and signal processing asymptotics. The resulting form, however, does not allow the posterior statistics of the modal parameters to be computed easily because its dependence on the modal parameters is complicated and there are typically a moderate to large number of parameters. Using linear algebra techniques, fast equivalent formulations have been developed that allow efficient algorithms to be developed. The Bayesian identification results are governed characteristically by the modal signal-to-noise ratio. The posterior covariance matrix also admits remarkably simple closed form when the s/n ratio is high, leading to a set of uncertainty laws that govern the limit of ambient modal identification.

## Cross-References

- ▶ [Ambient Vibration Testing of Cultural Heritage Structures](#)
- ▶ [Building Monitoring Using a Ground-Based Radar](#)
- ▶ [Modal Analysis](#)
- ▶ [Operational Modal Analysis in Civil Engineering: An Overview](#)
- ▶ [Uncertainty Quantification in Structural Health Monitoring](#)

## References

- Au SK (2011) Fast Bayesian FFT method for ambient modal identification with separated modes. *J Eng Mech-ASCE* 137(3):214–226
- Au SK (2012a) Fast Bayesian ambient modal identification in the frequency domain, Part I: posterior most probable value. *Mech Syst Signal Process* 26(1):60–75
- Au SK (2012b) Connecting Bayesian and frequentist quantification of parameter uncertainty in system Identification. *Mech Syst Signal Process* 29:328–342
- Au SK (2014a) Uncertainty law in ambient modal identification. Part I: theory. *Mech Syst Signal Process* 48(1–2):15–33
- Au SK (2014b) Uncertainty law in ambient modal identification. Part II: implication and field verification. *Mech Syst Signal Process* 48(1–2):34–48
- Au SK, To P (2012) Full-scale validation of dynamic wind load on a super-tall building under strong wind. *J Struct Eng ASCE* 138(9):1161–1172
- Au SK, Zhang FL (2012a) Fast Bayesian ambient modal identification incorporating multiple setups. *J Eng Mech* 138(7):800–815
- Au SK, Zhang FL (2012b) Ambient modal identification of a primary-secondary structure using fast Bayesian FFT approach. *Mech Syst Signal Process* 28:280–296
- Au SK, Ni YC, Zhang FL, Lam HF (2012a) Full scale dynamic testing of a coupled slab system. *Eng Struct* 37:167–178
- Au SK, Zhang FL, To P (2012b) Field observations on modal properties of two tall buildings under strong wind. *J Wind Eng Ind Aerodyn* 101:12–23
- Au SK, Zhang FL, Ni YC (2013) Bayesian operational modal analysis: theory, computation, practice. *Comput Struct* 126:3–14
- Brillinger DR (1981) *Time series: data analysis and theory*. Holden-Day, San Francisco
- Fan YL, Xiao Y, Kunnath SK (2012) Modal parameter identification of a rigid frame-continuous girders bridge under ambient excitation by fast bayesian FFT method. *Adv Civil Infrastruct Eng* 639–640:985–991
- Lutes DL, Sarkani S (1997) *Stochastic analysis of structural and mechanical vibrations*. Prentice Hall, Upper Saddle River
- Yuen KV (1999) Structural modal updating using ambient dynamic data. Master of philosophy thesis, Department of Civil Engineering, Hong Kong University of Science and Technology, Hong Kong
- Yuen KV, Katafygiotis LS (2001a) Bayesian time-domain approach for modal updating using ambient data. *Probab Eng Mech* 16(3):219–231
- Yuen KV, Katafygiotis LS (2001b) Bayesian spectral density approach for modal updating using ambient data. *Earthq Eng Struct Dyn* 30:1103–1123
- Yuen KV, Katafygiotis LS (2003) Bayesian fast fourier transform approach for modal updating using ambient data. *Adv Struct Eng* 6(2):81–95
- Yuen KV, Kuok SC (2010a) Modeling of environmental influence in structural health assessment for reinforced concrete buildings. *Earthq Eng Eng Vib* 9(2):295–306
- Yuen KV, Kuok SC (2010b) Ambient interference in long-term monitoring of buildings. *Eng Struct* 32(8):2379–2386
- Yuen KV, Kuok SC (2011) Bayesian methods for updating dynamic models. *Appl Mech Rev* 64(1):010802-1–010802-18
- Zhang FL, Au SK (2013) Erratum to “fast Bayesian FFT method for ambient modal identification with separated modes” by Siu-Kui Au. *J Eng Mech, ASCE* 139(4):545–545
- Zhang FL, Au SK, Lam HF (2015) Assessing uncertainty in operational modal analysis incorporating multiple setups using a Bayesian approach. *Struct Control Health Monit* 22(3):395–416

---

## Bayesian Statistics: Applications to Earthquake Engineering

Alin C. Radu and Mircea Grigoriu  
Civil and Environmental Engineering, School of  
Civil & Environmental Engineering, Cornell  
University, Ithaca, NY, USA

## Synonyms

Bayesian statistics; Earthquake probabilities; Fragility analysis; Ground motion simulation; Seismic activity matrix; Seismic hazard; Seismological model

## Introduction

Bayesian statistics are related to Bayes' rule after Thomas Bayes, a Presbyterian minister, probably born in 1701. Thomas Bayes' fame rests in his paper "An Essay Towards Solving a Problem in the Doctrine of Chances" communicated to the Royal Society in 1763, after his death in 1761, by his friend Richard Price (1723–1791) (Bellhouse 2004). Bayes addresses the following question in his essay: "Given the number of times in which an unknown event has happened and failed: Required the chance that the probability of its happening in a single trial lies somewhere between any two degrees of probability that can be named (Bayes (1763), p. 376)" (Dale 1986; Edwards 1978). The question is answered in its famous Bayes' model table problem (Bellhouse 2004).

Gillies (1987) calls this problem "Bayes' billiard table example." The problem assumes a unit-square table and two balls O and W. The ball W is thrown across the table once, and its rest point defines level  $p$  with respect to one of the sides of the table. The ball O is then thrown  $n$  times, and it is said that if ball O stops below level  $p$ , the event is a success. If we call the number of successes  $r$ , then the probability that ball O will stop between levels  $a$  and  $b$  is given by

$$\frac{\int_a^b x^r (1-x)^{n-r} dx}{\int_0^1 x^r (1-x)^{n-r} dx}.$$

As Bayes' rule becomes popular in many fields of science and engineering, earthquake engineering problems began to be solved in the Bayesian framework. One of the first Bayesian approaches on site seismicity is proposed in Esteva (1969) for the rate of seismic event occurrence and later in Suzuki and Kiremidjian (1991). The Bayesian framework is also used in other seismology-related areas to update ground motion prediction models' parameters to new data in Wang and Takada (2009) and Atkinson and Boore (2011). Earthquake engineering also deals with the probabilistic assessment of the structural response

under seismic loads. The probability of structural response to exceed critical states is known as seismic fragility. Early papers by Goodman (1986) and Mosleh and Apostolakis (1986) deal with failure and fragility analyses in a Bayesian context. Recently, the Bayesian framework has been used in a wide range of applications for calculating fragility curves (Straub and Kiureghian 2008; Koutsourelakis 2010).

Bayes' rule stays at the basis of the Bayesian framework and is a statement of conditional probability. It provides information on the probability of unknown parameters  $\Theta = [\theta_1, \dots, \theta_n]$  given some data  $x$ ,

$$p(\Theta|x) \propto f(\Theta)l(\Theta|x), \quad (1)$$

where  $f(\Theta)$  and  $p(\Theta|x)$  are referred to as the *prior* and *posterior* probability density functions of  $\Theta$  and  $l(x|\Theta)$  is called the *likelihood* function, which accounts for the significance of the observed data  $x$  on the distribution of  $\Theta$  (Gelman et al. 2003). The prior probability density function  $f(\Theta)$  should contain all possible values of  $\Theta$ . The probability associated with the values of  $\Theta$ , i.e.,  $f(\Theta)$ , can be interpreted as the current knowledge about  $\Theta$ . When all the values of the unknown parameters  $\Theta$  are assumed to be equally likely, we call the prior *non-informative*. If the prior and the posterior densities have the same functional form for the probability distributions, we refer to the prior as a *conjugate prior*.

Sampling from the posterior distribution of  $\Theta$  may be challenging. Direct sampling from  $p(\Theta|x)$  in the case of non-conjugate prior densities is even more difficult, and sampling techniques have been developed. Markov Chain Monte Carlo (MCMC) is a general algorithm of drawing samples of  $\Theta$  from a random distribution  $p(\Theta|x)$ .

Applications of the Bayesian theory in earthquake engineering are shown in the next section. This material is based upon work supported by the National Science Foundation under Grants No. CMMI-0925714 and No. CMMI-1265511. This support is gratefully acknowledged. Any opinions, findings, and conclusions or recommendations expressed in this material are those



of the authors and do not necessarily reflect the views of the National Science Foundation.

## Bayesian Framework in Earthquake Engineering

### Seismic Hazard Analysis

#### Earthquake Probabilities

A seismic activity matrix is defined as a two-dimensional histogram which gives the probability of occurrence  $p_j$  of earthquakes characterized by moment magnitude  $m$  and source-to-site distance  $r$ , denoted by  $(m, r)_j$ . Each point in this matrix with coordinates  $(m, r)_j$  is referred to as a cell  $j = 1, \dots, n_c$ , where  $n_c$  is the total number of cells. Note that  $\sum_{j=1}^{n_c} p_j = 1$ . Seismic activity matrices can be calculated for each zip code in the United States by using the earthquake probability tool available on the US Geological Survey website (USGS 2009). Figure 1 shows the seismic activity matrix for Los Angeles.

A Bayesian approach is used to update earthquake probabilities in light of new data. For this, we seek a probabilistic parametric model with parameters, the earthquake probabilities. Let  $Z_j$  be a random variable which counts the number of new earthquakes recorded in each cell  $j$ . The vector  $\mathbf{Z} = \{Z_j, j = 1, \dots, n_c\}$  has a

multinomial distribution with parameters  $\Theta = \{\theta_j, j = 1, \dots, n_c\}$ , a random vector whose coordinates  $\theta_j$  capture earthquake probabilities in each cell  $j$ , such that  $\sum_{j=1}^{n_c} \theta_j = 1$ . We call  $N_Z = \sum_{j=1}^{n_c} Z_j$  the total number of newly recorded earthquakes. The new records are used in the Bayesian framework to update earthquake probabilities  $p_j$ .

**Numerical example.** For illustration, a hypothetical example is considered. It is assumed that at a site only three earthquakes  $j = 1, 2, 3$  are likely to occur with known probabilities  $p_1 = 0.2, p_2 = 0.3, p_3 = 0.5$ . The seismic activity matrix, shown in Fig. 3a, has  $n_c = 3$  cells. If an earthquake of type  $j = 1$  occurs at that site and it is used for the update of the earthquake probabilities  $p_1, p_2, p_3$ , then  $N_Z = 1$  and  $\mathbf{z} = [z_1 \ z_2 \ z_3] = [1 \ 0 \ 0]$ , which is a sample of  $\mathbf{Z}$ .

The unknown parameters  $\{\theta_1, \dots, \theta_{n_c}\}$  are assumed to have a Dirichlet distribution with parameters  $\{\alpha_1, \dots, \alpha_{n_c}\}$ , that is,

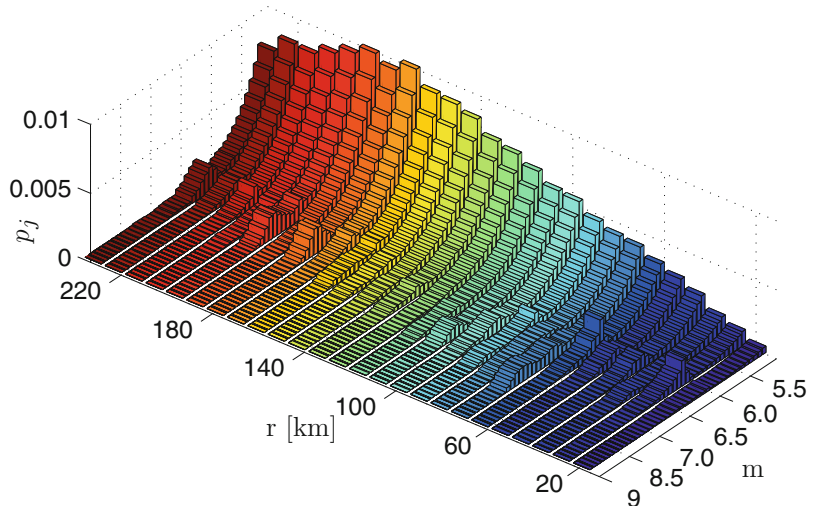
$$f(\theta_1, \dots, \theta_{n_c}) \propto \prod_{j=1}^{n_c} \theta_j^{\alpha_j - 1}, \forall \theta_j \geq 0. \quad (2)$$

Moreover, we impose that

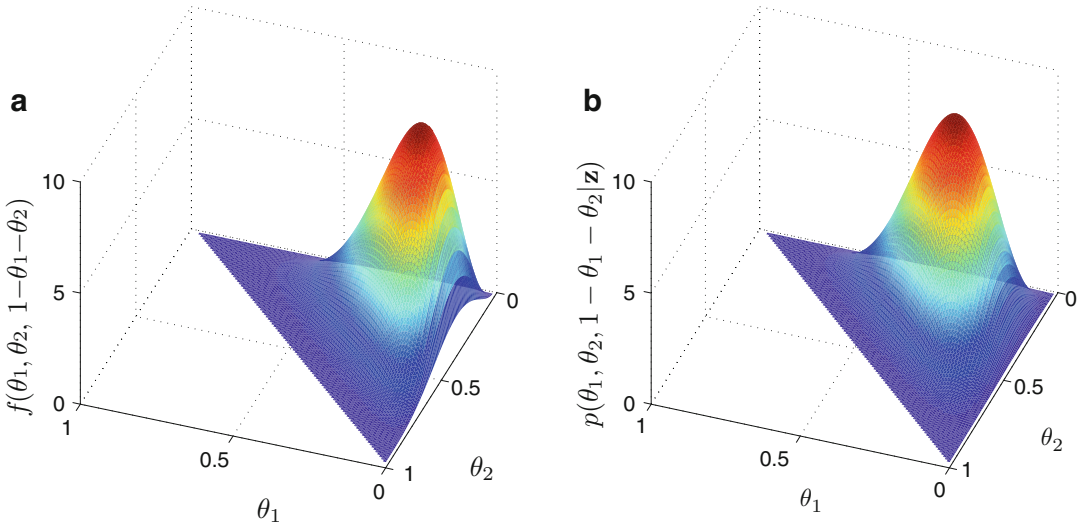
$$\mathbb{E}[\theta_j] = \frac{\alpha_j}{\alpha_0} = p_j, \quad (3)$$

### Bayesian Statistics: Applications to Earthquake Engineering,

**Fig. 1** Seismic activity matrix for Los Angeles







**Bayesian Statistics: Applications to Earthquake Engineering, Fig. 2** (a) Prior density  $f(\theta_1, \theta_2, 1 - \theta_1 - \theta_2)$  and (b) posterior density  $p(\theta_1, \theta_2, 1 - \theta_1 - \theta_2 | \mathbf{z})$

in order to reflect the prior knowledge from the seismic activity matrix, where  $\alpha_0 = \sum_{j=1}^{n_c} \alpha_j$ . For a given value of  $\alpha_0$ , parameters  $\alpha_j = p_j \alpha_0$  have deterministic values, and they are known as hyper-parameters. The value  $\alpha_0$  can be interpreted as the total number of recorded earthquakes to have occurred at the site until the new earthquakes in  $\mathbf{Z}$  were recorded.

Based on the assumption that  $\mathbf{Z}$  has a multinomial distribution, the likelihood function is written as

$$l(\mathbf{z} | \Theta) = \prod_{j=1}^{n_c} \theta_j^{z_j}. \quad (4)$$

The posterior probability density of the unknown parameters  $\Theta$  is calculated as shown in Eq. 1:

$$p(\Theta | \mathbf{z}) = \prod_{j=1}^{n_c} \theta_j^{\alpha_j + z_j - 1}, \quad (5)$$

which is also a Dirichlet distribution with parameters  $\alpha_j + z_j, j = 1, \dots, n_c$ . Note that the Dirichlet distribution is the conjugate prior of the multinomial distribution. The seismic activity matrix in light of new data is, then, given by the expectation of  $\Theta$ :

$$\mathbb{E}[\theta_j] = \frac{\alpha_j p_j + z_j}{\alpha_0 + n_z}. \quad (6)$$

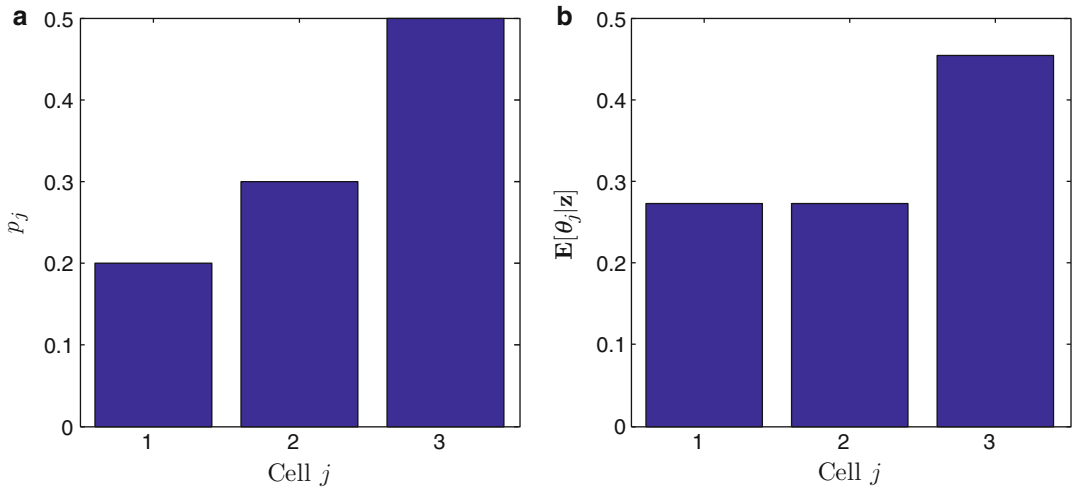
For the hypothetical case presented above, the prior density  $f(\theta_1, \theta_2, \theta_3)$  and the posterior density  $p(\theta_1, \theta_2, \theta_3 | \mathbf{z})$  are shown in Fig. 2 in the form of  $f(\theta_1, \theta_2, 1 - \theta_1 - \theta_2)$  and  $p(\theta_1, \theta_2, 1 - \theta_1 - \theta_2 | \mathbf{z})$ , respectively, since  $\theta_1 + \theta_2 + \theta_3 = 1$ . The results are shown for  $\alpha_0 = 10$ .

The updated seismic activity matrix with the new data  $\mathbf{z}$ , i.e.,  $\mathbb{E}[\Theta | \mathbf{z}]$ , is shown in Fig. 3b.

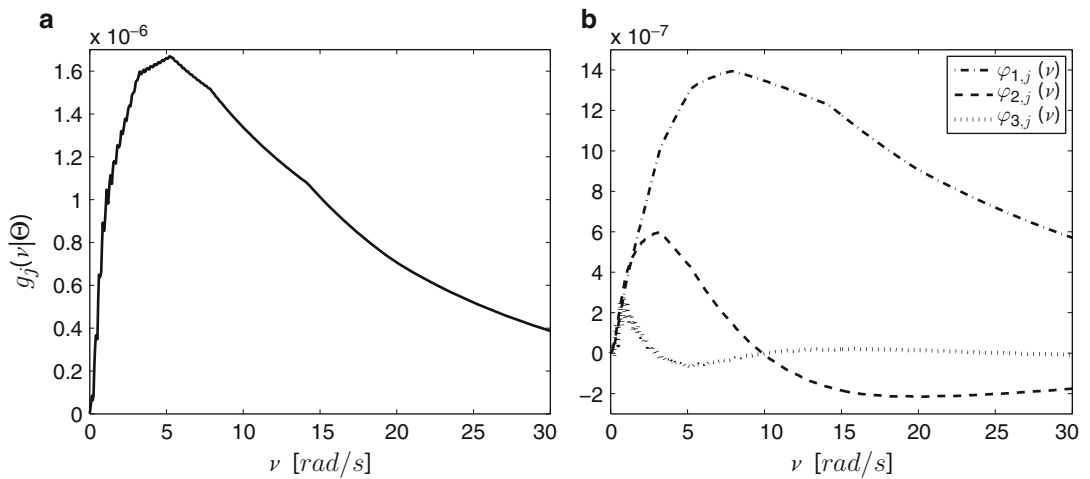
#### Seismological Model Update

The specific barrier model (Halldorsson and Papageorgiou 2005) is a source model which characterizes the frequency content of the ground motion process in the form of a function  $g(v; (m, r)_j)$  of  $(m, r)_j$ , called power spectral density. The specific barrier model is calibrated to regional data and cannot provide information about ground motions at particular sites. For simplicity, the following notation  $g_j(v) := g(v; (m, r)_j)$  is used.

A Bayesian framework is used to update the spectral density model with site-specific records (Radu and Grigoriu 2014). The power spectral density function  $g_j(v)$  is only available in



**Bayesian Statistics: Applications to Earthquake Engineering, Fig. 3** Two-dimensional seismic activity matrix: (a) original earthquake probabilities  $p_j, j = 1, 2, 3$ , and (b) updated earthquake probabilities  $\mathbb{E}[\theta_j|\mathbf{z}], j = 1, 2, 3$



**Bayesian Statistics: Applications to Earthquake Engineering, Fig. 4** (a) Power spectral density  $g_j(v)$  and (b) linear components  $\varphi_{k,j}, k = 1, 2, 3$ , for  $(m, r)_j = (8, 200)$  km

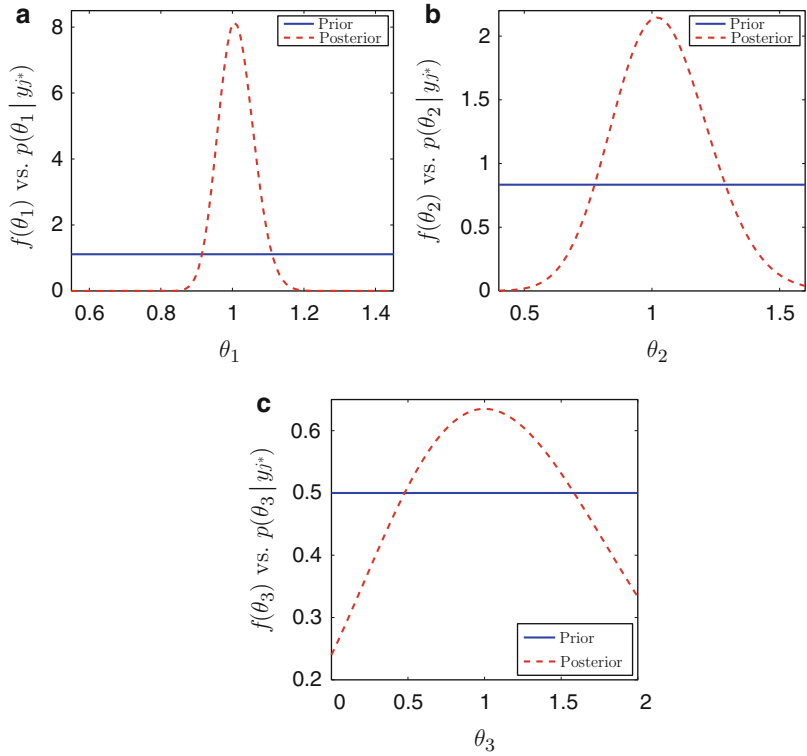
algorithmic form. For the Bayesian approach, a parametric model for  $g_j(v)$  is sought, and it is written as

$$g_j(v : \Theta) = \theta_1 \varphi_{1,j} + \theta_2 \varphi_{2,j} + \theta_3 \varphi_{3,j} \quad (7)$$

using the singular value decomposition, where  $\{\theta_k = 1, k = 1, 2, 3\}$  are some global parameters and  $\varphi_{k,j}, k = 1, 2, 3$ , are deterministic

functions which depend on  $(m, r)_j$ . In the Bayesian context, the vector  $\Theta = \{\theta_k, k = 1, 2, 3\}$  is seen as a random vector with mean  $\mathbb{E}[\Theta] = [111]$ . The range  $\Psi$  of  $\Theta$  is defined such that it ensures the existence of the spectral density, i.e.,  $g_j(v) \geq 0, \forall_j = 1, \dots, n_c, \forall_v \geq 0$ , and  $\forall \theta \in \Psi$ . A uniform prior  $f(\Theta)$  on  $\Psi$  is assumed for the vector of unknown parameters  $\Theta$ . Figure 4 shows the spectral density  $g_j(v)$  for  $(m, r)_j = (8, 200)$  km and its components  $\varphi_{k,j}, k = 1, 2, 3$ .

**Bayesian Statistics: Applications to Earthquake Engineering, Fig. 5** Marginal prior and posterior densities for (a)  $\theta_1$ , (b)  $\theta_2$ , and (c)  $\theta_3$



Let  $x = \{x_{j,i}, i = 1, \dots, n_j, j = 1, \dots, n_c\}$  be a set of  $n = \sum_{j=1}^{n_c} n_j$  ground motion records available at a site, where  $n_j$  is the number of earthquakes with  $(m, r)_j$  and  $n_c$  is the number of cells in the seismic activity matrix in Fig. 1. It is assumed that  $x_{j,i}$  are the discrete versions of the records' strong motion parts, i.e., the part of the earthquake where most of its energy is concentrated (Trifunac 1971). Under the assumption that  $x_{j,i}$  are samples of a zero-mean, stationary, Gaussian process (Zerva 2009), Chap. 7; Rezaeian and Kiureghian 2010), the logarithmic form of the likelihood function is written as

$$\ln(l(x|\Theta)) \propto -\frac{n}{2} \ln(|C_j(\Theta)|) - \frac{1}{2} \sum_{i=1}^{n_c} \sum_{j=1}^{n_j} x_{j,i}^T C_j(\Theta)^{-1} x_{j,i}, \quad (8)$$

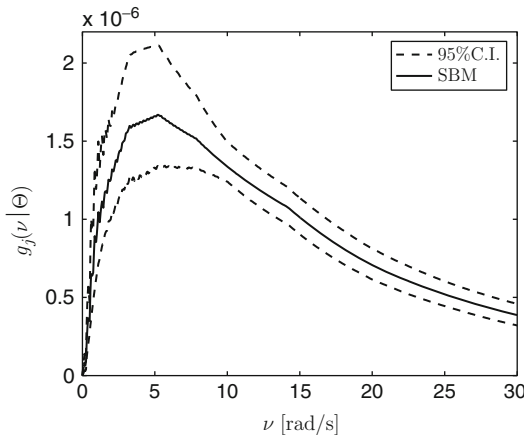
where  $\ln$  denotes the natural logarithm and  $|C_j(\Theta)|$  is the determinant of the covariance

matrix  $C_j(\Theta)$  of the ground motion process in cell  $j$ . The components of the covariance matrix can be calculated from the Fourier transform of the spectral density function  $g_j(v; \Theta)$  (Grigoriu 2012, Section 3.6).

The posterior probability density function  $p(\Theta | x)$  follows directly from Eq. 1.

**Numerical example.** For numerical results,  $n = 5,000$  samples of zero-mean, stationary, Gaussian processes with spectral densities  $g_j(v)$ ,  $j = 1, \dots, n_c$ , were simulated in cells  $j$  according to the multinomial distribution given by the seismic activity matrix of Los Angeles (Fig. 1). The marginal prior and posterior densities of the unknown parameters  $\theta_i$ ,  $i = 1, 2, 3$  are shown in Fig. 5.

The resulting posterior 95 % confidence interval for the spectral density  $g_j(v; \Theta)$  shown in Fig. 6, i.e., the interval  $[g_j^{lw}(v), g_j^{up}(v)]$  such that  $\mathbb{P}\{g_j(v; \Theta) \in [g_j^{lw}(v), g_j^{up}(v)]\} = 0.95$ , is also calculated based on the density  $p(\Theta | x)$ .



**Bayesian Statistics: Applications to Earthquake Engineering, Fig. 6** Ninety-five percent confidence interval (CI) for the spectral density  $g_j(v; \Theta)$ ,  $j = 1, 2, 3$

**Seismic Fragility Analysis**

Seismic fragility of a structural or nonstructural system is the probability that the system’s response exceeds a critical value under seismic ground motions of specified intensities, e.g., peak ground acceleration (PGA) or pseudo-spectral acceleration (PSa) (Kafali and Grigoriu 2010). Graphical representations of seismic fragilities are called fragility curves.

Reliable fragility analyses require the use of large numbers of seismic records, which are not usually available. Thus, Monte Carlo simulations of synthetic seismic motions or scaling of actual records to common intensity measures are among the most popular methods. The Bayesian framework allows calculation of seismic fragility curves using just the data available.

It is assumed that  $n$  ground motion records  $x_i(t)$ ,  $i = 1, \dots, n$ , are available at a site. The response displacement  $y_i(t)$  of a system to record  $x_i(t)$  is characterized by a second-order differential equation:

$$y_i'' = D(y_i, y_i', x_i), \tag{9}$$

where  $D$  can be either a linear or a nonlinear operator. For example, for a linear single-degree-of-freedom system with frequency  $\omega_0$  and damping ratio  $\zeta_0$ ,

$$D(y_i, y_i', x_i) = -(2\omega_0\zeta_0y_i' + \omega_0^2y_i + x_i). \tag{10}$$

Two intensity measures for the ground motion  $x_i(t)$  are defined:

1. Peak ground acceleration (PGA)

$$\xi_i = \max_{0 \leq t \leq \tau} |x_i(t)| \tag{11}$$

2. Pseudo-spectral acceleration (PSa)

$$\xi_i(\omega; \zeta) = \max_{0 \leq t \leq \tau} |y_i(t; \omega, \zeta)|, \tag{12}$$

where  $y_i(t; \omega, \zeta)$  is the solution of Eq. 10.

For illustration purposes, we present the methodology for calculating fragility curves for the single-degree-of-freedom system in Eq. 10. In this context, we define the seismic fragility as

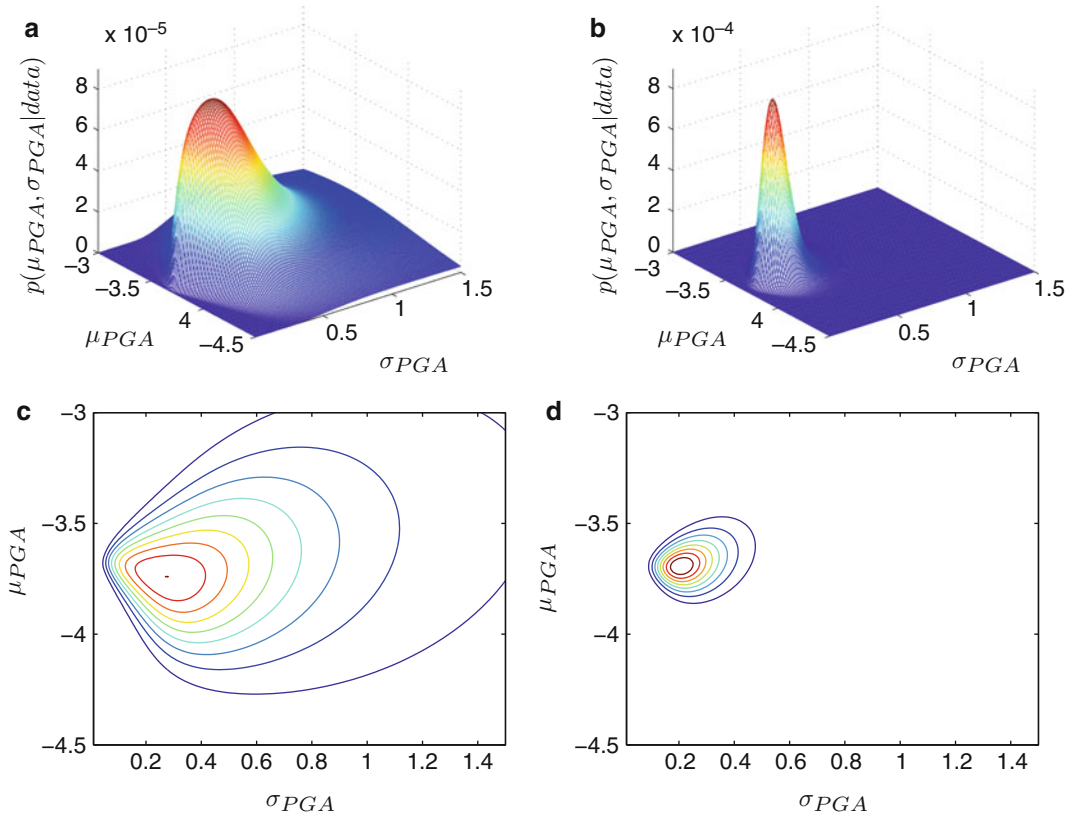
$$P_f(\xi; y_{cr}) = \mathbb{P}\left(\max_{0 \leq t \leq \tau} |y_i(t; \omega_0, \zeta_0)| > y_{cr} | \xi_i = \xi\right), \tag{13}$$

where  $y_{cr}$  is a critical displacement imposed for the system. Fragility curves can be calculated for any other engineering design parameters, e.g., the inter-story drift in the case of multi-degree-of-freedom systems. For simplicity, parameters  $y_{cr}$  is dropped from notation  $P_f(\xi; y_{cr})$ .

In order to calculate fragility curves in a Bayesian framework, a parametric model for  $P_f(\xi)$  is sought. Fragility curves are increasing functions plotted against positive ground motion intensity measures  $\xi > 0$  and left-bounded at zero.

Therefore, it is common to assume that they are well modeled by log-normal cumulative distribution functions  $F(\xi; \mu, \sigma)$  with mean  $\mu$  and standard deviation  $\sigma$ . The log-normal cumulative distribution function is defined as

$$F(\xi; \mu, \sigma) = \int_0^\xi \phi_{LN}(x; \mu, \sigma) dx, \tag{14}$$



**Bayesian Statistics: Applications to Earthquake Engineering, Fig. 7** Three-dimensional and corresponding contour plots for the posterior density functions of  $(\mu_{PGA}, \sigma_{PGA})$ , for (a), (c)  $n = 10$  and (b), (d)  $n = 50$  records

where

$$s_i = 1\{y_i(t) > y_{cr}\}, \tag{16}$$

$$\phi_{LN}(x; \mu, \sigma) = \frac{1}{x\sigma\sqrt{2\pi}} \exp\left\{-\frac{(\ln(x) - \mu)^2}{2\sigma^2}\right\}, x > 0, \tag{15}$$

and  $\phi_{LN}(x; \mu, \sigma)$  is the probability density function of the log-normal distribution with mean  $\mu \in \mathbb{R}$  and standard deviation  $\sigma \geq 0$ .

The model for the fragility curve in Eq. 13 is  $P_f(\xi; \Theta) = F(\xi; \mu, \sigma)$ , where  $\Theta = (\mu, \sigma)$  is the vector of unknown parameters to be estimated from the data. Parameters  $(\mu, \sigma)$  define uniquely the fragility curve.

A non-informative uniform prior  $f(\Theta)$  is assumed for  $\Theta = (\mu, \sigma)$  in a custom range within previously defined bounds, i.e.,  $\mu \in \mathbb{R}, \sigma \geq 0$ .

Let  $s = \{s_i, i = 1, \dots, n\}$  be a vector with values:

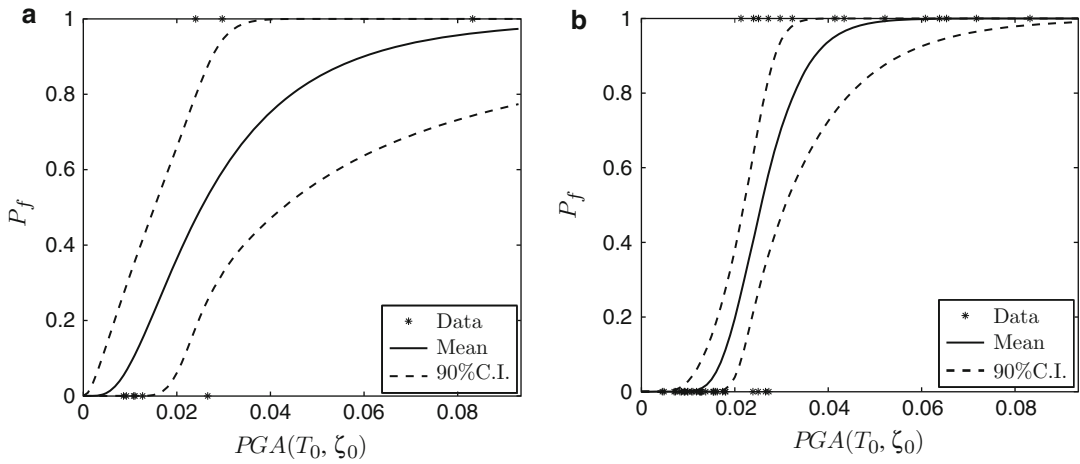
where 1 denotes the indicator function. The vector  $s$  is a sample of a binomial random vector with parameters  $(n, \{F(\xi_i; \mu, \sigma), i = 1, \dots, n\})$ . Then, the likelihood function is defined as

$$l(s|\mu, \sigma) = \prod_{i=1}^n (1 - F(\xi; \mu, \sigma))^{1-s_i} F(\xi; \mu, \sigma)^{s_i}. \tag{17}$$

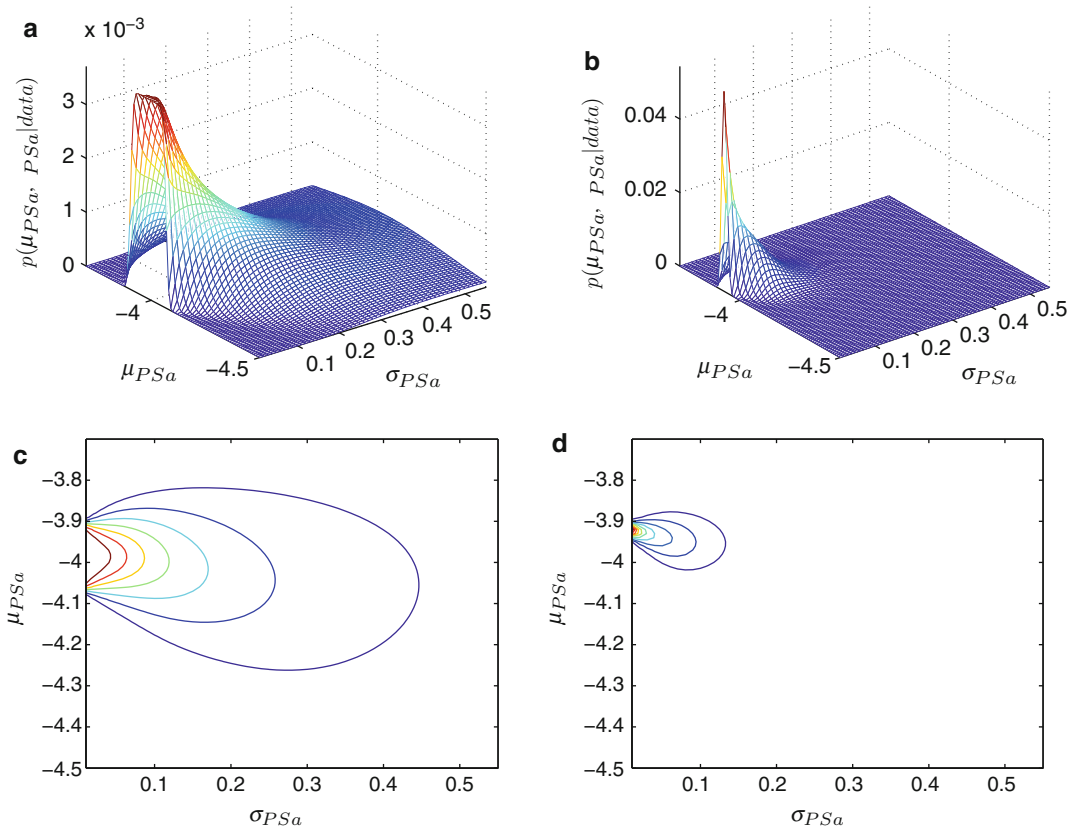
Finally, the posterior density of parameters  $\Theta$  is

$$p(\mu, \sigma|s) \propto f(\mu, \sigma)l(s|\mu, \sigma). \tag{18}$$

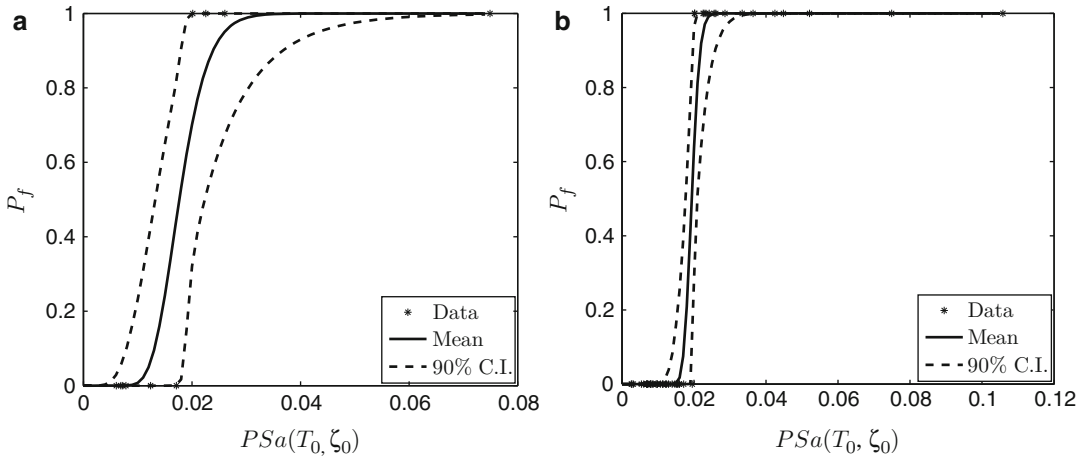
**Numerical examples** Numerical examples are shown for the linear single-degree-of-freedom system in Eq. 10 with  $\omega_0 = \pi \text{ rad/s}, \zeta_0 = 2\%$ ,



**Bayesian Statistics: Applications to Earthquake Engineering, Fig. 8** Fragility curves (mean)  $P_f(PGA)$  and 95 % confidence intervals (CIs) for (a)  $n = 10$  and (b)  $n = 50$  records



**Bayesian Statistics: Applications to Earthquake Engineering, Fig. 9** Three-dimensional and corresponding contour plots for the posterior density functions of  $(\mu_{PSa}, \sigma_{PSa})$ , for (a), (c)  $n = 10$  and (b), (d)  $n = 50$  records



**Bayesian Statistics: Applications to Earthquake Engineering, Fig. 10** Fragility curves (mean  $Pf(PSa)$  and 95 % confidence intervals (CIs) for (a)  $n = 10$  and (b)  $n = 50$  records

and  $y_{cr} = 2$ , for two sets of  $n = 10$  and  $n = 50$  ground motion records, respectively. The ground motion samples used in the fragility analysis were simulated as zero-mean, nonstationary Gaussian processes with probability density functions  $g_j(v)$  from the specific barrier model in Halldorsson and Papageorgiou (2005). Samples are generated for various  $(m, r)$ , according to the seismic activity matrix of Los Angeles. Fragility curves are constructed for both PGA and PSa intensity measures.

Figures 7 and 9 show the posterior distributions of the unknown parameters  $\Theta = (\mu_{PGA}, \sigma_{PGA})$  and  $\Theta = (\mu_{PSa}, \sigma_{PSa})$ , which define the fragility curves for the PGA and PSa intensity measures, respectively. Plots (a) and (c) of each figure show the posterior of  $\Theta$  obtained for  $n = 10$  records and (b) and (d) for  $n = 50$  records, respectively. Fragility curves for PGA and their corresponding 90 % confidence intervals calculated based on the posterior densities of  $\Theta$  shown in Fig. 7a and c are illustrated in Fig. 8a and b, respectively. Fragility curves and their 90 % confidence intervals for the PSa intensity measure are plotted in Fig. 10 for the  $n = 10$  and  $n = 50$  ground motion sample sets. The posterior densities are less spread on the domain of  $\Theta$  as the number of samples  $n$  increases. Consequently, the more data is used in the analysis, the narrower the confidence intervals for the fragility curves are.

## Summary

The Bayesian framework, widely used in earthquake engineering, produces statistical inferences about uncertain parameters of a probabilistic model by combining observable data with available prior information about the parameters. The entry presents applications of Bayes' theorem for several concepts used in earthquake engineering.

The data is usually composed of ground motion records, which are used to develop probabilistic parametric models for fragility curves or to improve and update existent models on earthquake probabilities and frequency content of seismic motions. The Bayesian framework also facilitates the calculations of various statistics by using limited amounts of data.

## Cross-References

- ▶ [Analytic Fragility and Limit States \[P\(EDP|IM\)\]: Nonlinear Dynamic Procedures](#)
- ▶ [Engineering Characterization of Earthquake Ground Motions](#)
- ▶ [Nonlinear Dynamic Seismic Analysis](#)
- ▶ [Performance-Based Design Procedure for Structures with Magneto-Rheological Dampers](#)
- ▶ [Physics-Based Ground-Motion Simulation](#)



- ▶ Probabilistic Seismic Hazard Models
- ▶ Seismic Actions Due to Near-Fault Ground Motion
- ▶ Seismic Fragility Analysis
- ▶ Site Response for Seismic Hazard Assessment
- ▶ Stochastic Analysis of Linear Systems
- ▶ Stochastic Analysis of Nonlinear Systems
- ▶ Stochastic Ground Motion Simulation
- ▶ Time History Seismic Analysis

## References

- Atkinson G, Boore D (2011) Modification to existing ground-motion prediction equations in light of new data. *Bull Seismol Soc Am* 101(3):1121–1135
- Bayes T (1763) An essay towards solving a problem in the doctrine of chances. *Philosophical Transactions* 53, p. 370–418. [Reprinted (1958) *Studies in the history of probability and statistics IX*. Thomas Bayes' essay towards solving a problem in the doctrine of chances. *Biometrika* 45, p. 296–315]
- Bellhouse D (2004) The reverend Thomas Bayes, FRS: a biography to celebrate the tercentenary of his birth. *Stat Sci* 19(1):3–43
- Dale A (1986) A newly-discovered result of Thomas Bayes. *Arch Hist Exact Sci* 35(2):101–113
- Edwards A (1978) Commentary on the arguments of Thomas Bayes. *Scand J Stat* 5(2):116–118
- Esteva L (1969) Seismicity prediction: a Bayesian approach. In: *Proceedings of the fourth world conference on earthquake engineering*, Santiago de Chile
- Gelman A, Carlin JB, Stern HS, Rubin DB (2003) *Bayesian data analysis*, 2nd edn. *Texts in statistical sciences*. Chapman Hall CRC, Boca Raton
- Gillies D (1987) Was Bayes a Bayesian? *Hist Math* 14:325–346
- Goodman J (1986) Interval estimates of average failure rate and unavailability per demand. *Reliab Eng* 14:107–121
- Grigoriu M (2012) *Stochastic systems. Uncertainty quantification and propagation*. Springer, London
- Halldorsson B, Papageorgiou A (2005) Calibration of the specific barrier model to earthquake to different tectonic regions. *Bull Seismol Soc Am* 95(4):1276–1300
- Kafali C, Grigoriu M (2010) Seismic fragility analysis: application to simple linear and nonlinear systems. *Earthq Eng Struct Dyn* 36(13):1885–1900
- Koutsourelakis P (2010) Assessing structural vulnerability against earthquakes using multi-dimensional fragility surfaces: a Bayesian framework. *Probab Eng Mech* 25:49–60
- Mosleh A, Apostolakis G (1986) The assessment of probability distributions from expert opinions with an application to seismic fragility curves. *Risk Anal* 6(4):447–461
- Radu A, Grigoriu M (2014) A site-specific seismological model for probabilistic seismic-hazard assessment. *Bull Seismol Soc Am* 104(6):3054–3071
- Rezaeian S, Kiureghian A (2010) Simulation of synthetic ground motions for specified earthquake and site characteristics. *Earthq Eng Struct Dyn* 39(10):1155–1180
- Straub D, Kiureghian A (2008) Improved seismic fragility modeling from empirical data. *Struct Saf* 30:320–336
- Suzuki S, Kiremidjian A (1991) A random slip rate model for earthquake occurrences with Bayesian parameters. *Bull Seismol Soc Am* 81(3):781–795
- Trifunac MD (1971) A method for synthesizing realistic strong ground motions. *Bull Seismol Soc Am* 61(6):1739–1753
- USGS (2009) U.S. geological survey: 2009 earthquake probability mapping. Last checked on 9 Sept 2013. <https://geohazards.usgs.gov/eqprob/2009/index.php>
- Wang M, Takada T (2009) A Bayesian framework for prediction of seismic ground motion. *Bull Seismol Soc Am* 99(4):2348–2364
- Zerva A (2009) Spatial variation of seismic ground motions: modeling and engineering applications. In: *Advances in engineering*. CRC Press – Taylor Francis Group, LLC, 6000 Broken Sound Parkway, Boca Raton, FL

---

## Beginner's Guide to Fragility, Vulnerability, and Risk

Keith Porter

Civil, Environmental, and Architectural Engineering, University of Colorado, Boulder and SPA Risk LLC, Denver, CO, USA

## Introduction

This entry provides a primer for earthquake-related fragility, vulnerability, and risk. Many of its concepts can be applied to other perils. Section “**Fragility**” discusses fragility – the probability of an undesirable outcome as a function of excitation. Vulnerability (the measure of loss as a function of excitation) is discussed in section “**Vulnerability**.” Section “**Hazard**” presents enough information about seismic hazard for the reader to understand risk, which is discussed in section “**Risk for a Single Asset**.” Section “**Conclusions**” provides brief conclusions. For solved exercises, see Porter (2014).

## Fragility

### Uncertain Values

Many of the terms used here involve uncertain quantities, often called random variables. “Uncertain” is used here because it applies to quantities that change unpredictably (e.g., whether a tossed coin will land heads or tails side up on the next toss) and to quantities that do not vary but that are not known with certainty. For example, a particular building’s capacity to resist collapse in an earthquake may not vary much over time, but one does not know that capacity before the building collapses, so it is uncertain. In this entry, uncertain variables are denoted by capital letters, e.g.,  $D$ ; particular values are denoted by lower case, e.g.,  $d$ ; probability is denoted by  $P[\ ]$ ; and conditional probability is denoted by  $P[A|B]$ , that is, probability that statement  $A$  is true given that statement  $B$  is true.

### Meaning and Form of a Fragility Function

The stage is now set to discuss fragility functions. A fragility function expresses the probability that an undesirable event will occur as a function of the value of some (potentially uncertain) environmental excitation. Let  $X$  denote the excitation. A fragility function is usually shown on an  $x$ - $y$  chart with probability on the  $y$ -axis (bounded by 0 and 1) and excitation  $X$  on the  $x$ -axis (usually bounded below by 0 and above by infinity). (The variable  $X$  is used more than once in this entry. It may have different meanings in different places.)

When the undesirable outcome has to do with damage to a whole building, bridge, or other large facilities, excitation is generally measured in terms of ground motion. Common measures of ground motion are addressed later. When the undesirable outcome has to do with damage to a building component, excitation is often measured in terms of one of the following:

**Peak floor acceleration (PFA).** Maximum zero-period acceleration in any direction at any time during an earthquake at the base of floor-mounted components or at the soffit of

the slab from which a component is suspended.

**Peak floor velocity (PFV).** Like PFA, except maximum velocity at the base of the floor-mounted components or at the soffit of the slab from which a component is suspended.

**Peak transient interstory drift ratio (PTD).** This is the maximum value at any time during seismic excitation of the displacement of the floor above relative to the floor below the story on which a component is installed, divided by the height difference of the two stories. The displacements are commonly measured parallel to a horizontal axis of the component, such as along a column line.

**Peak residual drift ratio (PRD).** Like PTD, except measures the displacement of the floor above relative to the floor below after the cessation of motion.

Some people use the term fragility curve to mean the same thing as fragility function. Some use fragility and vulnerability interchangeably. This work will not do so and will not use the expression “fragility curve” or “vulnerability curve” at all. A function allows for a relationship between loss and one, two, or more inputs, whereas a curve only allows for one input.

The most common form of a seismic fragility function is the lognormal cumulative distribution function (CDF). It is of the form

$$\begin{aligned} F_d(x) &= P[D \geq d | X = x] \quad d \in \{1, 2, \dots, n_D\} \\ &= \Phi\left(\frac{\ln(x/\theta_d)}{\beta_d}\right) \end{aligned} \quad (1)$$

$P[A/B]$  = probability that  $A$  is true given that  $B$  is true.

$D$  = uncertain damage state of a particular asset such as a building component or a building. It can take on a value in  $\{0, 1, \dots, n_D\}$ , where  $D = 0$  denotes the undamaged state,  $D = 1$  denotes the first damage state, etc.  
 $d$  = a particular value of  $D$ , i.e., with no uncertainty.

$n_D$  = number of possible damage states,  $n_D \in \{1, 2, \dots\}$ .

$X$  = uncertain excitation, e.g., peak zero-period acceleration at the base of the asset in question. Here excitation is called demand parameter (DP), using the terminology of FEMA P-58 (Applied Technology Council 2012). FEMA P-58 builds upon work coordinated by the Pacific Earthquake Engineering Research (PEER) Center and others. PEER researchers use the term engineering demand parameter (EDP) to mean the same thing. Usually  $X \in \{\mathfrak{R} \geq 0\}$  but it does not have to be. Note that  $X \in \{\mathfrak{R} \geq 0\}$  means that  $X$  is a real, nonnegative number.

$x$  = a particular value of  $X$ , i.e., with no uncertainty.

$F_d(x)$  = a fragility function for damage state  $d$  evaluated at  $x$ .

$\Phi(s)$  = standard normal cumulative distribution function (often called the Gaussian) evaluated at  $s$ , e.g., `normsdist(s)` in Excel.

$\ln(s)$  = natural logarithm of  $s$ .

$\theta_d$  = median capacity of the asset to resist damage state  $d$  measured in terms of  $X$ . Usually  $\theta_d \in \{\mathfrak{R} > 0\}$  but it could in principle have a vector value and perhaps negative values. The subscript  $d$  appears because a component can sometimes have  $n_D > 1$ .

$\beta_d$  = logarithmic standard deviation of the uncertain capacity of the asset to resist damage state  $d$ .

For example, see the PACT fragility database at [https://www.atcouncil.org/files/FEMAP-58-3\\_2\\_ProvidedFragilityData.zip](https://www.atcouncil.org/files/FEMAP-58-3_2_ProvidedFragilityData.zip) (Applied Technology Council 2012). See the tab PERFORMANCE DATA, the line marked C3011.002c. It employs the lognormal form to propose two fragility functions for Wall Partition, Type: Gypsum + Ceramic Tile, Full Height, Fixed Below, Slip Track Above w/ returns (friction connection). The demand parameter is “Story Drift Ratio,” meaning the time-maximum absolute value of the peak transient drift ratio for the story at which partition occurs. For that component,  $n_D = 2$ , which occur sequentially, meaning that a component must enter damage state

1 before it can enter damage state 2. Damage state 1 is defined as “minor cracked joints and tile.” Damage state 2 is defined as “cracked joints and tile.”  $\theta_1 = 0.0020$ ,  $\beta_1 = 0.70$ ,  $\theta_2 = 0.0050$ , and  $\beta_2 = 0.40$ . The repair for  $D = 1$  is described as “carefully remove cracked tile and grout at cracked joints, install new ceramic tile and re-grout joints for 10 % of full 100 foot length of wall. Existing wall board will remain in place.” Repair for  $D = 2$  is “install ceramic tile and grout all joints for full 100 foot length of wall. Note: gypsum wall board will also be removed and replaced which means the removal of ceramic tile will be part of the gypsum wall board removal.”

### The Lognormal Distribution

The lognormal is ubiquitous in probabilistic seismic hazard analysis (PSHA) and probabilistic seismic risk analysis (PSRA). To understand it, consider first the normal (*not* the lognormal) distribution. If a quantity  $X$  is normally distributed with mean  $\mu$  and standard deviation  $\sigma$ , it can take on any scalar value in  $-\infty < X < \infty$ . Its cumulative distribution function (CDF) can be expressed as follows:

$$P[X \leq x] = \Phi\left(\frac{x - \mu}{\sigma}\right) \quad (2)$$

Note that:

$\mu \in \{\mathfrak{R}\}$ , meaning that  $\mu$  is any real scalar value  
 $\sigma \in \{\mathfrak{R} > 0\}$ , meaning that  $\sigma$  is any positive scalar value.

One can also find the value  $x$  associated with a specified nonexceedance probability,  $p$ .

$$x = \mu + \sigma \cdot \Phi^{-1}(p) \quad (3)$$

Now consider to the lognormal distribution. If a variable is lognormally distributed, that means its natural logarithm is normally distributed, which means it must take on a positive real value and the probability of it being zero or negative is zero. One can write the CDF several different, equivalent, ways:

$$\begin{aligned}
 P[X \leq x] &= \Phi\left(\frac{\ln x - \ln \theta}{\beta}\right) \\
 &= \Phi\left(\frac{\ln(x/\theta)}{\beta}\right) \\
 &= \Phi\left(\frac{\ln x - \mu_{\ln X}}{\sigma_{\ln X}}\right)
 \end{aligned} \tag{4}$$

where  $\mu_{\ln X}$  denotes the mean value of  $\ln(X)$ , which is the same as the natural logarithm of the median,  $\ln(\theta)$ . It is sometimes desirable to calculate  $\theta$  and  $\beta$  in terms of  $\mu$  and  $\sigma$ . Here are the conversion equations. (The reader can learn more about probability distributions from various sources, such as the free online source NIST/SEMATECH (2013) or Ang and Tang (1975).) Let  $v$  denote the coefficient of variation of  $X$ . Then

$$v = \frac{\sigma}{\mu} \tag{5}$$

$$\beta = \sqrt{\ln(1 + v^2)} \tag{6}$$

$$\theta = \frac{m}{\sqrt{1 + v^2}} \tag{7}$$

Note well: there is nothing fundamental about the lognormal distribution that makes it ideal or exact for fragility functions, ground motion, and so on. It is commonly used for several reasons:

1. Simplicity. It only requires two parameter values to completely define.
2. Precedent. The lognormal has been used for fragility functions for decades.
3. Information-theory reasons. Given a median and logarithmic standard deviation of some uncertain positively valued quantity like component capacity, the lognormal is the most uncertain distribution, that is, it assumes the least amount of information.
4. Sometimes it fits the data well.

But the lognormal may fit data badly, sometimes worse than other competing parametric and nonparametric forms. Beware oversimplification,

and never confuse a mathematical simplification or model with reality. Ideally one's model approximates reality, but the model is not the thing itself.

### Multiple Fragility Functions

Consider situations where a component, asset, or person can experience multiple possible damage states. This entry considers only discrete damage states, meaning that one can number the damage states  $D = 1, 2, \text{etc.}$ , but not 1.5. If a component is damaged, one can number damage states in at least one of three ways. First, let  $D = 0$  denote the undamaged state. If the component or asset is damaged, let the damage state be denoted by  $D \in \{1, 2, \dots, n_D\}$ . The three kinds of fragility functions dealt with here are:

1. Sequential damage states. A component must enter damage state 1 before it can enter damage state 2, and it must enter 2 before 3, and so on.
2. Simultaneous damage states. A damaged component can be in more than one damage state at the same time. Order does not matter.
3. Mutually exclusive and collectively exhaustive (MECE) damage states. A damaged component can be in one and only one damage state. Order does not matter.

There are other ways to express fragility, such as with a vector that combines numbers of various types. For example, one might want to talk about a scalar quantity  $Q$  of a component that is in a particular sequential damage state  $D$ , such as the fraction of a reinforced concrete shear wall that has cracks of at least 3/8 in. width, which would be indicative of the quantity of steel that has to be replaced. But the present discussion is limited to the three kinds noted above.

### Sequential Damage States

In sequential damage states, the damage states are ordered ( $D$  is therefore an ordinal number, subject to certain mathematical rules of ordinal numbers), so one can talk about lower damage states

and higher ones. The probability of reaching or exceeding a lower damage state is greater than or

equal to the probability of reaching or exceeding a higher damage state.

$$\begin{aligned}
 P[D = d|X = x] &= 1 - P[D \geq 1|X = x] & d = 0 \\
 &= P[D \geq d|X = x] - P[D \geq d + 1|X = x] & 1 \leq d < n_D \\
 &= P[D \geq d|X = x] & d = n_D
 \end{aligned} \tag{8}$$

The first line is the probability that the component is undamaged. The next is the probability that the component is damaged, but not in damage state  $n_D$ , called the maximum damage state. The last line is the probability that the component is damaged in the maximum damage state.

### Simultaneous Damage States

With simultaneous damage states, one can evaluate the probability that a component is in each damage state independently of the others. Because order does not matter, damage states  $D$  are nominal numbers, like the numbers on football jerseys without any order, although  $D = 0$  is reserved for the undamaged state.

$$\begin{aligned}
 P[D = d|X = x] &= 1 - P[D \geq 1|X = x] & d = 0 \\
 &= P[D \geq 1|X = x] \cdot P[D = d|D \geq 1] & 1 \leq d \leq n_D
 \end{aligned} \tag{9}$$

where

$P[D \geq 1 | X = x]$  = probability that the component is damaged in some way, which can be quantified just like any fragility function, such as with a lognormal CDF:

$$P[D \geq 1|X = x] = \Phi\left(\frac{\ln(x/\theta)}{\beta}\right) \tag{10}$$

where there are only one value of  $\theta$  and only one value of  $\beta$  – no subscripts as in Eq. 1 – that is, a single median and logarithmic standard deviation of capacity. Note that the fragility function does not have to be a lognormal CDF, but that is common.

$P[D = d | D \geq 1]$  = probability that, if damaged, it is in damage state  $d$ . It can be in others as well.

Since under simultaneous damage states a component can be in more than one damage state,

$$\left(\sum_{d=1}^{n_D} P[D = d|D \geq 1]\right) > 1 \tag{11}$$

How can one estimate the probability that a component is in one and only one damage state? Let  $d_i$  denote one particular value of  $D$  and  $d_j$  another particular value of  $D$ , but  $d_i \neq d_j$ ,  $d_i \neq 0$ , and  $d_j \neq 0$ . Let  $P[D = d_i \& D \neq d_j | X = x]$  denote the probability that the component is in damage state  $d_i$  and it is not in any other damage state  $d_j$  given that  $X = x$ . It is given by

$$\begin{aligned}
 P[D = d_i \& D \neq d_j | X = x] &= P[D \geq 1, D = d_i | X = x] \cdot \prod_j (1 - P[D = d_j | D \geq 1, X = x]) \\
 &= P[D \geq 1 | X = x] \cdot P[D = d_i | D \geq 1, X = x] \cdot \prod_j (1 - P[D = d_j | D \geq 1, X = x]) \\
 &= P[D \geq 1 | X = x] \cdot P[D = d_i | D \geq 1] \cdot \prod_j (1 - P[D = d_j | D \geq 1])
 \end{aligned} \tag{12}$$

Consider now the probability that the component is in exactly two damage states. Let  $D_1$  denote the first of two nonzero damage states that the component is in and  $D_2$  the second. Let  $P[D_1 = d_i \& D_2 = d_j \& D \neq d_k | X = x]$  denote the probability

that the component is in two damage states  $D_1 = d_i$  and  $D_2 = d_j$  but not any other damage state  $d_k$  ( $k \neq i, k \neq j, i \neq j, i \neq 0, j \neq 0, \text{ and } k \neq 0$ ) given  $X = x$ . It is given by

$$\begin{aligned} P[D_1 = d_i \& D_2 = d_j \& D = d_k | X = x] \\ = P[D \geq 1 | X = x] \cdot P[D = d_i | D \geq 1] \cdot P[D = d_j | D \geq 1] \cdot \prod_k (1 - P[D = d_k | D \geq 1]) \end{aligned} \quad (13)$$

One could repeat for three damage states  $i, j,$  and  $k$  by repeating the pattern. It is the product of the probabilities that the component is in each damage state  $i, j,$  and  $k$  and the probabilities that it is not in each remaining damage state  $l, m, n,$  etc.

### MECE Damage States

Remember that MECE means that, if the component is damaged (denoted by  $D \geq 1$ ), it is in one and only one nonzero damage state. One can evaluate it by

$$\begin{aligned} P[D = d | X = x] &= 1 - P[D \geq 1 | X = x] & d = 0 \\ &= P[D \geq 1 | X = x] \cdot P[D = d | D \geq 1] & d \in \{1, 2, \dots, N_D\} \end{aligned} \quad (14)$$

$P[D \geq 1 | X = x]$  = probability that the component is damaged in some way, which one evaluates with a single fragility function. If the fragility function is taken as a lognormal CDF, see Eq. 10. Note that the fragility function does not have to be a lognormal CDF, but that is common.

$P[D = d | D \geq 1]$  = probability that, if damaged, it is damaged in damage state  $d$  (and not any other value of  $D$ ). Since under MECE damage states a component can only be in one damage state,

$$\left( \sum_{d=1}^{N_D} P[D = d | D \geq 1] \right) = 1 \quad (15)$$

## Creating Fragility Functions

### What to Know Before Trying to Derive a Fragility Function

Consider now how fragility functions are made. Much of this section is drawn from Porter et al. (2007). Before trying to derive a fragility

function, the analyst should define failure in unambiguous terms that do not require the exercise of judgment, i.e., where two people observing the same specimen would reach the same conclusion as to whether a specimen has failed or not. Beware damage scales that do not meet this test. Second, define the excitation to which specimens are subjected (maximum base acceleration, peak transient drift ratio, etc.) in similarly unambiguous terms. Third, select specimens without bias with respect to failure or nonfailure. That is, one cannot use data about specimens that were observed *because* they were damaged or because the damage was prominent or interesting in some way. (Failure data gathered by reconnaissance surveys tend to be biased in this way.) Fourth, ensure that specimens were subjected to multiple levels of excitation.

### Actual Failure Excitation

In the unusual case where specimens were all tested in a laboratory to failure and the actual excitation at which each specimen failed is known, then one can fit a lognormal fragility



function to the data as follows. This kind of data is referred to here as type A data, A for actual failure excitation. Before using the following math, the analyst must clearly define “failure” and should know both the means of observing specimen excitation and failure, as well as a clear definition of the component or other asset category in question:

- $n_i$  = number of specimens,  $n_i \geq 2$ .
- $i$  = index to specimens,  $i \in \{1, 2, \dots, n_i\}$ .
- $r_i$  = excitation at which specimen  $i$  failed.

$$\theta = \frac{1}{n_i} \sum_{i=1}^{n_i} \ln(r_i) \tag{16}$$

$$\beta = \sqrt{\frac{1}{n_i - 1} \sum_{i=1}^{n_i} (\ln(r_i/\theta))^2} \tag{17}$$

**Bounding-Failure Excitation**

Suppose one possesses observations where at least one specimen did not fail, at least one specimen did fail, and one knows the peak excitation to which each specimen was subjected, but not the actual excitation at which each specimen failed. These data are referred to here as bounding, or type B, data. Specimens are grouped by the maximum level of excitation to which each specimen was subjected. Assume the fragility function is reasonably like a lognormal cumulative distribution function and find the parameter values  $\theta$  (median) and  $\beta$  (logarithmic standard deviation) as follows:

- $m_i$  = numbers of levels of excitation among the data, referred to here as bins,  $m_i \geq 2$ .
- $i$  = bin index,  $i \in \{1, 2, \dots, m_i\}$ .
- $r_i$  = maximum excitation to which specimens in bin  $i$  were subjected.
- $n_i$  = number of specimens in bin  $i$ ,  $n_i \in \{1, 2, \dots\}$ .
- $f_i$  = number of specimens in bin  $i$  that failed,  $f_i \in \{0, 1, \dots, n_i\}$ .

One proper way to estimate  $\theta$  and  $\beta$  is by the maximum likelihood method, i.e., by finding the

values of  $\theta$  and  $\beta$  that have the highest likelihood of producing the observed data. At any level of excitation  $r_i$ , there is a probability of any individual specimen failing that is given by the lognormal CDF. Let  $p_i$  denote this probability:

$$p_i = \Phi\left(\frac{\ln(r_i/\theta)}{\beta}\right) \tag{18}$$

Assume that the failure of any two different specimens is independent conditioned on excitation. In that case, if one were to estimate the number of failed specimens in bin  $i$ , it would be proper to take that number as a random variable with a binomial distribution. Let  $F_i$  denote that random variable. The following equation gives the probability that one will observe  $f_i$  failures among  $n_i$  specimens with the per-occurrence failure probability  $p_i$ :

$$P[F_i = f_i] = \frac{n_i!}{f_i!(n_i - f_i)!} \cdot p_i^{f_i} \cdot (1 - p_i)^{n_i - f_i} \tag{19}$$

This is the binomial distribution. One finds the  $\theta$  and  $\beta$  values that maximize the likelihood of observing all the data  $\{n_1, f_1, n_2, f_2, \dots\}$  given excitations  $\{r_1, r_2, \dots\}$ . That likelihood is given by the product of the probabilities in Eq. 19, multiplied over all the bins. That is, find  $\theta$  and  $\beta$  that maximize  $L(\theta, \beta)$  in:

$$L(\theta, \beta) = \prod_{i=1}^{m_i} P[F_i = f_i] \tag{20}$$

One can explicitly maximize  $L(\theta, \beta)$ , but it is easier to use Excel or similar MATLAB or other software. Excel’s solver is straightforward.

It may be easier to remember a more approximate approach of minimizing the weighted squares of the difference between the observed data and the idealized fragility function. That is, find  $\theta$  and  $\beta$  that minimize the squared error term  $\varepsilon^2(\theta, \beta)$  in:

$$\varepsilon^2(\theta, \beta) = \sum_{i=1}^{m_i} n_i \cdot \left(p_i - \frac{f_i}{n_i}\right)^2 \tag{21}$$

The difference between the fragility functions derived by these two different methods generally appears to be small compared with the scatter about the regression lines, so arguments about what is more proper tend to be academic compared with the choice of which one is easier. There is at least one more reasonable approach, called logistic regression, but again this approach tends to produce roughly the same values of  $\theta$  and  $\beta$ , with differences that are small compared with data scatter.

#### Other Data Conditions

There are cases where none of the specimens failed (type C, or capable, data), where failure is derived by structural analysis (type D data), where expert opinion is used (type E), or where Bayesian updating is used to update an existing fragility function with new evidence (type U). For such situations, see Porter et al. (2007).

#### Dealing with Under-Representative Specimens

If the specimens used to create the fragility function are very few in number or unrepresentative of the broader class whose fragility is desired, or if the excitation to which they were subjected was unlike real-world earthquake shaking, one can reflect added uncertainty associated with unrepresentative conditions by increasing the fragility function's logarithmic standard deviation. The FEMA P-58 guidelines, for example, suggest always increasing the logarithmic standard deviation of a fragility function that is derived from test data or observations, as follows:

$$\beta' = \sqrt{\beta^2 + \beta_u^2} \quad (22)$$

where  $\beta'$  is the new, increased value of the logarithmic standard deviation of the fragility function,  $\beta$  is the value derived using the test or post-earthquake observation data, and  $\beta_u$  is a term to reflect uncertainty that the tests represent real-world conditions of installation and loading or uncertainty that the available data are an adequate sample size to accurately represent the true variability.

FEMA P-58 recommends values of  $\beta_u$  depending on how under-representative are the

data. If any of the following is true, use a minimum value of  $\beta_u = 0.25$ ; otherwise, use  $\beta_u = 0.10$ .

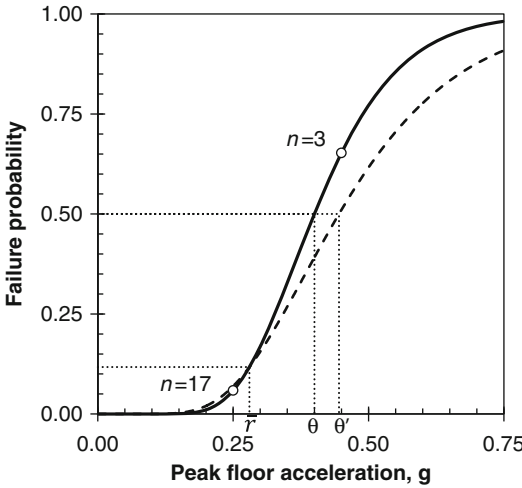
1. Data are available for five or fewer specimens.
2. In an actual building, a component can be installed in a number of different configurations, but all specimens were tested with the same configuration.
3. All specimens were subjected to the same loading protocol.
4. Actual behavior of the component is expected to be dependent on two or more demand parameters (e.g., simultaneous drift in two orthogonal directions), but specimens were loaded using only one demand parameter.

In the case of type B data, increasing  $\beta$  using Eq. 22 introduces a bias in long-term failure probability and can cause the fragility function not to pass through the actual failure data well. If the data generally lie at excitation levels below the derived median capacity  $\theta$ , which is common, then increasing  $\beta$  without adjusting  $\theta$  will cause the fragility function to move up (to higher probabilities) relative to the data. To increase  $\beta$  while still ensuring that the derived fragility function passes through the data, one can adjust  $\theta$  as follows:

$$\bar{r} = \frac{\sum_{i=1}^{N_i} r_i \cdot n_i}{\sum_{i=1}^{N_i} n_i} \quad (23)$$

$$\theta' = \bar{r} \cdot \left( \frac{\bar{r}}{\theta} \right)^{(-\beta'/\beta)} \quad (24)$$

In the case of type A data, use  $n_i = 1$  for all  $i$  in Eq. 23. For example, imagine that 17 suspended ceilings of identical construction are installed in a large, stiff single-story building, a block away from a 2-story building with three suspended ceilings on the upper floor. A ceiling in the 1-story building and two ceilings in the 2-story building collapse in a particular earthquake. The estimated roof accelerations in the two buildings are 0.25 and 0.45 g, respectively. These type



**Beginner's Guide to Fragility, Vulnerability, and Risk, Fig. 1** Increasing beta and adjusting theta to account for under-representative samples

B data are used to derive a fragility function in terms of peak floor acceleration, with  $\beta = 0.3$  and  $\theta = 0.4$  g. These conditions meet FEMA P-58's criteria 2 and 3, so  $\beta_u = 0.25$ . Applying the FEMA P-58-recommended value  $\beta_u = 0.25$  and evaluating Eqs. 22, 23, and 24 yields

$$\beta' = \sqrt{0.3^2 + 0.25^2} = 0.39$$

$$\bar{r} = \frac{(17 \cdot 0.25 + 3 \cdot 0.45)}{20} = 0.28$$

$$\theta' = 0.28 \cdot \left(\frac{0.28}{0.4}\right)^{(-0.39/0.30)} = 0.45$$

Figure 1 illustrates the data, the fragility function before increasing  $\beta$  (the solid line) and the fragility function after increasing  $\beta$ . Note how the two curves cross at  $r = \bar{r}$  and how  $\theta' > \theta$ . The solid curve passes through the data because there are only two data points, but it passes over the first data point and below the second, closer to the first because the first represents more data.

**Some Useful Sources of Component Fragility Functions**

FEMA P-58 produced a large suite of component fragility functions. See [https://www.atcouncil.org/files/FEMAP-58-3\\_2\\_ProvidedFragilityData.zip](https://www.atcouncil.org/files/FEMAP-58-3_2_ProvidedFragilityData.zip).

“Component” means a building component, like an RSMeans assembly such as glass curtain walls. The component fragility functions in FEMA P-58 mostly use as excitation measures the peak transient interstory drift ratio to which a drift-sensitive specimen is subjected or the peak absolute acceleration of the floor or roof to which the specimen is attached, for acceleration-sensitive components. In some cases peak residual drift is used (e.g., doors getting jammed shut). There are other measures of excitation as well. FEMA P-58 failure modes are defined with symptoms of physical damage or nonfunctionality requiring particular, predefined repair measures. They are never vague qualitative states such as “minor damage” that require judgment to interpret. Most of the FEMA P-58 fragility functions are derived from post-earthquake observations or laboratory experiments. Some are based on structural analysis and some are derived from expert opinion. All were peer reviewed. Johnson et al. (1999) also offer a large library of component fragility functions, many based on post-earthquake observations of standard mechanical, electrical, and plumbing equipment in power facilities.

The HAZUS-MH technical manual (NIBS and FEMA 2009) offers a number of whole-building fragility functions, defining for instance probabilistic damage to all the drift-sensitive nonstructural components in the building in four qualitative damage states (slight, moderate, extensive, complete) as a function of a whole-building measure of structural response (spectral acceleration response or spectral displacement response of the equivalent nonlinear SDOF oscillator that represents the whole building).

**Vulnerability**

**Vulnerability Terminology**

So far, this entry has discussed damageability in terms of the occurrence of some undesirable event such as a building collapse that either occurs or does not occur. Damageability is also measured in terms of the degree of the

undesirable outcome, called loss here, in terms of repair costs, life-safety impacts, and loss of functionality (dollars, deaths, and downtime) or in terms of environmental degradation, quality of life, historical value, and other measures. When loss is depicted as a function of environmental excitation, the function can be called a vulnerability function. A seismic vulnerability function relates uncertain loss to a measure of seismic excitation, such as spectral acceleration response at some damping ratio and period. A seismic vulnerability function usually applies to a particular asset class.

Vulnerability is not fragility. Vulnerability measures loss; fragility measures probability. Vulnerability functions are referred to many ways: damage functions, loss functions, vulnerability curves, and probably others.

When a vulnerability function measures repair cost, it is commonly normalized by replacement cost new (RCN), a term which here means the cost of a similar new property having the nearest equivalent utility as the property being appraised, as of a specific date (American Society of Appraisers 2013). RCN excludes land value and usually refers to part or all of the fixed components of a building or other assets (structural, architectural, mechanical, electrical, and plumbing components) or to its contents. Repair cost divided by RCN is referred to here as damage factor (DF). Some authors call it damage ratio, fractional loss, or other terms. The expected value of DF conditioned on excitation is commonly called mean damage factor (MDF). Sometimes it is assumed that if DF exceeds some threshold value such as 0.6, the property is not worth repairing and is a total loss, so repair-cost vulnerability functions can jump abruptly from 0.6 (or other threshold value) to 1.0 with increasing excitation. In principle DF can exceed 1.0 because it can cost more to repair a building than to replace it.

When a vulnerability function measures life-safety impacts, it commonly measures the fraction of indoor occupants who become casualties (that is, they are killed or experience a nonfatal injury to some specified degree) as a function of excitation. There are a variety of human-injury

scales, some used by civil engineers and others used by public health professionals. Before using a terms such as minor injury, one should be sure its meaning is entirely clear and meaningful to the intended user of the vulnerability information. Civil engineers sometimes use casualty scales that are ambiguous or not useful to public health professionals.

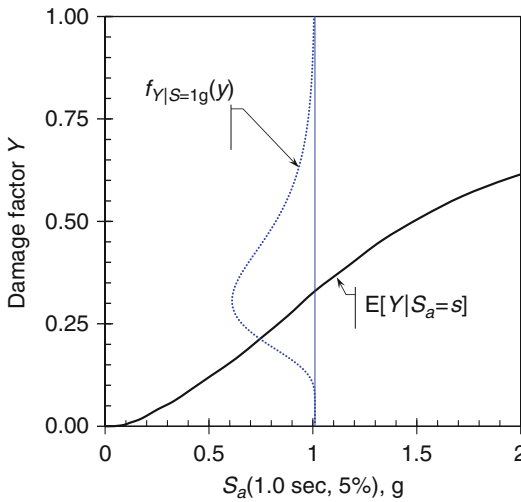
Downtime is commonly measured in terms of days or fractions of a year during which the asset cannot be used for its intended purposes. Sometimes it measures the time from the environmental shock (the earthquake, in the case of a seismic vulnerability function) to the time when all repairs are completed, which includes both the time required to perform the repairs and a previous period during which damage is assessed, repairs are designed, financing is arranged, repairs are bid out, and the repair contractor mobilizes to the site.

Many vulnerability functions are expressed with conditional probability distributions that give a probability that loss will not exceed some specified value given the excitation, for a particular asset class. The distribution is often assigned a parametric form such as lognormal or beta, in which case the parameters of the distribution are all required, some or all of them conditioned on excitation. Figure 2 presents a sample probabilistic vulnerability function.

### **Brief Summary of Vulnerability Derivation Methods**

While this entry does not provide guidance on how to derive vulnerability functions, it is worthwhile to understand the different approaches to doing so and some of the relevant history. There are three distinct approaches – sometimes referred to as empirical, analytical, and expert opinion – and some hybrids that combine aspects of two or more approaches. They are briefly explained here.

An empirical vulnerability function is one derived by regression analysis of observations of pairs of excitation and loss for specimens of an asset class. Professional users of vulnerability functions such as insurance loss estimators tend to prefer empirical vulnerability functions over



**Beginner's Guide to Fragility, Vulnerability, and Risk, Fig. 2** Sample vulnerability function that relates damage factor to 1-s spectral acceleration response for some asset class. The *solid line* depicts the expected value of damage factor, and the *dotted curve* depicts the probability density function of damage factor at 1 g of excitation

other approaches, because they are known to be based on real-world observations. One of the best examples of an empirical vulnerability function is the one derived by Wesson et al. (2004), who performed regression analysis of losses to single-family housing from ground motion in the 1994 Northridge earthquake. Among the challenges to deriving empirical vulnerability functions are the scarcity of nearby ground motion observations, the difficulty getting reliable loss information, and relatively few observations at high levels of ground motion.

Analytical methods are useful when empirical data are lacking and one has the time and other resources to create and analyze a model. An analytical approach generally involves defining one or more specimens to represent the class, creating and analyzing a structural model to estimate structural response as a function of ground motion, estimating component-level damage given structural response, and then estimating loss given component damage. The interested reader is referred to FEMA P-58 (ATC 2012) for the current state of the practice for individual buildings and to Porter et al. (2009a, b; 2010,

2014) for building classes. Analytical methods offer the advantage of being able to distinguish the effect of any feature of interest and any asset class the analyst can model, but the disadvantages of cost and often a lack of data to validate the results.

Expert opinion can quickly provide vulnerability functions where empirical data are missing and the analyst lacks the resources for an analytical model. Briefly, one convenes a group of experts familiar with the performance of the asset class of interest and with a structured interview process elicits their judgment of the performance of the class at each of many levels of excitation. ATC-13 (1985) represents one of the earliest and most thorough expert-opinion models of the seismic vulnerability of buildings and other asset classes. Jaiswal et al. (2012) offers a more recent example.

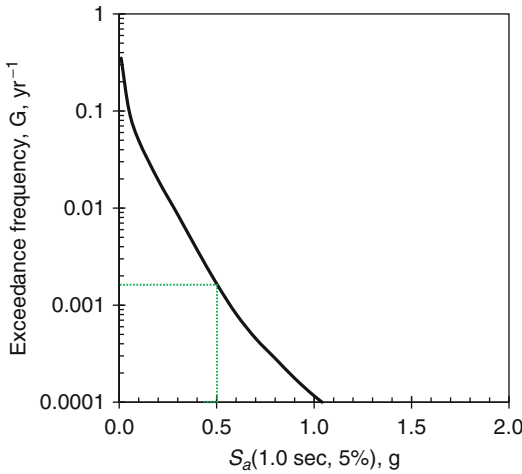
## Hazard

### Probabilistic Seismic Hazard Analysis

Seismic hazard refers here to an uncertain relationship between the level of some measure of seismic excitation and the frequency or probability of a particular location experiencing at least that level of excitation. It is *not* the measure of excitation, the occurrence of an earthquake, nor the probability or frequency of excitation. These terms are not to be used interchangeably.

Seismic hazard is quantified many ways. One is through a hazard curve, commonly depicted on an *x-y* chart where the *x*-axis measures shaking intensity at a site and the *y*-axis measures either exceedance probability in a specified period of time or exceedance rate in events per unit time. See Fig. 3 for an example Cornell (1968) applied the theorem of total probability to create a hazard curve. What follows here is a summary of current procedures to perform probabilistic seismic hazard analysis (PSHA), but is conceptually identical to Cornell's work.

Engineers sometimes refer to the quantity by which intensity is measured as the intensity measure. Earth scientists call it ground motion. The present work uses the term intensity measure (IM).



**Beginner's Guide to Fragility, Vulnerability, and Risk, Fig. 3** Sample hazard curve. The *solid line* shows the mean rate at which various levels of 1 s spectral acceleration response are exceeded. The *dotted line* shows that 0.5 g is exceeded on average about once in 600 years

Some authors distinguish between the intensity measure type (IMT), such as 5 % damped spectral acceleration response at 0.2 s period, and the intensity measure level (IML), a particular value of the IM such as 0.4 g. In any case, IMT must be completely specified. If using damped elastic spectral acceleration response, one states the period, damping ratio, and whether one is referring to the geometric mean of two orthogonal directions or the maximum direction or other directional references.

To estimate seismic hazard, one applies the theorem of total probability to combine the uncertain shaking at the site caused by a particular fault rupture and the occurrence frequency or probability of that rupture. Earth scientists create models called earthquake rupture forecasts that specify the locations and rates at which various fault produce earthquakes of various sizes, e.g., the Uniform California Earthquake Rupture Forecast version 2 (UCERF2, Field et al. 2007). The uncertain shaking given a fault rupture is quantified using a relationship variously called an attenuation relationship or a ground-motion prediction equation, such as the next-generation attenuation (NGA) relationships presented in the

February 2008 issue of *Earthquake Spectra*. Mathematically, a hazard curve is created as follows. Let:

$H$  = uncertain severity of ground motion at the building site, e.g.,  $S_a(T, 5\%)$ .

$h$  = a particular value of  $H$ .

$G(h)$  = frequency (events per unit time) with which  $H > h$ , i.e., the number of events per unit time in which at least once during the event,  $H > h$ .

$n_E$  = number of earthquake rupture forecast models to consider,  $n_E \in \{1, 2, \dots\}$ . For example, in UCERF2, there were 480 discrete combinations of fault model, rupture model, magnitude-area relationship, and several other modeling choices that together are represented by a logic tree that begins with fault model, branches to rupture model, then to magnitude-area relationship, etc. For UCERF2,  $n_E = 480$ .

$E$  = the “correct” earthquake rupture forecast, which is uncertain.  $E \in \{1, 2, \dots, n_E\}$ .

$e$  = an index to a particular earthquake rupture forecast,  $e \in \{1, 2, \dots, n_E\}$ .

$P[E = e]$  = Bayesian probability assigned to earthquake rupture forecast  $e$ . In UCERF2, this would be the product of the conditional probabilities (weights) of the individual branches in the logic tree that represents UCERF2. Conditional probability means that each branch’s probability can (though only sometimes do) depend on which choices came before it.

$n_A$  = number of attenuation relationships (also called ground motion prediction equations) to be employed,  $n_A \in \{1, 2, \dots\}$

$A$  = the “correct” ground-motion-prediction equation, i.e., the one that expresses the true state of nature, which is uncertain.

$a$  = an index to ground-motion prediction equations.

$P[A = a]$  = Bayesian probability assigned to ground-motion-prediction equation  $a$ , i.e., the probability that ground-motion-prediction equation  $a$  actually reflects the true state of nature and is therefore the correct ground-motion-prediction equation.



$n_F(e)$  = number of fault sections in earthquake rupture forecast  $e$ ,  $n_F(e) \in \{1, 2, \dots\}$ .  
 $f$  = an index to faults section,  $f \in \{1, 2, \dots, n_F(e)\}$ .  
 $m_0$  = minimum magnitude to consider.  
 $\Delta m$  = an increment of magnitude, say,  $\Delta m = 0.1$ .  
 $M_{\max}(f|E = e)$  = maximum magnitude of which fault  $f$  is deemed capable under earthquake rupture forecast  $e$ ,  $M_{\max}(f|E = e) \in \{m_0 + \frac{1}{2} \cdot \Delta m, m_0 + \frac{3}{2} \cdot \Delta m, \dots\}$ .  
 $n_o(f,m)$  = number of locations within fault section  $f$  that can generate a rupture of magnitude  $m$ ,  $n_o(f,m) \in \{1, 2, \dots\}$ .  
 $o$  = an index to locations on fault section  $f$ , in  $o \in \{1, 2, \dots, n_o(f,m)\}$ .  
 $G(f,m,o|E = e)$  = frequency (events per unit time) with which fault section  $f$  ruptures at location  $o$  producing earthquake of magnitude  $m \pm \frac{1}{2} \cdot \Delta m$  given earthquake rupture forecast  $e$ .  
 $V_S$  = uncertain site soil, potentially measured by NEHRP site soil classification or shearwave velocity in the top 30 m of soil (Vs30) or something else. To find Vs30, see the site data application at [www.opensha.org/apps](http://www.opensha.org/apps) for U.S. locations or Google the USGS's Global Vs30 map server for other locations  
 $v$  = a particular value of  $V$ .

$P[H > h | m,r,v,a]$  = probability that  $H > h$  given earthquake magnitude  $m$  at distance  $r$  on soil with soil type  $v$  using ground-motion prediction equation  $a$ . Note that, given a known site location, fault segment  $f$ , and location along the fault segment  $o$ , distance  $r$  from the site to the fault is known. Note that ground-motion prediction equations use a variety of distance measures. As of this writing, most ground-motion prediction equations give an equation for the mean of the natural logarithm of  $H$  given  $m$ ,  $r$ , and  $v$ , for the logarithmic standard deviation of  $H$  (i.e., the standard deviation of the natural logarithm of  $H$ ), and assume a lognormal distribution of  $H$  conditioned on  $m$ ,  $r$ , and  $v$ . Let  $m_{\ln H}$  and  $s_{\ln H}$  denote the mean of  $\ln(H)$  and the standard deviation of  $\ln(H)$ , respectively, given  $m$ ,  $r$ , and  $v$ , assuming ground-motion-prediction equation  $a$ . Under these conditions,

$$P[H > h | m, r, v, a] = 1 - \Phi\left(\frac{\ln(h) - m_{\ln H}}{s_{\ln H}}\right) \tag{25}$$

One can now estimate the hazard curve by applying the theorem of total probability. Suppose one always knew soil conditions  $V$  with certainty. Then

$$G(h) = \sum_{e=1}^{n_E} \sum_{a=1}^{n_A} \sum_{f=1}^{n_F(e)} \sum_{m} \sum_{o=1}^{n_o(f,m)} P[H > h | m, r, v, a] \cdot G(m, f, o | E = e) \cdot P[A = a] \cdot P[E = e] \tag{26}$$

where the summation over  $m$  means that one considers each  $m \in \{m_0 + \frac{1}{2} \cdot \Delta m, m_0 + \frac{3}{2} \cdot \Delta m, \dots, M_{\max}(f|E = e)\}$ .

**Hazard Rate Versus Probability**

Seismic hazard is often expressed in terms of exceedance probability, rather than in terms of exceedance rate. The distinction is this: exceedance probability is the probability that shaking of  $H > h$  will occur at least once in a given period of time. That means that it is the probability that it  $H > h$  will occur exactly once, plus the probability that it will occur exactly twice, etc. For some calculations, the analyst wants rate (number of

events per unit time) not probability (chance that it occurs one or more times in a given time period).

The two can be related using a concept called a Poisson process. From the Wikipedia's article on the Poisson Process: "In probability theory, a Poisson process is a stochastic process which counts the number of events and the time that these events occur in a given time interval. The time between each pair of consecutive events has an exponential distribution with parameter  $G$  [the parameter is the occurrence rate per unit time] and each of these inter-arrival times is ... independent of other

inter-arrival times [meaning that the time between the second and third occurrence is independent of the time between the first and second occurrence – knowing one tells you nothing about the other, so a Poisson process is called memoryless]. The process is named after the French mathematician Siméon-Denis Poisson and is a good model of radioactive decay, telephone calls, and requests for a particular document on a web server, among many other phenomena.”

Modeling earthquakes as Poisson arrivals is convenient in part because in a Poisson process, arrival rate and occurrence probability have this relationship:

$$G = \frac{-\ln(1 - P)}{t} \quad (27)$$

where

$G$  = occurrence rate, i.e., events per unit time,  
 $P$  = probability that at least one event will occur in time  $t$ .

So if a hazard curve were represented as  $P(h)$ , the probability that  $H > h$  at least once in a particular period of time  $t$ , one could use Eq. 27 to estimate the occurrence rate  $G(h)$ , the average number of times that  $H \geq h$  per unit time. One can also rearrange Eq. 27 to give probability as a function of rate:

$$P = 1 - e^{-G \cdot t} \quad (28)$$

So with the occurrence rate  $G(h)$  of earthquakes causing  $H > h$ , one can calculate the probability that at least one earthquake with  $H > h$  will occur in a given time  $t$ .

### Measures of Seismic Excitation

These are many common measures of seismic excitation. Some measure ground motion and some measure structural response or excitation to which the components of a building, bridge, or other structural systems are subjected. This section introduces common ones.

#### Some Commonly Used Measures of Ground Motion

**Peak ground acceleration (PGA).** This is the maximum value of acceleration of a particular point on the ground at any time during an earthquake. Often PGA is estimated as the geometric mean (the square root of the product) of the maximum values of PGA parallel to each of two orthogonal horizontal axes. PGA is sometimes called zero-period acceleration (ZPA), meaning the spectral acceleration response of a single-degree-of-freedom elastic oscillator with zero, or near-zero, period. Before using a PGA value, be sure you know whether it refers to geometric mean, maximum-direction value, or something else.

**Peak ground velocity (PGV).** This is like PGA, except maximum velocity of a point on the ground rather than acceleration.

**Peak ground displacement (PGD).** This is like PGA, except maximum displacement relative to a fixed datum.

**Spectral acceleration response ( $S_a(T,z)$ ).** This usually refers to damped elastic spectral acceleration response at some specified index period such as  $T = 0.3$  s, 1.0 s, 3.0 s, etc., and specified damping ratio such as  $z = 5\%$ , at a particular point on the ground. To be precise,  $S_a(T,z)$  is the absolute value of the maximum acceleration relative to a fixed datum of a damped elastic single-degree-of-freedom harmonic oscillator with period  $T$  and damping ratio  $z$  when subjected to a particular one-degree-of-freedom ground-motion time history at its base. In practice, it typically refers to the geometric mean of spectral acceleration response parallel to each of two orthogonal horizontal axes. It is so often measured for  $z = 5\%$  that damping ratio is often not mentioned. Before using  $S_a(T,z)$ , be sure you know  $T$ ,  $z$ , and whether it is a geometric mean value or the maximum-direction value or something else.

**Spectral displacement response ( $S_d(T,z)$ ).** This is like  $S_a(T,z)$  but for relative spectral displacement (displacement of the oscillator relative to its base, not relative to a fixed datum) rather than absolute acceleration of the oscillator.

**Pseudoacceleration response ( $PSA(T,z)$ ).**  $PSA(T,z)$  is defined as  $S_d(T,z) \cdot \omega^2$ , where  $\omega$  is

angular frequency,  $2 \cdot \pi/T$ . Some authors prefer to use  $PSA(T,z)$  rather than  $S_a(T,z)$ , but for values of  $z$  less than about 20 %, the two measures are virtually identical.

**Modified Mercalli Intensity (MMI) and European Macroseismic Scale (EMS).** These are macroseismic intensity measures, meaning that they measure seismic excitation over a large area, not at a particular point on the ground. They are measured with an integer scale in Roman numerals from I to XII. They measure whether and how people in a region such as a neighborhood or city felt and reacted to earthquake motion (did they run outside?) and what they observed to happen to the ground, buildings, and contents around them, such as plates rattling and weak masonry being damaged. They are subjective and generally easier for nontechnical audiences to understand than instrumental measures. On the MMI scale, building damage begins around MMI VI and it is rare for an earthquake to produce shaking of  $MMI \geq X$ . EMS is similar to MMI, but building-damage observations are related to common European building types. A version of EMS defined in 1998 is often referred to as EMS-98. For detail see Table 1, Wood and Neumann (1931) and European Seismic Commission Working Group—Macroseismic Scales (1998).

**Japan Meteorological Agency (JMA) seismic intensity scale.** This is like MMI, but with a 0–7 scale. It has both a macroseismic sense (observed effects of people and objects) and an instrumental sense (in terms of ranges of PGA). See [http://en.wikipedia.org/wiki/Japan\\_Meteorological\\_Agency\\_seismic\\_intensity\\_scale](http://en.wikipedia.org/wiki/Japan_Meteorological_Agency_seismic_intensity_scale) for details.

**Instrumental intensity measure (IMM).** This is a positively valued measure of intensity that can take on fractional values, e.g., 6.4. This is an estimate of MMI using functions of instrumental ground-motion measures such as PGA and PGV.

#### Conversion Between Instrumental and Macroseismic Intensity

It is often desirable to convert between instrumental ground-motion measures such as PGA or PGV and macroseismic intensity

measures, especially MMI. One reason is that MMI observations can be made by people exposed to shaking or who make post-earthquake observations, whereas instrumental measures require an instrument.

**Ground motion to intensity conversion equations (GMICE).** These estimate macroseismic intensity as a function of instrumental measures of ground motion. There are several leading GMICES. When selecting among them, try to match the region, magnitude range, and distance range closest to the conditions where the GMICE will be applied. More data for conditions like the ones in question are generally better than less data, all other things being equal. When considering building response, GMICES that convert from  $S_a(T,z)$  to macroseismic intensity are generally better than those that use PGA or PGV, which do not reflect anything building-specific. Two recent GMICES for the United States are as follows:

As of this writing, Worden et al.'s (2012) relationships in Eqs. 29 and 30 seem to be the best choice for estimating MMI from ground motion and vice versa for California earthquakes. The reason is they employ a very large dataset of California (ground motion, MMI) observations. The dataset includes 2092 PGA-MMI observations and 2074 PGV-MMI observations from 1207 California earthquakes  $M = 3.0\text{--}7.3$ ,  $MMI = 2.0\text{--}8.6$ ,  $R = 4\text{--}500$  km. It includes no observations from continental interior. It includes regressions for  $S_a(0.3$  s, 5 %),  $S_a(1.0$  s, 5 %),  $S_a(3.0$  s, 5 %), PGA, and PGV that operate in both directions, meaning that one can rearrange the relationships to estimate instrumental measures in terms of MMI, as well as MMI in terms of instrumental measures. The reason that the relationships are bidirectional is that Worden et al. (2012) used a total least-squares data modeling technique in which observational errors on both dependent and independent variables are taken into account. Equation 30 includes the option to account for the apparent effects of magnitude  $M$  and distance  $R$ . The columns for residual standard deviations show a modest reduction in uncertainty when accounting for  $M$  and  $R$  (Table 2).

**Beginner's Guide to Fragility, Vulnerability, and Risk, Table 1** MMI and EMS-98 macroseismic intensity scales (abridged)

MMI	Brief description	EMS-98	Brief description
I. Instrumental	Generally not felt by people unless in favorable conditions	I. Not felt	Not felt by anyone
II. Weak	Felt only by a couple people that are sensitive, especially on the upper floors of buildings. Delicately suspended objects (including chandeliers) may swing slightly	II. Scarcely felt	Vibration is felt only by individual people at rest in houses, especially on upper floors of buildings
III. Slight	Felt quite noticeably by people indoors, especially on the upper floors of buildings. Standing automobiles may rock slightly. Vibration similar to the passing of a truck. Indoor objects may shake	III. Weak	The vibration is weak and is felt indoors by a few people. People at rest feel swaying or light trembling. Noticeable shaking of many objects
IV. Moderate	Felt indoors by many people, outdoors by few. Some awakened. Dishes, windows, and doors disturbed, and walls make cracking sounds. Chandeliers and indoor objects shake noticeably. Like a heavy truck striking building. Standing automobiles rock. Dishes and windows rattle	IV. Largely observed	The earthquake is felt indoors by many people and outdoors by few. A few people are awakened. The level of vibration is possibly frightening. Windows, doors, and dishes rattle. Hanging objects swing. No damage to buildings
V. Rather strong	Felt inside by most or all and outside. Dishes and windows may break. Vibrations like a train passing close. Possible slight damage to buildings. Liquids may spill out of glasses or open containers. None to a few people are frightened and run outdoors	V. Strong	Felt indoors by most, outdoors by many. Many sleeping people awake. A few run outdoors. China and glasses clatter. Top-heavy objects topple. Doors and windows swing
VI. Strong	Felt by everyone; many frightened and run outdoors, walk unsteadily. Windows, dishes, glassware broken; books fall off shelves; some heavy furniture moved or overturned; a few instances of fallen plaster. Damage slight to moderate to poorly designed buildings; all others receive none to slight damage	VI. Slightly damaging	Felt by everyone indoors and by many outdoors. Many people in buildings are frightened and run outdoors. Objects on walls fall. Slight damage to buildings; for example, fine cracks in plaster and small pieces of plaster fall
VII. Very strong	Difficult to stand. Furniture broken. Damage light in buildings of good design and construction; slight to moderate in ordinarily built structures; considerable damage in poorly built or badly designed structures; some chimneys broken or heavily damaged. Noticed by people driving automobiles	VII. Damaging	Most people are frightened and run outdoors. Furniture is shifted and many objects fall from shelves. Many buildings suffer slight to moderate damage. Cracks in walls; partial collapse of chimneys

*(continued)*

**Beginner’s Guide to Fragility, Vulnerability, and Risk, Table 1** (continued)

MMI	Brief description	EMS-98	Brief description
VIII. Destructive	Damage slight in structures of good design, considerable in normal buildings with possible partial collapse. Damage great in poorly built structures. Brick buildings moderately to extremely heavily damaged. Possible fall of chimneys, monuments, walls, etc. Heavy furniture moved	VIII. Heavily damaging	Furniture may be overturned. Many to most buildings suffer damage: chimneys fall; large cracks appear in walls and a few buildings may partially collapse. Can be noticed by people driving cars
IX. Violent	General panic. Damage slight to heavy in well-designed structures. Well-designed structures thrown out of plumb. Damage moderate to great in substantial buildings, with a possible partial collapse. Some buildings may be shifted off foundations. Walls can collapse	IX. Destructive	Monuments and columns fall or are twisted. Many ordinary buildings partially collapse and a few collapse completely. Windows shatter
X. Intense	Many well-built structures destroyed, collapsed, or moderately damaged. Most other structures destroyed or off foundation. Large landslides	X. Very destructive	Many buildings collapse. Cracks and landslides can be seen
XI. Extreme	Few if any structures remain standing. Numerous landslides, cracks, and deformation of the ground	XI. Devastating	Most buildings collapse
XII. Catastrophic	Total destruction. Objects thrown into the air. Landscape altered. Routes of rivers can change	XII. Completely devastating	All structures are destroyed. The ground changes

**Beginner’s Guide to Fragility, Vulnerability, and Risk, Table 2** Parameter values for Worden et al. (2012) GMICE for California

Y	c <sub>1</sub>	c <sub>2</sub>	c <sub>3</sub>	c <sub>4</sub>	c <sub>5</sub>	c <sub>6</sub>	c <sub>7</sub>	t <sub>1</sub>	t <sub>2</sub>	Eq. 29		Eq. 30	
										σ <sub>MMI</sub>	σ <sub>log10Y</sub>	σ <sub>MMI</sub>	σ <sub>log10Y</sub>
PGA	1.78	1.55	-1.60	3.7	-0.91	1.02	-0.17	1.57	4.22	0.73	0.39	0.66	0.35
PGV	3.78	1.47	2.89	3.16	0.90	0.00	-0.18	0.53	4.56	0.65	0.40	0.63	0.38
PSA (0.3 s)	1.26	1.69	-4.15	4.14	-1.05	0.60	0.00	2.21	4.99	0.84	0.46	0.82	0.44
PSA (1.0 s)	2.50	1.51	0.20	2.90	2.27	-0.49	-0.29	1.65	4.98	0.80	0.51	0.75	0.47
PSA (3.0 s)	3.81	1.17	1.99	3.01	1.91	-0.57	-0.21	0.99	4.96	0.95	0.69	0.89	0.64

**Beginner’s Guide to Fragility, Vulnerability, and Risk, Table 3** Parameter values for Atkinson and Kaka (2007) GMICE for the United States

Y	c <sub>1</sub>	c <sub>2</sub>	c <sub>3</sub>	c <sub>4</sub>	c <sub>5</sub>	c <sub>6</sub>	c <sub>7</sub>	σ <sub>MMI</sub>	
								Eq. 31	Eq. 32
PGA	4.37	1.32	3.54	3.03	0.47	-0.19	0.26	0.80	0.76
PGV	2.65	1.39	-1.91	4.09	-1.96	0.02	0.98	1.01	0.89
PSA(0.3 s)	2.40	1.36	-1.83	3.56	-0.11	-0.20	0.64	0.88	0.79
PSA(1.0 s)	3.23	1.18	0.57	2.95	1.92	-0.39	0.04	0.84	0.73
PSA(2.0 s)	3.72	1.29	1.99	3.00	2.24	-0.33	-0.31	0.86	0.72

$$\begin{aligned}
 MMI &= c_1 + c_2 \cdot \log_{10}(Y) & \log_{10}(Y) \leq t_1 & & MMI &= c_1 + c_2 \log_{10}(Y) & MMI \leq 5 \\
 &= c_3 + c_4 \cdot \log_{10}(Y) & \log_{10}(Y) > t_1 & & &= c_3 + c_4 \cdot \log_{10}(Y) & MMI > 5
 \end{aligned} \tag{29}$$

$$\begin{aligned}
 MMI &= c_1 + c_2 \cdot \log_{10}(Y) + c_5 + c_6 \cdot \log_{10}(R) \\
 &+ c_7 \cdot M & MMI \leq t_2 \\
 &= c_3 + c_4 \cdot \log_{10}(Y) + c_5 + c_6 \cdot \log_{10}(R) \\
 &+ c_7 \cdot M & MMI > t_2
 \end{aligned} \tag{30}$$

$$\begin{aligned}
 MMI &= c_1 + c_2 \cdot \log_{10}(Y) + c_5 + c_6 \cdot M \\
 &+ c_7 \cdot \log_{10}(R) & MMI \leq 5 \\
 &= c_3 + c_4 \cdot \log_{10}(Y) + c_5 + c_6 \cdot M \\
 &+ c_7 \cdot \log_{10}(R) & MMI > 5
 \end{aligned} \tag{32}$$

Units of Y are cm/s or cm/s, 5 % damping. Units of R are km. Columns labeled σ show residual standard deviation and depend on whether the M and R adjustment is used or not. Use σ<sub>log10Y</sub> with rearranged equations to give log<sub>10</sub>Y in terms of MMI.

Atkinson and Kaka’s (2007) relationships, shown in Eqs. 31 and 32, employ smaller dataset of California observations than Worden et al. (2012), but they reflect data from central and eastern and US observations. There are 986 observations: 710 from 21 California earthquakes, M = 3.5–7.1, R = 4–445 km, MMI = II–IX, and 276 central and eastern US observations from 29 earthquakes M = 1.8–4.6 R = 18–799 km. They include regression for Sa (0.3 s, 5 %), Sa(1.0 s, 5 %), Sa(3.0 s, 5 %), PGA, and PGV. Equation 32 accounts for the apparent effects of magnitude M and distance R. As suggested by the difference between the columns for residual standard deviation, the information added by M and R only modestly reduces uncertainty. The Atkinson and Kaka (2007) relationships are not bidirectional, meaning that one cannot rearrange them to estimate ground motion as a function of MMI.

Units of Y are cm/s or cm/s<sup>2</sup>, 5 % damping. Units of R are km. Columns labeled σ show residual standard deviation and depend on whether the M and R adjustment is used or not (Table 3).

Other GMICES of potential interest include the following. Wald et al.’s (1999) relationship draws on 342 (PGA, PGV, MMI) observations from eight California earthquakes. Kaestli and Faeh (2006) offer a PGA-PGV-MMI relationship for Switzerland, Italy, and France. Tselentis and Danciu (2008) offer relationships for MMI as functions of PGA, PGV, Arias intensity, cumulative absolute velocity, magnitude, distance, and soil conditions for Greece. Kaka and Atkinson (2004) offer GMICES relating MMI to PGV and three periods of PSA for eastern North America. Sørensen et al. (2007) offer a GMICE relating EMS-98 to PGA and PGV for Vrancea, Romania.

For relationships that give ground motion as a function of MMI (intensity to ground-motion conversion equations, IGMCE), consider Faenza and Michelini (2010) for Italy, Murphy, and O’Brien (1977) for anywhere in the world and Trifunac and Brady (1975) for the western United States. Unless explicitly stated, GMICE and IGMCE relationships are not



interchangeable – it is inappropriate to simply rearrange terms of a GMICE to produce an IGMCE. The reason is that both GMICE and IGMCE are derived by regression analysis. Given  $(x,y)$  data, a least-squares regression of  $y$  as a function of  $x$  will generally produce a different curve than a least-squares regression of  $x$  as a function of  $y$ .

### Hazard Deaggregation

When evaluating the risk to an asset, it is often desirable to perform nonlinear dynamic structural analyses at one or more intensity measure levels. To do so, one needs a suite of ground-motion time histories scaled to the desired intensity. The ground-motion time histories should be consistent with the seismic environment. That is, they should reflect the earthquake magnitudes  $m$  and distances  $r$  that would likely cause that level of excitation in that particular place. The reason is that magnitude and distance affect the duration and frequency content of the ground-motion time history, which in turn affects structural response. See McGuire (1995) or Bazzurro and Cornell (1999) for more information.

There is another term (commonly denoted by  $\varepsilon$ ) that also matters. It relates to how the spectral acceleration response at a specified period in a particular ground-motion time history differs from its expected value, given magnitude and distance. Let  $y$  denote the natural logarithm of the intensity measure level, e.g., the natural logarithm of the spectral acceleration response at the building's estimated small-amplitude fundamental period of vibration. Let  $\mu$  and  $\sigma$  denote the expected value and standard deviation of the natural logarithm of the intensity measure level, respectively, calculated from a ground-motion prediction equation. The  $\varepsilon$  term is a normalized value of  $y$ , as follows:

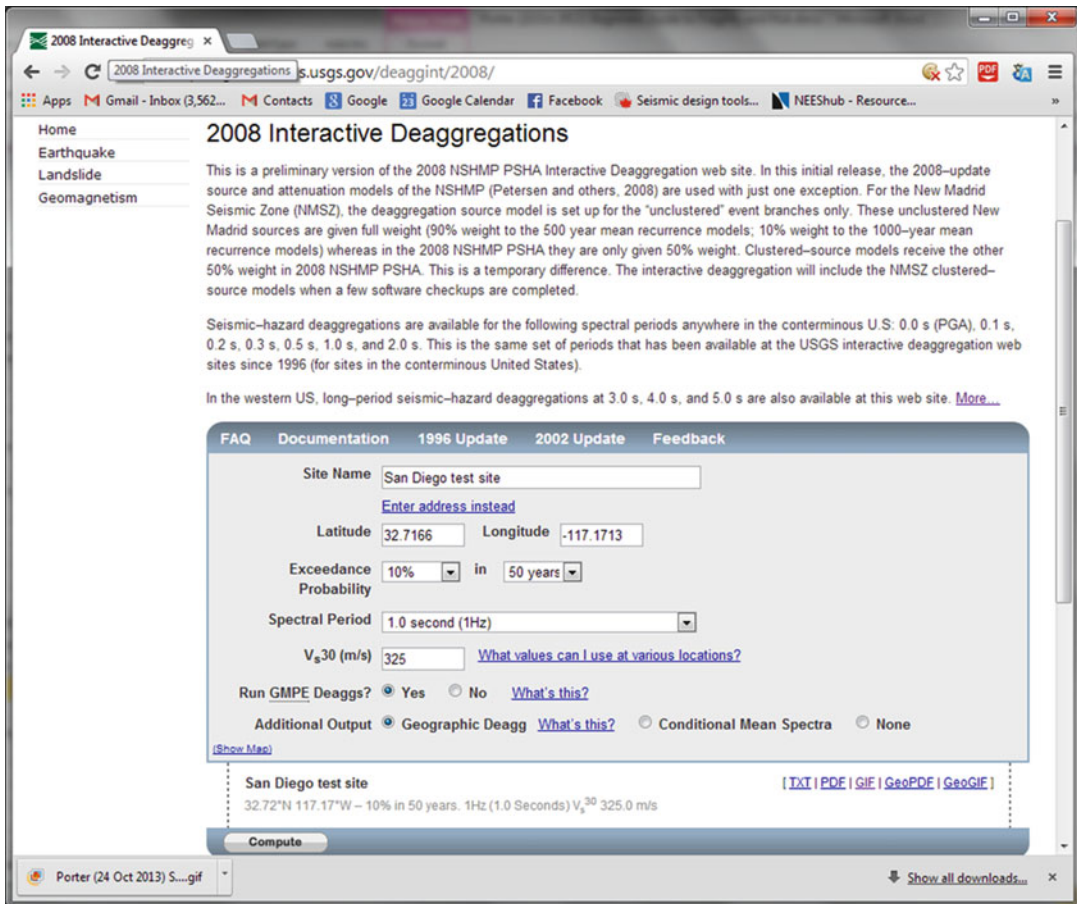
$$\varepsilon = \frac{y - \mu}{\sigma} \quad (33)$$

When calculating the motion  $y_0$  that has a specified exceedance probability  $p_0$ , one labels the  $\varepsilon$  from a specific source and this particular value of motion  $y_0$  as  $\varepsilon_0$ . The equation is the same as

Eq. 33, except with the subscript 0 on  $y$  and  $\varepsilon$ . It is practical to calculate for a given location, intensity measure type, and intensity measure level, the contribution of each fault segment, magnitude, rupture location, and value of  $\varepsilon_0$  to the frequency with which the site is expected to experience ground motion of at least the specified intensity measure level. In fact, Eq. 26 shows that the site hazard is summed from such values. (For simplicity that equation omits mention of  $\varepsilon$ , but the extension is modest.) See Baker and Cornell (2005) for more information.

Rather than leading the reader through the math, suffice it to say that there are online tools to do that hazard deaggregation, and an example is given here. The USGS offers a website that does interactive hazard deaggregation for the United States. As of this writing, the URL includes the year associated with the hazard model, so it will change over time. The most recent tool at this writing is <https://geohazards.usgs.gov/deaggint/2008/>. When that site becomes obsolete, the reader should be able to find the current one by googling “interactive hazard deaggregation USGS.”

Consider an imaginary 12-story building in San Diego, California at 1126 Pacific Hwy, San Diego CA, whose geographic coordinates are 32.7166 N -117.1713 E (North America has negative east longitude). Suppose its small-amplitude fundamental period of vibration is 1.0 s, its  $V_{s30}$  is 325 m/s, and its depth to bedrock (defined as having a shearwave velocity of 2,500 m/s) is 1.0 km. One wishes to select several ground-motion time histories with geometric mean  $S_a(1.0 \text{ s}, 5 \%)$  equal to that of the motion with 10 % exceedance probability in 50 years. The input data look like Fig. 4. The results look like Fig. 5, which shows that 10%/50-year motion at this site tends to result from earthquakes with Mw 6.6 at 1.8 km distance and a value of  $\varepsilon_0 = -1.22$ . One can then draw sample ground-motion time histories with approximately these values of magnitude, distance, and  $\varepsilon_0$  from a database such as PEER's strong motion database, currently located at [http://peer.berkeley.edu/peer\\_ground\\_motion\\_database](http://peer.berkeley.edu/peer_ground_motion_database).



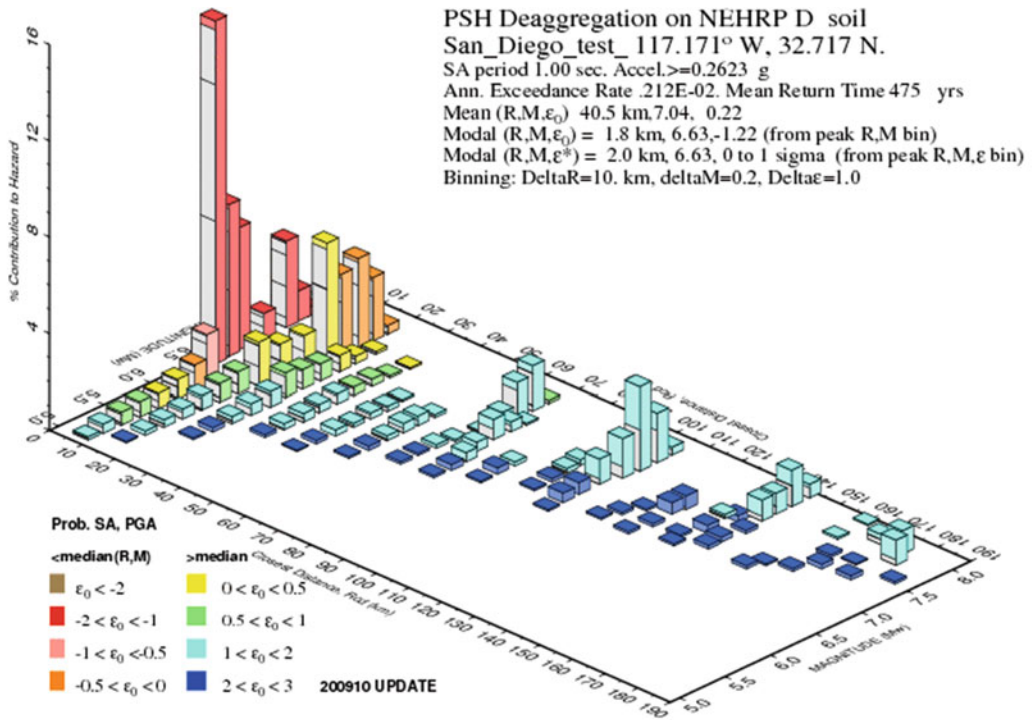
**Beginner's Guide to Fragility, Vulnerability, and Risk, Fig. 4** USGS interactive hazard deaggregation website

### Convenient Sources of Hazard Data

For California sites, see [www.OpenSHA.org/apps](http://www.OpenSHA.org/apps) for a very powerful hazard curve calculator. See <http://earthquake.usgs.gov/hazards/products/> for several sets of gridded hazard data from the National Seismic Hazard Mapping Program. For example, for the 2008 NSHMP hazard curves for  $S_a(1.0 \text{ s}, 5 \%)$ , see <http://earthquake.usgs.gov/hazards/products/conterminous/2008/data/> and look for the data file labeled “Hazard curve data 1 Hz (1.0 s).” If you use NMSMP’s hazard curves (as opposed to uniform seismic hazard maps), the data will reflect hazard on site class B, so adjust for other site classes. A good way to do that is by multiplying by the site coefficient  $F_a$  (for the 3.33 Hz or 5 Hz curves) or  $F_v$  (for the 1 Hz curves) from ASCE 7-10 Tables 11.4-1 and 11.4-2, respectively. You will also find at the

same location gridded uniform seismic hazard data such as the values of  $S_a(1.0 \text{ s}, 5 \%)$  with 2 % exceedance probability in 50 years (the so-called  $MCE_G$  map). For that map, see the data file labeled “Gridded Hazard Map 1 Hz (1.0 s) 2 % in 50 Years” at <http://earthquake.usgs.gov/hazards/products/conterminous/2008/data/>. For elsewhere in the world, see [www.globalquakemodel.org](http://www.globalquakemodel.org).

The risk analyst typically also needs a convenient and authoritative source of soil information. As of this writing, the USGS offers a global map of estimated average shearwave velocity in the upper 30 m of soil ( $V_{s30}$  in ASCE 7-10 notation). See <http://earthquake.usgs.gov/hazards/apps/vs30/> or Google “Global  $V_{s30}$  Map Server” for this useful resource. Find your latitude and longitude using Google Earth, then look up your



GMT 2015 May 18 15:28:42 Distance (R), magnitude (M), epsilon (ε₀) deaggregation for a site on soil with average vs: 325 m/s top 30 m. USGS CGMT PSH42006 UPDATE Bins with 110.05% contrib. omitted

**Beginner's Guide to Fragility, Vulnerability, and Risk, Fig. 5** Sample output of the USGS' interactive hazard deaggregation website

location at the USGS site by centering a grid around it, adding and subtracting 0.01 degrees of latitude and longitude for a Vs30 map about 2km × 2km grid centered at your location. See Wald and Allen (2007) for its technical basis. In the United States, the site data app at [www.OpenSHA.org/apps](http://www.OpenSHA.org/apps) is more powerful and easier to use. It offers the Wald-Allen Vs30 along with other sources, such as the Wills and Clahan (2006) map of Vs30 in California.

**Risk for a Single Asset**

**Risk**

This entry has dealt so far with fragility, vulnerability, and seismic hazard. Risk is analogous to hazard, but as used here it refers to the relationship between probability or frequency of the undesirable outcome and a measure of the degree of that undesirable outcome. If there are only two

possible values of that undesirable outcome – it occurs or it does not occur – one can apply the theorem of total probability, combining fragility and hazard, to estimate the mean frequency with which it occurs or the probability that it will occur in a specified period of time. If the undesirable outcome is measured in terms of loss, then one can apply the theorem of total probability, combining vulnerability and hazard, to estimate the mean annualized loss or the probability that at least a specified degree of loss will occur in a specified period of time. This entry deals with risk only for a single asset.

**Expected Failure Rate for a Single Asset**

Let  $F(s)$  denote a fragility function for a component with a single damage state and let  $G(s)$  denote the mean rate of shaking  $S \geq s$  (mean number of events per year in which the shaking is at least  $s$  at the site of interest). The mean rate of failures (number of times per year that the

component reaches or exceeds the specified damage state) is given by

$$\lambda = \int_{s=0}^{\infty} -F(s) \frac{dG(s)}{ds} ds \tag{34}$$

where  $G(s)$  = mean annual frequency of shaking exceeding intensity  $s$ . One can also use integration by parts and show that

$$\lambda = \int_{s=0}^{\infty} \frac{dF(s)}{ds} G(s) ds \tag{35}$$

If, for example,  $F(s)$  is taken as a cumulate log-normal distribution function,  $dF(s)/ds$  is the log-normal probability density function, i.e.,

$$\begin{aligned} F(s) &= \Phi\left(\frac{\ln(s/\theta)}{\beta}\right) \\ \frac{dF(s)}{ds} &= \phi\left(\frac{\ln(s/\theta)}{\beta}\right) \end{aligned} \tag{36}$$

Equation 34 only rarely can be evaluated in closed form. More commonly,  $G(s)$  is available only at discrete values of  $s$ . If one has  $n + 1$  values of  $s$ , at which both  $F(s)$  and  $G(s)$  are available, and these are denoted by  $s_i$ ,  $F_i$ , and  $G_i$ ;  $i = 0, 1, 2, \dots, n$ , respectively, then Eq. 34 can be evaluated numerically by

$$\begin{aligned} \lambda &= \sum_{i=1}^n \left( F_{i-1} G_{i-1} (1 - \exp(m_i \Delta s_i)) \right. \\ &\quad \left. - \frac{\Delta F_i}{\Delta s_i} G_{i-1} \left( \exp(m_i \Delta s_i) \left( \Delta s_i - \frac{1}{m_i} \right) + \frac{1}{m_i} \right) \right) \\ &= \sum_{i=1}^n (F_{i-1} a_i - \Delta F_i b_i) \end{aligned} \tag{37}$$

where

$$\begin{aligned} \Delta s_i &= s_i - s_{i-1} \quad \Delta F_i = F_i - F_{i-1} \\ m_i &= \ln(G_i/G_{i-1})/\Delta s_i \quad \text{for } i = 1, 2, \dots, n \end{aligned}$$

$$\begin{aligned} a_i &= G_{i-1} (1 - \exp(m_i \Delta s_i)) \\ b_i &= \frac{G_{i-1}}{\Delta s_i} \left( \exp(m_i \Delta s_i) \left( \Delta s_i - \frac{1}{m_i} \right) + \frac{1}{m_i} \right) \end{aligned}$$

Equation 37 is exact for piecewise linear  $F$  and piecewise loglinear  $G$ .

**Probability of Failure During a Specified Period of Time**

If one assumes that hazard and fragility are memoryless and do not vary over time, then failure is called a Poisson process, and the probability that failure will occur at least once in time  $t$  is given by

$$P_f = 1 - \exp(-\lambda \cdot t) \tag{38}$$

where  $\lambda$  is the expected value of failure rate, calculated for example using Eq. 37.

**Expected Annualized Loss for a Single Asset**

Now consider risk in terms of degree of loss to a single asset. There are many risk measures in common use. First, consider the expected annualized loss (*EAL*). It is analogous to mean rate of failures as calculated in Eq. 34. If loss is measured in terms of repair cost, *EAL* is the average quantity that would be spent to repair the building every year. It can be calculated as

$$EAL = V \int_0^{\infty} y(s) \frac{-dG(s)}{ds} ds \tag{39}$$

where  $V$  refers to the replacement value of the asset and  $y(s)$  is the expected value of loss given shaking  $s$  as a fraction of  $V$ . Equation 39 can only rarely be evaluated in closed form. More commonly,  $y(s)$  and  $G(s)$  are available at discrete values of  $s$ . If one has  $n + 1$  values of  $s$ , at which both  $y(s)$  and  $G(s)$  are available, and these are denoted by  $s_i$ ,  $y_i$ , and  $G_i$ ;  $i = 0, 1, 2, \dots, n$ , respectively, then *EAL* in Eq. 39 can be replaced by

$$\begin{aligned}
 EAL &= V \sum_{i=1}^n \left( y_{i-1} G_{i-1} (1 - \exp(m_i \Delta s_i)) \right. \\
 &\quad \left. - \frac{\Delta y_i}{\Delta s_i} G_{i-1} \left( \exp(m_i \Delta s_i) \left( \Delta s_i - \frac{1}{m_i} \right) + \frac{1}{m_i} \right) \right) \\
 &= V \sum_{i=1}^n (y_{i-1} a_i - \Delta y_i b_i)
 \end{aligned}
 \tag{40}$$

where

$$\begin{aligned}
 \Delta s_i &= s_i - s_{i-1} \quad \Delta y_i = y_i - y_{i-1} \\
 m_i &= \ln(G_i/G_{i-1})/\Delta s_i \quad \text{for } i = 1, 2, \dots, n
 \end{aligned}$$

$$\begin{aligned}
 a_i &= G_{i-1} (1 - \exp(m_i \Delta s_i)) \\
 b_i &= \frac{G_{i-1}}{\Delta s_i} \left( \exp(m_i \Delta s_i) \left( \Delta s_i - \frac{1}{m_i} \right) + \frac{1}{m_i} \right)
 \end{aligned}$$

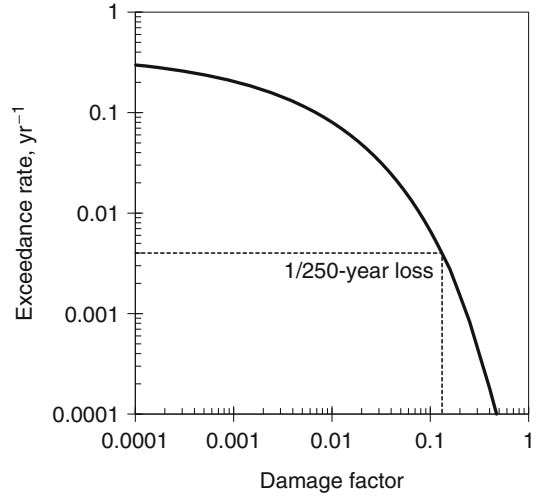
**Risk Curve for a Single Asset**

It is often desirable to know the probability that loss will exceed a particular value during a given time period  $t$  as a function of loss. Here, that function is called a risk curve or a loss-exceedance curve. It is like the hazard curve, except that the  $x$ -axis measures loss instead of excitation. Suppose one knows the hazard curve and the uncertain vulnerability function for a single asset. Figure 6 shows an example. The risk curve for a single asset can be calculated as

$$R(x) = \int_{s=0}^{\infty} -(1 - P[X \leq x | S = s]) \frac{dG(s)}{ds} ds
 \tag{41}$$

where

- $X$  = uncertain degree of loss to an asset, such as the uncertain damage factor,
- $x$  = a particular value of  $X$ ,
- $s$  = a particular value of the excitation, such as the shaking intensity in terms of the 5 % damped spectral acceleration response at some index period of vibration,



**Beginner's Guide to Fragility, Vulnerability, and Risk, Fig. 6** Sample risk curve. The *solid line* is the risk curve; the *dotted line* shows that the asset experiences a damage factor of 0.13 with an average exceedance rate of 0.004

- $R(x)$  = annual frequency with which loss of degree  $x$  is exceeded,
- $G(s)$  = the mean annual frequency of shaking exceeding intensity  $s$ ,
- $P[X \leq x | S = s]$  = cumulative distribution function of  $X$  evaluated at  $x$ , given shaking  $s$

If  $X$  is lognormally distributed at  $S = s$ , then

$$P[X \leq x | S = s] = \Phi \left( \frac{\ln(x/\theta(s))}{\beta(s)} \right)
 \tag{42}$$

where

- $\theta(s)$  = median vulnerability function, i.e., the value of the damage factor with 50 % exceedance probability when the asset is exposed to excitation  $s$ ,
- $v(s)$  = coefficient of variation of vulnerability, i.e., the coefficient of variation of the damage factor of the asset exposed to excitation  $s$ ,
- $\beta(s)$  = logarithmic standard deviation of the vulnerability function, i.e., the standard deviation of the natural logarithm of the damage factor when the asset is exposed to excitation  $s$ .

If one has the mean vulnerability function  $y(s)$  and coefficient of variation of loss as a function of shaking  $v(s)$ , use Eqs. 6 and 7 to evaluate  $\theta(s)$  and  $\beta(s)$ .

Suppose the analyst has  $y(s)$ ,  $v(s)$ , and  $G(s)$  at a number  $n$  of discrete values of  $s$ , denoted here by  $s_i$ , where  $i$  is an index  $i \in \{1, 2, \dots, n\}$ . One can numerically integrate Eq. 41 by

$$\begin{aligned} R(x) &= \sum_{i=1}^n \left( p_{i-1}(x) G_{i-1} (1 - \exp(m_i \Delta s_i)) \right. \\ &\quad \left. - \frac{\Delta p_i(x)}{\Delta s_i} G_{i-1} \left( \exp(m_i \Delta s_i) \left( \Delta s_i - \frac{1}{m_i} \right) + \frac{1}{m_i} \right) \right) \\ &= \sum_{i=1}^n (p_{i-1}(x) \cdot a_i - \Delta p_i(x) \cdot b_i) \end{aligned} \quad (43)$$

where

$$\begin{aligned} p_i(x) &= P[X \geq x | S = s_i] \\ &= 1 - \Phi \left( \frac{\ln(x/\theta(s_i))}{\beta(s_i)} \right) \end{aligned} \quad (44)$$

$$\Delta p_i(x) = p_i(x) - p_{i-1}(x) \quad (45)$$

$$\begin{aligned} \Delta s_i &= s_i - s_{i-1} \quad m_i = \ln(G_i/G_{i-1})/\Delta s_i \quad \text{for } i \\ &= 1, 2, \dots, n \end{aligned}$$

$$\begin{aligned} a_i &= G_{i-1} (1 - \exp(m_i \Delta s_i)) \\ b_i &= \frac{G_{i-1}}{\Delta s_i} \left( \exp(m_i \Delta s_i) \left( \Delta s_i - \frac{1}{m_i} \right) + \frac{1}{m_i} \right) \end{aligned}$$

Equation 43 is exact if  $p(x)$  and  $\ln G(s)$  vary linearly between values of  $s_i$ .

### Probable Maximum Loss for a Single Asset

There is no universally accepted definition of probable maximum loss (PML) for purposes of earthquake risk analysis, but it is often understood to mean the loss with 90 % nonexceedance probability given shaking with 10 % exceedance probability in 50 years. For a single asset, PML can be calculated from the seismic vulnerability function by inverting the conditional distribution

of loss at 0.90, when conditioned on shaking with 10 % exceedance probability in 50 years.

For example, assume that loss is lognormally distributed conditioned on shaking  $s$ , with median  $\theta(s)$  and logarithmic standard deviation  $\beta(s)$  as described near Eq. 42, which are related to the mean vulnerability function  $y(s)$  and coefficient of variation  $v(s)$  as in Eqs. 6 and 7. Under the assumption of Poisson arrivals of earthquakes, shaking with 10 % exceedance probability in 50 years is the shaking with exceedance rate  $G(s_{PML}) = 0.00211$  per year, so PML can be estimated as a fraction of value exposed by

$$PML = \theta(s_{PML}) \cdot \exp(1.28 \cdot \beta(s_{PML})) \quad (46)$$

where  $s_{PML} = G^{-1}(0.00211 \text{ year}^{-1})$ , that is, the hazard curve (events per year) inverted at 0.00211.

## Conclusions

This entry has provided a primer on fragility, vulnerability, and risk for the student or professional who is new to the topic. It briefly introduced basic concepts of fragility, vulnerability, hazard, and risk. Fragility is used to relate excitation, such as ground motion, to the probability that some undesirable event will occur, such as the probability that a component will become nonfunctional or that a building will be damaged. In some situations, multiple fragility functions can apply to the same asset; the entry presented three distinct situations and presented several approaches to deriving fragility functions and some useful sources of fragility functions. Vulnerability relates excitation to the degree of loss, such as the uncertain repair cost to a building. Three distinct approaches exist to deriving vulnerability functions: empirical, analytical, and expert opinion, each with its advantages and disadvantages. This entry briefly summarized the approaches, though it did not provide detail.

Hazard relates the exceedance probability or exceedance frequency to various levels of excitation, such as the rate at which earthquakes occur causing or exceeding various levels of spectral



acceleration response. The entry introduced probabilistic seismic hazard analysis, distinguished probability from exceedance rate, summarized some leading measures of excitation and conversion between them, explained hazard deaggregation, and offered some convenient sources of hazard data. Risk relates the degree of loss to its rate of exceedance, or it can express long-term average loss. This entry presented methods for estimating and depicting risk for a single asset.

## References

- American Society of Appraisers (2013) Definitions of value relating to MTS assets, Machinery & Technical Specialties Committee of the American Society of Appraisers. Reston VA, <http://www.appraisers.org/Disciplines/Machinery-Technical-Specialties/mts-appraiser-resources/DefinitionsOfValue>. Accessed 18 May 2015
- Ang AHS, Tang WH (1975) Probability concepts in engineering planning and design, 1 – basic principles. Wiley, New York, 409 pp
- Applied Technology Council (ATC) (1985) ATC-13, Earthquake Damage Evaluation Data for California. Redwood City, CA, 492 pp
- Applied Technology Council (ATC) (2012) Seismic performance assessment of buildings volume 1 – methodology FEMA P-58-1. Federal Emergency Management Agency, Washington, DC. <http://goo.gl/QN8AQz>
- Atkinson GM, Kaka SI (2007) Relationships between felt intensity and instrumental ground motion. *Bull Seismol Soc Am* 97:497–510
- Baker JW, Cornell CA (2005) A vector-valued ground motion intensity measure consisting of spectral acceleration and epsilon. *Earthq Eng Struct Dyn* 34(10):1193–1217
- Bazzurro P, Cornell A (1999) Disaggregation of seismic hazard. *Bull Seismol Soc Am* 89(2):501–520
- Cornell CA (1968) Engineering seismic risk analysis. *Bull Seismol Soc Am* 58(5):1583–1606
- European Seismic Commission Working Group—Macroseismic Scales (1998) European macroseismic scale 1998 EMS-98. Luxembourg. [http://www.gfz-potsdam.de/pb5/pb53/projekt/ems/eng/index\\_eng.html](http://www.gfz-potsdam.de/pb5/pb53/projekt/ems/eng/index_eng.html). Accessed 17 July 2006
- Faenza L, Michelini A (2010) Regression analysis of MCS intensity and ground motion parameters in Italy and its application in ShakeMap. *Geophys J Int* 180:1138–1152
- Field EH, Dawson TE, Felzer KR, Frankel AD, Gupta V, Jordan TH, Parsons T, Petersen MD, Stein RS, Weldon RJ II, Wills CJ (2007) The Uniform California earthquake rupture forecast, version 2 (UCERF 2). USGS open file report 2007–1437
- Jaiswal KS, Aspinall WP, Perkins D, Wald D, Porter KA (2012) Use of expert judgment elicitation to estimate seismic vulnerability of selected building types. Proc 15th World Conference on Earthquake Engineering, September 2012, Lisbon, Portugal
- Johnson GS, Sheppard RE, Quilici MD, Eder SJ, Scawthorn CR (1999) Seismic reliability assessment of critical facilities: A handbook, supporting documentation, and model code provisions, MCEER-99-0008. Multidisciplinary Center for Earthquake Engineering Research, Buffalo, NY, 384 pp
- Kaestli P, Faeh D (2006) Rapid estimation of macroseismic effects and ShakeMaps using macroseismic data. In: Proceedings of First European conference on earthquake engineering and seismology, Geneva
- Kaka SI, Atkinson GM (2004) Relationships between instrumental ground-motion parameters and Modified Mercalli intensity in Eastern North America. *Bull Seismol Soc Am* 94(5):1728–1736
- McGuire RK (1995) Probabilistic seismic hazard analysis and design earthquakes: closing the loop. *Bull Seismol Soc Am* 85(5):1275–1284
- Murphy JR, O'Brien LJ (1977) The correlation of peak ground acceleration amplitude with seismic intensity and other physical parameters. *Bull Seismol Soc Am* 67:877–915
- National Institute of Building Sciences and Federal Emergency Management Agency (NIBS and FEMA) (2009) Multi-hazard loss estimation methodology, Earthquake Model, HAZUS<sup>®</sup> MH MR4 Technical Manual. Federal Emergency Management Agency, Washington, DC
- NIST/SEMATECH (2013) e-Handbook of statistical methods. <http://www.itl.nist.gov/div898/handbook/>. Accessed 3 Mar 2015
- Porter KA (2009a) Cracking an open safe: HAZUS vulnerability functions in terms of structure-independent spectral acceleration. *Earthq Spectra* 25(2):361–378
- Porter KA (2009b) Cracking an open safe: more HAZUS vulnerability functions in terms of structure-independent spectral acceleration. *Earthq Spectra* 25(3):607–618
- Porter KA (2010) Cracking an open safe: uncertainty in HAZUS-based seismic vulnerability functions. *Earthq Spectra* 26(3):893–900
- Porter KA (2014) A beginner's guide to fragility vulnerability and risk, with solved exercises. Resource document. <http://spot.colorado.edu/~porterka/Porter-beginners-guide.pdf>. Accessed 28 Apr 2014
- Porter KA, Kennedy RP, Bachman RE (2007) Creating fragility functions for performance-based earthquake engineering. *Earthq Spectra* 23(2):471–489
- Porter K, Farokhnia K, Vamvatsikios D, Cho I (2014) Analytical derivation of seismic vulnerability functions for highrise buildings, global vulnerability

- consortium. Available from [www.nexus.globalquakemodel.org/gem-vulnerability/posts/](http://www.nexus.globalquakemodel.org/gem-vulnerability/posts/)
- Sørensen MB, Stromeyer D, Grünthal G (2007) Deliverable 4.1: generation of area-specific relationships between ground motion parameters (PGA, PGV) at certain sites, magnitude  $M$  and distance  $R$  to the causative fault and site intensities in terms of EMS-98. Databank of intensity data points and related parameters, seismic early warning for Europe. GFZ Potsdam 19–32, Potsdam, Germany
- Trifunac MD, Brady AG (1975) On the correlation of seismic intensity scales with the peaks of recorded strong ground motion. *Bull Seismol Soc Am* 65:139–162
- Tselentis GA, Danciu L (2008) Empirical relationships between modified Mercalli intensity and engineering ground-motion parameters in Greece. *Bull Seismol Soc Am* 98:1863–1875
- Wald DJ, Allen TI (2007) Topographic slope as a proxy for seismic site conditions and amplification. *Bull Seismol Soc Am* 97:1379–1395
- Wald DJ, Quitoriano V, Heaton TH, Kanamori H (1999) Relationships between peak ground acceleration, peak ground velocity and modified Mercalli intensity in California. *Earthq Spectra* 15(3):557–564
- Wesson RL, Perkins DM, Leyendecker EV, Roth RJ, Petersen MD (2004) Losses to single-family housing from ground motions in the 1994 Northridge, California, earthquake. *Earthq Spectra* 20(3):1021–1045
- Wills CJ, Clahan KB (2006) Developing a map of geologically defined site-conditions categories for California. *Bull Seismol Soc Am* 96(4A):1483–1501
- Wood HO, Neumann F (1931) Modified Mercalli intensity scale of 1931. *Bull Seismol Soc Am* 21:277–283
- Worden CB, Gerstenberger MC, Rhoades DA, Wald DJ (2012) Probabilistic relationships between ground-motion parameters and modified Mercalli intensity in California. *Bull Seismol Soc Am* 102(1):204–221

---

## Behavior Factor and Ductility

Christos A. Zeris

Department of Structural Engineering, Faculty of Civil Engineering, National Technical University of Athens, Athens, Greece

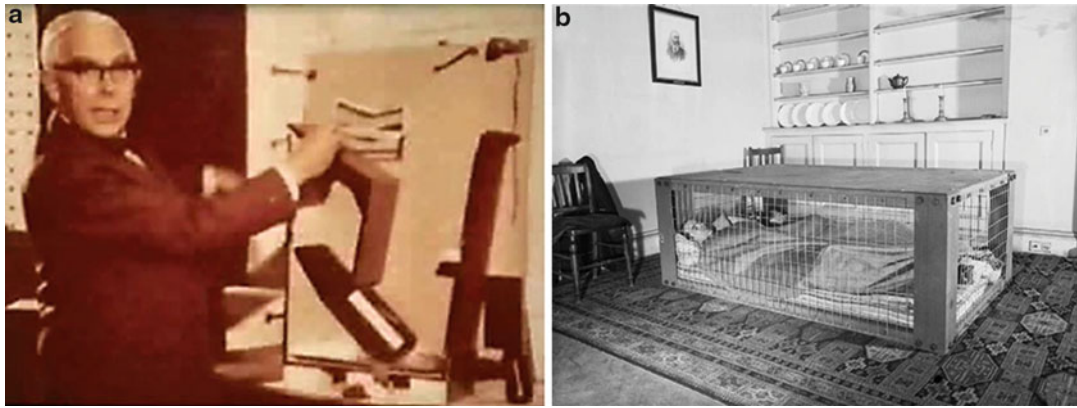
### Synonyms

Behaviour factor; Damage; Ductility; Inelastic design; Reinforced concrete; Response spectrum; Seismic design

## An Introduction: Evolution of Inelastic Design and Justification for Using a Behavior Factor for Extreme Transient Load Designs

The force-based design philosophy adopted by current design codes prescribes that the design of the structural system and the sizing and reinforcing of its structural elements are developed under prescribed equivalent statically applied forces. Structural design against seismic loads follows an ultimate limit state (ULS) design, since the excitation levels considered have very low probabilities of being exceeded. In this context, limit analysis of the structures is enforced possibly using a load factor and unfactored resistance approach or, in most cases, a partial factor – load and resistance factor – design approach (e.g., EC8 2004). Historically, earlier generations of seismic design codes adopted throughout the world a serviceability level approach, whereby the prescribed seismic loads were applied to the structure unfactored and the corresponding verification at the member level was evaluated using linear elastic analysis – including cracking, for reinforced concrete (RC) structures – and code prescribed allowable stress for the structural materials (concrete, reinforcement, structural steel or timber). These allowable stress limits were a factored percentage of the actual material strength and represented the safety factor built in the design inequality, since the loads were unfactored, thereby justifying linear elastic analysis. Such an allowable (working) stress force-based design has been the traditional design approach up until the 1970s in most seismically affected countries.

Direct inelastic design through limit analysis through the relaxation of the prevailing design assumption of an elastic response, accepting the fact that the structure can survive an extreme transient action by entering into the inelastic range in a controlled damage response, is traced in protective civilian designs against military action during World War II in England. Although plasticity theory, namely, the mathematical formulation of the ideal plastic flow of metal-type



**Behavior Factor and Ductility, Fig. 1** (a) Baron J. Baker demonstrating the effectiveness of a model Morrison shelter to survive a collapsed building floor following a bomb hit, with controlled inelastic deformation in order to ensure survival of its occupants ([http://en.wikipedia.org/wiki/Baron\\_Baker](http://en.wikipedia.org/wiki/Baron_Baker), also: <http://www-g.eng.cam.ac.uk/125/1925-1950/baker6.html>). (b) Picture of a Morrison shelter deployed inside a house for civilian protection ([http://en.wikipedia.org/wiki/Morrison\\_shelter#cite\\_note-21](http://en.wikipedia.org/wiki/Morrison_shelter#cite_note-21))

materials, was well developed in the early nineteenth century, it was at this time that through the formulation of the plasticity theorems that limit analysis design methods for reduced loading capacity were adopted, for the design of simple steel structures for civilian protection under extreme blast loads (Fig. 1). Specifically for seismic loading and following the observation/evaluation of the response of simple structures following severe earthquakes in California in the 1950s, it was demonstrated by Housner (1956) that a sufficient inelastic deformation supply by the structure through controlled (hierarchical) underdesign of the elements and local detailing resulted in these structures behaving in an acceptable manner during the extreme earthquake event.

Taking therefore into account the transient time-varying nature of the loading and of the response, the type of the loading and inertia effects, and the extreme magnitude of the load intensity, a reduction factor was proposed to be used in order to reduce the design force (therefore resistance) of the structure to levels (often considerably) lower than those required for full elastic response, at the expense of increased inelastic global (structural) and local (element, section) deformations of a controlled magnitude and distribution. This reduction is enforced through

recognizing (and thereby enforcing) the fact that such an intentionally (or accidentally) underdesigned structure with adequate ductility capacity will survive the extreme loading event scenario with tolerable inelastic deformations, to a level that is acceptable for the safety of its occupants and equipment. As an extension of this initial collapse limitation design approach adopted in the 1970s, additional intermediate performance requirements for occupants and equipment have been adopted, leading to a complete performance-based design (PBD) philosophy for the safety and/or operability of the structure, occupants, and equipment.

In order to reduce the design load for elastic response, a factor greater than 1.0 is adopted, which, depending on the code, is denoted as: the behavior factor  $q$  (Europe), the response reduction coefficient or response modification factor  $R$  (United States and the Americas), the structural performance factor  $S_p$  (New Zealand), or the structural characteristic factor  $D_s$  (Japan), all these factors denoted as the behavior factor  $q$  herein, for simplicity. The magnitude of  $q$ , obtained for (design) or by (assessment) the quantification of the limiting structural resistance versus the magnitude of the corresponding inelastic global or local element, section, or material inelastic deformations (axial or shear strains, flexural rotations,

and so on) – expressed as the corresponding ductilities  $\mu$  – and the interrelation of these two, is the topic of discussion of this entry.

## The Behavior Factor: Its Types, Definitions, and Uses in Seismic Design

### Behavior Factor for Ductility $q_\mu$ of SDOF Equivalent Structural Systems

The behavior factor for ductility (denoted as  $q_\mu$ ) of an inelastic SDOF system is defined, for a particular base excitation  $g(t)$ , as the ratio of its yield resistances  $R_y$  in order to develop two ductility levels, a prescribed ductility level  $\mu = \mu_i$  and a ductility  $\mu = 1.0$ , namely, entirely elastic response (Eq. 1):

$$q_\mu(T_0, \xi, f(R, \mu), g(t), \mu_i) = \frac{R_y(\max|\mu| = 1.0)}{R_y(\max|\mu| = \mu_i)} \quad (1)$$

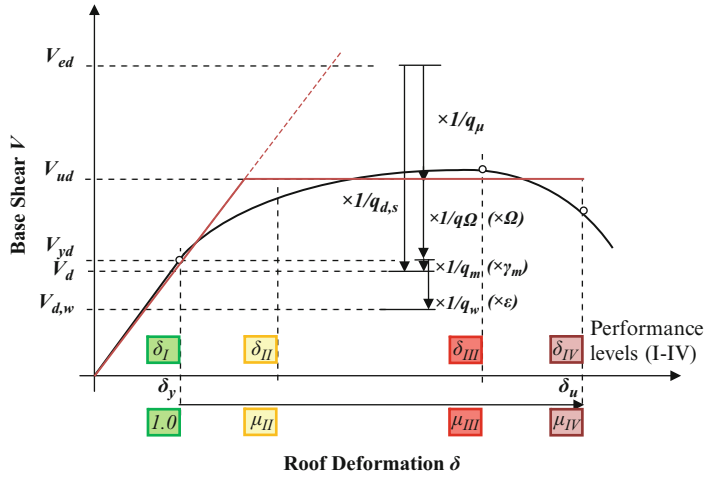
where  $q_\mu$ , besides  $g(t)$ , depends on the initial elastic response parameters, namely, elastic period  $T_0$  and critical damping ratio  $\xi$ , and on the parameters characterizing the inelastic response, namely,  $R_y$  and the cyclic hysteretic response shape  $f(R, \mu)$ .

Both terms of the fraction above are evaluated from time history integration of the equation of motion under the base excitation  $g(t)$ . Solution of the equation over a range of periods  $T_0$  yields the ductility spectrum for the given earthquake excitation, also denoted as the  $q_{\mu-\mu-T}$  spectrum of this excitation. For design applications, such spectra are evaluated for an ensemble of base excitation inputs characterizing the local seismicity of the region and local soil effects; the resulting average plus percent fractile  $q_{\mu-\mu-T}$  spectrum is obtained for the design and evaluation of structures in the region exhibiting compatible hysteretic response characteristics and initial damping. The definition of  $q_\mu$  and its dependence on structural and excitation parameters is discussed in section “[Evaluation of the Behaviour Factor Due to Ductility  \$q\_\mu\$  of SDOF Systems](#)” herein.

### Behavior Factors for Seismic Design or Evaluation and Redesign of Structural Systems, $q_d$ and $q_s$

The earliest use of a ductility reduction coefficient can be traced to the seismic design regulations in California, in which a force reduction coefficient was adopted depending on the building properties, namely, seismic resisting system and construction material. The 1959 edition of the Structural Engineers Association of California (SEAOC) Blue Book and its successive editions (e.g., SEAOC 1974) used this horizontal force factor  $K$ , in the context of an allowable stress design procedure, for the estimation of the design base shear. ATC (1978) was the first seismic design code that adopted an  $R$  factor greater than 1.00 as a divisor of the elastic design response spectrum (EDRS) forces, which depended on the type of structural system but was, as yet, independent of the building period. The early uses of  $R$  were based not only on SDOF analysis but, primarily, on consensus values through the earthquake engineering design community, with typical values of  $R$  and comparisons among different codes given in ATC (1995). Since then, the reduction coefficient  $R$  – initially as  $R_w$ , for codes based on working stress design methods such as UBC (1988) – has been adopted in all ultimate level design codes (e.g., NEHRP 1985; FEMA-356 2000; ASCE 2013). In Europe, Eurocode 8, from the initial stages of development (EC8 ENV 1988) up to the final completion (EC8 2004), also adopted the behavior factor  $q$ . To date, most modern force-based seismic design codes adopt the behavior factor approach for quantifying the seismic design forces, with different levels of rationalization for the magnitude of  $q$  ( $R$ ) (see, for instance, an overview of  $R$  factors adopted in South American seismic design codes in Chavez et al. 2012).

Based on the way the behavior factor is applied in seismic design, one can identify two uses of  $q$ , namely: (i)  $q_d$  – specified for the design of new buildings in order to control the ductility demand (and thus damage level) for a given site seismicity and performance level. This is specified in the seismic codes as the maximum allowed behavior factor for the design of modern



**Behavior Factor and Ductility, Fig. 2** Definition of the design and supplied (available) behavior factors  $q_d$  and  $q_s$  and the contributing  $q$ , for non-base-isolated structures: (i)  $q$  for ductility ( $q_\mu$ ), (ii)  $q$  for structural overstrength ( $q_\Omega$ ), and (iii)  $q$  for material strength reduction ( $q_m$  or  $q_w$ ).

In the context of PBD,  $q_{s,d}$  are no longer unique and depend on the local (and therefore global) ductility demands  $\mu_I$  to  $\mu_{IV}$  for different performance levels  $I$  to  $IV$ , respectively

structures. (ii)  $q_s$  – supplied (also called available) behavior factor of a given building (new or existing), corresponding to an anticipated elastic demand defined by the building period and the local EDRS, for a given ductility capacity and therefore damage level at specified performance levels ( $I-IV$ , Fig. 2) of this structure; for existing structures designed by past code generations, this behavior factor is usually below the currently enforced design  $q_d$  due to de facto underdesign coupled with insufficient or complete lack of ductile response of such structures.

$$V_{yd} = \frac{V_{ed}}{q_d} = \frac{C_{sd}W}{q_d} \tag{2}$$

where the EDRS is representative of the local seismicity, earthquake return period, and system equivalent damping. Modern design typically codes specify for RC buildings the 5 % EDRS, giving suitable adjustment multipliers for systems with other damping coefficients such as steel, timber, or prestressed concrete (e.g., the EDRS modification coefficient  $\eta = \sqrt{10/(5 + \xi)} \geq 0,55$  in EC8 (2004), where  $\xi$  is the percent critical damping).

**Behavior Factor  $q_d$  for Seismic Design of New Structures**

In the context of force-based seismic design, the design behavior factor  $q_d$  is a design force reduction coefficient greater than 1.0 by which the EDRS-specified base shear  $V_{ed}$  of the structure’s equivalent SDOF system representation (Fig. 2) is divided, in order to establish the seismic design base shear level  $V_d$  of this structure (Eq. 2), expressed as the product of the seismic coefficient  $C_{sd}$  times the inertial weight  $W$  of the structure for the seismic load combination:

Considering the typical base shear versus roof deformation response under increasing lateral load in Fig. 2, it can be seen that  $q_d$  can be expressed (Uang 1991; Whittaker et al. 1999) as the product of four behavior factors that relate the elastic base shear demand of the EDRS to the design base shear force as follows (Eq. 3):

$$q_d = q_\mu \cdot q_\Omega \cdot q_\xi \cdot \{q_m \text{ or } q_w\} \tag{3}$$

where:

- (i)  $q_\mu$  is the behavior factor for ductility of the equivalent SDOF system,  $q_\mu = V_{ed}/V_{ud}$ : this



factor relates the elastic spectral base shear demand  $V_{ed}$  to the equivalent SDOF bilinear yield strength  $V_{ud}$ , obtained by assuming an elastoplastic equal area approximation of the inelastic base shear–roof displacement response under a given lateral load profile, up to the ultimate deformation  $\delta_u$ . The value of this factor varies with the base excitation(s), the dynamic and inelastic hysteretic characteristics of the system (including structural damping), and its ductility. It corresponds to the basic design behavior  $q_s$  in EC8 (2004): for concrete structures  $q_s$  takes values between  $1.5 < q_s < 3.0$  and  $2.0 < q_s < 4.5$ , for ductility classes medium and high, respectively.  $q_\mu$  is established from SDOF analysis, as described in section “Evaluation of the Behaviour Factor Due to Ductility  $q_\mu$  of SDOF Systems” of this work.

- (ii)  $q_\Omega$  is the behavior factor for structural overstrength,  $q_\Omega = V_{ud}/V_{yd}$ , relating  $V_{ud}$  to the base shear  $V_{yd}$  at incipient onset of yield within the structural elements, at a roof deformation  $\delta_y$ . The value of this factor, which in EC8 (2004) is defined as the ratio  $\alpha_u/\alpha_1$ , accounts for the overstrength of the structure and depends on the type of structural system and the degree of redundancy built in the system: for instance, for a typical soft ground story pilotis structure with limited redistribution of inelastic actions in the members of the upper stories, this factor is close to 1.0. For medium-rise RC frame buildings, however, where seismic loads govern the design and members exhibit sufficient local ductility for redistribution,  $q_\Omega$  is of the order of 1.5–1.8, while for fully infilled RC frames with good-quality masonry construction,  $q_\Omega$  can easily reach values of 2.50 and higher (Repapis et al. 2006b). For low-rise RC frame buildings, overstrengths of 4.0 have been reported. This factor can be quantified through static or dynamic inelastic analysis

of the structure. Its magnitude and mode of evaluation are discussed in section “Building Behaviour Factor  $q_s$ ” herein.

- (iii)  $q_\xi$  is the behavior factor contribution due to increased critical damping  $\xi$ ; this contributing factor is meaningful for base-isolated or artificially damped systems, since the contribution of the initial mass proportional damping (rather than the hysteretic damping, which is included in  $q_u$ ) is not as significant in non-base-isolated structures. This factor is therefore not considered further herein.
- (iv)  $q_m$  (or  $q_w$ ) is the behavior factor due to material strength  $q_m = V_{yd}/V_d$  or  $q_w = V_{yd}/V_{dw}$ , relating the base shear at incipient member yield  $V_{yd}$  to the design base shear level specified by the code  $V_d$  (for ULS design) or  $V_{d,w}$  (for working stress design). This factor is practically the ratio of the material strength partial factor in load and resistance factor design, in order to relate the design material stress level (for EC2 2004, the characteristic strength  $f_{yk}$ ) to the yield strength ( $f_{yd}$ ) of the material controlling the response, namely, the steel reinforcement in modern structural RC designs; for EC2 (2004),  $q_m = f_{yk}/f_{yd} = 1.15$ . For buildings in Greece constructed during the 1970s using reinforcement with a yield strength of 400 MPa and designed for an allowable stress in flexural design calculations of 230 MPa with a 20 % increase for the seismic load combination,  $q_m = 400/1.2 \cdot 230 = 1.45$  (Repapis et al. 2006a). It has been proposed that the factor  $q_m$  may also include strength gain due to strain rate effects, although this increase is not a factor to take into account since it is counterbalanced by strength reduction by cyclic degradation.

This behavior factor is implicitly taken into account in the design of new buildings and is of primary importance since it defines the

transition from allowable design level to peak member resistance in the assessment of existing buildings, in which their members may behave in a brittle manner with very little deformability reserves.

#### Behavior Factor $q_s$ Supplied by an Existing Structure Under a Given EDRS

In the context of performance-based design (PBD), the available behavior factor  $q_s$  supplied by an existing structure can also be established for a given EDRS demand and at specific performance limits of damage. The structure may have been designed using a prescribed design behavior factor  $q_d$  (different than  $q_s$ ) or none at all, as the case is for older existing buildings which have been designed using past force-based design philosophies (e.g., working stress).

The available behavior factor  $q_s$  of the structure *as is* (often reevaluated after strengthening and/or rehabilitation of the structure at hand) is evaluated (i) through dynamic analyses of the structure until the establishment of a collapse base excitation, which is then compared to the design base excitation of the currently enforced EDRS for this type of structural system, or (ii) through static inelastic analyses of the structure, using an often idealized bilinear approximation of the resulting base shear resistance–roof deformation capacity curve under an imposed lateral deformation. Following an initial idealization of the structure as an equivalent SDOF system, with a yield resistance equal to the base shear at the onset of yielding in the building and an effective period equal to the initial secant stiffness from the lateral pushover curve,  $q_s$  is the behavior factor which results in a ductility demand equal to the ductility actually supplied by the system equivalent SDOF system. Contributions to  $q_s$  in this case are accounted from the structure overstrength or the member overstrength due to material  $q_m$ , relating the yield strength (also obtained from in situ evaluation of material capacity) to the design strength.

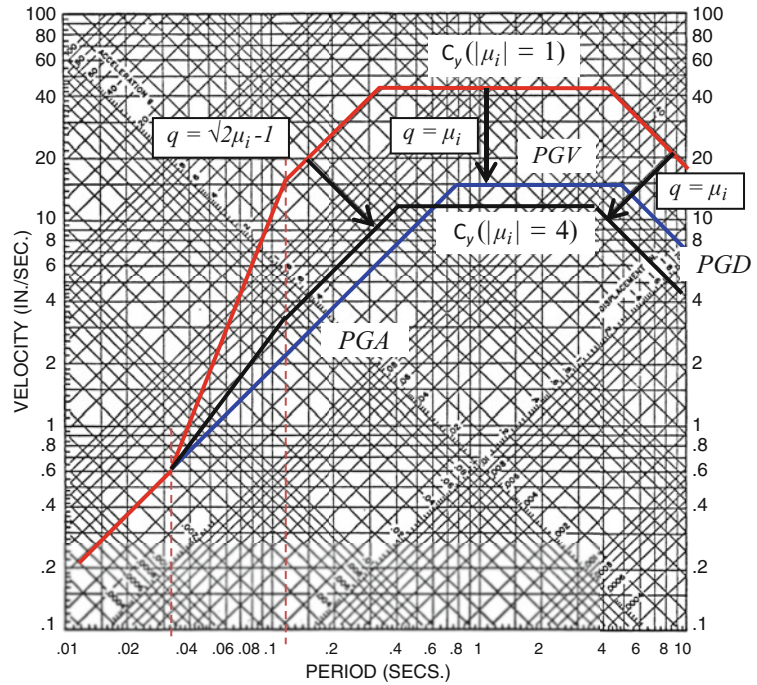
### Evaluation of the Behavior Factor Due to Ductility $q_\mu$ of SDOF Systems

The response of nonlinear SDOF systems under seismic excitation has traditionally been formulated in the form of  $q_{\mu-T}$  (or  $R_{\mu-T}$ ) spectra, representing an extension of earlier uses of such spectra, relating the ratio of yield to elastic resistance of the SDOF system ( $q_\mu$ ) to the corresponding displacement ductility  $\mu$ , under blast-type loads (Biggs 1964). Such inelastic response spectra (also known as shock spectra) have been formulated for different time-varying forcing shapes, such as impulse, triangular, or half sine, and are widely used in military and protective designs for blast. As discussed in the introduction, the use of such design load reductions has been well established in the design of protective structures against blast, where the introduction of a factored elastic design for controlled inelastic deformation was initially introduced.

The mathematics for the evaluation of the dynamic response of SDOF systems under seismic excitation is well established in textbooks of structural dynamics (Clough and Penzien 1975) and is not covered herein. The peak ductility demand  $\mu$  of a given inelastic system under a certain type of base (or force) excitation is obtained by step-by-step integration using explicit or implicit time integration procedures, depending on the duration of the forcing function. From the way the problem is posed in Eq. 1, given the SDOF characteristics ( $R_y, T_0, \zeta, f, g$ ), only the peak ductility can readily be estimated. Consequently, the numerical estimation of the  $q_{\mu-T}$  for a prescribed ductility  $\mu = \mu_i$  is necessarily an iterative process, involving successive iterative estimates of  $R_y$  and solution of the equation of motion to establish  $R_y(\max|\mu| = \mu_i)$ , for which the SDOF system attains a peak ductility  $\mu = \mu_i$ , e.g., using a variable bound bisection iterative solution scheme, to within a user-specified tolerance. Subsequent application of the procedure for  $\mu = 1$  as well (elastic response) will establish



**Behavior Factor and Ductility, Fig. 3** Indirect methods: Variation of  $q$  with period for ductility  $\mu_i = 4$  from the construction of the EDRS and the IDRS spectrum of the design base shear coefficient  $C_y$  according to the graphic methodology by Newmark and Hall (1973)



$R_y(\max|\mu| = 1)$  and  $q_\mu$ . It should be noted that in the case of strongly softening systems which are representative of structures with severe second-order effects or strength degradation, such an iterative solution may not converge, implying that the SDOF system may never attain this target ductility.

**Indirect Evaluation Methods**

For seismic design, the evaluation of the behavior factor through the formulation of an inelastic design response spectrum (IDRS) shape for a given seismicity condition – expressed in the form of a peak ground acceleration ( $PGA$ ), ground velocity ( $PGV$ ), and ground displacement ( $PGD$ ) at the site – has initially been based on indirect methods. Such methods specified amplification factors for the establishment of an EDRS and subsequent spectral reduction factors (i.e., period-dependent behavior factors) for constructing the IDRS. This approach was initially recognized by Veletsos and Newmark (1960), yet, later on, Newmark and Hall (1973) formulated the procedure for the construction of

the IDRS. Such indirect methods essentially provide  $q_\mu(\mu, T)$  relations, as a function of target  $\mu_i$ , for an assumed damping and form of inelastic hysteretic response (initially an elastic perfectly plastic (EPP) oscillator was considered).

Following estimations of SDOF inelastic response assuming EPP behavior and using limited accelerogram data available at the time, Newmark and Hall (1973) observed that (Fig. 3) (i) elastic and inelastic SDOF systems with sufficiently medium-to-long periods (medium-to-low frequencies) tend to displace equally and, consequently, the behavior factor is equal to the required ductility, (ii) elastic and inelastic SDOF systems with very short period (very high frequency) have spectral accelerations (and thus force demands) equal to the  $PGA$  and should be designed to remain elastic, and (iii) in between, the energy absorbed by an inelastic system having a yield strength  $1/q_\mu$  of the elastic demand and, as a consequence, deforming to a target  $\mu_i$  is nearly equal to the kinetic energy absorbed by the elastic SDOF system, thereby leading to an equal energy criterion between  $q_\mu$  and  $\mu_i$  (Fig. 3).

**Behavior Factor and Ductility, Table 1** Period dependent response reduction coefficients  $q_\mu$  following the Newmark and Hall (1973) procedure

Soil class EDRS region	I			II			III		
	<i>D</i>	<i>V</i>	<i>A</i>	<i>D</i>	<i>V</i>	<i>A</i>	<i>D</i>	<i>V</i>	<i>A</i>
$\mu_i = 1.5$	1.62	1.70	1.44	1.58	1.66	1.50	1.78	1.94	1.47
$\mu_i = 2.0$	2.28	2.21	1.76	2.16	2.19	1.83	2.46	2.70	1.79
$\mu_i = 5.0$	5.63	4.59	2.84	5.04	4.63	2.91	5.82	5.96	2.85

They therefore proposed the indirect construction of an IDRS from an EDRS, for a given target

ductility  $\mu_i$ , using the following period-dependent response reduction coefficients  $q_\mu$  (Eq. 4):

$$\begin{aligned}
 &0 \leq T < T_1/10 && q_\mu = 1 \\
 &T_1/10 \leq T < T_1/4 && q_\mu = \sqrt{2\mu_i - 1} \left(\frac{T_1}{4T}\right)^{2.513 \log\left(\frac{1}{\sqrt{2\mu_i - 1}}\right)} \\
 &T_1/4 \leq T < T'_1 && q_\mu = \sqrt{2\mu_i - 1} \\
 &T'_1 \leq T < T_1 && q_\mu = \mu_i \frac{T}{T_1} \\
 &T_1 \leq T < T_2, T_2 \leq T < 10 \text{ s} && q_\mu = \mu_i
 \end{aligned} \tag{4}$$

where  $T_1, T'_1$ , and  $T_2$  are the characteristic corner periods of the EDRS, defined from the peak ground response parameters (Newmark and Hall 1973):

$$\begin{aligned}
 T_1 &= 2\pi \frac{\phi_{ev} PGV}{\phi_{ea} PGA}, T_2 = 2\pi \frac{\phi_{ed} PGD}{\phi_{ev} PGV^2}, \\
 T'_1 &= T_1 \cdot \frac{\sqrt{2\mu_i - 1}}{\mu_i}
 \end{aligned} \tag{5}$$

where  $\phi_{ea}, \phi_{ev}, \phi_{ed}$  are the amplification factors defining the EDRS acceleration, velocity, and displacement from the corresponding  $PGA, PGV$ , and  $PGD$  for the site, defined by local seismicity considerations. Thus, in a log–log format, the Newmark and Hall  $q_\mu$ – $\mu$ – $T$  relation consisted of two constant  $q_\mu$  regions (Eq. 4) followed by intermediate linear transitions, as shown in Fig. 3. Based on a statistical parameter evaluation, they recommended averaged relations of  $PGV/PGA$  (48 in/s/g) and  $PGD/PGV^2$  (6 s/in.) and  $\phi_{ea}, \phi_{ev}, \phi_{ed}$  equal to 2.6, 1.9, and 1.4, respectively, for the construction of the EDRS at 5 % damping; different amplification values were given for stiff or soft soil or, in addition to the average values above, for average plus or minus one standard deviation.

Successive improvements of the indirect  $q_\mu$ – $\mu$ – $T$  construction model were proposed by Newmark and colleagues (for a review of the literature, see Miranda and Bertero 1994) (i) using additional ground motions and including the vertical excitation, (ii) for wider sets of critical damping ratios  $\xi$  (2–10 %) and target ductilities  $\mu_i$  (1–10), and (iii) for different hysteretic shapes  $f(u,t)$ .

Riddell (1995) extended the indirect method of evaluating  $q_\mu$  for different soil classification conditions, by considering 72 accelerograms which were obtained during the 1985 Chile earthquake, initially classified according to the prevailing soil conditions as records on rock (I), firm (II), and medium stiffness (III) soil sites. Following statistical analysis, soil-dependent corner frequencies and amplification values  $\Psi_\mu$  were proposed for obtaining the 5 % damping EDRS and the ductility-dependent IDRS, given the site  $PGA, PGV$ , and  $PGD$ , following the Newmark and Hall (1973) procedure. Based on the amplification factors reported, typical  $q_\mu$ , evaluated as  $q_\mu = \Psi_{\mu=1}/\Psi_\mu$  for  $\mu_i = 1.5, 2.0$ , and 5.0, are given below for the constant displacement ( $D$ ), velocity ( $V$ ), and acceleration ( $A$ ) regions of the EDRS (Table 1):

### Direct Evaluation Methods of $q_\mu$

Since the indirect evaluation of the behavior factor intrinsically included the uncertainty of both the elastic spectral amplification as well as the inelastic reduction, the scatter between target and actual ductilities or strength demands was high. Furthermore, use of a constant  $q_\mu$  over a period range or over the entire period range, as originally adopted in ATC (1978), was shown to be inadequate to limit the inelastic demands of SDOF systems, particularly for near-field earthquake events with severe velocity pulses (Mahin and Bertero 1981).

Consequently, direct methods of evaluating the behavior factor variation with period and ductility have been proposed, through statistical evaluation of SDOF time history analysis results. According to the direct estimation methodology, the elastic and inelastic response of a set of nonlinear SDOF oscillators over a period range was evaluated under a set of earthquake excitations and given oscillator characteristics, and the ratio of the required resistance of the system to remain elastic over that to develop a given ductility, as defined in Eq. 1, was evaluated in each case. The resulting variation of this ratio ( $q_\mu$ ) over the period range considered was statistically processed in order to establish  $q_{\mu-\mu-T}$  functional relations that directly fitted the corresponding spectra for the specific record(s) and oscillator characteristics. Although average prediction functions were often reported, several studies also gave sensitivity analyses or even additional equations to obtain the mean plus standard deviation approximation of the data.

An examination of the indirect method above for the construction of the EDRS and IDRS reveals the physical requirements for the variation of  $q_\mu$  with period for a given ductility  $\mu_i$  (Newmark and Hall 1973):

- (i) For very stiff systems, the SDOF system cannot develop any ductility and is therefore elastic; consequently, any functional describing a  $q_{\mu-\mu-T}$  variation must satisfy:

$$\lim_{T \rightarrow 0} q_\mu = 1$$

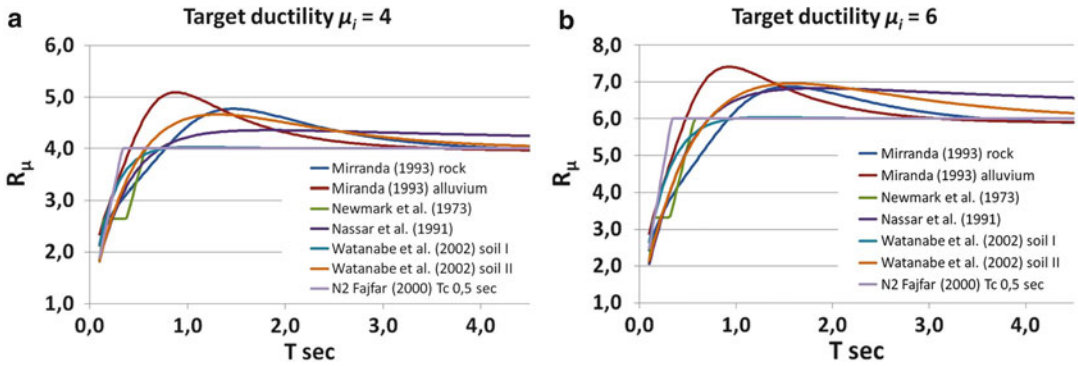
- (ii) For flexible long-period systems, the SDOF deformation of the elastic and the inelastic systems is equal to the imposed ground displacement; consequently  $q_\mu$  is equal to the SDOF ductility:

$$\lim_{T \rightarrow \infty} q_\mu = \mu$$

- (iii) In between, in the so-called constant velocity region, energies of the elastic and the inelastic systems are comparable. Direct and indirect methods of establishing  $q_\mu$  yield different requirements in this range.

Therefore, functional relations describing  $q_\mu$  in terms of period and ductility should satisfy these requirements. Such statistical estimations of  $q_\mu$  have shown that the latter limit is actually approached asymptotically from above (Nassar and Krawinkler 1991); however, the constraint imposed by the first limit has been relaxed in certain statistical studies in order to obtain better statistical correlations of  $q_{\mu-\mu-T}$  in the short period (Riddell 1995). A brief description of several such functional relations and the corresponding parametric studies involved are given herein; a graphical comparison of the different  $q_{\mu-\mu-T}$  spectral models for target ductilities  $\mu_i = 4$  and 6 is given in Fig. 4, as proposed by these studies.

**Influence of the SDOF oscillator inelastic characteristics.** One of the earliest proposed  $q_{\mu-\mu-T}$  expression that satisfied the functional limitations of the reduction factor spectrum by Newmark and Hall (1973) was the exponential function proposed by Nassar and Krawinkler (1991). In their statistical study, they considered 36 records to establish the attenuation of the ground motion parameters and 15 records from Western US earthquakes on firm-to-medium stiffness soils (plus 10 records from the Whittier Narrows earthquake, for verification) to establish  $q_\mu$ . Two hysteretic shapes were considered to



**Behavior Factor and Ductility, Fig. 4** Comparison of different  $q_{\mu}-\mu-T$  models for evaluating the behavior factor, for target ductilities of (a)  $\mu_i = 4$  and (b)  $\mu_i = 6$

model the hysteresis curve of the SDOF oscillator, namely, an EPP and a bilinear stiffness

degrading model. The  $q_{\mu}-\mu-T$  expression proposed is given in Eq. 6:

$$\begin{aligned}
 q_{\mu}(T, \mu, \alpha) &= (c \cdot (\mu_i - 1) + 1)^{1/c} \\
 \text{Elastoplastic systems } (\alpha = 0) & \quad c(T) = \frac{T}{T+1} + \frac{0.42}{T} \\
 \text{Elasto-hardening systems } (\alpha = 0.02) & \quad c(T) = \frac{T^{1.01}}{T^{1.01} + 1} + \frac{0.37}{T} \\
 \text{Elasto-hardening systems } (\alpha = 0.10) & \quad c(T) = \frac{T^{0.8}}{T^{0.8} + 1} + \frac{0.29}{T}
 \end{aligned}
 \tag{6}$$

The authors concluded that, with the exception of the short-period range, the stiffness degrading models with no hardening exhibited a 20 % higher behavior factor compared to the EPP system, with the effect diminishing for the 10 % hardening slope EPP and degrading oscillators. Furthermore, in addition to the quantification of the oscillator bias and based on the attenuation studies and the evaluation of the corresponding  $q_{\mu}$  for the subject datasets, they further established that  $q_{\mu}$  of SDOF systems for given  $\mu_i$  is not sensitive to the epicentral distance of the earthquake and the ground motion; this observation, however, is considered in more detail further on.

Lee and Han (1999) developed direct expressions of  $q_{\mu}$  for stiff soil and rock sites only, namely, soils exhibiting a shear-wave velocity larger than 750 m/s. In order to evaluate the

influence of the hysteretic response, they performed a statistical analysis of  $q_{\mu}-\mu-T$  using 40 ground motion records taking into account five different SDOF oscillator hysteretic shapes, namely, (i) EPP oscillator, (ii) bilinear hysteretic oscillator, (iii) degrading strength hysteretic oscillator, (iv) degrading stiffness oscillator (centered upon reversal), and (v) pinching hysteretic oscillator (in all cases initial damping of 5 % was assumed). They concluded that in the absence of the soil bias, additional factors that affect the  $q_{\mu}$  demand (given target ductility and period) are the hardening slope and the form and extent of pinching of the oscillator cyclic characteristic, in a statistically independent manner to each other. They subsequently proposed a  $q_{\mu}-\mu-T$  functional in terms of the hysteretic parameters  $\alpha_1, \alpha_2, \alpha_3,$  and  $\alpha_4$  (Eq. 7):

$$\begin{aligned}
q_\mu &= (0.99 \cdot \mu + 0.15) \left(1 - e^{-23.69 \cdot T \cdot \mu^{-0.83}}\right) \cdot C_{\alpha 1} \cdot C_{\alpha 2} \cdot C_{\alpha 3} \cdot C_{\alpha 4}, \text{ with :} \\
C_{\alpha 1} &= 1.0 + (2.07 \cdot \ln(\mu) - 0.28) \cdot \alpha_1 - (10.55 \cdot \ln(\mu) - 5.21) \cdot \alpha_1^2 \\
C_{\alpha 2} &= \frac{1}{(0.2 \cdot \mu + 0.42) \cdot \alpha_2 + 0.005 \cdot \mu + 0.98} \\
C_{\alpha 3} &= \frac{0.85 + (0.03 \cdot \mu + 1.02) \cdot \alpha_3}{1 + (0.03 \cdot \mu + 0.99) \cdot \alpha_3 + 0.001 \cdot \alpha_3^2} \\
C_{\alpha 4} &= \frac{1}{1 + 0.11 \cdot e^{(1.4 \ln(\mu) - 6.6) \cdot \alpha_4}}
\end{aligned} \tag{7}$$

where  $\alpha_1$  measures the hardening slope,  $\alpha_2$  measures the strength degradation upon reversal,  $\alpha_3$  measures the stiffness degradation, and  $\alpha_4$  measures the pinching response.

**Influence of the local soil conditions.** Miranda (1993) and Miranda and Bertero (1994) considered a wide dataset of ground motion excitations which had been previously classified according to the relevant earthquake parameters (magnitude, distance from the fault) and the local soil conditions prevalent at the site. Statistical equations of  $q_\mu$  in terms of the local soil conditions were subsequently obtained, proposing the following  $q_\mu$ - $\mu$ - $T$  evaluation function for different soil classifications (Eq. 8):

$$\begin{aligned}
q_\mu &= 1 + \frac{\mu_i - 1}{\Phi(T)} \\
\text{Rock sites} \quad \Phi(T) &= 1 + \frac{1}{10T - \mu_i T} - \frac{1}{2T} e^{-\frac{3}{2}(\ln T - 3/5)^2} \\
\text{Alluvium sites} \quad \Phi(T) &= 1 + \frac{1}{12T - \mu_i T} - \frac{2}{5T} e^{-2 \cdot (\ln T - 1/5)^2} \\
\text{Soft soil sites} \quad \Phi(T, T_s) &= 1 + \frac{T_s}{3T} - \frac{3T_s}{4T} e^{-3 \cdot (\ln(\frac{T}{T_s}) - 1/4)^2}
\end{aligned} \tag{8}$$

where, apart from the parameters defined already, the dominant soil period  $T_s$  was introduced for the soft soil sites. The analysis showed that there is a distinct trend in the shape of the  $q_\mu$ - $\mu$  curves for (primarily soft) soils that exhibit a predominant period, whereby in the vicinity of the oscillator resonance with the soil dominant period  $T_s$  ( $T/T_s \sim 1$ ), the behavior factor  $q_\mu$  is much larger than the target ductility (e.g.,  $q_{\mu i=3} = 8.5$  or  $q_{\mu i=5} = 18.0$  was obtained); this effect led to

conservative designs based on the  $q_\mu$ - $\mu$ - $T$  relations obtained on firm ground or alluvia proposed by other studies, while for lower  $T/T_s$  values, the opposite was observed, with the reduction factors in this case being lower than  $\mu_i$  (e.g.,  $q_{\mu i=3} = 2$  or  $q_{\mu i=5} = 2.8$  at  $T/T_s = 0.5$ ). Finally, for normalized periods above  $T_s$  ( $T/T_s > 2$ ), the behavior factor was close to the target ductility, as for stiff soils and rock, yielding similar or conservative designs compared to the use of rock spectra.

In order to investigate the influence of stiffness degradation on soft soils, Miranda and Ruiz-Garcia (2002) extended this study by expressing  $q_\mu$  in terms of the structural period normalized by the predominant soil period  $T_s$  (namely,  $q_\mu$ - $\mu$ - $T/T_s$ ), using a set of 116 ground motions on soft-to-medium soils and two hysteretic systems, a bilinear EPP and a stiffness degrading. It was shown that the influence of stiffness degradation was significant for soft soil excitations, since for period ratios lower than soil resonance, in the range of  $T/T_s \sim 2/3$  (also depending on  $\mu_i$ ), the average  $q_\mu$  of stiffness degrading systems was about 25 % lower than  $q_\mu$  of EPP systems, leading to unconservative designs based on the  $q_\mu$ - $\mu$ - $T$  relations obtained on firm ground for EPP systems. On the contrary,  $q_\mu$  of stiffness degrading systems at soil resonant periods and above was higher than that for EPP systems, indicating that the earlier onset of nonlinearity in these structures induced a drop in the required  $R_y$  for a given target ductility compared to EPP structures.

Vidiç et al. (1994) expressed  $q_\mu$  versus ductility relations in site-specific form, expressed in

terms of the accelerogram’s frequency parameter  $T_I$ , obtained at the period of change in slope of the idealized bilinear approximation of the pseudovelocity response spectrum  $PS_v(T, \xi)$  of the accelerogram. For their analyses they considered 24 records from California, Chile,

Italy, Montenegro, and the 1985 Mexico City earthquake, analyzing SDOF oscillators with either EPP or stiffness degrading characteristics, yielding the more general  $q_{\mu}-\mu-T$  exponential expression of Eq. 9 (a tangent stiffness proportional damping equal to 5 % critical was used):

$$\begin{aligned}
 & T < T_0 & q_{\mu} &= c_1(\mu_i - 1)^{c_R} \cdot \frac{T}{T_0} + 1 \geq 1, 0 \\
 & T_0 \leq T & q_{\mu} &= c_1(\mu_i - 1)^{c_R} + 1 \\
 & \text{where :} & T_0 &= c_2 \cdot \mu^{c_T} T_1 \\
 & \text{and :} & & \\
 \text{stiffness degrading SDOF :} & c_1 & c_2 & c_R & c_T \\
 & 0, 75 & 1, 0 & 0, 65 & 0, 30 \\
 \text{elastoplastic SDOF :} & 1, 10 & 0, 95 & 0, 75 & 0, 20
 \end{aligned} \tag{9}$$

In the context of PBD, Fajfar (1999) proposed more simplified conservative design envelopes for the estimation of the required target ductility

at a given  $q_{\mu}$  (Eq. 10), by adapting the statistical  $q_{\mu}-\mu-T$  estimations by Vidić et al. (1994) above in the N2 method:

$$\begin{aligned}
 & T < T_0 & q_{\mu} &= (\mu_i - 1) \cdot \frac{T}{T_0} + 1 \geq 1, 0 \\
 & T_0 \leq T & q_{\mu} &= \mu_i \\
 & \text{where :} & T_0 &= 0, 65 \cdot \mu^{0,3} T_c \leq T_c \\
 & \text{or, in a simplified form :} & T_0 &= T_c
 \end{aligned} \tag{10}$$

This expression has been adopted with refinements (soil effect, softening or hardening oscillator characteristics) as the displacement coefficient method (DCM) for PBD (NEHRP 1985; FEMA-356 2000), where  $q_{\mu}$  is equal to the coefficient  $C_I$  in the target roof estimation equation.

Riddell (1995) examined the influence of local soil conditions on  $q_{\mu}$  using 72 records obtained during the Magnitude 7.8 1985 Chile earthquake and aftershocks on rock (I), hard (II), or medium soil (III), as also previously described in the indirect evaluation method for  $q_{\mu}$ : following the indirect method analysis and recognizing that the variation in  $q_{\mu}$  was high, direct evaluation

expressions for spectral amplification factors  $\Psi(T, \mu)$  and therefore  $q_{\mu}$  in terms of ductility and period were also proposed, as being more reliable and less prone to statistical scatter than the former indirect method. The function proposed was of the exponential form given in Eq. 11 using five statistical parameters ( $\alpha_1-\alpha_5$ ) – although a dominant soil period was not explicitly considered (type IV soft soil records were not available).

$$\begin{aligned}
 q_{\mu} &= \frac{S_a(T, \mu = 1)}{S_a(T, \mu = \mu_i)}, \text{ where} \\
 \Psi(T, \mu = \mu_i) &= \frac{\alpha_1 + \alpha_2 \cdot T^{\alpha_3}}{1 + \alpha_4 \cdot T^{\alpha_5}}
 \end{aligned}$$



Soil Type	$\mu_i = 2$					$\mu_i = 5$				
	$a_1$	$a_2$	$a_3$	$a_4$	$a_5$	$a_1$	$a_2$	$a_3$	$a_4$	$a_5$
I	0,45	5,81	0,66	18,0	2,04	0,60	4,75	0,86	37,3	2,03
II	0,88	7,77	1,39	24,2	2,79	0,84	1,41	1,44	13,6	2,52
III	-33,96	35,65	0,005	1,4	2,62	0,86	0,06	2,967	2,303	2,72

The parameters were obtained from regression analysis after relaxing, for the sake of improved statistical correlation, the requirement that  $\Psi(T, \mu)$  should be equal to 1.0 for rigid structures.

Ordaz and Pérez-Rocha (1998) considered the direct evaluation of  $q_\mu$  as a force reduction parameter from the elastic relative displacement spectrum  $S_d$ , since both the inelastic and elastic displacements of the SDOF system are related to the ductility and  $q_\mu$ , the variation of  $S_d$  with period being the controlling factor for the variation of  $q_\mu$ , and also  $S_d$

includes local soil effects. They therefore proposed a functional for  $q_\mu$  in terms of the spectral displacement amplification  $S_{d/PGD}$  instead of  $T$  (Eq. 12) since, implicitly, it is a function of the period  $T$ . For their statistical analysis, they considered 445 records over a wide range of magnitudes, epicentral distance, and local soft soil to rock conditions.

$$q_\mu = 1 + (\mu_i - 1) \cdot \left( \frac{S_d(T)}{PGD} \right)^{\beta(\mu)}, \text{ where}$$

$$\beta(\mu) = 0.388 \cdot (\mu - 1)^{0,173}$$

Soil Type	$\mu_i = 2$			$\mu_i = 4$			$\mu_i = 6$		
	$a$	$b$	$c$	$a$	$b$	$c$	$a$	$b$	$c$
I	1,29	2,77	0,0218	1,12	2,18	0,0777	2,35	1,69	0,0080
II	1,12	2,18	0,0416	,989	1,62	0,2037	1,52	1,05	0,1334
III	2,35	1,69	0,0418	1,03	1,24	0,2707	1,85	,821	0,1184

Their expression  $q_{\mu-\mu-S_d(T)/PGD}$  yielded similar results as the proposed direct  $q_{\mu-\mu-T}$  relations by other investigators (e.g., Nassar and Krawinkler (1991) or Miranda (1993)), for either firm or soft soil, yet, unlike previous studies, is of a more general applicability over the entire range of soil types considered.

Watanabe and Kawashima (2002) investigated in detail the scattering of  $q_\mu$  from the mean value as well as the influence of initial damping under elastic and EPP inelastic response, using 70 free-field records from a relatively large dataset from Japanese earthquakes: ground motions were classified according to different soil conditions with predominant soil period  $T_g$ , following the Japanese seismic design

code classification. They showed that their predictions of the average  $\bar{q}_\mu$  approach reasonably well the equal energy and equal displacement approximation (Fig. 3). However, the average minus one standard deviation ( $\sigma_{q_\mu}$ ) values differ significantly from this simplification and on the unconservative side, since ( $\sigma_{q_\mu}$ ) increases disproportionately, and therefore, the use of  $\bar{q}_\mu$  for design may be unconservative, especially for larger target ductilities. They then proposed an exponential  $q_{\mu-\mu-T}$  relation and the corresponding expression for  $\sigma_{q_\mu}$  in Eq. 13:

$$q_\mu = 1 + (\mu_i - 1) \cdot \Psi(T), \text{ where}$$

$$\Psi(T) = 1 + c \cdot \frac{T - a}{e^{b(T-a)}}, c = \frac{1}{(a \cdot e^{ab})}$$

Soil Type	$\mu_i = 2$			$\mu_i = 4$			$\mu_i = 6$		
	<i>a</i>	<i>b</i>	<i>c</i>	<i>a</i>	<i>b</i>	<i>c</i>	<i>a</i>	<i>b</i>	<i>c</i>
I) $T_g < 0.2s$	1,29	2,77	0,0218	1,12	2,18	0,0777	2,35	1,69	0,0080
II) $T_g < 0.6s$	1,12	2,18	0,0416	,989	1,62	0,2037	1,52	1,05	0,1334
III) $T_g > 0.6s$	2,35	1,69	0,0418	1,03	1,24	0,2707	1,85	0,821	0,1184

and  $\sigma_{q_\mu} \sim 0.4 \cdot \mu_i - 0.3$  (all soil classes)

Additional soil-dependent  $q_{\mu-\mu-T}$  functions were proposed by Genshu and Yongfeng (2007) with a range of application of  $\mu_i$  between 1.0 and 6.0 and a period range between 0.1 and 6.0 s. A dataset of 370 records was used, divided according to the prevailing soil conditions at the site and classified in accordance with the four soil-type classifications adopted in the Chinese seismic code. Four different hysteretic oscillator characteristics were considered, namely, (i) an EPP model, (ii) a bilinear with hardening (5 %, 10 %, and 20 % hardening stiffness) and pinching

hysteresis, (iii) a shear slip model, and (iv) a bilinear elastic oscillator, in order to establish the influence of energy absorption. Three critical damping ratios were considered, namely, undamped, 3.5 % critical, and 5 % critical. Following a sensitivity study, the resulting  $q_{\mu-\mu-T}$  spectra were correlated to the ratio of  $T/T_g$ , where  $T_g$  is the characteristic ground motion period of each record, defined as the period at which  $q_\mu$  was maximized. They therefore proposed expressions with  $T$  for the estimation of  $q_\mu$  with 90 % confidence,  $q_{\mu,90}$  (Eq. 14):

$$q_{\mu,90} = \begin{cases} 1 + 0.36 \cdot [(2.5 \cdot \mu_i - 2)^{0.75} - 1] \cdot \left(\frac{T}{T_g}\right)^{(0,6-T/T_g)}, & 0 < T \leq 0.6T_g \\ 1 + [(2.5 \cdot \mu_i - 2)^{0.75} - 1] \cdot \left(\frac{T}{T_g}\right)^2, & 0.6T_g < T \leq T_g \\ (2.5\mu_i - 2)^{0.75} - [(2.5\mu_i - 2)^{0.75} - 0.5 - 0.6\mu_i] \left(\frac{T-1}{\chi-1}\right)^{2/\mu_i}, & T_g < T \leq \chi T_g \\ 0.5 + 0.6 \cdot \mu & , \chi \cdot T_g < T \end{cases}$$

Soil Type	A	B	C	D	(14)
$\chi$	1.5	2.1	2.5	3.0	

where  $\chi$  is a coefficient depending on the soil class. Their statistical analysis confirmed that expressing  $q_\mu$  in terms of the ratio  $T/T_g$  reduced the statistical scatter, making the governing parameter the target ductility; little influence of the critical damping and the hysteretic shape, apart from the short-period range, was observed on the magnitude of  $q_\mu$ .

**Influence of seismological and ground motion characteristics for near-field excitations.** So far, the overall consensus of the SDOF

studies reported has been (and the statistics proved it so) that the earthquake magnitude was not a governing parameter for the quantification of  $q_\mu$ , thereby the effort for parameter identification concentrated on the target ductility, the oscillator hysteretic shape, the damping, and, primarily, the soil characteristics and its predominant period.

Mavroeidis et al. (2004) investigated further the seismicity bias by considering the pulse duration  $T_p$  of near-field ground motions and

its effect on the strength demands for a given  $\mu_i$  of EPP systems. The pulse duration observed in near-field records was shown on geophysical (source mechanism) terms to be about twice the rise time of the rupture process generating the earthquake, namely, the time it takes for a point on the fault to reach the maximum fault displacement, which, therefore, was well

correlated to the earthquake moment magnitude  $M_w$ . Subsequent inelastic SDOF analyses using near-field pulses demonstrated that  $T_p$  was an important parameter for near-field events, particularly through the establishment of amplification factors along the lines of a modified Eq. 4 (Newmark and Hall 1973), in terms of  $T/T_p$  (Eq. 15):

$$q_\mu = \begin{cases} 1 & \frac{T}{T_p} < \left(\frac{T}{T_p}\right)_a \\ \sqrt{2\mu_i - 1} & \left(\frac{T}{T_p}\right)_b < \frac{T}{T_p} < \frac{\sqrt{2\mu_i - 1}}{\mu_i} \left(\frac{T}{T_p}\right)_c \\ \mu_i & \frac{T}{T_p} > \left(\frac{T}{T_p}\right)_c \end{cases}$$

where:

$M_w$	$\left(\frac{T}{T_p}\right)_a$	$\left(\frac{T}{T_p}\right)_b$	$\left(\frac{T}{T_p}\right)_c$	$\phi_{ev}$	$\phi_{ea}$
5.6 – 6.3	0.035	0.35	0.75	2.10	0.95
6.4 – 6.7	0.010	0.2	0.75	2.0	0.75
6.8 – 7.6	0.002	0.055	0.75	1.55	0.43

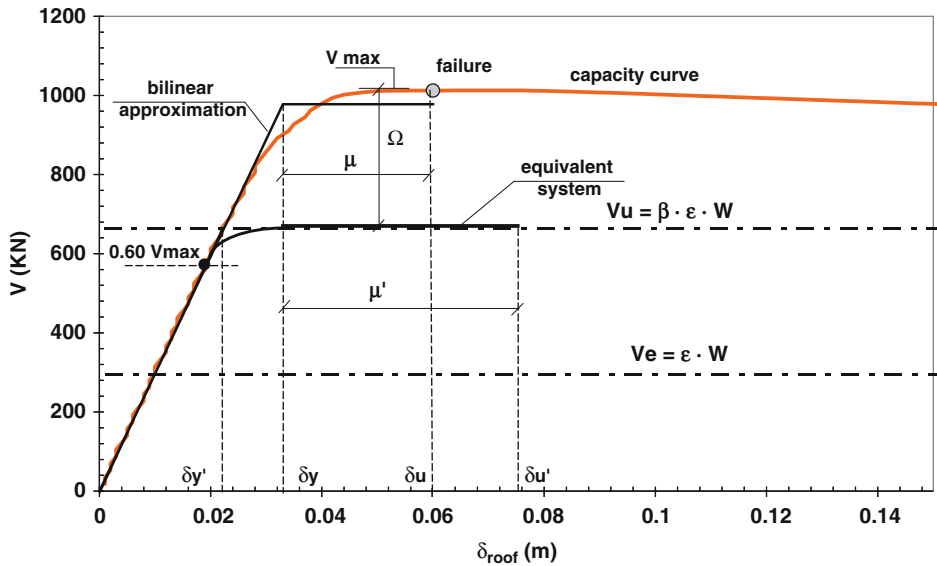
(15)

Gillie et al. (2010) also considered the sensitivity of the  $q_{\mu-\mu-T}$  relations of EPP systems on the fault directivity effects in near-field earthquake motions, namely, the content of a strong velocity pulse. Their study was based on a dataset of 82 near-field acceleration records with velocity pulse content due to fault directivity effects. They demonstrated that, in the near-field case, unlike the prevailing notions on published  $q_{\mu-\mu-T}$  functionals from statistical analysis of both near- and far-field events, there was a much stronger dependence of  $q_\mu$  on the earthquake magnitude and a much smaller dependence on the local soil conditions. Recognizing this dependence, they therefore examined the dependence of  $q_\mu$  to the predominant period  $T_p$  of the velocity pulse content or, equivalently, to  $T_{RSV}$ , the period at the peak velocity of the elastic velocity spectrum, which was found to be the influencing parameter for the magnitude of  $q_\mu$ . Overall, near-field events were proven to demand by the SDOF oscillators

lower  $q_\mu$  than those with no directivity effects, such as those considered by previous  $q_{\mu-\mu-T}$  relations proposed so far in the literature. They therefore also proposed  $q_\mu$  relations for near-field seismic events in terms of  $M_w$  (range of 6.0–7.5), since both  $T_p$  and  $T_{RSV}$  are not known a priori for a given earthquake; however, they are adequately correlated with the earthquake magnitude.

### Building Behavior Factor $q_s$

In addition to the development of IDRS and ductility-dependent behavior factors of SDOF systems, considerable interest has been given to the evaluation of the available behavior factor supplied by entire structural systems ( $q_s$ ) following different performance criteria, also compared to the behavior factor specified by modern building codes for design ( $q_d$ ) following allowable stress, ULS, or PBD design procedures. Such studies have been specifically related to typical RC or steel building construction, either modern designs according to a particular seismic design code or existing structures, designed using past regulations. The purpose of such studies aimed for the evaluation, calibration, or reliability analysis (often using stochastic analysis procedures) of the behavior factor(s) specified by the subject



**Behavior Factor and Ductility, Fig. 5** Evaluation of the overstrength, the ductility, and the behavior factor of an existing RC structure (From Repapis et al. 2006a)

code or structural system under scrutiny. Although most studies (especially related to code design parameter calibration and reliability analysis) have been aimed toward the evaluation of the overall design behavior factor  $q_s$ , studies of specific structural systems (e.g., RC shear wall or steel braced frame structures) have also been concerned with the evaluation of the behavior factor due to overstrength  $q_\Omega$ .

Generally, the evaluation of  $q_s$  of a new or an existing structure is based on either static push-over (SPO) or time history inelastic analyses under an earthquake excitation set. The resulting  $q$  is particular to the building type and structural material under scrutiny, the EDRS, and the performance level criteria adopted, as well as the entire set of underlying code-specific design requirements inherent in the seismic design of the structure. Such requirements include, among others, the design load level during earthquake, the relative magnitude of gravity and seismic loads under the seismic load combination, limiting section geometry or reinforcement requirements, the degree of conservatism in the design, the code prescribed detailing rules, and so on. Hence, these behavior factors can only be

used for the corresponding design environment over which they have been calibrated for.

### Evaluation of the Behavior Factor Using SPO Analysis

The evaluation of  $q_s$  using SPO methods involves the estimation of the capacity curve of the structure under a prescribed lateral load and/or displacement profile (modal, triangular, constant, adaptive) and crucial modeling assumptions (among others) of the strength and stiffness dependence of the member characteristics (also the finite element formulation itself), of the foundation and the joint models, including or not the second-order effects at the global and local element level. Following the definition of a set of local and global failure criteria (the damage indices), the available global ductility of the structural model is evaluated at the minimum roof deformation at incipient satisfaction of any of these indices, over the onset of yield roof deformation. Repapis et al. (2006a) have adopted SPO procedures in order to evaluate the available  $q_s$  and also  $q_\Omega$  of existing RC plane irregular frames, typical of structural designs between the 1960s and 1990s in Greece (Fig. 5). Their results were

compared to dynamic analysis estimates of  $q_s$ , as described in the next section.

### Evaluation of the Behavior Factor Using Dynamic Analysis

Several analytical estimations of  $q_s$  based on dynamic analysis have been published, in order to calibrate or verify the reliability of the behavior factor as a static analysis parameter in force-based seismic design, against local or global damage predictions. Two methods, the direct and the indirect method, have been proposed for evaluating  $q_s$  of a building using dynamic analysis (EC8 ENV 1988). Recently, in FEMA P-695 (2009), the procedure is formalized for a uniform reliability of evaluating  $q_s$  and  $q_\Omega$  in PBD.

(a) **Indirect evaluation of  $q_s$ .** A building initially designed for a given EDRS (shape, PGA equal to  $A_d$ , critical damping, and a design behavior factor  $q_d$ ) is analyzed in the time domain under a base excitation whose response spectrum matches the EDRS entirely or locally in the vicinity of the initial period of the structure for the same critical damping. The PGA is linearly increased until incipient violation of any of a set of failure criteria, at the nominal collapse value of  $A_c$ . The behavior factor  $q_s$  is equal to

$$q_s = q_d \cdot \frac{A_c}{A_d} \quad (16)$$

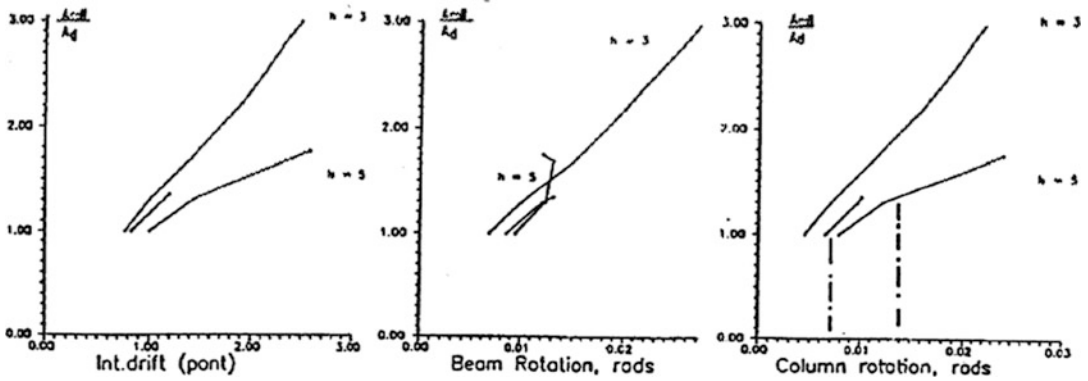
The process is repeated for different earthquake input sets, and a statistical estimate of  $q_s$  is established for this type of building, design procedure, and performance criteria. The method suffers from the drawback that the performance indices do not depend linearly on the PGA (Kappos 1991); however, it has been commonly used since  $q_s$  is obtained at the expense of only one initial structural design and model formulation. This method falls closely with the application of the incremental dynamic analysis method (IDA) proposed by Vamvatsikos and Cornell (2003) for evaluating existing structural systems.

(b) **Direct evaluation of  $q_s$ .** A set of collapse criteria is adopted together with an EDRS (shape, PGA, and damping) and a set of base excitation records matching the specific EDRS. The structure is designed for the assumed EDRS in a repetitive manner, initially assuming a design  $q_d$  as proposed by the code and, subsequently, for increasing (or possibly decreasing) values of  $q_d^i$  for each  $i_{th}$  design iteration; decreasing values may need to be considered in irregular or non-ductile structures in regions of high seismicity. For each  $i_{th}$  design, an inelastic model of the structure is formulated and analyzed over the design earthquake set. This design – analysis procedure – is repeated until any of the preset collapse criteria is incipiently violated: this limiting  $q_d^i$  is the behavior factor  $q_s$ .

$$q_s = \max(\text{or min})q_d^i \quad (17)$$

In this case, a direct redesign method is adopted for  $q_s$  at the expense of several structural (re)designs. As before, the resulting behavior factor is a function of the design assumptions as well as the performance level evaluation criteria and the design record set.

Kappos (1991) applied the direct method for the evaluation of  $q_s$  for two typical RC plane frames, namely, a moment frame and a dual frame-wall system, designed according to EC8 ENV (1988) for medium ductility class using a  $q_d$  of 3.50 and 2.10, respectively. Using performance limits of total and interstorey drift, member shear capacity, and local curvature ductility  $\mu_\varphi$ , the resulting available  $q_s$  were evaluated to be 4.9 and 3.4 of the bare frame and the dual system, respectively. Different criteria governed for each structure and base excitation: for the bare frame system, the story drift limit governed, while for the dual system, member failure governed the response (the ground story columns). Zeris et al. (1992) applied the direct method to medium-height RC frames with a relatively taller ground story designed according to EC8 ENV (1988) for ductility class II and a  $q_d$  of 3.50, observing design code limitations (e.g., member



**Behavior Factor and Ductility, Fig. 6** Variation of the structural behavior factor  $q_s$  of a tall first-story building with base excitation amplitude (Zeris et al. 1992)

**Behavior Factor and Ductility, Table 2** Comparison of building  $q_s$  using static and dynamic analysis for three excitations (minimum value, mean, and standard deviation) (Zeris et al. 2005)

Frame building type	$q$ (SPO)	$q$ (IDA)		
		$\bar{q}$	$q_{min}$	$\sigma_q$
Nonconforming ordinary frame, Zone I	2.03	2.18	1.92	0.33
Nonconforming ordinary frame, Zone II	1.77	3.15	2.43	1.25
Nonconforming frame with tall first story	2.34	2.82	2.41	0.70
Nonconforming frame with a recess	1.55	2.78	2.36	0.39
Nonconforming frame with discontinuous column	1.98	4.31	2.87	2.48
Nonconforming frame with discontinuous beam	2.14	2.12	1.81	0.43
Conforming ordinary frame, Zone I	5.44	6.78	5.22	1.84

geometry, reinforcement detailing). Adopting failure limits in interstory drift and  $\mu_\varphi$  as a function of confinement, it was shown that for a  $\mu_\varphi$  of 5 and 10, the  $q_s$  of the regular RC frame was 4.4 and 7.1, while the tall first-story frame was marginally able to satisfy the  $\mu_\varphi$  limit of 5.0 at  $q_s = q_d = 3.5$ , supplying a  $q_s = 4.6$  for  $\mu_\varphi = 10$  (Fig. 6).

For the case of modern building designs, Kappos (1999) and Borzi and Elnashai (2000) evaluated the ductility and  $q_s$  of typical low- to medium-rise RC buildings designed according to the CEB model seismic code or EC8, using both SPO and dynamic analysis SPO. In addition to comparisons of SDOF  $q_\mu$  predictions of their record datasets with those available in the literature (e.g., by Miranda and Bertero 1994), the problems associated with comparing  $q_\mu$  of entire structural systems (after excluding  $q_\Omega$ ) with

SDOF analysis were considered in detail. The studies concluded that the design behavior factor in EC8 was conservative for the cases considered, although their results were conflicting (proving the fact that the design and building bias affects the end result), attributing the conservatism of  $q_s$  to either the structural overstrength or the ductility supply or both.

In order to establish  $q_s$  of typical existing irregular buildings in Greece constructed in the 1960s and 1970s, Zeris et al. (2005) applied IDA analysis methods for evaluating  $q_s$  using the indirect method of evaluation; these values were compared with values obtained from SPO analysis by Repapis et al. (2006b), taking into account both interstory drift and local critical region rotational ductility limits comparable to the previous study. The resulting estimates are compared in Table 2, showing that (i) the available behavior



factors are well below currently adopted and (ii) dynamic analysis predictions of  $q_s$  for irregular buildings tend to be more conservative than those using dynamic analysis, being closer to the minimum predictions obtained in the latter case.

Chryssanthopoulos et al. (2000) evaluated the reliability of the design behavior factor  $q_d$  adopted by the Eurocode for the case of a regular ten-story RC frame designed for ductility class M. Using the indirect method of evaluation of the available  $q_s$ , they assumed a statistical variation of the structural material properties (concrete and steel yield strength and ultimate failure strain of the reinforcement), the uncertainty in confinement (and therefore supplied  $\mu_\varphi$  in the critical regions), and a set of spectrum compatible base excitation records, in order to evaluate the reliability of ULS design following EC8 recommendations for the subject building. At the same time, they established the variation of the available  $q_s$  of the subject frame under the base input set. They concluded that for a seismic hazard model with a return period of 475 years for Southern Europe, the violation of the initial design value ( $q_d$ ) of 3.75 was to be expected in 0.6 % of the frames exhibiting this type of building and design characteristics and the material property variability assumed.

## Summary and Conclusions

It should be noted at the outset that such an intentional underdesign approach (i.e., using a behavior factor) is by no means a socially irresponsible approach from the point of view of the engineers' role to the society. It is well accepted that economic limitations and design feasibility will define the intensity level that is socially acceptable for the design of structures for the extreme earthquake; furthermore, it is well known that the gradual increase of records through more dense earthquake monitoring grids of digital instruments has proven more and more often that the actual seismic load intensity at a site will surprise us, when an extreme

earthquake event happens. Consequently, until sufficient seismic data are available, structures will continue to be constructed in regions in which, historically or otherwise, a fault was not known to exist or the existing faults' ability to induce a given seismic magnitude has been underestimated. Such famous examples, among others, were (i) the unexpected 1983 Coalinga earthquake in a quiet region in California; (ii) the 1971 Sylmar earthquake with its surprising (*at the time*) Pacoima Dam record exceeding 1.0 g; (iii) the numerous strong motion records since then that have well exceeded 1.0 g in Chile, New Zealand, Taiwan, and elsewhere; and (iv) for Greece, the 1999 Athens earthquake that ruptured an unknown extension of a known fault in a low- to medium-seismicity zone with a design effective PGA of 0.16 g, yielding estimated PGAs of 0.5 g, and the 2014 earthquakes in a well-known seismically active region in Kefallinia, exceeding the design effective PGA by as high as 200 %. Such consistent overshoots of our impression of the expected level of shaking in a seismically affected region demonstrate the need for introducing to our designs reasonable reduction factors coupled with excess ductility capacity and structural redundancy, rather than adopting  $q_d = 1.0$ -type designs with no built-in ductility.

Extensive statistical studies have demonstrated that the  $q$ (or  $R$ ) factors of SDOF systems are not sensitive to the earthquake magnitude unless near the causative fault, while they show a reasonable similarity (in terms of the estimated  $q_\mu-\mu-T$  relations) between earthquake faults of similar tectonic characteristics. Furthermore, they do not seem to be sensitive to the hysteretic shape of the system, for EPP and hardening systems of conventional new buildings. They are sensitive, however, to softening cyclic response, such as the case of structures with excessively softening or brittle failure mechanisms, such as existing RC frame or frame-wall structures, buildings with strong  $P-\delta$  effects, or infilled RC frames with weak infills. They also depend strongly on the EDRS (de)amplification in the case of a resonant (or not) structural period near

the predominant period of the local soil conditions, in soft soil sites. These observations make the specification in earlier codes of constant system-dependent  $q_\mu$  for design unconservative.

Can the behavior factor  $q_\mu$  be increased to 1.0 (elastic response) at the gain of lack of implementing ductility into the system (i.e.,  $q_s = q_\Omega$ )? Although the incorporation of ductility was initially imperative in seismic designs, this is no longer the case, and the codes are coming at the end of closed circle situation at this point, where one may (at the national level) relax this compulsory requirement. In this context, EC8 (2004), for instance, accounts for the case of a low ductility class (DCL) design, whereby a contemporary seismic design may for all practical purposes ignore all seismic detailing provisions for ductility, provided that a  $q_d$  close to 1.0–1.50 is adopted; in fact, the New Greek Code for Concrete Works still in effect in parallel usage with EC8 (2004) during the publication of this work allows for such a non-ductile design, even though the Greek National Annex of EC8 (2004) wisely, in the authors' opinion, precludes the use of DCL buildings in Greece. Given the performance of non-ductile structures in strong earthquakes and the possibly increased cost of introducing ductility detailing into the structure, it is believed that the practice of neglecting to incorporate ductility may lead to unsafe designs; therefore, adequate behavior factors with ductile detailing should be introduced, so that incorporating ductility is financially feasible.

### Cross-References

- ▶ [Assessment of Existing Structures Using Inelastic Static Analysis](#)
- ▶ [Equivalent Static Analysis of Structures Subjected to Seismic Actions](#)
- ▶ [Nonlinear Finite Element Analysis](#)
- ▶ [Numerical Modeling of Masonry Infilled Reinforced Concrete Frame Buildings](#)
- ▶ [Seismic Vulnerability Assessment: Reinforced Concrete Structures](#)

### References

- ASCE (2013) Minimum design loads for buildings and other structures. Standards SEI/ASCE 7-10. American Society of Civil Engineers, Reston
- ATC (1978) Tentative provisions for the development of seismic regulations for buildings. Report ATC 3-06. Applied Technology Council, Redwood City
- ATC (1995) Structural response modification factors. Report ATC-19. Applied Technology Council, Redwood City
- Biggs J (1964) Introduction to structural dynamics. McGraw-Hill, New York
- Borzi A, Elnashai AS (2000) Refined force reduction factors for seismic design. *Eng Struct* 22(10):1244–1260
- Chavez J, Khemici O, Khater M, Keshishian P (2012) Building codes and relative seismic vulnerability in Latin American Countries. In: Proceedings of 15th world conference of earthquake engineering, Lisbon
- Chryssanthopoulos MK, Dymiotis C, Kappos AJ (2000) Probabilistic evaluation of behaviour factors in EC8-designed R/C frames. *Eng Struct* 22(8):1028–1041
- Clough RW, Penzien J (1975) Dynamics of structures. McGraw Hill, New York
- EC2 (2004) Eurocode No. 2, design of concrete structures - part 1-1: general rules and rules for buildings, EN-1992-1-1. European Committee for Standardization, Brussels
- EC8 (2004) Eurocode No. 8, design of structures for earthquake resistance - part 1: general rules, seismic actions and rules for buildings, EN-1998-1. European Committee for Standardization, Brussels
- EC8 ENV (1988) Background documents for Eurocode 8, Part 1. Vol. 2 - Design rules. Commission of the European Communities, Brussels
- Fajfar P (1999). Capacity spectrum method based on inelastic demand spectra. *Earthq Eng Struct Dyn* 28(9):979–993
- FEMA-356 (2000) Prestandard and commentary for the seismic rehabilitation of buildings. FEMA, Washington, DC
- FEMA-695 (2009) Quantification of building seismic performance factors. FEMA, Washington, DC
- Genshu T, Yongfeng Z (2007) Seismic force modification factors for modified-Clough hysteretic model. *Eng Struct* 29(11):3053–3070
- Gillie J, Rodriguez-Marek A, McDaniel C (2010) Strength reduction factors for near-fault forward-directivity ground motions. *Eng Struct* 32(1):273–285
- Housner G (1956) Limit design of structures to resist earthquakes. In: Proceedings, world conference of earthquake engineering. Earthquake Engineering research Institute, Berkeley
- Kappos A (1991) Analytical prediction of the collapse earthquake for R/C buildings: case studies. *Earthq Eng Struct Dyn* 20(2):177–190

- Kappos A (1999) Evaluation of behaviour factors on the basis of ductility and overstrength studies. *Eng Struct* 21(9):823–835
- Lee LH, Han SW (1999) Determination of ductility factor considering different hysteretic models. *Earthq Eng Struct Dyn* 28(9):957–977
- Mahin SA, Bertero VVB (1981) An evaluation of inelastic seismic design spectra. *J Struct Div ASCE* 107(9):1777–1795
- Mavroeidis GP, Dong G, Papageorgiou AS (2004) Near-fault ground motions, and the response of elastic and inelastic single-degree-of-freedom (SDOF) systems. *Earthq Eng Struct Dyn* 33(9):1023–1049
- Miranda E (1993) Site-dependent strength reduction factors. *J Struct Eng ASCE* 119(12):3503–3519
- Miranda E, Bertero VVB (1994) Evaluation of strength reduction factors for earthquake-resistant design. *Spectra* 10(2):357–379
- Miranda E, Ruiz-Garcia J (2002) Influence of stiffness degradation on strength demands of structures built on soft soil sites. *Eng Struct* 24(10):1271–1281
- Nassar AA, Krawinkler H (1991) Seismic demands for SDOF and MDOF systems, TR 95, The J. Blume Earthquake Engineering Center, Stanford University, Palo Alto
- NEHRP (1985) NEHRP Recommended provisions for the development of seismic regulations for new buildings. Building Seismic Safety Council, Washington, DC
- Newmark NM, Hall WJ (1973) Seismic design criteria for nuclear reactor facilities. Report No. 46, Building Practices for Disaster Mitigation, National Bureau of Standards, US Department of Commerce, pp 209–236
- Ordaz M and Pérez-Rocha LE (1998) Estimation of strength-reduction factors for elastoplastic systems: a new approach. *Earthq Eng Struct Dyn* 27(9):889–901
- Repapis K, Vintzeleou E, Zeris C (2006a) Evaluation of the seismic performance of existing RC buildings: I suggested methodology. *Eur J Earthq Eng* 10(2):265–288
- Repapis K, Zeris C, Vintzeleou E (2006b) Evaluation of the seismic performance of existing RC buildings: II a case study for regular and vertically irregular buildings. *Eur J Earthq Eng* 10(3):429–452
- Riddell R (1995) Inelastic design spectra accounting for soil conditions. *Earthq Eng Struct Dyn* 24(11):1491–1510
- SEAOC (1974) Recommended lateral force requirements and commentary, 4th edn. Struct. Engineers Assoc. of California, San Francisco
- Uang CM (1991) Establishing  $R$  (or  $R_w$ ) and  $C_d$  factors for building seismic provisions. *J Struct Eng ASCE* 117(1):19–28
- UBC (1988) Uniform building code. International Conference of Building Officials, Washington, DC
- Vamvatsikos D, Cornell CA (2003) Applied incremental dynamic analysis. *Earthquake Spectra* 20(2):525–533
- Veletsos A, Newmark NM (1960) Effect of inelastic behaviour on the response of simple systems to earthquake motions. In: Proceedings second world conference on earthquake engineering, Japan, pp 895–912
- Vidić T, Fajfar P, Fischinger M (1994) Consistent inelastic design spectra: strength and displacement. *Earthq Eng Struct Dyn* 23(5):507–521
- Watanabe G, Kawashima K (2002) An evaluation of the forced reduction factor in the force-based seismic design. In: Proceedings of 39th joint meeting, panel on wind and seismic effect, UJNR, NIST Special Publication, Gaithersburg
- Whittaker A, Hart G, Rojahn C (1999) Seismic response modification factors. *J Struct Eng* 125(4):438–444
- Zeris C, Tassios TP, Lu Y, Zhang GF (1992) Influence of irregularity on the  $q$  factor of RC frames. In: Proceedings, 10th world conference of earthquake engineering, Madrid
- Zeris C, Repapis K, Vintzeleou E (2005) Seismic performance of existing irregular RC buildings. Paper No. 32, Proceedings of the 4th European workshop on the seismic behaviour of irregular and complex structures, Thessaloniki

---

## Blind Identification of Output-Only Systems and Structural Damage via Sparse Representations

Satish Nagarajaiah<sup>1,2</sup> and Yongchao Yang<sup>1</sup>

<sup>1</sup>Department of Civil and Environmental Engineering, Rice University, Houston, TX, USA

<sup>2</sup>Department of Mechanical Engineering, Rice University, Houston, TX, USA

### Synonyms

Blind source separation; Modal identification; Sparse representation; Structural health monitoring; Time-frequency analysis

### Introduction

Traditional model-based structural modal analysis and damage identification methods are typically parametric and user involved; as such, they are usually associated with demanding computational resources and require quite a lot of prior knowledge of structures. For practical

applications, it would be useful to seek efficient structural identification methods that may be able to extract the salient information directly from the measured structural signals. The recently widely deployed advanced structural health monitoring (SHM) systems in structures with dense sensors also support such an effort: the massive recorded data especially call for efficient data-driven algorithms (Yang and Nagarajaiah 2014c, d) for further structural assessment.

Recently, blind source separation (BSS) has emerged as a new unsupervised machine learning tool (Hyvärinen and Oja 2000) and has been extensively studied in structural dynamics and output-only modal identification (Antoni 2005; Kerschen et al. 2007; Yang and Nagarajaiah 2013a, b, c, 2014a, b; Poncelet et al. 2007; Zhou and Chelidze 2007; McNeill and Zimmerman 2008; Hazra et al. 2010; Hazra and Narasimhan 2010; Sadhu et al. 2011, 2012; Abazarsa et al. 2013; Antoni and Chuahan 2013; Ghahari et al. 2013). Essentially, BSS techniques are able to recover the hidden source signals and their underlying factors using only the observed mixtures; it is thus suitable to perform output-only structural identification when structural input or excitation is usually extremely difficult or expensive to obtain.

This entry presents the authors' recent work on data-driven output-only modal identification and damage detection of structures. It is found that exploiting the sparse essences of modal expansion and damage information can efficiently and effectively address some challenging problems in output-only modal identification and damage detection via BSS. A series of novel algorithms are developed with experimental and real-world structure examples for demonstrations.

### Blind Identification of Damage via Sparse Independent Component Analysis (ICA)

The sparse damage features hidden in the structural information can be blindly extracted via a

BSS technique called independent component analysis (ICA), as detailed in the following.

ICA is popularly used to estimate the blind source separation (BSS) model (Hyvärinen and Oja 2000),

$$\mathbf{x}(t) = \mathbf{A}\mathbf{s}(t) = \sum_{i=1}^n \mathbf{a}_i s_i(t) \quad (1)$$

using only the observed mixture vector  $\mathbf{x}(t) = [x_1(t), x_2(t), \dots, x_m(t)]^T$ ;  $\mathbf{s}(t) = [s_1(t), s_2(t), \dots, s_n(t)]^T$  and  $\mathbf{A}$  denote the latent source vector and the unknown constant  $m \times n$  linear mixing matrix, respectively, to be simultaneously estimated.  $\mathbf{a}_i$  is the  $i$ th column of  $\mathbf{A}$  and is associated with the corresponding source  $s_i(t)$ . The assumption of  $m = n$  is imposed herein, i.e., the number of mixtures equals that of the sources and  $\mathbf{A}$  is square. With only  $\mathbf{x}(t)$  known, Eq. 1 may not be mathematically solved by classical methods; additional assumption is thus needed to estimate the BSS model.

The principle of ICA estimation is based on the classical central limit theorem (CLT), which states that a sum of independent random variables tends to distribute toward Gaussian, i.e., a mixture of independent random variables is always more Gaussian than any one of the original variables (except that the mixture only contains one random variable). As seen in Eq. 1, mixtures are expressed as a weighted sum of the sources themselves; they are thus always more or equally Gaussian than the sources. ICA therefore searches for proper demixing matrix  $\mathbf{W}$  such that the recovered independent components (ICs)  $\mathbf{y}(t) = [y_1(t), y_2(t), \dots, y_n(t)]^T$  obtained by

$$\mathbf{y}(t) = \mathbf{W}\mathbf{x}(t) \quad (2)$$

are as non-Gaussian as possible and thus approximate  $\mathbf{s}(t)$ . Each IC  $y_i(t)$  is computed by

$$y_i(t) = \mathbf{w}_i \mathbf{x}(t) \quad (3)$$

with  $\mathbf{w}_i$  denoting the  $i$ th row of  $\mathbf{W}$ . By seeking those ICs which maximize non-Gaussianity, the

sources (and simultaneously the mixing matrix) can therefore be recovered by ICA.

Non-Gaussianity of a random variable can be measured by some contrast function, e.g., negentropy. The entropy of a discrete random variable  $v = \{v^1, v^2, \dots, v^i, \dots\}$  is defined by

$$H(v) = -\sum_i p(v = v^i) \cdot \log p(v = v^i) \quad (4)$$

where  $p(\cdot)$  is the probability mass operator. Entropy measures the uncertainty or randomness of a random variable. For example, for a random variable with impulse probability mass function, its entropy is zero, i.e., it is completely determined.

The Gaussian random variable has the largest entropy among all other random variables with equal variance (Hyvärinen and Oja 2000), i.e., it is the most random or uncertain one. On the other hand, a random variable with sparse representation has small entropy as it is less random or easier to be predicted. This conclusion yields the definition of negentropy as a measure of non-Gaussianity given by

$$J(v) = H(v_{\text{gau}}) - H(v) \quad (5)$$

in which  $v_{\text{gau}}$  is a standardized Gaussian random variable (zero mean and unit variance); it quantitatively evaluates the entropy distance of a (standardized) random variable from a Gaussian variable. Finding the ICs that maximize the negentropy by ICA thus yields random variables with sparse representation (Yang and Nagarajaiah 2014a). This finding turns out very useful for damage identification, as subsequently described.

A simplified approximation to the negentropy is the classical kurtosis, which is defined by

$$\text{kurt}(v) = E[v^4] - 3(E[v^2])^2 \quad (6)$$

where  $E[\cdot]$  denotes the expectation operator. The kurtosis of a Gaussian random variable is zero, and that of a non-Gaussian random variable is nonzero. It is easy to estimate and computationally efficient. The FastICA is one of the most

efficient algorithms implementing ICA estimation and is adopted in this study.

Damage may behave as pulse-like information hidden in the structural vibration response signals once they are processed further such as in the wavelet domain. The pulse-like feature containing damage information may be buried in the noisy wavelet-domain signals on a certain scale. Because ICA biases to extract sparse components from the observations, feed the wavelet-domain responses  $\mathbf{x}^l(t)$  at the  $l$ th scale as mixtures into the BSS model,

$$\mathbf{x}^l(t) = \mathbf{A}\mathbf{s}(t) \quad (7)$$

If there is any pulse-like feature hidden in  $\mathbf{x}^l(t)$ , then ICA will extract it, which is to be revealed in the recovered sparse component  $y_j(t)$  with sharp spikes indicating damage

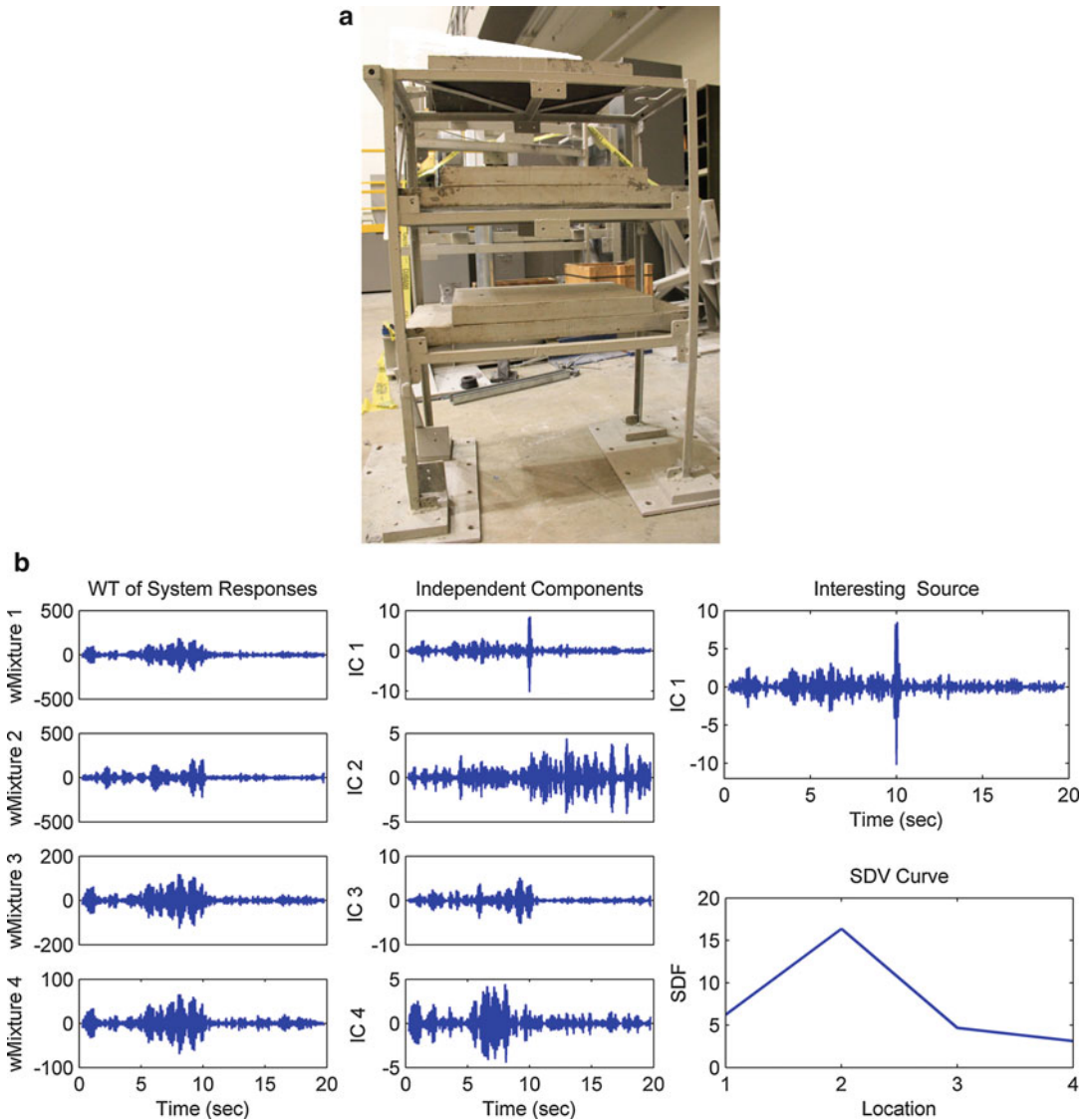
$$\mathbf{y}(t) = \mathbf{W}\mathbf{x}^l(t) \quad (8)$$

Such  $y_j(t)$  is proposed as the “interesting” source within the damage identification framework. Note that  $\mathbf{x}^l(t)$  inherits the temporal information of the responses; this implies that the recovered “interesting” source  $y_j(t)$  retains temporal signatures of the inflicted damage, which is indicated by the time instant location of the sharp spike.

Expanding the WT-BSS model Eq. 7 as

$$\begin{aligned} \mathbf{x}^l(t) &= \sum_{i=1}^n \mathbf{a}_i s_i(t) \\ x_1^l &= \sum_{i=1}^n a_{1i} s_i(t) = a_{11} s_1(t) + a_{12} s_2(t) + \dots + a_{1n} s_n(t) \\ x_j^l &= \sum_{i=1}^n a_{ji} s_i(t) = a_{j1} s_1(t) + a_{j2} s_2(t) + \dots + a_{jn} s_n(t) \\ x_n^l &= \sum_{i=1}^n a_{ni} s_i(t) = a_{n1} s_1(t) + a_{n2} s_2(t) + \dots + a_{nn} s_n(t) \end{aligned} \quad (9)$$

Observe that the mixing coefficient  $a_{ji}$  locates the mixture and the source by its indices  $j$  and  $i$ , respectively, and the columnwise vector  $\mathbf{a}_i = [a_{1i}, a_{2i}, \dots, a_{ji}, \dots, a_{ni}]^T$  contains the spatial signature of the corresponding source  $s_i(t)$ . Herein,  $\mathbf{a}_i$  and its element  $a_{ji}$  are proposed as the



**Blind Identification of Output-Only Systems and Structural Damage via Sparse Representations, Fig. 1** Sparse ICA simultaneous identification of both structural damage instant and damage location: (a) the

experimental structure with four sensors embedded subject to white noise excitation at the base and (b) the WT-ICA identification results

source distribution vector (SDV) and source distribution factor (SDF), respectively; they describe how source  $s_i(t)$  is distributed among  $n$  mixtures. Specifically, if  $a_{ji}$  has the largest (absolute) value among  $\mathbf{a}_i = [a_{1i}, a_{2i}, \dots, a_{ji}, \dots, a_{ni}]^T$ , then  $x_j(t)$  contains most  $s_i(t)$  components among all the mixtures (Yang and Nagarajaiah 2014a).

The proposed concepts of SDV and SDF are readily extended to damage localization issues. As the structural response in the vicinity of damage naturally contains most spike-like features, damage can be localized by tracking the spike in the SDV of the recovered impulse-like IC, which is the “interesting” source. Figure 1 shows an experimental structure application of WT-ICA



in simultaneous identification of both damage instant (at the 10th second) and damage location (the second sensor, left column in the first floor) by the spike feature in the recovered “interesting” source and the corresponding spatial signature, respectively; the detail of this experiment is referred to Yang and Nagarajaiah (2014a).

### Output-Only Modal Identification by Sparse Time-Frequency ICA

In the above section, the sparse wavelet ICA is introduced for identification of the hidden spike-like features that typically indicate structural damage information. In the following, the sparse properties of modal expansion are further exploited and lead to a new output-only modal identification method STFT-ICA within the BSS framework which can handle even highly damped structures, as detailed in the following.

For a linear time-invariant system with  $n$  degrees-of-freedom (DOF), the governing equation of motion is

$$\mathbf{M}\ddot{\mathbf{x}}(t) + \mathbf{C}\dot{\mathbf{x}}(t) + \mathbf{K}\mathbf{x}(t) = \mathbf{f}(t) \quad (10)$$

where  $\mathbf{M}$ ,  $\mathbf{C}$ , and  $\mathbf{K}$  are the symmetric mass, (diagonalizable) damping, and stiffness matrices, respectively, and  $\mathbf{f}(t)$  is the external force.

The system responses  $\mathbf{x}(t) = [x_1(t), \dots, x_n(t)]^T$  can be expressed using the modal expansion

$$\mathbf{x}(t) = \mathbf{\Phi}\mathbf{q}(t) = \sum_{i=1}^n \varphi_i q_i(t) \quad (11)$$

where  $\mathbf{\Phi} \in \mathbb{R}^{n \times n}$  denotes the inherent vibration mode matrix (real-valued normal modes) with its  $i$ th column (modeshape), and  $\varphi_i \in \mathbb{R}^n$  is the modal response (real-valued).

The output-only identification issue pursues to identify the modal parameters by solely relying on the knowledge of  $\mathbf{x}(t)$  without any excitation or input information to the system, such like identification of both  $\mathbf{\Phi}$  and  $\mathbf{q}(t)$  only from  $\mathbf{x}(t)$  in Eq. 11. Such is an ill-posed problem and may

not be solved mathematically. Traditional output-only modal identification methods usually presume a parametric model (e.g., a stochastic state space model) to proceed with the identification; however, they have a serious drawback of the model order determination problem. Other methods may suffer from sensitivity to noise, dependence on expert experience, and heavy computational burden. The BSS technique provides a straightforward and efficient algorithm for output-only modal identification, as detailed in the following.

The BSS problem has a similar pursuit with the output-only modal identification issue. The close similarity is implied between the modal expansion Eq. 11 and the BSS model Eq. 1. If the system responses are fed as mixtures into the BSS model, then the target of output-only identifying  $\mathbf{\Phi}$  and  $\mathbf{q}(t)$  in Eq. 11 can be solved by blind recovery of  $\mathbf{A}$  and  $\mathbf{s}(t)$  using those BSS techniques dependent on the independence assumption since  $\mathbf{q}(t)$  typically with incommensurable frequencies are independent on the modal coordinates.

It has been shown, however, that such direct extraction of time-domain modal responses by ICA has failed for higher-damped structures (only within 1 %) (Kerschen et al. 2007; Yang and Nagarajaiah 2013a, b, 2014a, Brewick and Smyth 2015). The primary reason lies in that ICA ignores the temporal information of signals, while the targeted modal responses possess significant time structure – exponentially decaying monotone sinusoids.

To address the aforementioned issues of ICA, it is proposed by Yang and Nagarajaiah (2013a) to transform the time-domain modal expansion Eq. 11 to the time-frequency domain where the target modal responses have sparse representations, using the short-time Fourier transform (STFT) prior to the ICA estimation,

$$\mathbf{X}_{f\tau} = \mathbf{\Phi}\mathbf{Q}_{f\tau} = \sum_{i=1}^n \varphi_i Q_{f\tau,i} \quad (12)$$

where  $f$  and  $\tau$  are the frequency and window indices, respectively. ICA then extracts the most

independent (sparse) components that are the time-frequency representation of the modal responses,

$$\tilde{\mathbf{Q}}_{f\tau} = \tilde{\mathbf{W}}\mathbf{X}_{f\tau} \quad (13)$$

The recovered independent sources  $\tilde{\mathbf{Q}}_{f\tau} = [\tilde{Q}_{1,f\tau}, \dots, \tilde{Q}_{n,f\tau}]^T$  are supposed to be as sparse as possible and approximate the targeted sparse time-frequency representations of the monotone modal responses. The obtained mixing matrix is therefore the estimated normal mode, i.e.,  $\tilde{\mathbf{\Phi}} = \tilde{\mathbf{A}} = \tilde{\mathbf{W}}^{-1}$ . Once the normal modes are estimated, the time-domain modal responses can be recovered using the demixing matrix

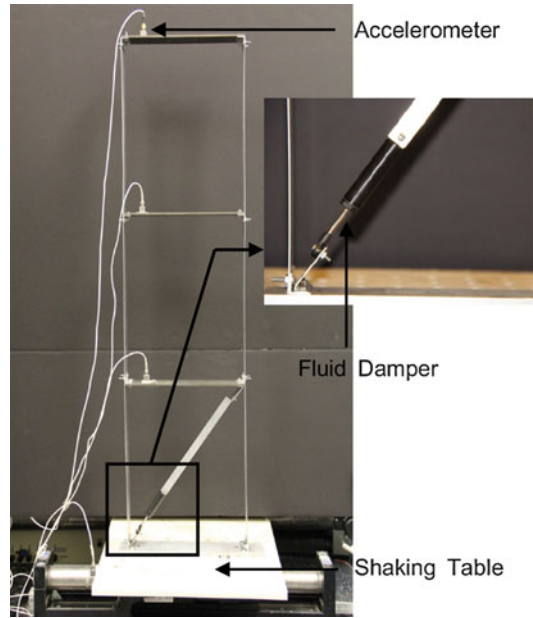
$$\tilde{\mathbf{q}}(t) = \tilde{\mathbf{W}}\mathbf{x}(t) \quad (14)$$

whereby readily estimating the modal frequencies and damping ratios in free vibration are readily estimated by Fourier transform (FT) and Hilbert transform (HT) or logarithm-decrement technique (LT) (Nagarajaiah and Basu 2009; Basu et al. 2008; Nagarajaiah and Li 2004; Dharap et al. 2006; Koh et al. 2005a, b; Li et al. 2007).

Figures 2, 3, 4, and 5 as well as Tables 1 and 2 present the successful application of STFT-ICA in identification of the modal parameters of an experimental structure (Fig. 2) and a real-world structure subject to the Northridge Earthquake 1994 (Nagarajaiah and Dharap 2003; Nagarajaiah and Sun 2000, 2001), both of which are highly damped. The details are referred to Yang and Nagarajaiah (2013a).

### Complexity Pursuit on “Independent” Modal Coordinates

Exploiting the properties of the system responses and modal responses can lead to an efficient output-only modal identification method (Yang and Nagarajaiah 2013b) that enjoys even wider success based on a new BSS learning rule complexity pursuit (Stone 2001), which states that the complexity of any mixture signal



**Blind Identification of Output-Only Systems and Structural Damage via Sparse Representations, Fig. 2** The experimental highly-damped 3-story steel frame and the zoomed fluid damper

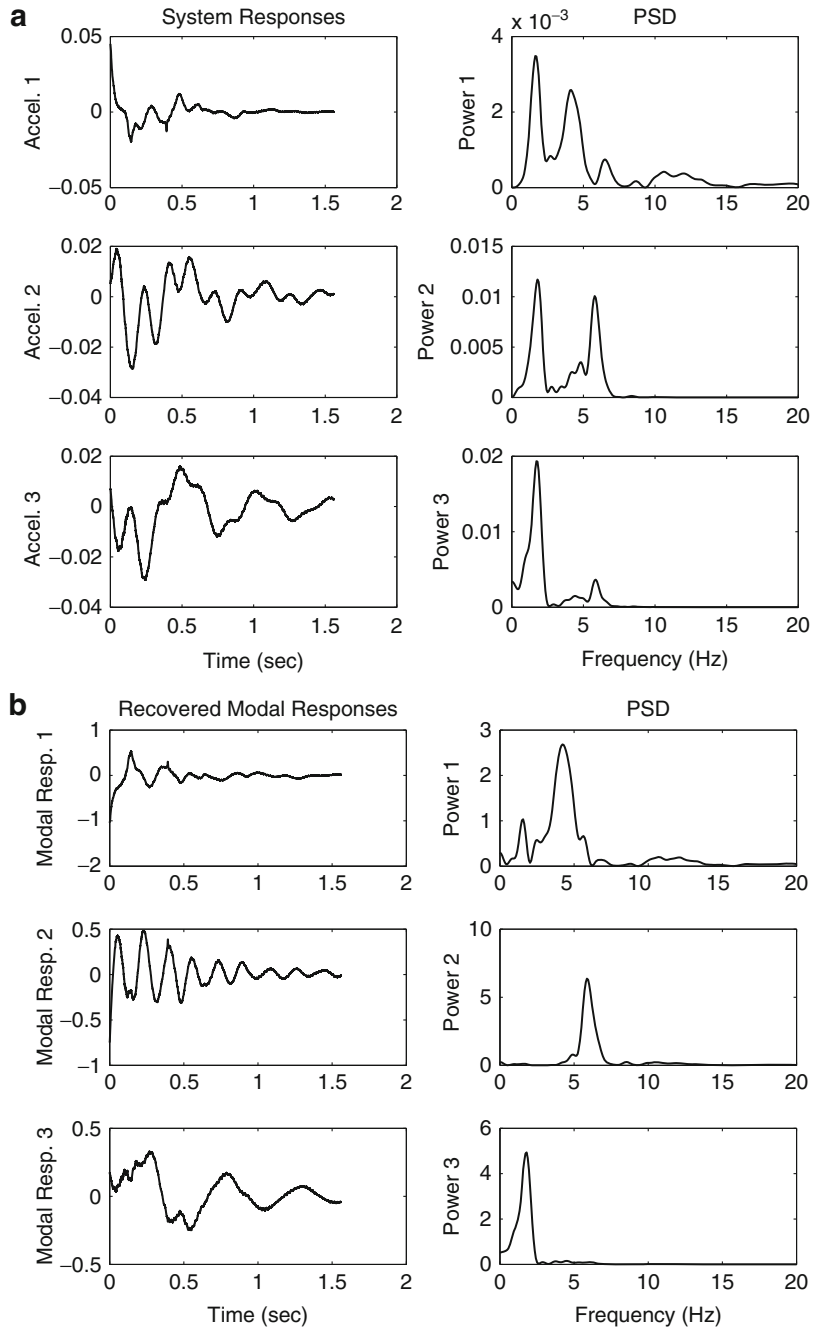
(system response) always lies between that of the simplest source (simplest modal response) and most complicated source (most complex modal response).

In statistics, the complexity of a signal, say,  $y_i = \mathbf{w}_i\mathbf{x}$  (the temporal index is made implicit), is rigorously measured by Kolmogorov complexity. Given that Kolmogorov complexity is not intuitive and difficult to approximate in practice, Stone (2001, 2004) provided a simple yet robust complexity measure of a signal, temporal predictability, which is defined by

$$F(y_i) = \log \frac{V(y_i)}{U(y_i)} = \log \frac{\sum_{t=1}^N (\bar{y}_i(t) - y_i(t))^2}{\sum_{t=1}^N (\hat{y}_i(t) - y_i(t))^2} \quad (15)$$

where the long-term predictor  $\bar{y}_i(t)$  and short-term predictor  $\hat{y}_i(t)$  are given, respectively, by

**Blind Identification of Output-Only Systems and Structural Damage via Sparse Representations, Fig. 3** (a) System responses (free vibration) of the experimental structure (b) the recovered modal responses by STFT-ICA

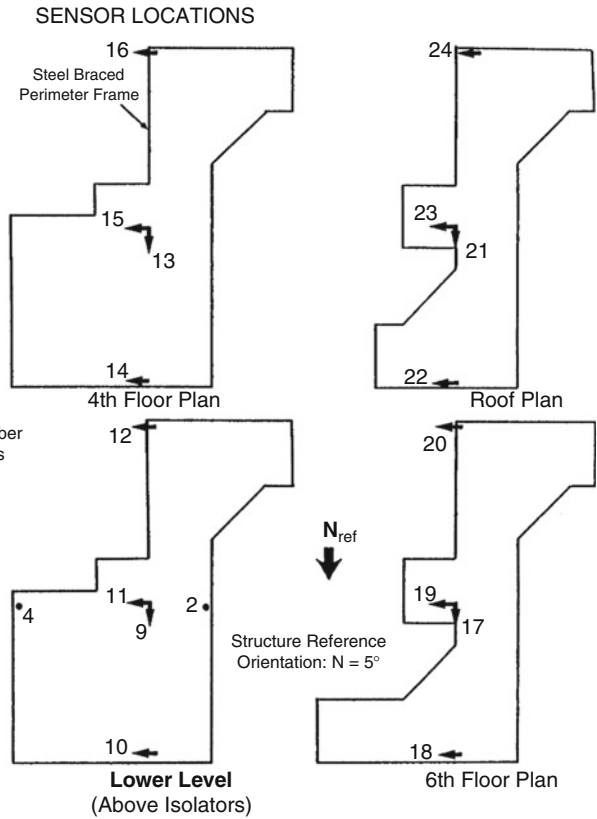
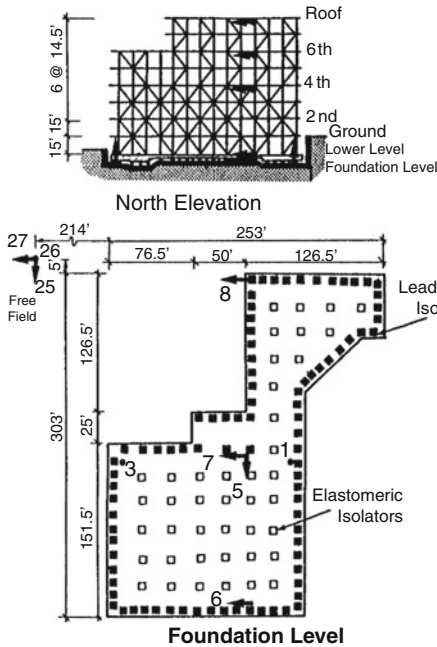


$$\begin{aligned} \bar{y}_i(t) &= \lambda_L \bar{y}_i(t-1) + (1 - \lambda_L) y_i(t-1) \quad 0 \leq \lambda_L \leq 1 \\ \hat{y}_i(t) &= \lambda_S \hat{y}_i(t-1) + (1 - \lambda_S) y_i(t-1) \quad 0 \leq \lambda_S \leq 1 \end{aligned} \tag{16}$$

$$\lambda = 2^{-1/h} \tag{17}$$

The parameter  $\lambda$  is defined by the half-life parameter  $h$  as

where  $h_S = 1$  and  $h_L$  is arbitrarily set (say, 900, 000) as long as  $h_L \gg h_S$  (Stone 2001, 2004). Incorporate  $y_i = \mathbf{w}_i \mathbf{x}$  into Eq. 15,

Los Angeles -7-story University Hospital  
(CSMIP Station No. 24605)

B

**Blind Identification of Output-Only Systems and Structural Damage via Sparse Representations, Fig. 4** Sensor outline of the highly-damped USC hospital building

$$F(y_i) = F(\mathbf{w}_i, \mathbf{x}) = \log \frac{V(\mathbf{w}_i, \mathbf{x})}{(\mathbf{w}_i, \mathbf{x})} = \log \frac{\mathbf{w}_i \bar{\mathbf{R}} \mathbf{w}_i^T}{\mathbf{w}_i \hat{\mathbf{R}} \mathbf{w}_i^T} \quad (18)$$

where  $\bar{\mathbf{R}}$  and  $\hat{\mathbf{R}}$  are the  $n \times n$  long-term and short-term covariance matrix between the mixtures, respectively; their elements are defined as

$$\begin{aligned} \bar{r}_{ij} &= \sum_{t=1}^N (x_i(t) - \bar{x}_i(t)) (x_j(t) - \bar{x}_j(t)) \\ \hat{r}_{ij} &= \sum_{t=1}^N (x_i(t) - \hat{x}_i(t)) (x_j(t) - \hat{x}_j(t)) \end{aligned} \quad (19)$$

Therefore, given a set of mixtures  $\mathbf{x}(t)$ , the CP learning rule is formulated to search for the demixing vector  $\mathbf{w}_i$  which maximizes the temporal predictability contrast function  $F(\cdot)$ ; this can

be solved by the classic gradient ascent technique as described in the following.

Following Eq. 18, the derivative of  $F$  with respect to  $\mathbf{w}_i$  is

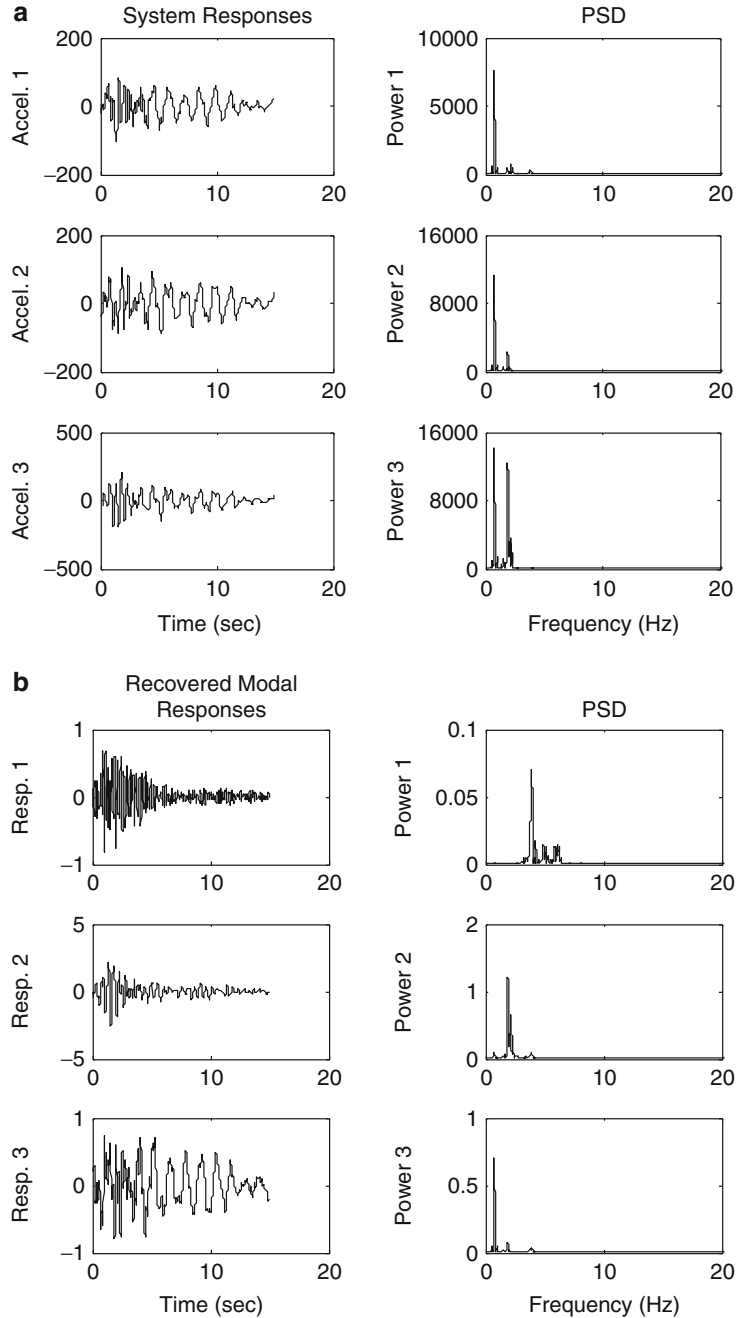
$$\nabla_{\mathbf{w}_i} F = \frac{2\mathbf{w}_i}{V_i} \bar{\mathbf{R}} - \frac{2\mathbf{w}_i}{U_i} \hat{\mathbf{R}} \quad (20)$$

By iteratively updating  $\mathbf{w}_i$ , a maximum of  $F$  is guaranteed to be found; the extracted component  $y_i = \mathbf{w}_i \mathbf{x}$  with maximum temporal predictability is the least complex signal and thus approaches the simplest source hidden in the mixtures, according to Stone's theorem in the CP learning rule.

Restricted to Stone's theorem (Xie et al. 2005), however, the sources can only be extracted one by one by maximizing the temporal

**Blind Identification of Output-Only Systems and Structural Damage via Sparse Representations,**

**Fig. 5** (a) System responses (during the Northridge Earthquake 1994) of the USC hospital building (b) the recovered modal responses by STFT-ICA



predictability using the gradient ascent technique. Stone (2001) proposed a more elegant algorithm that can efficiently extract all the hidden sources simultaneously, described as follows.

The gradient of  $F$  reaches zero in the solution, where

$$\nabla_{\mathbf{w}_i} F = \frac{2\mathbf{w}_i}{V_i} \bar{\mathbf{R}} - \frac{2\mathbf{w}_i}{U_i} \hat{\mathbf{R}} = 0 \quad (21)$$

### Blind Identification of Output-Only Systems and Structural Damage via Sparse Representations,

**Table 1** Identified results of the experimental model

Mode	Frequency (Hz)		Damping ratio (%)		MAC
	ERA	STFT-ICA	ERA	STFT-ICA	
	1	1.649	1.800	12.9	
2	4.226	4.126	16.8	16.5	0.69
3	5.999	5.869	5.0	5.1	0.91

### Blind Identification of Output-Only Systems and Structural Damage via Sparse Representations,

**Table 2** Identified results of the USC building

Mode	Frequency (Hz)		MAC
	Analytical	STFT-ICA	
1	0.746	0.766	0.98
2	1.786	1.907	0.93
3	3.704	3.941	0.30

Rewriting as

$$\mathbf{w}_i \bar{\mathbf{R}} = \frac{V_i}{U_i} \mathbf{w}_i \hat{\mathbf{R}} \quad (22)$$

yields a well-defined generalized eigenproblem (Stone 2001); the solution for  $\mathbf{w}_i$  can thus be obtained as the eigenvector of the matrix  $\hat{\mathbf{R}}^{-1} \bar{\mathbf{R}}$ , with the eigenvalue  $\gamma_i = V_i/U_i$ . The sources can then be efficiently extracted simultaneously by

$$\mathbf{s}(t) = \mathbf{y}(t) = \mathbf{W}\mathbf{x}(t) \quad (23)$$

where the eigenvector matrix  $\mathbf{W}$ , with  $\mathbf{w}_i$  as its  $i$ th row, is the target demixing matrix such that  $\mathbf{A} = \mathbf{W}^{-1}$  and  $\mathbf{y}(t) = [y_1(t), \dots, y_n(t)]^T$  is the recovered component vector which approaches the source vector  $\mathbf{s}(t)$ .

The aforementioned CP framework can then be cast into the modal identification whose physical interpretation is based on a new concept of “independent physical system on modal coordinates” (Yang and Nagarajaiah 2013b). The CP method is successful as shown in Figs. 6, 7, 8, and 9 and Tables 3 and 4 in identification of closely spaced couples with high-damped modes and in the presence of nonstationary seismic excitation.

### Sparse Component Analysis of Modal Expansion

Existing BSS-based output-only modal identification methods may not be applied to the underdetermined problem where  $m < n$  (i.e., only partial observations are available), which also often arises; e.g., for a large-scale structure, compared to its complexity with quite a few active modes, the measurement sensors may be limited. In this situation, the SCA method (Gribonval and Lesage 2006; Yang and Nagarajaiah 2013c) is used to tackle both the determined and underdetermined problem by exploiting the sparsity essence of the modal response. The targeted modal responses, which are viewed as sources in the BSS framework, are monotone, implying that they are active at only one distinct frequency, respectively. Therefore, they are most sparsely and disjointly distributed in the frequency domain and naturally satisfy the source sparsity assumption of SCA. Hence, transform the modal expansion Eq. 11 into the sparse frequency domain to incorporate modal identification to the SCA framework

$$\mathbf{x}(f) = \tilde{\Phi} \mathbf{q}(f) = \sum_{i=1}^n \varphi_i q_i(f) \quad (24)$$

with

$$\begin{aligned} \mathbf{x}(f) &= \mathcal{F}(\mathbf{x}(t)) = \int_{-\infty}^{\infty} \mathbf{x}(t) e^{-j2\pi f t} dt \\ \mathbf{q}(f) &= \mathcal{F}(\mathbf{q}(t)) = \int_{-\infty}^{\infty} \mathbf{q}(t) e^{-j2\pi f t} dt \end{aligned} \quad (25)$$

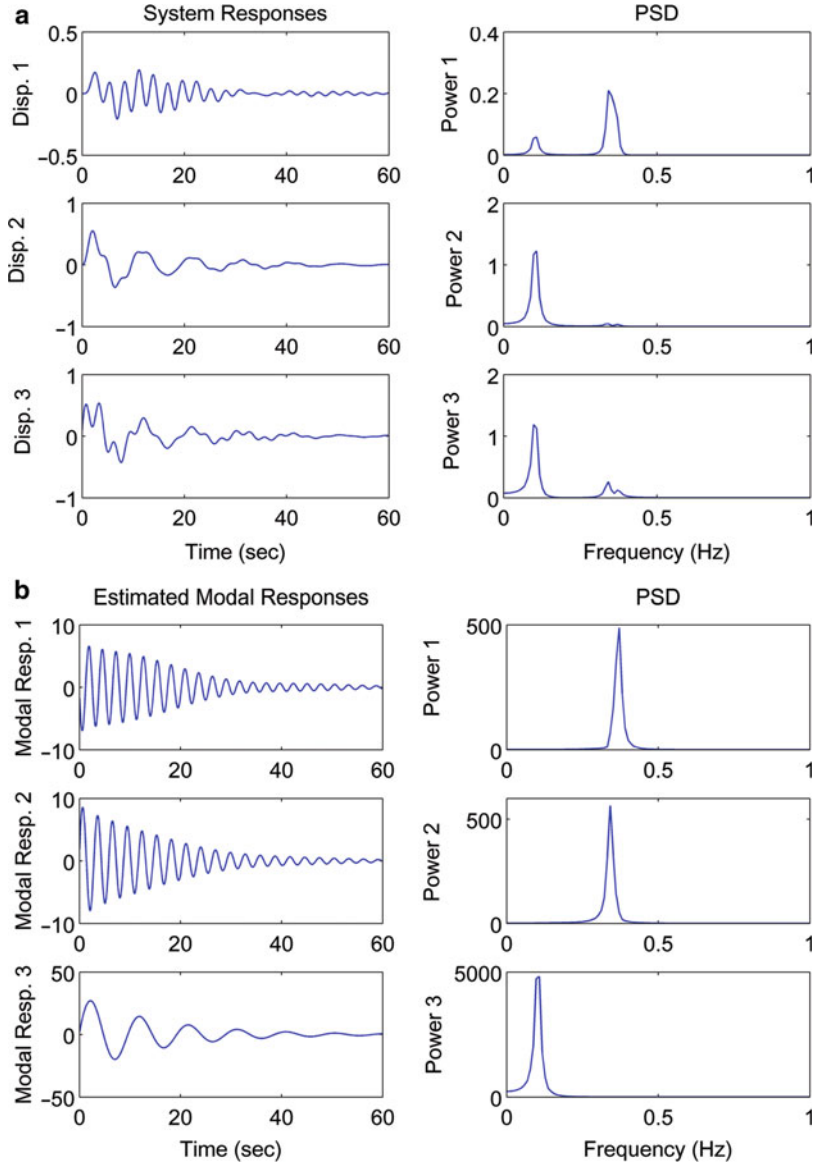
where  $\mathcal{F}$ ,  $f$ , and  $j$  denote the Fourier transform operator, frequency index, and the imaginary operator, respectively. Note that  $\mathcal{F}$  is an invertible linear transform; it holds the form of the modal expansion such that Eq. 24 is valid and  $\Phi$  remains invariant.

To avoid complex elements in Eq. 24, it is more practical to use the cosine transform  $\mathcal{F}^c$  (also linear) to yield real-valued  $\mathbf{x}(f)$ , simply replacing the Fourier basis  $e^{-j2\pi f t}$  with the cosine



**Blind Identification of Output-Only Systems and Structural Damage via Sparse Representations,**

**Fig. 6** (a) The system responses of a 3-DOF numerical model and (b) the modal responses recovered by CP in free vibration (closely-spaced coupled with high-damped modes)



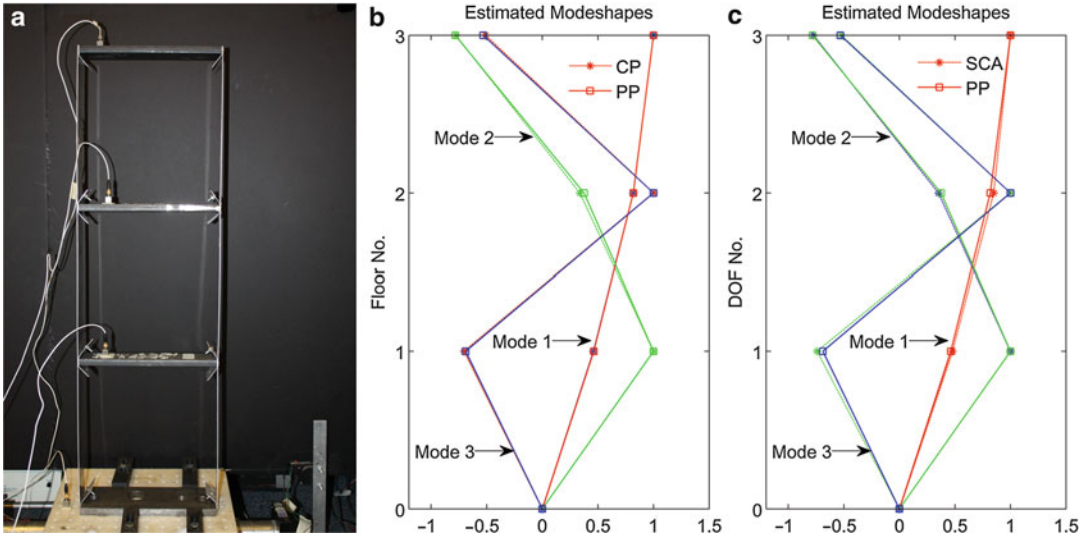
basis  $\cos 2\pi ft$  in Eq. 24. The DCT is adopted in the proposed SCA method, then  $\mathbf{x}(f)$  and  $\mathbf{q}(f)$  are understood as real-valued cosine transform coefficients.

Using the disjoint sparsity property of modal responses with distinct frequencies, at some  $f_k$  where only one modal response

$q_j(j = 1, \dots, n)$  is active and  $q_i = 0$  for  $i \neq j$ , Eq. 24 becomes

$$\mathbf{x}(f_k) = \varphi_j q_j(f_k) \tag{26}$$

Therefore, the points of  $\mathbf{x}(f)$  will cluster to the direction of the  $j$ th modeshape  $\varphi_j(j = 1, \dots, n)$



**Blind Identification of Output-Only Systems and Structural Damage via Sparse Representations, Fig. 7** (a) The experimental 3-story structure, (b) the modeshapes estimated by CP, and (c) the modeshapes estimated by SCA

such that the estimated vibration mode matrix  $\tilde{\Phi}$  can be extracted by the automatic fuzzy C-means clustering algorithm.

For determined cases,  $\tilde{\Phi}$  is square, and the time-domain modal responses can be recovered directly by

$$\tilde{\mathbf{q}}(t) = \tilde{\Phi}^{-1} \mathbf{x}(t) \quad (27)$$

from which the frequency and damping ratio can be estimated by straightforward Fourier transform and logarithm decrement, respectively. In underdetermined cases,  $\tilde{\Phi}$  is rectangular. The frequency-domain modal sources  $\tilde{\mathbf{q}}(f)$  can first be recovered using  $\ell_1$ -minimization ( $P_1$ ): at each  $f \in \Omega$ ,

$$\begin{aligned} \tilde{\mathbf{q}}(f) &= \arg \min \|\mathbf{q}(f)\|_{\ell_1} \quad \text{subject to} \quad \tilde{\Phi} \mathbf{q}(f) \\ &= \mathbf{x}(f) \end{aligned} \quad (28)$$

where  $\|\mathbf{q}(f)\|_{\ell_1} = \sum_{i=1}^n |q_i(f)|$ . The validity of this strategy resides in the ability of the  $\ell_1$ -minimization to recover the sparsest solution to Eq. 28, which is exactly the desired monotone frequency-domain modal responses since they are the sparsest solution among all feasible solutions to Eq. 28.

Using the inverse cosine transform, the time-domain modal responses can be readily recovered by

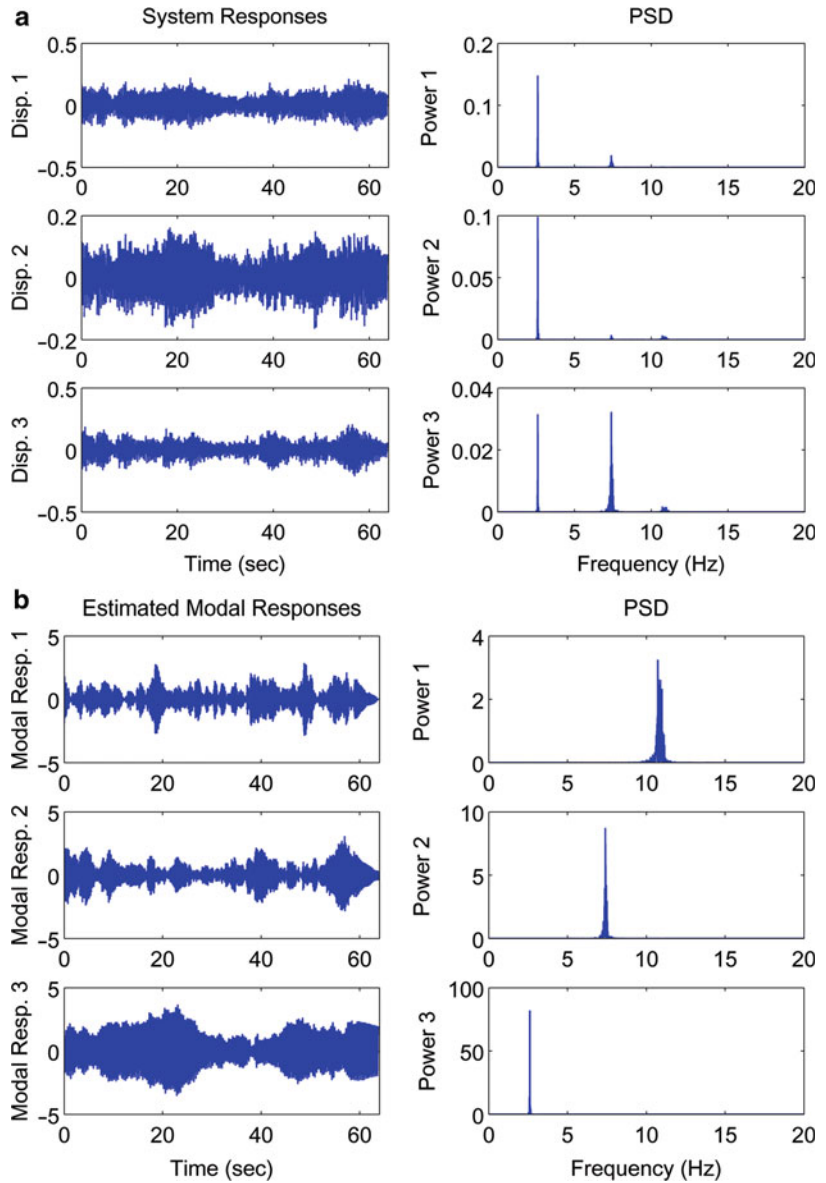
$$\tilde{\mathbf{q}}(t) = \mathcal{F}^{c-1}(\tilde{\mathbf{q}}(f)) \quad (29)$$

thereby estimating the frequency and damping ratio.

For demonstrations, Fig. 10 shows that SCA is able to recover the close modes coupled with high damping using only two sensors of the 3-DOF numerical model.

**Blind Identification of Output-Only Systems and Structural Damage via Sparse Representations,**

**Fig. 8** (a) The measured system responses and (b) the modal responses recovered by CP of the experimental model subject to white noise excitation



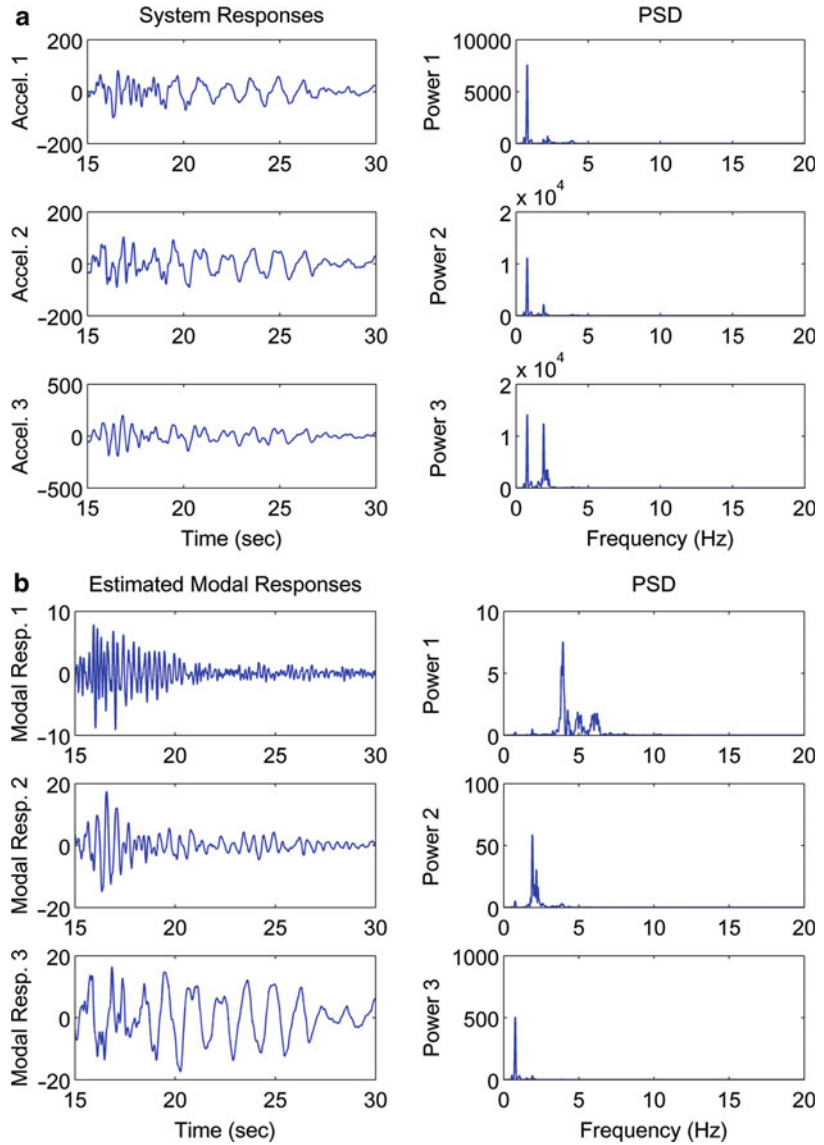
Figures 7c, 11, 12, and 13 and Table 5 show that SCA works very well even with limited sensors in the three-story experimental structure. Details are referred to Yang and Nagarajaiah (2013c).

**Summary**

This study shows that properly exploiting the sparse essences of modal expansion and damage information could efficiently and

**Blind Identification of Output-Only Systems and Structural Damage via Sparse Representations,**

**Fig. 9** (a) The measured system responses and (b) the modal responses recovered by CP of the USC hospital building in the Northridge earthquake 1994



**Blind Identification of Output-Only Systems and Structural Damage via Sparse Representations, Table 3** CP identified results of the experimental model

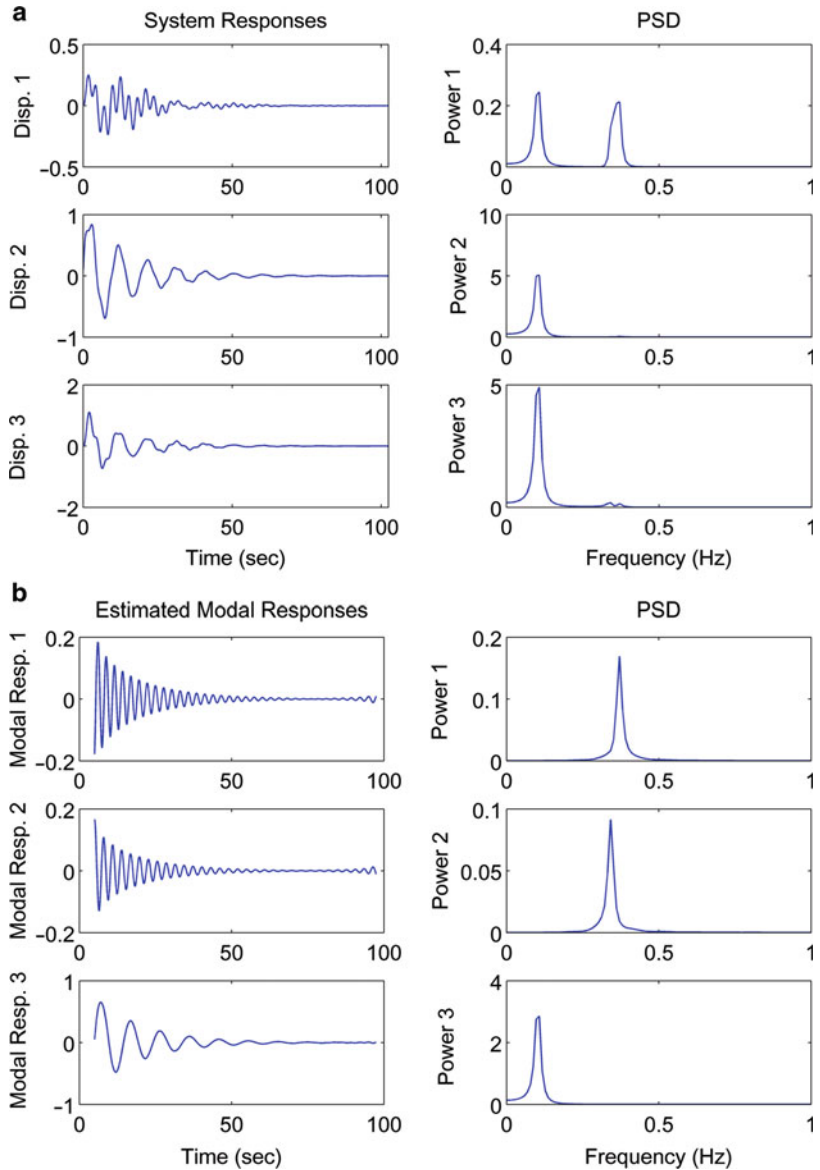
Mode	Frequency (Hz)		MAC
	Peak picking	CP	
1	2.550	2.600	1.0000
2	7.330	7.395	0.9993
3	10.460	10.720	0.9997

**Blind Identification of Output-Only Systems and Structural Damage via Sparse Representations, Table 4** CP identified results of the USC building

Mode	Frequency (Hz)		MAC
	Analytical	CP	
1	0.746	0.768	0.9751
2	1.786	1.907	0.9054
3	3.704	3.941	0.7874

**Blind Identification of Output-Only Systems and Structural Damage via Sparse Representations,**

**Fig. 10** The modal responses recovered by SCA using only two sensors (close modes coupled with high damping case)

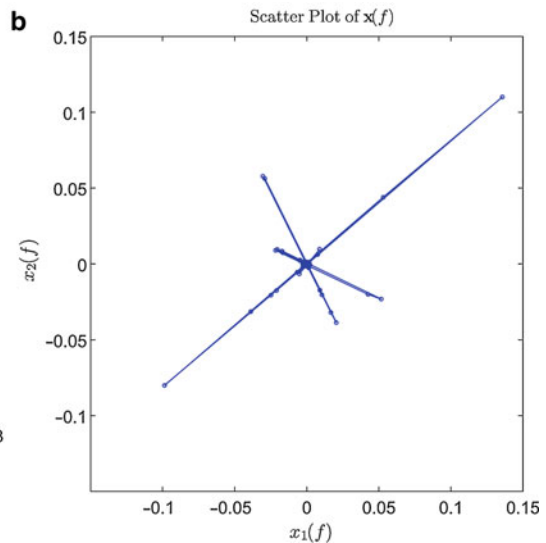
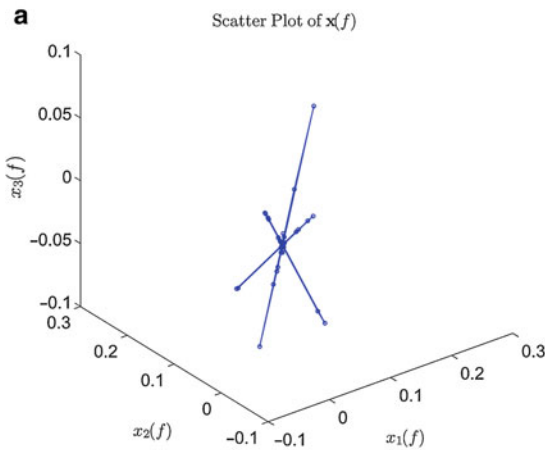
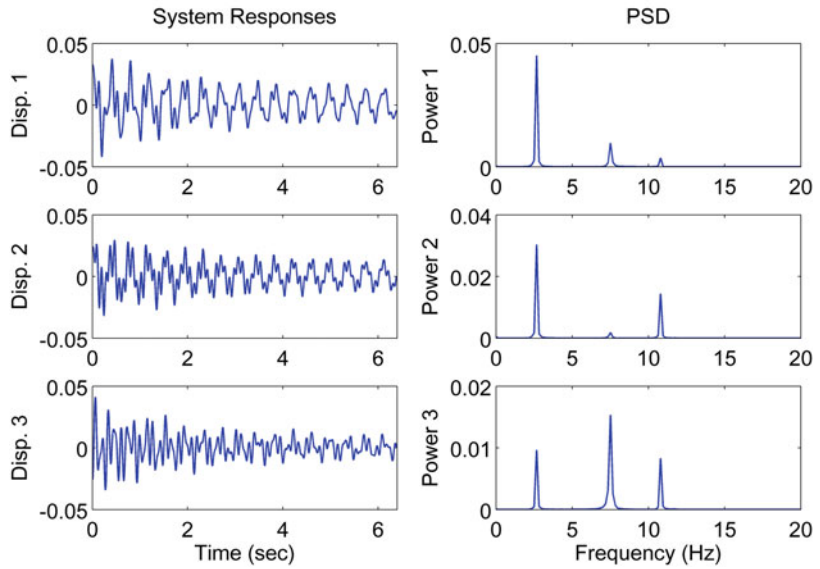


effectively address some challenging problems in output-only modal identification and damage detection via the unsupervised blind source separation (BSS) method. Sparse ICA is first introduced to simultaneously identify

both damage time instants and damage locations and then further employed to exploit the sparse nature of modal expansion to handle the problem of identification of highly damped structures. What is more, two new

**Blind Identification of Output-Only Systems and Structural Damage via Sparse Representations,**

**Fig. 11** The free-vibration system responses of the 3-story experimental model (Fig. 7a)



**Blind Identification of Output-Only Systems and Structural Damage via Sparse Representations,**  
**Fig. 12** The scatter plot in frequency domain of the

system responses of (a) all three sensors; (b) Sensor 1 and 2 in the 3-story experimental model (shown in Fig. 7a)

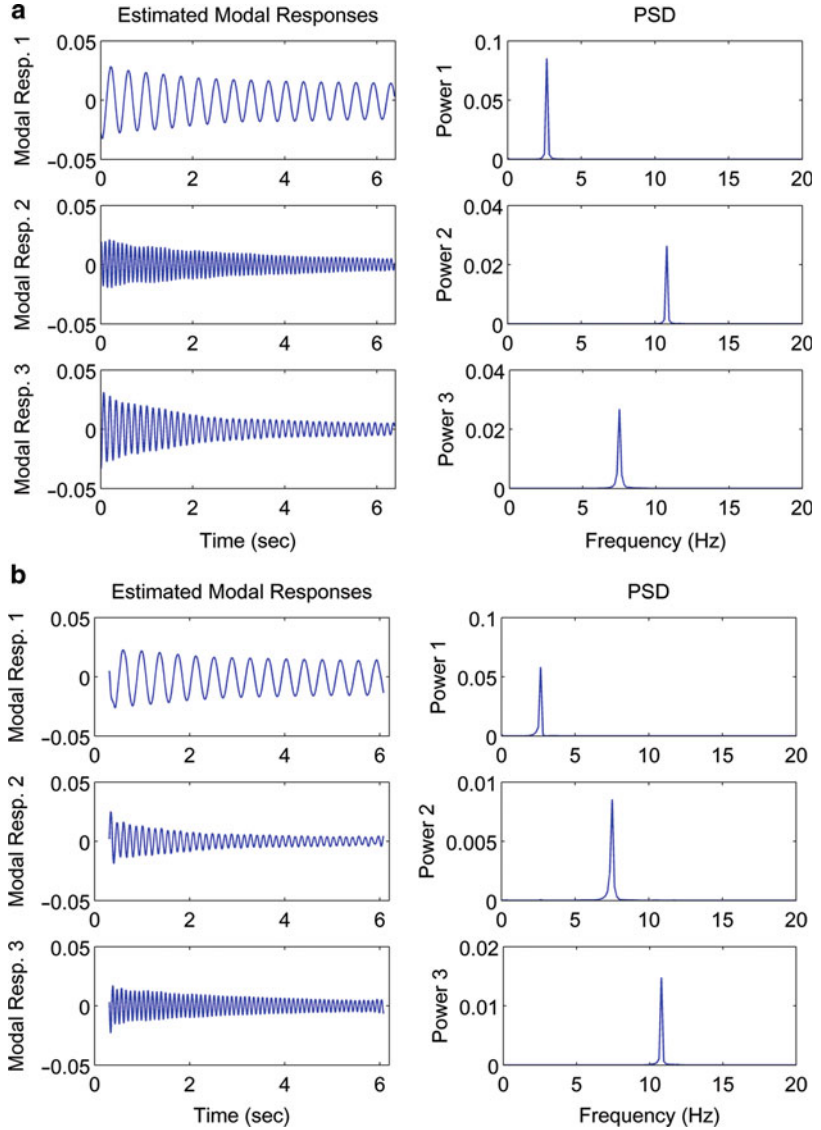
output-only modal identification methods are presented: the time-domain CP method and the SCA method which can handle the underdetermined problems with limited

sensors. The interpretations of CP and SCA in output-only modal identification are presented, and the successful implementations are also demonstrated using both



**Blind Identification of Output-Only Systems and Structural Damage via Sparse Representations, Fig. 13**

The modal responses recovered by SCA (a) using all the three sensors and (b) using Sensor 1 and 2 of the experimental model



**Blind Identification of Output-Only Systems and Structural Damage via Sparse Representations, Table 5** Identified modal parameters by SCA of the experimental system

Mode	Frequency (Hz)			Damping ratio (%)		MAC	
	PP	Determined	Under-	Determined	Under-	Determined	Under-
1	2.55	2.66	2.66	1.12	1.04	0.9997	0.9995
2	7.33	7.51	7.51	1.08	1.03	0.9997	0.9996
3	10.46	10.80	10.80	0.68	0.67	0.9988	1.0000

experimental and real-world structure examples. The established data-driven output-only modal identification and damage identification framework is nonparametric and enjoys

efficient computation and little user involvement, which is expected to have potential for real-time structural identification and health monitoring.

## Cross-References

- ▶ [Advances in Online Structural Identification](#)
- ▶ [Ambient Vibration Testing of Cultural Heritage Structures](#)
- ▶ [Bayesian Operational Modal Analysis](#)
- ▶ [Modal Analysis](#)
- ▶ [Stochastic Structural Identification from Vibrational and Environmental Data](#)
- ▶ [System and Damage Identification of Civil Structures](#)
- ▶ [Vibration-Based Damage Identification: The Z24 Bridge Benchmark](#)

## References

- Abazarsa F, Ghahari SF, Nateghi F, Taciroglu E (2013) Response-only modal identification of structures using limited sensors. *Struct Control Health Monit* 20:987–1006
- Antoni J (2005) Blind separation of vibration components: principles and demonstrations. *Mech Syst Signal Process* 19:1166–1180
- Antoni J, Chuahan S (2013) A study and extension of second-order blind source separation to operational modal analysis. *J Sound Vib* 332:1079–1106
- Basu B, Nagarajaiah S, Chakraborty A (2008) Online identification of linear time-varying stiffness of structural systems by wavelet analysis. *Struct Health Monit Int J* 7(1):21–36
- Brewick P, Smyth A (2015) Exploration of the impacts of driving frequencies on damping estimates. *J Eng Mech* 141(3): 04014130
- Dharap P, Koh B, Nagarajaiah S (2006) Structural health monitoring using ARMarkov observers. *J Intell Mater Syst Struct* 17(6):467–481
- Ghahari S, Abazarsa F, Ghannad M, Taciroglu E (2013) Response-only modal identification of structures using strong motion data. *Earthq Eng Struct Dyn* 42:1221–1242
- Gribonval R, Lesage S (2006) A survey of sparse component analysis for blind source separation: principles, perspectives, and new challenges. In: *Proceedings of European symposium on artificial neural networks, Bruges, Apr 2006*, pp 323–330
- Hazra B, Narasimhan S (2010) Wavelet-based blind identification of the UCLA Factor building using ambient and earthquake responses. *Smart Mater Struct* 19(2):205005
- Hazra B, Roffel AJ, Narasimhan S, Pandey MD (2010) Modified cross-correlation method for the blind identification of structures. *J Eng Mech* 136(7):889–897
- Hyvärinen A, Oja E (2000) Independent component analysis: algorithms and applications. *Neural Netw* 13:411–430
- Kerschen G, Poncelet F, Golinval J-C (2007) Physical interpretation of independent component analysis in structural dynamics. *Mech Syst Signal Process* 21:1561–1575
- Koh BH, Dharap P, Nagarajaiah S, Phan MQ (2005a) Real-time structural damage monitoring by input error function. *AIAA J* 43(8):1808–1814
- Koh BH, Li Z, Dharap P, Nagarajaiah S, Phan MQ (2005b) Actuator failure detection through interaction matrix formulation. *J Guid Control Dyn AIAA* 28(5):895–901
- Li Z, Koh BH, Nagarajaiah S (2007) Detecting sensor failure via decoupled error function and inverse input-output model. *J Eng Mech ASCE* 133(11):1222–1228
- McNeill SI, Zimmerman DC (2008) A framework for blind identification using joint approximate diagonalization. *Mech Syst Signal Process* 22:1526–1548
- Nagarajaiah S, Basu B (2009) Output only identification and structural damage detection using time frequency and wavelet techniques. *Earthq Eng Eng Vib* 8:583–605
- Nagarajaiah S, Dharap P (2003) Reduced order observer based identification of base isolated buildings. *Earthq Eng Eng Vib* 2(2):237–244
- Nagarajaiah S, Li Z (2004) Time segmented least squares identification of base isolated buildings. *Soil Dyn Earthq Eng* 24(8):577–586
- Nagarajaiah S, Sun X (2000) Response of base-isolated USC hospital building in Northridge earthquake. *J Struct Eng ASCE* 126(10):1177–1186
- Nagarajaiah S, Sun X (2001) Base-isolated FCC building: impact response in Northridge earthquake. *ASCE J Struct Eng* 127:1063–1075
- Poncelet F, Kerschen G, Golinval J-C, Verhelst D (2007) Output-only modal analysis using blind source separation techniques. *Mech Syst Signal Process* 21:2335–2358
- Sadhu A, Hazra B, Narasimhan S, Pandey MD (2011) Decentralized modal identification using sparse blind source separation. *Smart Mater Struct* 20:125009
- Sadhu A, Hazra B, Narasimhan S (2012) Blind identification of earthquake-excited structures. *Smart Mater Struct* 21:045019
- Stone JV (2001) Blind source separation using temporal predictability. *Neural Comput* 13:1559–1574
- Stone JV (2004) Independent component analysis: a tutorial introduction. The MIT Press, Cambridge
- Xie S, He Z, Fu Y (2005) A note on Stone's conjecture of blind source separation. *Neural Comput* 17:321–330
- Yang Y, Nagarajaiah S (2013a) Time-frequency blind source separation using independent component analysis for output-only modal identification of highly-damped structures. *ASCE J Struct Eng* 139(10):1780–1793
- Yang Y, Nagarajaiah S (2013b) Blind identification of modal parameters in time domain based on complexity pursuit. *Earthq Eng Struct Dyn* 42(13):1885–1905

- Yang Y, Nagarajaiah S (2013c) Output-only modal identification with limited sensors using sparse component analysis. *J Sound Vib* 332:4741–4765
- Yang Y, Nagarajaiah S (2014a) Blind identification of damage in time-varying system using independent component analysis with wavelet transform. *Mech Syst Signal Process* 47(1):3–20
- Yang Y, Nagarajaiah S (2014b) Structural damage identification via a combination of blind feature extraction and sparse representation classification. *Mech Syst Signal Process* 45(1):1–23
- Yang Y, Nagarajaiah S (2014c) Blind denoising of structural responses with outliers via principal component pursuit. *Struct Control Health Monit* 21(6):962–978
- Yang Y, Nagarajaiah S (2014d) Data compression of structural seismic responses using principled independent component analysis. *ASCE J Struct Eng* 140(7):04014032
- Zhou W, Chelidze D (2007) Blind source separation based vibration mode identification. *Mech Syst Signal Process* 21(8):3072–3087

---

## Bridge Foundations

Ayman A. Shama<sup>1</sup> and Hesham El Naggar<sup>2</sup>  
<sup>1</sup>Ammann & Whitney, New York, NY, USA  
<sup>2</sup>Geotechnical Research Centre, Department of Civil and Environmental Engineering, The University of Western Ontario, London, ON, Canada

### Introduction

The poor performance of bridges during the 1971 San Fernando earthquake has urged the engineering community to further investigate methods of analysis and evaluation of seismic loads and their effects on these structures. Later, earthquakes such as Northridge, 1994, and Kobe, 1995, have further increased engineers' awareness of the effects of earthquakes on bridges. The past two decades have witnessed a great evolution in seismic design codes, advance modeling, and analysis. Moreover, the importance of the interaction between the structure and the surrounding soil on the seismic response of bridge structures during earthquakes has been fully realized.

Past performance of foundations was satisfactory in moderate earthquakes and poor in large

earthquakes with magnitudes greater than seven. Examples include the 1964 M9.2 Alaskan Earthquake, the 1991 M7.6 Costa Rica Earthquake, the 1999 M7.8 Izmit-Turkey Earthquake, the 2010 M8.8 Chile Earthquake, the 2011 M9.0 Tohoku-Oki Earthquake in Japan, and the 2012 M7.4 Guatemala Earthquake. In all these earthquakes, spread footings failures were due to loss of bearing capacity and lateral spreading due to soil liquefaction. Figure 1 depicts photo of a collapsed bridge during the Limon Province, Costa Rica Earthquake. The piers have disappeared in the river a result of liquefaction and both bridge spans have collapsed during the earthquake.

The seismic response of bridge foundations depends on: the type, geometry, and embedment of the foundation; the characteristics of the surrounding soil; and the interaction between the foundation and the surrounding soil. Soil–structure interaction is the influence of the soil and structure both on each other simultaneously. Seismic ground motions that are not influenced by the presence of the structure are known as free-field motions. If the structure exists, the deformations of the foundations deviate from the deformations of the free-field motion and the dynamic response of the structure induces deformation of the supporting soil. The process in which the response of the soil influences the motion of the structure and the motion of the structure influences the response of the soil is known as soil–structure interaction (SSI). There are two approaches used to incorporate the effect of SSI in seismic analyses of structures, direct methods and simplified methods. In the direct approach, the entire soil–foundation–structure system is modeled and analyzed simultaneously in one step using finite element or finite difference methods with the seismic waves applied at the model boundaries. This approach requires specific programs that can idealize the nonlinear behavior of the soil and large CPU time for analysis. Although it is conceptually very attractive, it is fairly complex and very seldom been applied for practical bridge problems. Simplified methods include the substructure approach and the Winkler approach. The substructure approach includes subdividing the structure into two

**Bridge Foundations,**

**Fig. 1** A bridge collapse due to foundation failure  
Costa Rica  
Earthquake 1993



B

substructures, foundation and superstructure, with a convenient interface between the two. First, the stiffness and damping properties of the foundation system, for each degree of freedom, are first evaluated and then applied to the bridge superstructure in the form of springs and dashpots at the point of interface. The Winkler spring model (Winkler 1867) acts in conjunction with the foundation to eliminate rotational springs. The p-y curve method, which was developed for off-shore structures and used for analysis of deep foundations, originates from the Winkler spring method.

The most common types of bridge foundations are: (i) spread footings for sites of rock and stiff soil; (ii) pile-supported cap foundations for sites with soft soil or for sites with soil layers vulnerable to liquefaction; (iii) drilled shafts for cohesive soils, especially with deep groundwater or when construction of new foundations requires a small footprint wherein, a single drilled shaft under a single column can avoid the large footprint that would be necessary with a group of piles; and (iv) large gravity caissons for complex bridges such as cable supported bridges.

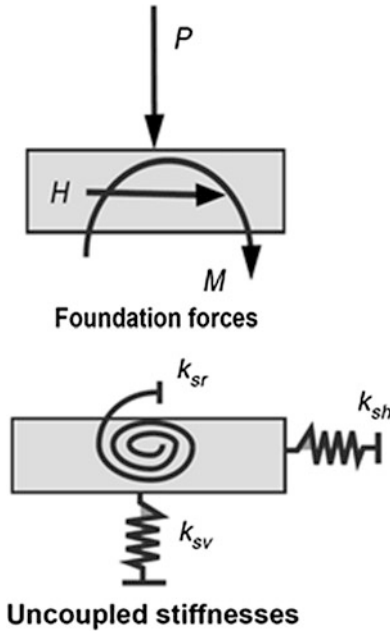
The subsequent sections of this chapter discuss the procedures for modeling bridge foundations for analysis including effects of SSI. Methods for designing these foundations to resist seismically induced forces and displacements are also explained.

## Spread Footings

Spread footings are usually suitable for sites of rock and firm soils. The stability of these foundations under seismic loads can be evaluated using a pseudostatic bearing capacity procedure. The applied loads for this analysis can be taken directly from the results of a global dynamic response analysis of the bridge with the soil-foundation-interaction effects represented in the structural model.

### Spread Footing Stiffness

A method to be selected for evaluating the foundation stiffness must adequately reflect the shape of the foundation–soil interface; the amount of embedment; the nature of the soil profile; and the mode of vibration and frequencies of excitation. The uncoupled spring approach satisfies all these conditions. It is accomplished through determining the dynamic impedance functions for the foundation. This method is adequate if the seismic foundation loads are not expected to exceed twice the ultimate foundation capacities. As illustrated in Fig. 2, the dynamic impedance model is an uncoupled single node model that represents the foundation element. An upper and lower bound approach to evaluating the foundation stiffness is often used because of the uncertainties in the soil properties and the static loads on the foundations. As a general rule of thumb, a factor



**Bridge Foundations, Fig. 2** Analysis model for spread footings

of 4 is taken between the upper and lower bound (ATC-1995).

The dynamic impedance model is based on earlier studies on machine foundation vibrations, in which, it is assumed that the response of rigid foundations excited by harmonic external forces can be characterized by the impedance or dynamic stiffness matrix for the foundation. The impedance matrix depends on the frequency of excitation, the geometry of foundation and the properties of the underlying soil deposit.

The evaluation of the impedance functions for a foundation with an arbitrary shape has been solved mathematically using a mixed boundary-value problem approach or discrete variation problem approach. Currently, there are two commonly used approaches for evaluating the dynamic impedance functions for a shallow foundation. The first is based on the approximate solution for a circular footing rigidly connected to the surface of isotropic homogeneous elastic half space. The second approach is more general and is applicable to a foundation with an arbitrary shape.

In the equivalent circular base approach the impedance function of a foundation is obtained from the elastic solution of a rigid massless circular base resting on the surface of the soil for each degree of freedom independently. The impedance function for each degree of freedom is a frequency dependent complex expression, where its real part represents the elastic stiffness (spring constant) of the soil-foundation system and its imaginary part represents the damping in the soil-foundation system. The impedance function is expressed as:

$$\bar{k}_j = k_j(a_0, \nu) + i\omega c_j(a_0, \nu) \quad (1)$$

where,  $k_j$  is the real part represent the dynamic stiffness for a specific degree of freedom  $j$ ,  $c_j$  is the imaginary part represent the damping for a degree of freedom  $j$ ,  $\nu$  is Poisson's ratio of the soil medium,  $a_0$  is a dimensionless frequency expressed as:

$$a_0 = \frac{\omega r_j}{V_s} \quad (2)$$

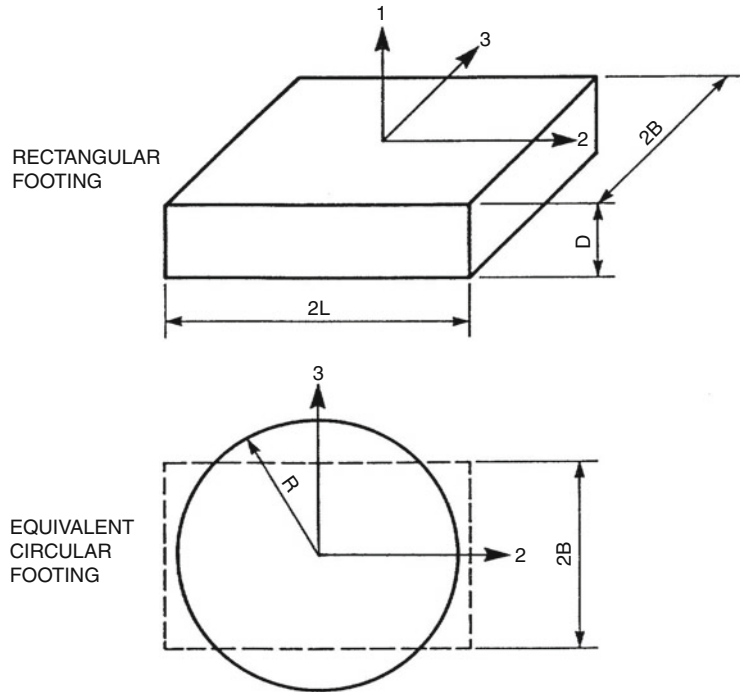
in which,  $\omega$  is the circular frequency of excitation in rad/s,  $r_j$  is equivalent radius for a specific degree of freedom, and  $V_s$  is the shear wave velocity of the soil medium. Both the dynamic stiffness  $k_j$  and the damping  $c_j$  are obtained in terms of the static stiffness  $K_j$  as:

$$k_j = \alpha_j K_j \quad \text{and} \quad c_j = \beta_j \frac{K_j r_j}{V_s} \quad (3)$$

where  $\alpha_j$  and  $\beta_j$  are dynamic modifiers are evaluated as function of the dimensionless frequency  $a_0$  and Poisson's ratio  $n$ .

Evaluation of the static stiffness coefficients can be obtained using the equivalent circular footing, wherein it is assumed that the footing is rigid and founded on top of a semi-infinite elastic half space. The rectangular footing is converted to an equivalent circular footing for each degree of freedom. The stiffness coefficients are evaluated for the circular footing and then multiplied

**Bridge Foundations,**  
**Fig. 3** Procedure for evaluating equivalent radius of a rectangular footing



EQUIVALENT RADIUS:

TRANSLATIONAL:  $R_0 = \sqrt{\frac{4BL}{\pi}}$

ROTATIONAL:  $R_1 = \left[ \frac{(2B)(2L)^3}{3\pi} \right]^{1/4}$  (x-AXIS ROCKING)

$R_2 = \left[ \frac{(2B)^3(2L)}{3\pi} \right]^{1/4}$  (y-AXIS ROCKING)

$R_3 = \left[ \frac{4BL(4B^2 + 4L^2)}{6\pi} \right]^{1/4}$  (z-AXIS TORSION)

by shape and embedment factors to obtain the solution for the rectangular base. The solution is carried out in five steps as follows:

*Step 1:* Determine the equivalent radius for each degree of freedom, which is the radius of a circular footing with the same area as the rectangular footing as shown in Fig. 3.

*Step 2:* Calculate the stiffness coefficients  $K_0$  for the transformed circular footing (Table 1), where,  $G$  and  $\nu$  in the table are the shear modulus and Poisson's ratio for the soil-foundation system.

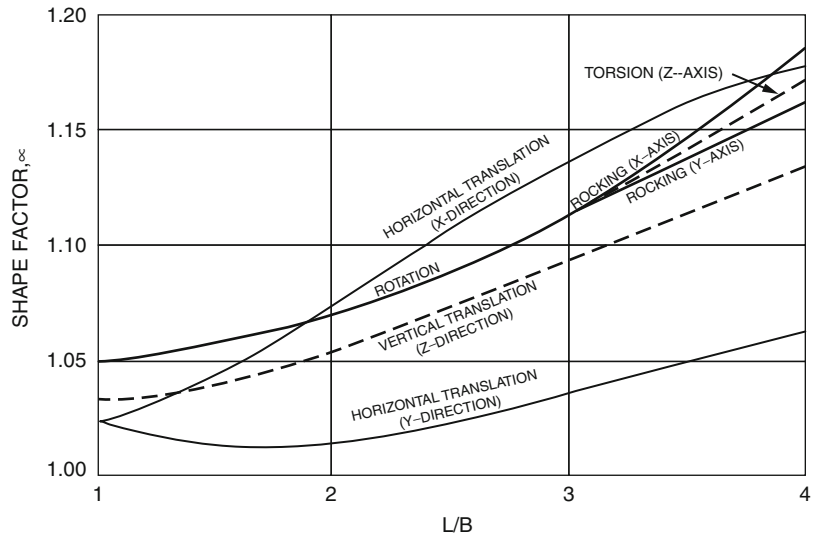
**Bridge Foundations, Table 1** Static stiffness coefficients for a circular footing resting on the surface of soil

Displacement degree-of-freedom	$k_0$
Vertical translation	$\frac{4Gr}{1-\nu}$
Horizontal translation	$\frac{8Gr}{2-\nu}$
Torsional rotation	$\frac{16}{3} Gr^3$
Rocking rotation	$\frac{8Gr^3}{3(1-\nu)}$

*Step 3:* Multiply each of the stiffness coefficients values obtained in step 2 by the appropriate shape correction factor  $\alpha$  from Fig. 4 (Lam and Martin 1986). This figure provides the shape



**Bridge Foundations,**  
**Fig. 4** Shape factors for rectangular footings (Lam and Martin 1986)



factors for different aspect ratios  $L/B$  for the foundation.

*Step 4:* Multiply the values obtained from step 3 by the embedment factor  $\beta$  using Fig. 5.  $D$  in these figures is the footing thickness.

*Step 5:* Calculate the dynamic stiffness and the damping coefficients using Eq. 3 and the charts displayed in Figs. 6, 7, and 8 (Veletsos and Verbic 1973),

The static stiffness can be calculated using the second approach for calculating the impedance functions for the soil-foundation system (Gazetas 1991). Using Fig. 9, a two-step calculation process is required. First, the stiffness terms are calculated for a foundation at the surface. Then, an embedment correction factor is calculated for each stiffness term. The stiffness of the embedded foundation is the product of these two terms. According to Gazetas, the height of effective sidewall contact,  $d$ , in Fig. 9 should be taken as the average height of the sidewall that is in good contact with the surrounding soil.

Considering the range of frequencies and amplitudes in earthquake ground motions compared to machine foundations, it is reasonable to ignore the frequency dependence of the stiffness as well as the damping parameters.

Based upon the results of the dynamic analysis, the peak dynamic loads and deformations of

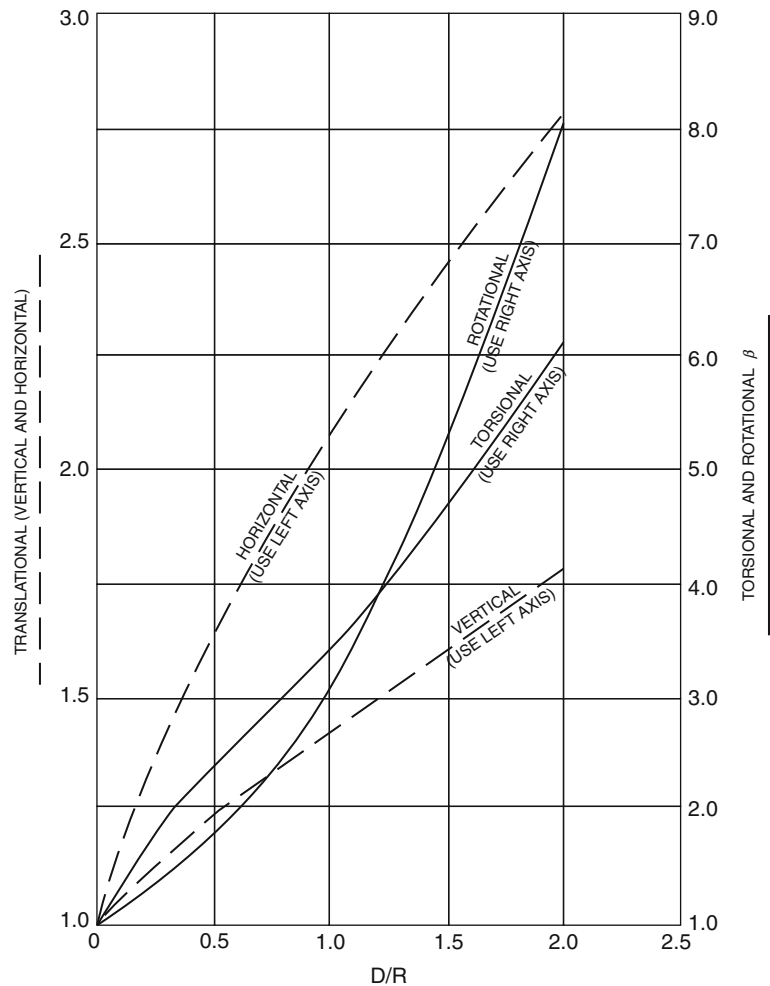
the foundation are determined and compared to acceptable values. The foundation must be evaluated for bearing capacity and sliding resistance due to the seismic loads.

### Seismic Design of Spread Footings

Earthquakes will induce moments and horizontal loads in addition to the traditional vertical loads applied to a spread footing. In low seismic hazard areas, spread footings may be proportioned to resist overturning, sliding, flexure, and shear due to forces obtained from the seismic analysis of the bridge. In high seismic regions, the flexural and shear demands are those associated with the over-strength plastic moment capacity of the column or pier attached to the footing. To represent the combined effect of the seismic forces and moments a resultant load that may have to be inclined and applied eccentrically can be applied in lieu of the seismic vertical forces, seismic horizontal forces, and seismic moments. Therefore, a procedure is established to account for load inclination and load eccentricity of footing through which the general bearing capacity equation of shallow footing is adjusted to account for these effects. This procedure is carried out in three steps as follows:

*Step 1:* Compute the seismic vertical loads, seismic horizontal loads, and seismic moments

**Bridge Foundations,**  
**Fig. 5** Embedment factors  
 for rectangular footings  
 (Lam and Martin 1986)



B

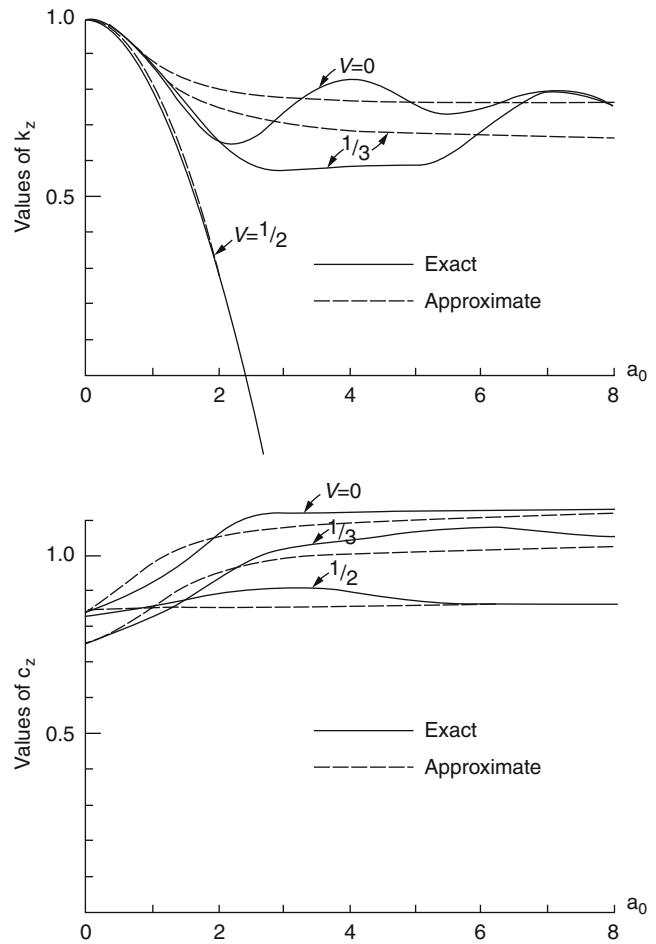
imposed to the footing. These seismic loads and moments can be taken directly from the results of a global dynamic response analysis of the structure with the soil–foundation interaction SFI effects represented in the structural model. For each direction, these forces are then combined into a single resultant force with an inclination angle  $\beta$  with respect to the vertical.

*Step 2:* Calculate the equivalent dimensions for the footing to account for the load eccentricity, which is caused by the seismic moments applied to the foundation in both directions. The vertical load can be transferred to an eccentric position defined by  $e_b = M_b/Q$  and  $e_l = M_l/Q$ , where  $Q$  is the central vertical load due to seismic load plus other service loads;

$M_b$  and  $M_l =$  seismic moments about the short and long axes of the footing; and  $e_b$  and  $e_l =$  eccentricities of the load  $Q$  about the centroid of the footing in the direction of the short and long axes respectively.

It is known from basic principles of strength of materials that if the eccentricity in one direction is less than 1/6 of the foundation’s length in that direction, the footing is in compression throughout. As eccentricity exceeds this value, a loss of contact occurs. The concept of effective width was introduced by Meyerhof (1953) who proposed that at the ultimate bearing capacity of the foundation, it could be assumed that the contact pressure is identical to that for a centrally loaded foundation but of reduced width. The reduced

**Bridge Foundations,**  
**Fig. 6** Dynamic modifiers  
 for vertically excited  
 footing



dimensions as indicated in AASHTO-LRFD (AASHTO 2012) for a footing subjected to two-way eccentricity can be adopted as illustrated in Fig. 10.

*Step 3:* Adjust the static bearing capacity equation for inclination and eccentricity. Load inclination factors may be calculated as Vesic 1970 and added to the static bearing capacity equation to count for load inclination.

The sliding resistance of a spread footing should be evaluated independently of the bearing capacity, wherein, the unit adhesion and/or frictional resistance of the footing's base to sliding are multiplied by the area of the base to obtain the sliding resistance.

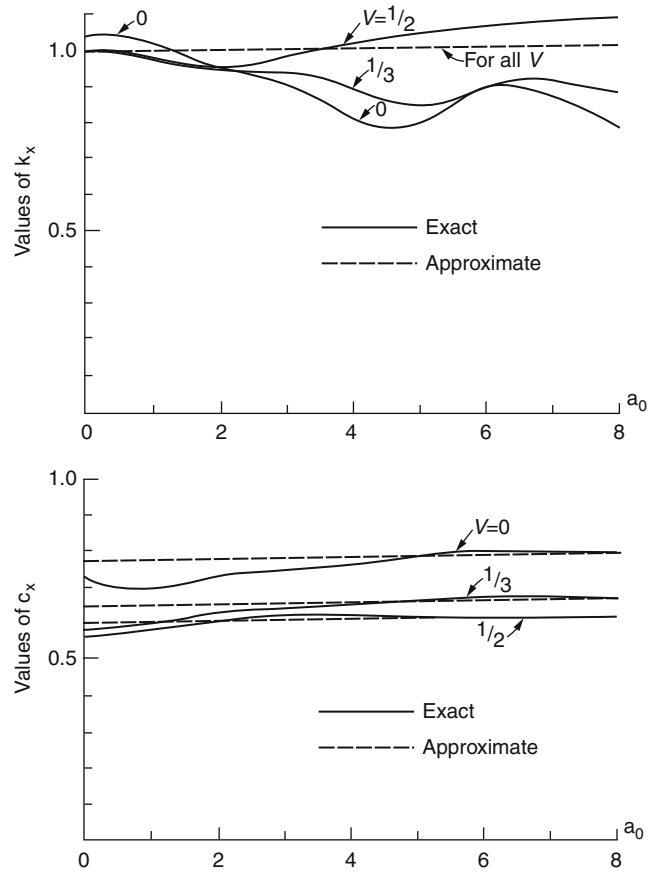
Spread footings are not allowed to be located in soils that are susceptible to liquefaction unless the footing is below the

maximum depth of liquefaction. Soil densifications or other acceptable methods for mitigating the potential for liquefaction may be used. Spread footings can be used in this case only if verification studies confirm that liquefaction potential has been mitigated.

### Pile Footings

Pile footings generally consist of pile groups connected to a pile cap with pile diameters usually less than or equal to 24 in. They are preferred if the upper soil layers are weak or susceptible to liquefaction. Essentially, the seismic response of piles requires consideration of six degrees of freedom; that is, three translational components and three rotational components. The lateral soil

**Bridge Foundations,**  
**Fig. 7** Dynamic modifiers  
 for horizontally excited  
 footing



B

reactions are usually mobilized along the top 5–10 pile diameters. The axial soil resistances, however, develop at greater depths. Hence, the axial and lateral capacities of piles are considered to be uncoupled.

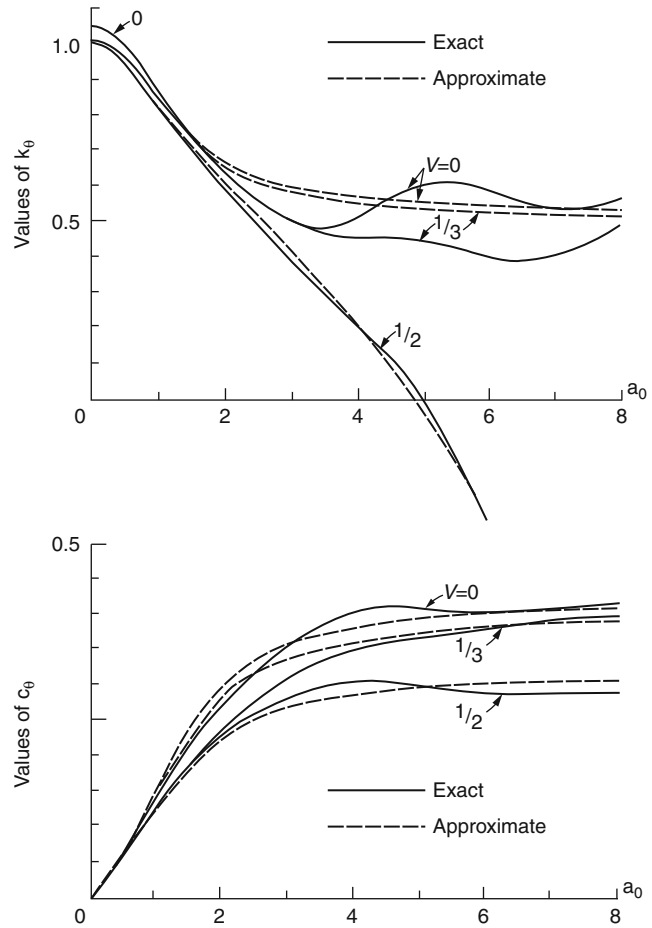
In general, seismic design of pile foundations is evaluated by the substructure method. First, the total structure is divided into two substructure models with a convenient interface between the two at the pile cap level. Next, the stiffness matrix of the pile group, which implies soil effects, is established using the foundation substructure model or simple methods. The stiffness matrix is then implemented in the superstructure model and seismic analysis is conducted using the superstructure model to determine the demands at the interface point. Finally, capacities of individual piles are evaluated and compared to the demands by back substitution in the substructure model. For a proper determination of the seismic

demand, it is imperative to estimate precisely the foundation stiffness to be included in the overall structural model for determination of the demands.

**Pile Foundation Stiffness**

Soils are inherently nonlinear, starting from incredibly small load levels. Lateral loads on piles are resisted by the surrounding soil. Therefore, piles exhibit nonlinear load deflection characteristics. This behavior is represented assuming the pile as a beam supported on Winkler springs that are characterized by nonlinear p-y curves for lateral loading, or t-z and q-z for vertical loading. These curves characterize the lateral soil resistance per unit length of pile as a function of the displacement. These relationships are generally developed on the basis of semiempirical curves, which reflect the nonlinear resistance of the local soil surrounding the pile at a certain depth.

**Bridge Foundations,**  
**Fig. 8** Dynamic modifiers  
 for footing in rocking  
 motion



The two most commonly used p-y models are those proposed by Matlock (1970) for soft clay and by Reese et al. (1974) for sand. The most commonly used t-z and q-z models are those developed by McVay et al. (1998).

There are two methods for modeling the behavior of pile groups for seismic response studies, the soil-pile stiffness as will be explained in the following subsections.

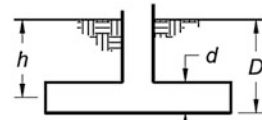
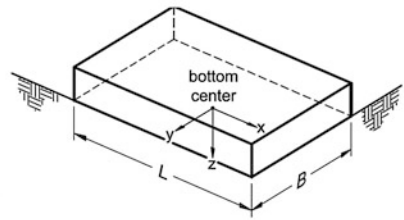
**Coupled Pile Foundation Stiffness Matrix**

In this method, a quasi-dynamic analysis for the pile group is conducted by applying loading (either as forces or displacements) at the interface node between the superstructure and foundation model using linearized properties for the soils. Linearized properties for a single pile can be achieved by assuming secant foundation stiffness

at 0.5–0.65 of peak deflection (Lam et al. 1998). A stiffness matrix can be obtained by prescribing a unit deformation vector for each degree of the six degrees of freedom, while keeping the other five degrees zero. The resultant force vector corresponding to each unit deformation vector can be used to form the corresponding column vector in the stiffness matrix. The stiffness matrix must be positive definite otherwise, numerical problems may be expected when the stiffness matrix is implemented in the overall structural model. One way to ensure that the stiffness matrix is positive definite is to invert it and check that the diagonal elements in the inverted (compliance) matrix are positive values. Programs such as LPILE (2010), FLPIER (Hoit and McVay 2010), and SWM (Ashour and Norris 2000) may be used to establish the foundation

Stiffness Parameter	Stiffness at Surface, $K_i$
Vertical Translation, $K_z$	$\frac{GL}{(1-\nu)} \left[ 0.73 + 1.54 \left( \frac{B}{L} \right)^{0.75} \right]$
Horizontal Translation, $K_y$ (toward long side)	$\frac{GL}{(2-\nu)} \left[ 2 + 2.5 \left( \frac{B}{L} \right)^{0.85} \right]$
Horizontal Translation, $K_x$ (toward short side)	$\frac{GL}{(2-\nu)} \left[ 2 + 2.5 \left( \frac{B}{L} \right)^{0.85} \right] - \frac{GL}{(0.75-\nu)} \left[ 0.1 \left( 1 - \frac{B}{L} \right) \right]$
Rotation, $K_{\theta_x}$ (about x axis)	$\frac{G}{(1-\nu)} I_x^{0.75} \left( \frac{L}{B} \right)^{0.25} \left( 2.4 + 0.5 \frac{B}{L} \right)$
Rotation, $K_{\theta_y}$ (about y axis)	$\frac{G}{(1-\nu)} I_y^{0.75} \left[ 3 \left( \frac{L}{B} \right)^{0.15} \right]$

Stiffness Parameter	Embedment Factors, $e_i$
Vertical Translation, $e_z$	$\left[ 1 + 0.095 \frac{D}{B} \left( 1 + 13 \frac{B}{L} \right) \right] \left[ 1 + 0.2 \left( \frac{2L + 2B}{LB} d \right)^{0.67} \right]$
Horizontal Translation, $e_y$ (toward long side)	$\left[ 1 + 0.15 \left( \frac{2D}{B} \right)^{0.5} \right] \left\{ 1 + 0.52 \left[ \frac{(D-d) 16(L+B)d}{BL^2} \right]^{0.4} \right\}$
Horizontal Translation, $e_x$ (toward short side)	$\left[ 1 + 0.15 \left( \frac{2D}{L} \right)^{0.5} \right] \left\{ 1 + 0.52 \left[ \frac{(D-d) 16(L+B)d}{LB^2} \right]^{0.4} \right\}$
Rotation, $e_{\theta_x}$ (about x axis)	$1 + 2.52 \frac{d}{B} \left( 1 + \frac{2d}{B} \left( \frac{d}{D} \right)^{-0.20} \left( \frac{B}{L} \right)^{0.50} \right)$
Rotation, $e_{\theta_y}$ (about y axis)	$1 + 0.92 \left( \frac{2d}{L} \right)^{0.60} \left( 1.5 + \left( \frac{2d}{L} \right)^{1.9} \left( \frac{d}{D} \right)^{-0.60} \right)$



$d$  = height of effective sidewall contact (may be less than total foundation height)

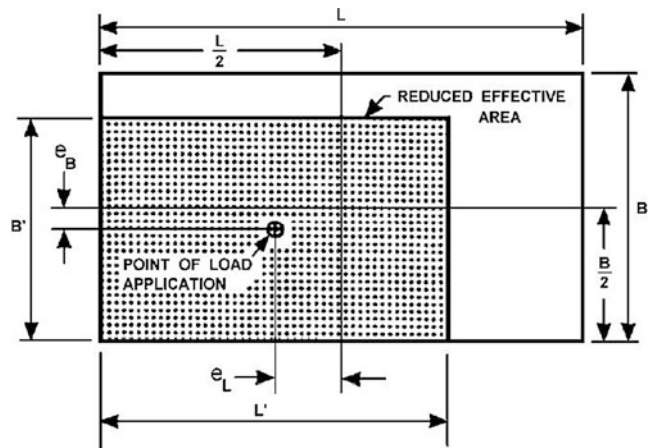
$h$  = depth to centroid of effective sidewall contact

For each degree of freedom, calculate

$$K_{emb} = \beta K_{sur}$$

**Bridge Foundations, Fig. 9** Static stiffness coefficients (Gazetas 1991)

**Bridge Foundations, Fig. 10** Effective footing dimensions due to eccentric loads (After AASHTO LRFD 2012)



$$B' = B - 2e_B$$

$$L' = L - 2e_L$$

where:

$e_B$  = eccentricity parallel to dimension  $B$  (ft)

$e_L$  = eccentricity parallel to dimension  $L$  (ft)



stiffness matrix of the pile group through an iterative process.

#### Simplified Procedure for Pile Group Stiffness Matrix

The simplified method assumes coupling only between shear and overturning moment for the single pile. The general form of a single pile stiffness matrix can take the form:

$$\begin{bmatrix} K_{xx} & 0 & 0 & 0 & -K_{x\theta_y} & 0 \\ 0 & K_{yy} & 0 & K_{y\theta_x} & 0 & 0 \\ 0 & 0 & K_{zz} & 0 & 0 & 0 \\ 0 & K_{\theta_x y} & 0 & K_{\theta_x} & 0 & 0 \\ -K_{\theta_y x} & 0 & 0 & 0 & K_{\theta_y} & 0 \\ 0 & 0 & 0 & 0 & 0 & K_{\theta_z} \end{bmatrix} \quad (4)$$

in which,  $K_{xx}$ ,  $K_{yy}$  are the lateral stiffnesses;  $K_{zz}$  is the axial stiffness; and  $K_{x\theta_y}$  and  $K_{y\theta_x}$  are corresponding coupled stiffnesses between shear and overturning moment.

The simplified method involves five basic steps (Lam et al. 1991) as follows:

1. Determine the stiffness coefficient of a single pile under lateral loading.
2. Determine the stiffness coefficient of a single pile under axial loading.
3. Superimpose the stiffness of individual piles to obtain the pile group stiffness.
4. Solve for the stiffness contribution of the pile cap.
5. Superimpose the stiffness of the pile cap to the pile group.

These steps are described herein.

**Step 1: Single Pile Under Lateral Load** Lam and Martin (1986) came to a realization that lateral load-deflection characteristics representing the overall stiffness of the soil pile system are dominated by the elastic pile stiffness over the nonlinear soil behavior. Moreover, the localized zone of influence is limited to the upper 5–10 pile diameters. Hence, they concluded that linear solutions may be adequate for pile stiffness evaluations. They developed single-layer, pile-head

stiffness design charts for lateral loading as presented in Figs. 11, 12, and 13. These charts are applicable for piles up to 24 in. Two parameters are required to define the soil-pile system: the pile bending stiffness,  $EI$ , and the coefficient of variation  $f$  of soil reaction modulus  $E_s$  with depth. The coefficient  $f$  has units of force/unit volume.

**Step 2: Single Pile Under Axial Load** The recommended LRFD guidelines for the seismic design of highway bridges proposed the following simple equation for the determination of the axial stiffness of the pile:

$$K_v = 1.25 \frac{E_p A}{L} \quad (5)$$

Wherein,  $E_p$  is the modulus of elasticity of pile material;  $A$  is cross sectional area of pile; and  $L$  is length of pile.

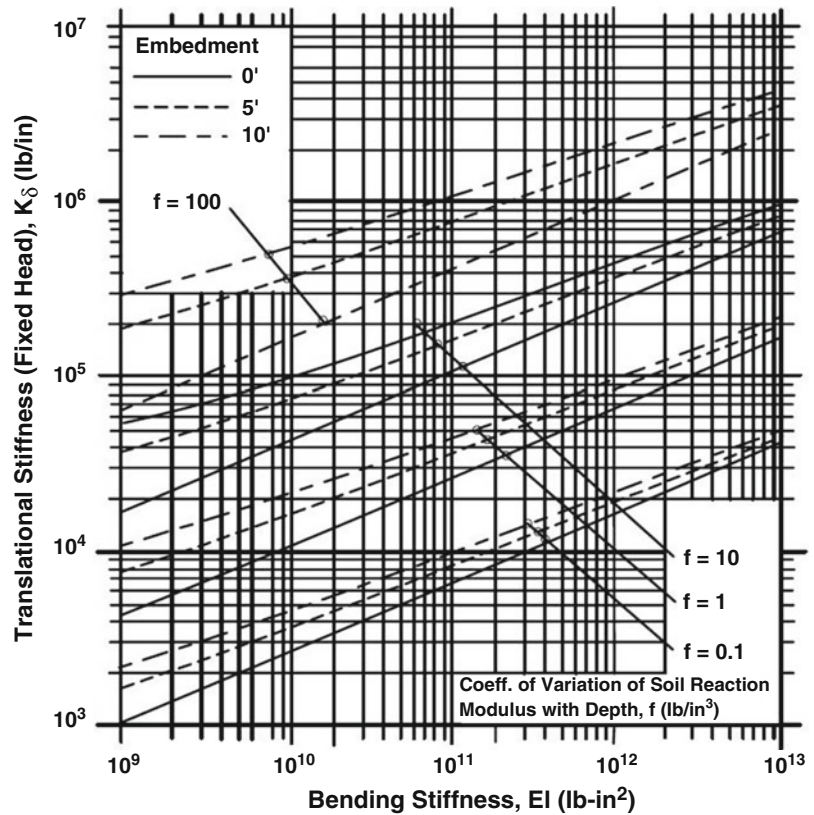
**Step 3: Pile Group Stiffness** The stiffness of the single pile can be used to establish the pile group stiffness matrix. If the pile group consists of vertical piles, the stiffness summation procedure is relatively straight forward. The stiffness for the translational displacement terms (the two horizontal and the vertical displacements) and the cross-coupling terms can be obtained by multiplying the corresponding stiffness components of an individual pile by the number of piles.

In general, the axial stiffness of the piles will dominate the rotational stiffness of the group. Therefore, the rotational stiffness terms require consideration of this additional stiffness component. Similarly, there is an interaction between the translational stiffness of piles and the torsional stiffness of the group. The following equation (Lam et al. 1991) can be used to develop the rotational terms of a pile group:

$$K_{RG} = NK_{RP} + \sum_{n=1}^N K_{\delta n} S_n^2 \quad (6)$$

In which,  $K_{RG}$  and  $K_{RP}$  are the rotational stiffness of the pile group and an individual pile respectively;  $N$  is the number of piles in the pile group;

**Bridge Foundations,**  
**Fig. 11** Pile translational  
 stiffness



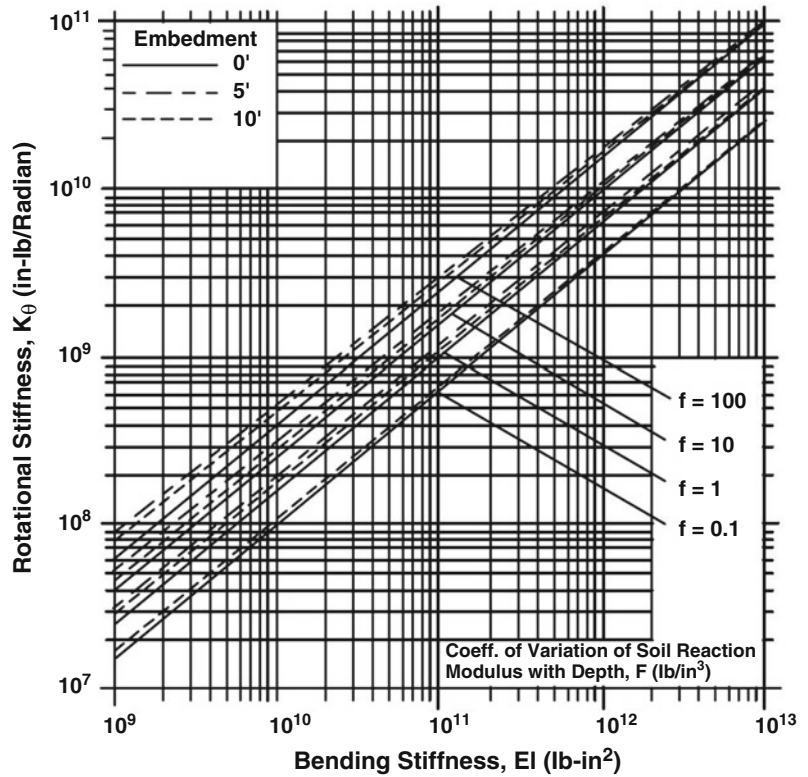
$K_{\delta_n}$  is the translational stiffness coefficient of an individual pile (axial for group rocking stiffness and lateral for group torsional stiffness); and  $S_n$  is the distance between the nth pile and the axis of rotation.

**Step 4: Stiffness Contribution of the Pile Cap** In addition to the component of soil resistance acting on piles, the passive pressure soil resistance on the vertical pile cap face can be added to the stiffness and resistance obtained from the pile members. This is contingent on stable level ground conditions. The pile cap stiffness can be estimated as the ultimate soil capacity divided by an estimated displacement to mobilize this capacity. Centrifuge tests (Gadre 1997) showed that the deflection level to reach the ultimate pile cap capacity occurs at about 0.02 times the embedment depth. This equivalent linear secant stiffness can be added to the stiffness of the piles.

**Step 5: Superimpose the Stiffness of the Pile Cap to the Pile Group** The resultant pile cap stiffness obtained from step 4 can be added to the diagonal lateral translational stiffness coefficients in the pile group stiffness matrix for the total pile group–pile cap stiffness matrix.

The above procedure does not account for group effects which relate to the influence of the adjacent piles in affecting the soil support characteristics. Full-scale tests by a number of investigators demonstrate that the lateral capacity of a pile in a pile group may be less than that of a single pile due to the interaction between closely spaced piles in the group (group efficiency). As the pile spacing reduced, the reduction in lateral capacity becomes more pronounced. In general, pile spacing of less than 3–5 pile diameters are necessary before the effects of pile interaction becomes significant in practical terms. Type and strength of soil, number of piles, and loading level are other factors that may affect the

**Bridge Foundations,**  
**Fig. 12** Pile rotational  
 stiffness



efficiency and lateral stiffness of the pile. Moreover, in addition to group effect, gapping, and potential cyclic degradation were also subject of many investigations (e.g., Brown et al. 1987; McVay et al. 1995). It has been shown that a concept based on p-multiplier applied on the standard stiffness matrix can work reasonably to account for pile group and cyclic degradation effects.

**Seismic Design of Pile Footings**

Design of pile footings for seismic effects is often relatively a complex process. The strategy of the seismic design is to determine capacity and deflection of the piles under the action of the seismic lateral loads and ensure the integrity of the pile group against liquefaction.

**Moment Capacity of Pile Groups**

Typically, the foundation system is designed to be capacity protected, which ensures that damage occurs above ground, where it can be accessed and repaired. The seismic moment capacity of the

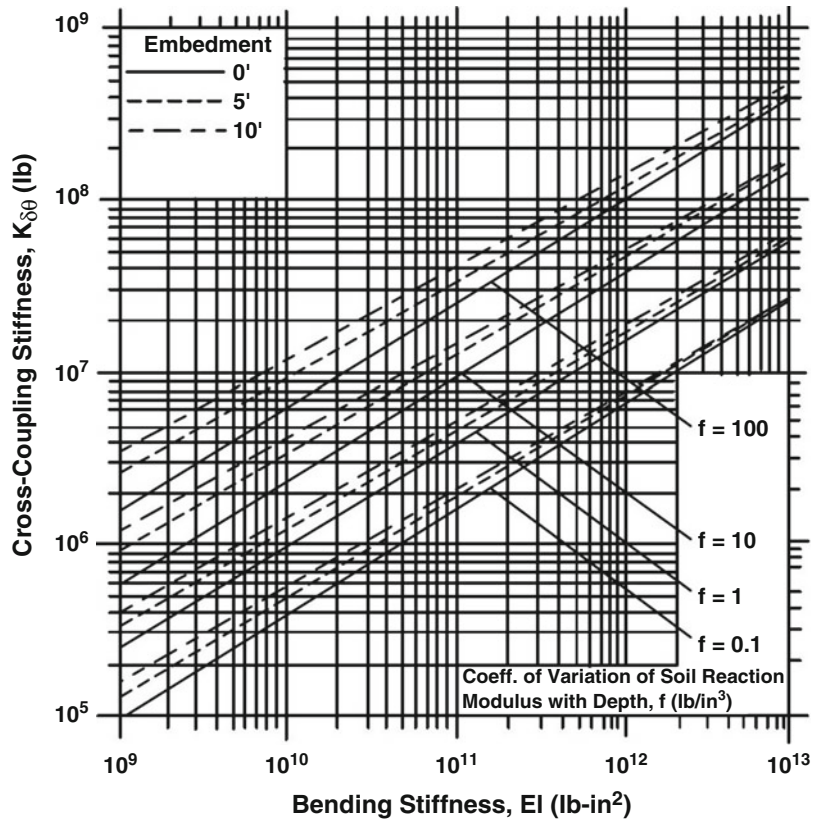
pile group will govern the design. For a fixed-head pile group, the piles must be designed for the plastic hinging moment capacity of the column/pier connected to the pile cap. The maximum negative moment occurs at the base of the pile cap while the maximum positive moments occur in the pile at a short depth below the base. In this regard, the pile cap has to be designed to behave rigidly. The rigid response of the footing may be assumed if the following equation is satisfied (AASHTO 2011):

$$\frac{L}{D} \leq 2.5 \tag{7}$$

where,  $L$  is the cantilever overhang length measured from the face of pier or column to the outside edge of the pile cap and  $D$  is the depth of the pile cap. Due to the interaction between the rocking response and the vertical response of a pile group, the axial demands on an individual pile can be estimated as:

**Bridge Foundations,**

**Fig. 13** Pile cross-coupling stiffness



$$F = \frac{P}{N} \pm \frac{M_Y^{col} C_{X_i}}{I_{pgy}} \pm \frac{M_X^{col} C_{Y_i}}{I_{pgx}} \quad (8)$$

in which,  $P$  is the total axial load due to dead load, footing weight, and seismic load;  $N$  is the total number of piles in a group;  $C_{X_i}$  and  $C_{Y_i}$  are the distances from neutral axis of pile group to  $i$ th row of piles measured parallel to the  $x$  and  $y$  axes respectively;  $M_X^{col}$  and  $M_Y^{col}$  are the plastic moment capacities of the pier or column connected to the footing about the  $x$  and  $y$  axes respectively; and  $I_{pgx}$  and  $I_{pgy}$  are the effective moment of inertia of pile group about the  $x$  and  $y$  axes evaluated as:

$$I_{pgx} = \sum_{i=1}^{N_x} n_x c_{yi}^2 \quad \text{and} \quad I_{pgy} = \sum_{i=1}^{N_y} n_y c_{xi}^2 \quad (9)$$

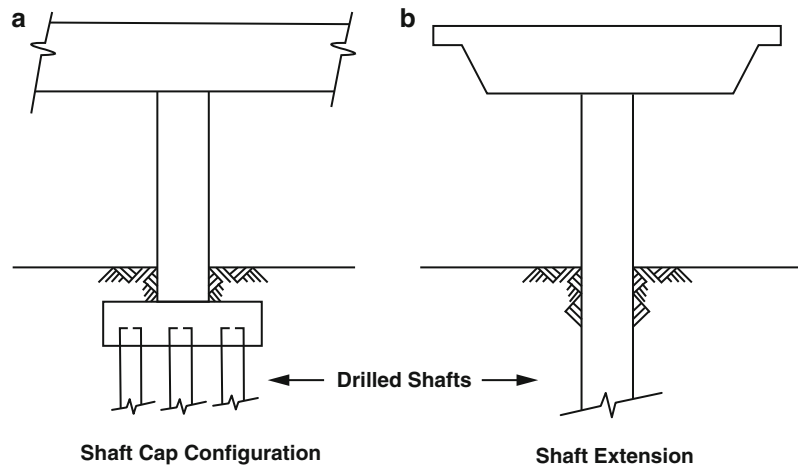
where  $n_x$  and  $n_y$  are the number of piles in a single row parallel to the  $x$  and  $y$  axes.

For a foundation protected design strategy, the connection of pile to cap should be designed such that its moment capacity exceeds that of the pile.

**Pile-to-Cap Connection**

The moment capacity at the connection depends on both the depth of embedment of the pile into the cap and the reinforcement arrangement. Driven precast piles should be constructed with considerable spiral confining steel to ensure good shear strength and tolerance of yield curvatures that may be exerted during the seismic event. Parametric studies (Harris and Petrou 2001) with prestressed piles suggest that the embedment length should be taken as the larger of the pile diameter or 12 in.. Experimental studies (Shama and Mander 2004) have showed that an embedment of one pile diameter of a timber pile into a pile cap was sufficient to develop the full moment capacity of the pile and provide a ductile response. Experimental studies (Rollins and Stenlund 2011) also showed that steel pipe piles

**Bridge Foundations,**  
**Fig. 14** Drilled shafts  
 configuration



embedded 24 in. into a pile cap can produce a sufficient moment capacity for the connection without the need for a reinforcement detail. These observations agree with the results of cyclic tests on steel HP piles (Shama et al. 2002).

#### Lateral Capacity of Pile Footings

The lateral capacity of piles requires compiling of both geotechnical and structural engineering principles. For a successful design, it is important to get the soil resistance mobilized before structural failure of the pile. The relative importance of the pile cap lateral capacity to the individual piles needs to be considered. Therefore, the lateral capacity evaluation must include the resistance developed by the pile cap in addition to the lateral shear resistance of the piles. Including the lateral capacity of the pile cap is contingent upon efficient compaction of the soils around the pile cap to improve the cap resistance. The lateral capacity of the pile cap must include the passive pressure mobilized at the front face of the cap perpendicular to the seismic load and the interface shear resistance developed along the sides of the cap parallel to the application of the seismic load.

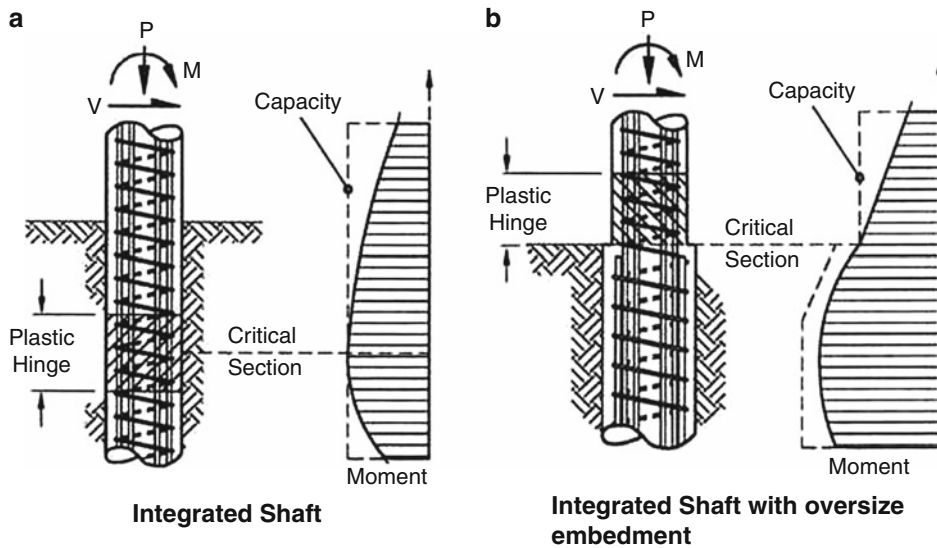
### Drilled Shafts

Drilled shafts are large diameter piles that are designed to sustain high axial loads and overturning moments. They are constructed

using drilling (excavating) equipment capable of auguring or coring 30" to 120" diameter excavations into soil and rock. After the excavation is completed, a reinforcing cage is placed in the excavation and the excavation is filled with high slump concrete. Drilled shafts are usually constructed with steel shells.

Drilled shafts are attached to the superstructure in two configurations as illustrated in Fig. 14. In the first configuration a group of drilled shafts, usually 4–6 are connected to a cap that supports the bridge pier or column. In the second configuration, a large diameter shaft is extended as a structural unit to support the bridge superstructure. The second configuration comes in two alternatives as illustrated in Fig. 15 (Priestley et al. 1996). In the first alternative, the section of the column above the ground is similar to that of the shaft. The maximum moment forms at a depth of typically 1.5–2.5 shaft diameter. A disadvantage of this alternative is that the extent of damage to the plastic hinge region will be below ground after an earthquake and needs excavation of the soil material for inspection. With the alternative detail of Fig. 15b, the moment capacity of the shaft below ground is increased above that of the column above ground to ensure that hinging occurs at the base of the column and damage can be expected after an earthquake. The disadvantage of this detail is that it is more expensive with respect to the alternative of Fig. 15a.





**Bridge Foundations, Fig. 15** Extended shaft seismic design alternatives (Priestley et al. 1996)

**Stiffness of Drilled Shaft Foundations**

The most common methods for modeling drilled shaft behavior in a global bridge model for seismic response analysis are categorized to three classes:

- (a) Beam supported on nonlinear Winkler springs
- (b) Equivalent cantilever model
- (c) Coupled foundation stiffness matrix

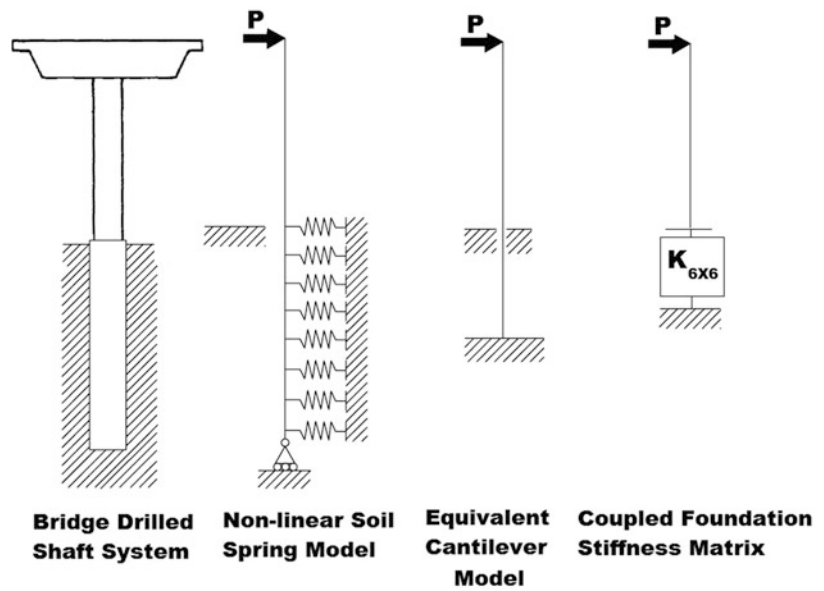
**Beam Supported on Nonlinear Winkler Model**

The beam supported on nonlinear Winkler springs method can be implemented in the structural model without any difficulty as the number of large diameter drilled shafts for a typical bridge is limited. This model, as illustrated in Fig. 16, is based on representing the soil by a series of nonlinear springs. It provides a complete representation of the soil–structure interaction. Furthermore, nonlinear behavior as plastic hinging of the shaft cross-section can be included as well as soil yielding. This approach is usually required for bridges located in highly active seismic regions. Two analytical methods are available to establish the nonlinear springs. These are the p-y method and the strain wedge method. The p-y model, as described in section “**Pile**

**Foundation Stiffness,”** simply describes the force displacement relationship of a soil spring, in which  $p$  is the soil reaction per unit length at a certain location along the embedment length of the pile into soil and  $y$  is the corresponding deflection of the pile. A major shortage of this method is that the p-y curves are semiempirical relationships and were developed based on a limited number of full-scale lateral load tests on piles of diameters ranging from 12 to 24 in.. Hence, they might underestimate the soil stiffness for larger diameter drilled shafts. Also, the p-y method uses a P-multiplier to account for group effects. Selection of values of this parameter is still controversial as treated by different codes and specifications. The strain wedge method (Ashour and Norris 1998), on the other hand, fills all these gaps. The nonlinear springs, obtained using this method, are based on modeling the three-dimensional interaction between the surrounding soil and the shaft. The method considers the alternative effects of the pile properties (stiffness and cross-section) and soil properties in developing the p-y curve. Furthermore, there is no need to use P-multipliers to the strain wedge method because this method accounts for the group effects through an assessment of the overlap of the passive wedges that develop due to



**Bridge Foundations, Fig. 16** Methods of representing shaft foundation stiffness



pushing the shaft in the lateral direction. For a group, the strain wedges for different shafts will interfere together, depending on the spacing, diameter, and location of the shaft within the group leading to strength reduction and softening.

The nonlinear spring modeling technique can include the Masing hysteretic behavior of the soil, which when implemented includes automatically in the model the energy dissipation associated with material damping. The radiation damping component can be included by attaching additional viscous dashpots. Recent studies (Wang et al. 1998) showed that placing the viscous dashpots (representing radiation damping in the far field) in series with the hysteretic component of the soil–structure element (representing the nonlinear soil-pile response in the near field) is technically preferable to a parallel arrangement of the viscous and hysteretic damping components.

**Equivalent Cantilever Model**

The equivalent cantilever model is the simplest approach to represent the effects of the surrounding soil, wherein the sectional properties of the cantilever are the same as that of the shaft, but its length (depth to fixity) is adjusted to provide the same maximum bending moment as in the actual

soil-pile system. The effective length of the shaft shall be equal to the laterally unsupported length  $L_C$  plus an embedded depth to fixity  $L_F$ . The depth to fixity below the ground in ft. may be taken as (AASHTO-LRFD 2012):

For clays:

$$1.4 \left[ \frac{E_p l_w}{E_s} \right]^{0.25} \tag{10}$$

and for sands:

$$1.8 \left[ \frac{E_p l_w}{n_h} \right]^{0.20} \tag{11}$$

Where  $E_p$  is the modulus of elasticity of the shaft material;  $l_w$  is the weak axis moment of inertia for the shaft;  $E_s$  is the soil modulus for clays;  $S_u$  is the undrained shear strength of clay; and  $n_h$  is the rate of increase of soil modulus with depth for sand.

**Coupled Foundation Stiffness Matrix**

This approach is usually employed in regions of low to moderate seismicity. As illustrated in Fig. 16, a  $6 \times 6$  can be determined for a single shaft at the ground line. As indicated in section “**Coupled Pile Foundation Stiffness Matrix,**”

linearization of p-y curves is required for the development of a  $6 \times 6$  coupled stiffness matrix.

**Seismic Design of Drilled Shafts**

The following design requirements shall apply (ATC-32 1996) to bridges on drilled shaft foundations:

- (I) Seismic lateral foundation design forces shall be based on either plastic hinging of the bridge column or pier; linear dynamic analysis; or more advanced nonlinear dynamic response analysis.
- (II) Foundation stiffness must be accounted for in the dynamic response analysis of the overall bridge.
- (III) The capacity of shaft foundations and their individual components shall be based on the safety evaluation earthquake.
- (IV) Earth pressures generated by lateral ground displacements due to liquefaction shall be accounted for at poor soil sites.
- (V) Strong connection details shall be evaluated at poor soil sites.

**Large Gravity Caissons**

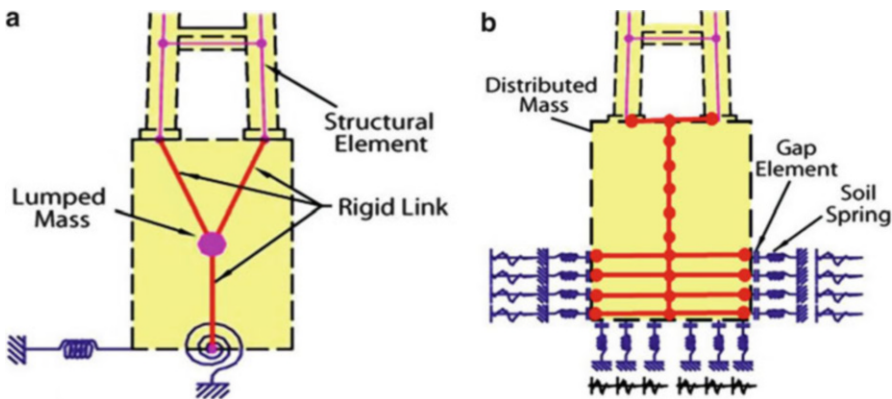
Large caissons are very large concrete boxes that are excavated or sunk to a predetermined depth. They are usually used for the construction of bridge piers or other heavy waterfront structures,

and they often become advantageous where water depths exceed 30–36 ft. Caissons are divided into three major types: (1) open caissons, (2) box caissons (or closed caissons), and (3) pneumatic caissons. A common feature of large caissons produced by the three methods is that they are massive structures that respond to seismic loads in a primarily rocking mode about the base plus some translations.

**Seismic Evaluation of Large Caissons**

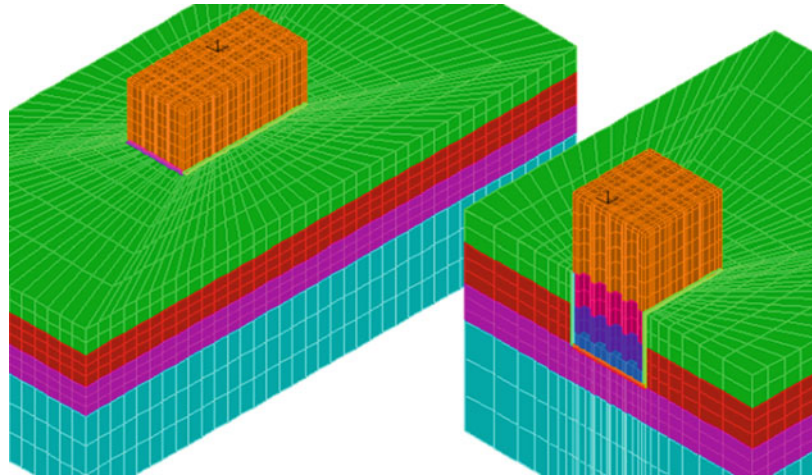
The behavior of caissons under lateral seismic loads is essentially nonlinear. Geometric nonlinearity dominates this behavior due to rocking of the caisson and gapping at the soil-caisson interface. The weight of caissons constitutes the major portion of the entire structure due to its large volume. Hence, the fundamental natural period of vibration of the large caisson is short and very different from the long period response of the bridge. This difference in the two modes of vibrations enables uncoupled seismic analyses of the two structures. However, when evaluating the bridge structural response, the caisson as an element must be included in the total bridge model. Two approaches are usually used for representing large caissons for seismic design.

The uncoupled spring approach represents the caisson as a lumped mass and establishes the interaction between the caisson and soil by the impedance approach. Figure 17a displays a



**Bridge Foundations, Fig. 17** Modeling techniques of caisson foundations: (a) Uncoupled spring approach; and (b) Winkler approach

**Bridge Foundations,**  
**Fig. 18** Continuum  
 models of caissons



schematic of the caisson model using this approach, wherein a rigid link is established between the node located at the center of mass of the caisson where its mass is lumped and another node at the bottom where a set of springs is attached. This method has been presented in section “[Spread Footing Stiffness](#).” This method overlooks the propensity of gapping at the base and at the embedded sides of the caisson during the seismic event and may lead to irrelevant results in the large displacement range of loading. Hence, it is only recommended for regions of low seismicity.

The nonlinear spring Winkler approach (Fig. 17b), as mentioned earlier, treats the soil supporting the foundation as a series of springs. It represents linear and nonlinear soil properties and hence favorable for life safety performance based design. It also accounts for the separation and gapping between the caisson walls and the surrounding soils. The properties of these nonlinear springs are established through static pushover analyses of three dimensional finite element continuum models as. Figure 18 depicts an example of such continuum model, where both the caisson and surrounding soil are modeled by three dimensional brick elements. The detailed 3-D finite element shall include constitutive relationships for the nonlinear behavior of the soil and special interface elements that can capture gapping

between the soil and the caisson at the base and side walls. Nonlinear static pushover analyses shall be carried out to establish the soil–structure interaction behaviors for implementation in the global model. Pushover analyses of the local model shall be performed by applying a point load at the center of gravity of the rigid caisson for each mode of soil resistance. The soil response results from the different pushover analyses of the local model in each direction shall be extracted and distributed to the soil spring elements at various nodal points in accordance with the discretization scheme of the global model. The behavior of the caissons under seismic loads shall be assessed through nonlinear time history analysis of the global model. The performance of the caissons is evaluated by comparing the maximum drifts from the results of the time history analysis to the permissible levels according to the performance based design criteria of the project.

### Cross-References

- ▶ [Dynamic Soil Properties: In Situ Characterization Using Penetration Tests](#)
- ▶ [Seismic Analysis of Masonry Buildings: Numerical Modeling](#)
- ▶ [Soil-Structure Interaction](#)

## References

- American Association of State Highway and Transportation Officials (2011) AASHTO LRFD seismic guidelines. Washington, DC
- American Association of State Highway and Transportation Officials (2012) AASHTO LRFD bridge design specifications. Washington, DC
- Applied Technology Council (1995) Seismic evaluation and retrofit of concrete buildings volume 1, ATC-40. Applied Technology Council, Redwood City
- Applied Technology Council (1996) Improved seismic design criteria for California bridges: provisional recommendations ATC-32. Applied Technology Council, Redwood City
- Ashour M, Norris G (1998) Lateral loading of a pile in layered soil using the strain wedge model. *J Geotech Eng Div ASCE* 124(4):303–315
- Ashour M, Norris G (2000) Modeling lateral soil-pile response based on soil-pile interaction. *J Geotech Eng Div ASCE* 126(5):420–428
- Brown D, Reese L, O’Niell M (1987) Cyclic lateral loading of a large-scale pile. *J Geotech Eng Div ASCE* 113(11):1326–1343
- Gadre A (1997) Lateral response of pile-cap foundation systems and seat-type bridge abutments in dry sand. PhD dissertation, Rensselaer Polytechnic Institute
- Gazetas G (1991) Formulas and charts for impedances of surface and embedded foundations. *J Geotech Eng Div ASCE* 117(9):1363–1381
- Harris KA, Petrou MF (2001) Behavior of precast prestressed concrete pile to cast-in-place pile cap connections. *PCI Journal*, 46(4)
- Hoit MI, McVay MC (2010) FLPIER user’s manual. University of Florida, Gainesville
- Lam IP, Martin GR (1986) Seismic design of highway bridge foundations. Report no. FHWA/RD-86-102, U.S. Department of Transportation, Federal Highway Administration, McLean, 167 p
- Lam IP, Martin GR, Imbsen R (1991) Modeling bridge foundations for seismic design and retrofitting. *Transp Res Rec* 1290 p.113–126
- Lam IP, Kapuskar M, Chaudhuri D (1998) Modeling of pile footings and drilled shafts for seismic design. Technical report MCEER-98-0018, Multidisciplinary Center for Earthquake Engineering Research. Buffalo
- LPILE (2010) Program LPILE plus, version 6.0. Ensoft, Austin
- Matlock H (1970) Correlations for design of laterally loaded piles in soft clay. In: 2nd offshore technology conference, vol 1. Houston, pp 579–594
- McVay MC, Casper R, Shang T (1995) Lateral response of three-row groups in loose to dense sands at 3D and 5D pile spacing. *Journal of Geotechnical Engineering, ASCE*, 121(5)
- McVay MC, O’Brien M, Townsend FC, Bloomquist DG, Caliendo JA (1998) Numerical analysis of vertically loaded pile groups. In: ASCE foundation engineering congress, Northwestern University, Evanston, pp 675–690
- Meyerhof GG (1953) The bearing capacity of foundations under eccentric loads. In: Proceedings 3rd international conference on soil mechanics and foundation engineering, vol 1. pp 440–445
- Priestley MJN, Seible F, Calvi GM (1996) Seismic design and retrofit of bridges. Wiley, New York
- Reese LC, Cox WR, Koop FD (1974) Analysis of laterally loaded piles in sand. In: Proceedings 6th Offshore Technology Conference, Paper 2080, Houston, pp 473–483
- Rollins K, Stenlund T (2011) Experimental testing of pile-to-cap connections for embedded pipe piles. *J Bridge Eng* 16(2):286–294
- Shama AA, Mander JB, Aref AA (2002) Seismic performance and retrofit of steel pile to concrete cap connections. *ACI Struct J* 99(1):185–192
- Shama AA, Mander JB (2004) Behavior of timber pile-to-cap connection under cyclic lateral loading. *J Struc Eng ASCE* 130(8):1252–1262
- Shama AA, Mander JB, Chen SS (2002) Seismic investigation of steel pile bents: II. Retrofit and vulnerability analysis. *Earthq Spectra EERI* 18(1):143–160
- Veletsos AS, Verbic B (1973) Vibration of viscoelastic foundations. *J Earthq Eng Struct Dyn* 2(1):87–102
- Vesic AS (1973) Analysis of ultimate loads of shallow foundations, chapter 3. In: Fang H-Y (ed) Foundation engineering handbook, 1st edn. Van Nostrand Reinhold, New York, pp 553–593
- Wang S, Kutter BL, Chacko JM, Wilson DW, Boulanger RW, Abghari A (1998) Nonlinear seismic soil-pile-interaction. *Earthq Spectra EERI, Oakland* 14(2) pp. 377–396
- Winkler E (1867) Die lehre von elasticizitat and festigkeit (on elasticity and fixity). Verlag von H. Dominicus Prague, 182 p

---

## Buckling-Restrained Braces and Their Implementation in Structural Design of Steel Buildings

Justin D. Marshall  
Auburn University, Auburn, AL, USA

### Synonyms

Ductile design of steel frames; Hysteretic energy dissipation; Passive energy dissipation; Steel braced frames

## Introduction

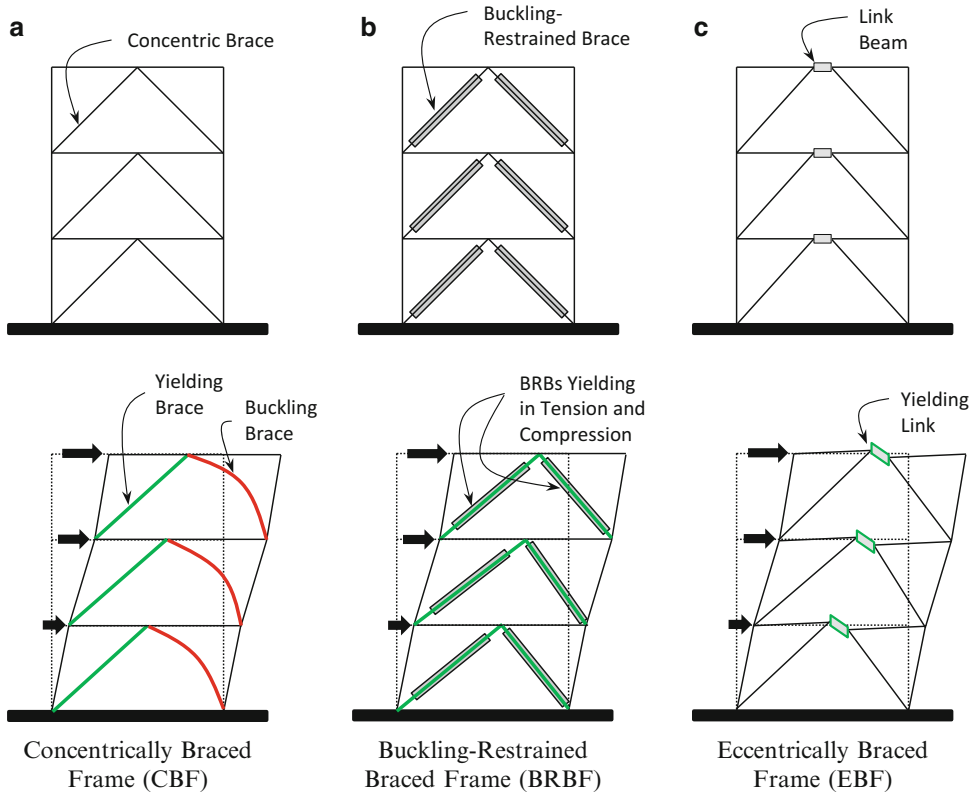
For a structural engineer, selection of the lateral load-resisting system for a building is a critical decision. While it is easy to understand the requirement to select beams and columns to support the gravity loads (i.e., self-weight of the building itself and the live loads related to building occupancy), a lateral system is required for any building to resist horizontal loading. Lateral loads routinely considered in design are wind and earthquake, although blast, flood, and tsunami are also possible. The lateral system can be especially critical when the building is to be constructed in a region where significant seismic activity is expected. In the case of a steel building, a wide variety of lateral resisting systems are available. These tested and approved lateral systems have the capability to maintain structural integrity in the face of significant lateral loads and inelastic behavior. One of the key elements to steel structures resisting seismic loads is a properly designed energy-dissipating fuse element. This critical element yields and subsequently dissipates energy during an earthquake without causing instability or collapse of the structure. In moment-resisting frames, the beams and columns resist both gravity and lateral loads although typically only the perimeter frames resist lateral forces. In this case, the beam elements are the fuse where inelastic behavior is expected. The challenge with these systems is that repairing or replacing beams after an earthquake is extremely difficult and costly. The other common lateral resisting system for steel buildings is a braced frame. The three most common braced frame systems are concentrically braced frames (CBF), eccentrically braced frames (EBF), and buckling-restrained braced frames (BRBF). Representative schematics for all three steel brace systems are shown in Fig. 1. Buckling-restrained braces (BRB) are a somewhat recently developed structural device that has a balanced force-deformation behavior (i.e., nearly equal strength in tension and compression) and are one of the few manufactured, rather than fabricated, products in common use in the structural steel construction industry. This entry will briefly

explore the three common types of braced frames and then discuss in greater depth the mechanics, performance, and design of BRBs and the BRBF system.

## Steel Braced Frame Lateral Resisting Systems

The basic premise of braced frame systems is that diagonal braces are placed in certain bays creating a vertical truss system to resist lateral loads. This results in primarily axial forces and axial deformations to control response of the lateral force-resisting system. The most common type of braced frame is the concentrically braced frame (CBF) (Fig. 1a). For CBFs, the centerline of the braces, beams, and columns is concentric at beam-column-brace joints and beam-brace intersections so that axial forces are induced in the braces, beams, and columns and significant moments are not developed in the members. The braces are the fuse elements, and the stiffness and strength of the system are controlled by the geometric and material properties of the braces. There are several drawbacks to this system, the first being the asymmetry of the system due to the braces yielding in tension and buckling in compression. This unbalance results in a significant difference in brace forces as well as degradation in both strength and stiffness during an earthquake. In addition, the potential exists for brace fracture due to multiple cycles of compression buckling and tension yielding. The benefit of this system is that typically the system is stiff resulting in small interstory drifts. CBFs have been extensively studied and tested experimentally such that if proper detailing methods are followed, the structure will be safe and the braces can be replaced following a significant earthquake.

A second type of braced frame is the eccentrically braced frame (EBF) (Fig. 1c). For these systems, the braces are intentionally eccentric relative to the element joints resulting in a combination of axial, shear, and moment in certain structural elements. The fuse element in this case is typically a link beam. The case shown in



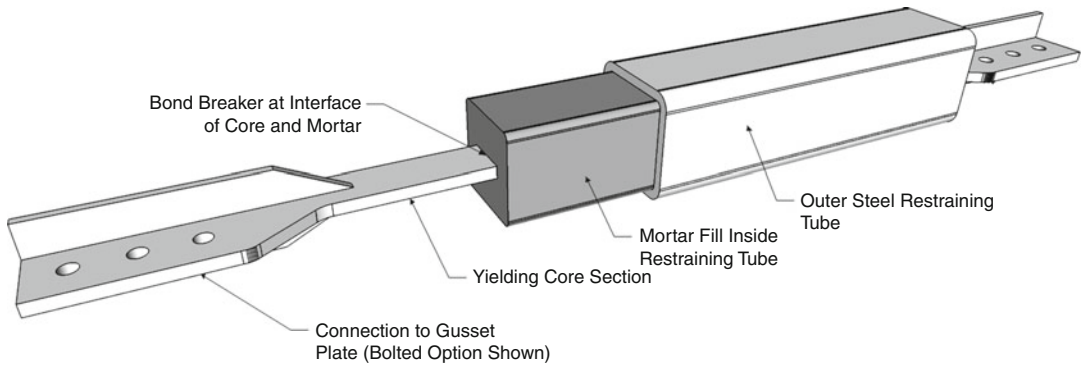
**Buckling-Restrained Braces and Their Implementation in Structural Design of Steel Buildings, Fig. 1** Types of steel braced frames

Fig. 1c shows a link in the middle of the beam span although it is also commonly adjacent to the column. The diagonal braces used in EBFs are designed to remain elastic for the maximum forces and moments that can develop in the link beam. An EBF system is more flexible than a CBF and has a symmetric response as the yielding under shear and flexure is symmetric. The primary drawback for EBFs is that replacing the link beam is more difficult and costly than replacing a diagonal brace. There has been recent work in developing and testing replaceable link beams to overcome this problem (Mansour et al. 2011).

The third type of braced frame system is the buckling-restrained braced frame, which is a type of concentrically braced system. The BRB is the primary structural element in the BRBF providing the necessary ductile energy dissipation. The difference between a typical fabricated steel

brace and the BRB is the symmetry of the response. A BRB is specially designed to prevent buckling during the compression cycle. This results in highly ductile behavior in both tension and compression and prevents the force unbalance present in other brace configurations due to the significantly lower buckling strength as compared to the tension yield (see Fig. 1b). Brace fracture is not a problem due to the fact that the large stresses in the core are primarily axial. There is no strength or stiffness degradation for BRBs that are detailed correctly. The stiffness of a BRBF is less than a CBF as the BRB strength is directly related to the tension strength, whereas in a CBF the area generally must be increased to get the required capacity in compression. Buckling-restrained braces are unique in that they are a manufactured device rather than a fabricated steel section. Since their development and introduction into the industry, BRBs have taken a





**Buckling-Restrained Braces and Their Implementation in Structural Design of Steel Buildings, Fig. 2** Isometric cutaway of buckling-restrained brace

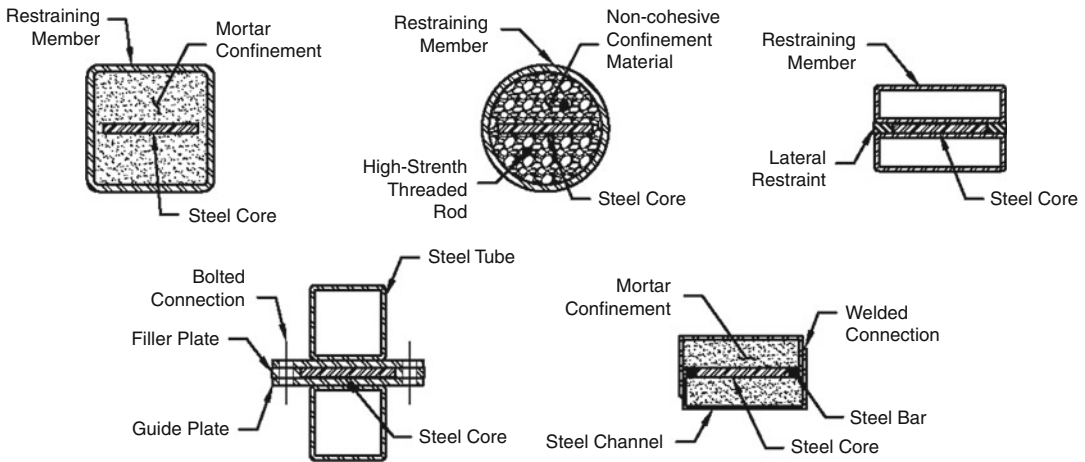
large market share in braced steel frame systems due to their cost competitiveness and their reliable, resilient performance in seismic events.

### Buckling-Restrained Brace Description

Because braced frames have very beneficial characteristics, significant work was undertaken to determine ways to overcome the negative aspects of brace buckling. The early beginnings of a brace restrained against buckling were in the 1970s in Japan where steel plates were encased in a precast concrete wall (Wakabayashi et al. 1973). Since then, significant improvements and modifications have been made to the original configuration that has enabled the reliable and ductile BRB commonly used today (Black et al. 2004; Fahnestock et al. 2006; Xie 2005). The key to the mechanism is the axial load going through the steel core while sufficient buckling resistance (flexural rigidity) is provided in another component. This has been accomplished in several ways although the most common is shown in Fig. 2. The basic premise of the BRB is that the core steel element has a cross section designed to yield in tension and compression. In order for this to occur, sufficient flexural rigidity must be provided so the overall buckling load of the composite device is greater than the ultimate strength of the steel core. This is accomplished through the use of a steel tube which is most commonly square or circular. The core steel

runs through the center of the tube which is then filled with a mortar paste to fill the space allowing the steel tube to provide the required flexural resistance to brace the core. It is not desirable for any axial load to go through the mortar or the steel outer tube. This is accomplished by providing a bond breaker between the mortar and the steel core. Several different options have been used for this including a lubricant or a material wrapped around the steel core prior to filling the outer tube. In addition to the BRB shown in Fig. 2, several other systems have been developed by researchers to create a BRB system for lower cost, to simplify manufacturing, or to replace damaged cores more simply after an event. Several of the BRB systems developed through these research efforts are shown in Fig. 3, although this is a sample of the different variations that have been investigated. Figure 4 shows a photograph of a building retrofitted with BRBs.

The geometry and yield strength of the core section play an important role in the performance of BRBs. From a material specification, it is desirable to have a known value or at least a small range where yielding will occur. An A36 material with controlled yield is commonly used for this purpose. The yielding core section can be fabricated to any area specified by the structural engineer. The area of the yielding core is the prime cross-sectional characteristic used to determine strength. There are two primary shapes for the core region, flat plate or cruciform.



**Buckling-Restrained Braces and Their Implementation in Structural Design of Steel Buildings, Fig. 3** Various BRB cross sections

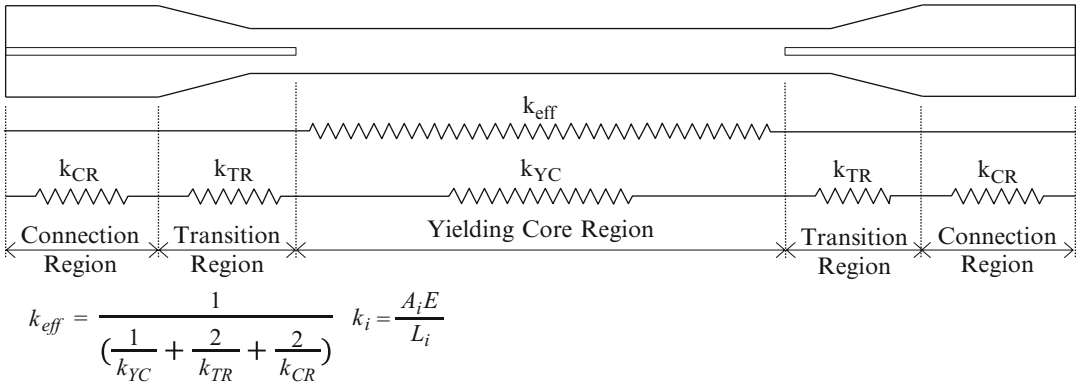
**Buckling-Restrained Braces and Their Implementation in Structural Design of Steel Buildings,**

**Fig. 4** Photograph of building retrofitted with BRBs (Courtesy of Core Brace, LLC)



In addition, some BRBs use multiple cores within the restraining tube to achieve the desired core area. The length of the yielding core is an important part in determination of the stiffness of the brace. Figure 5 shows the breakdown of a typical core with the flat plate yielding core, transition region, and connection region. The flexural stiffness of the transition region and connection region is important as the flexural rigidity of these regions must be sufficient to sustain the

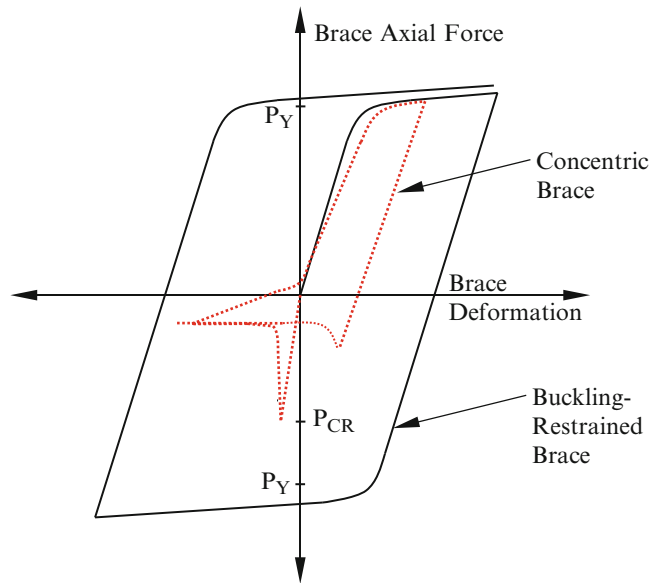
core axial strength. The equation for the equivalent elastic stiffness of the brace is shown in Fig. 4 and is based on a combination of springs in series representing the axial stiffness of each segment. The overall stiffness of the brace is important for accurate analysis of the frame with BRBs and can be modified if the brace stiffness is too low. This modification is typically done by shortening the yielding core length (i.e., increasing the transition length) which is the most flexible segment.



**Buckling-Restrained Braces and Their Implementation in Structural Design of Steel Buildings,**  
**Fig. 5** Stiffness calculation and different regions of BRB steel core

**Buckling-Restrained Braces and Their Implementation in Structural Design of Steel Buildings,**

**Fig. 6** Hysteresis plot for buckling-restrained brace and concentric brace



However, it is important to recognize that a shorter yielding length results in higher inelastic strains in the core which will result in higher forces in the braces, an important design criterion.

The overall representative hysteretic behavior of a BRB and a concentric brace is shown in Fig. 6. The BRB has full hysteresis loops in both tension and compression including strain hardening. The capacity for significant deformation ductility in both directions is apparent where deformation ductility is defined as the total

deformation divided by the yield deformation. There is a small increase in strength on the compression side, typically about 10 % larger than the brace tension strength. This is due to friction between the core and the mortar. Even with a bond breaker, the core will dilate under compression resulting in greater frictional force and some axial load transfer. By contrast, a concentric brace performs well in tension but experiences buckling in compression which typically results in formation of a flexural plastic hinge near the

center of the brace. Once the brace has buckled one time, it quickly loses strength in compression upon subsequent cycles. The formation of the hinge can result in brace fracture in tension due to the damage occurring during compression buckling. The lower compression capacity and potential brace fracture significantly limit the energy dissipation and deformation ductility capacity of CBFs when compared to BRBs.

As was stated previously, BRBs are a manufactured product. In the United States there are three primary brace producers, Core Brace (<http://www.corebrace.com/>), Star Seismic (<http://www.starseismic.net/>), and Unbonded Brace (<http://www.unbondedbrace.com/>). Each of these companies has tested their braces to meet the requirements put forth in the applicable building codes and reference documents. In addition to the braces, they provide design and engineering guidance associated with their products. While the basic premise of the BRB is the same for each manufacturer, many specific details of the various brace manufacturers differ as they compete based on price and performance in the marketplace.

BRBs, as manufactured products, have a high degree of quality control requirement placed on them in the American Institute of Steel Construction (AISC) *Seismic Provisions for Structural Steel Buildings* Section K3 (AISC 2010), which is a reference standard in the United States (USA) governing the design of steel buildings for seismic loads. The requirements include testing which includes both axial demands on the brace and the consideration of rotations at the connections due to frame deformations. The primary requirements of the testing are to show (1) the required ductility, both for a single cycle and cumulatively; (2) repeatable stable hysteresis with positive post-yield slope; and (3) avoidance of core rupture, brace instability, and connection failure. The required testing for a wide variety of brace sizes has been completed by the three primary producers. The specification however allows for these tests to be run on a project-specific basis if a new or unique brace configuration is specified.

## Buckling-Restrained Brace Design

Buckling-restrained braces were first used in the USA in 1999, over a decade after the first usage in Japan in 1987 (UBB 2014). Part of the motivation for this new system was due to the failure of steel moment frames that occurred in the 1994 Northridge, California, and the 1995 Kobe, Japan, earthquakes. As with other new developments in structural engineering practice, it was implemented in building practice in the USA prior to inclusion in building codes or reference standards. The first inclusion of BRB design provisions was in the *NEHRP Recommended Provisions for Seismic Regulations for New Buildings and Other Structures* (FEMA 2003), FEMA 450. The information included in FEMA 450 was developed by a joint committee including AISC and the Structural Engineers Association of California (SEAOC). FEMA 450 is not a building code or reference standard, but inclusion is typically the first step in the process. The buckling-restrained braced frame was included in the 2005 version of ASCE/SEI 7, *Minimum Standard for Design Loads for Buildings and Other Structures* (2005), as an acceptable seismic force-resisting system. In ASCE/SEI 7-05, a BRBF had the following seismic performance factors (SPF):  $R = 7$ ,  $\Omega_o = 2$ ,  $C_d = 5.5$ . A dual system with BRBs and moment-resisting connections at the beam-column joints without a bracing connection had slightly different SPFs:  $R = 8$ ,  $\Omega_o = 2.5$ ,  $C_d = 5$ . One change of note that appeared in ASCE 7-10 was that the SPFs for BRBs with and without moment frames were made the same as the dual system based on research that had taken place in the interim. In addition to ASCE 7, BRB provisions were included in AISC Standard 341-05, *Seismic Provisions for Structural Steel Buildings* (2005). This document deals with more detailed requirements for design of not only the BRBs but also the other elements of the lateral force-resisting system. This document also lists the required testing protocol for BRBs. The subsequent versions of the ASCE/SEI 7 and AISC 341 standards continued to include provisions for BRBs with

modifications based on continuing research. An early and still applicable reference for the design of BRBs is by Lopez and Sabelli (2004) which has detailed examples of design provisions. A more recent textbook (Bruneau et al. 2011) also has a chapter on BRBFs.

From the design perspective, sizing of BRBs is a very straightforward process. The size of the core is based on the maximum axial demand according to the limit state of yielding based on the load combinations from the applicable building code. Equation 1 shows the basic premise where  $P_{y_{sc}}$  is the nominal axial yield strength,  $A_{sc}$  is the area of the steel core, and  $F_{y_{sc}}$  is either the minimum specified yield stress or the actual yield stress from a coupon test. If the manufacturer provides coupon tests from the steel used to fabricate the core, this value can be used in design. Otherwise, a range of values should be used to determine the upper and lower limits that could occur.

$$P_{y_{sc}} = F_{y_{sc}} A_{sc} \quad (1)$$

Once determined, the nominal yield strength value is then modified by a resistance factor of 0.9 for LRFD design to determine the design axial strength. One of the benefits of BRBs is that any cross-sectional area can be provided so each floor can have a BRB sized to the demand. Typically the area will be rounded to some degree based on the manufacturer's practice, but this is not generally a significant change. In addition to nominal yield, the adjusted brace strength must also be established as part of the design. The adjusted brace strength has two components, the tension ( $\omega R_y P_{y_{sc}}$ ) and compression adjusted brace strength ( $\beta \omega R_y P_{y_{sc}}$ ), where  $\omega$  is the strain hardening adjustment factor,  $\beta$  is the compression strength adjustment factor, and  $R_y$  is the ratio of expected to specified minimum yield stress.  $R_y$  can be set to 1 if coupon tests are used to determine the yield strength. The values for  $\beta$  and  $\omega$  are taken from coupon tests that are carried out to the strain equivalent to that occurring in the brace at the expected deformation. The expected deformation is defined as the larger of 2% story drift or two times the design story drift. Figure 7 shows a

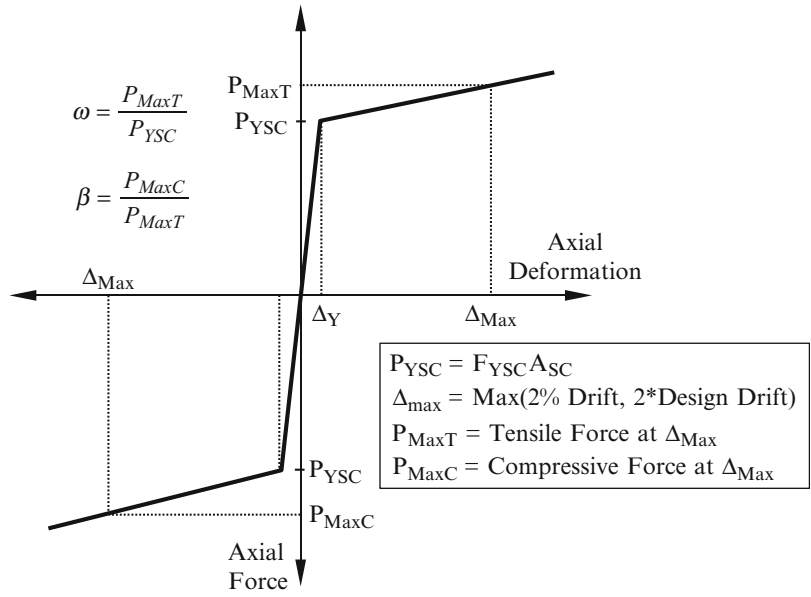
plot of how these values would be determined. This is one of several items that will require input from a brace manufacturer. The adjusted brace strength is used to ensure that the beams, columns, and connections in the frame have the required strength to remain elastic through the expected strength of the BRB. The design of brace connections must be designed to 1.1 times the adjusted brace strength in compression.

The other component of design that is important is accurate modeling of brace stiffness. As discussed previously, the stiffness of the brace represents a combination of the stiffness of the different segments. This versatility provides additional mechanisms to control response by modifying the stiffness of the brace. For example, if the brace is too flexible, the yield length could be shortened. However, this will have an effect on other components as the inelastic strains in the brace for the same deformation will increase which will also increase the adjusted brace strengths. Brace manufacturers will provide assistance to create the appropriate balance of stiffness and required strength.

One of the final design considerations is that of the connection of the BRB to the framing. There are three typical options for connecting BRBs to gusset plates although the specific details of the connections vary based on the different manufacturer's brace geometry. The three options are bolted, welded, and pinned connections. Example details are shown in Fig. 8 although many variations can be found and have been used. As opposed to CBFs where the gusset plate is designed to allow for the out-of-plane rotation due to brace buckling, BRBs can sustain significant moments. These large moments are developed based on the large deformations in the frame inducing rotations in the beam and columns. The pin allows for these rotations to occur in the connection rather than the structural element. This allowance for rotation can also be developed using welded and bolted gusset connections by providing a beam stub off the column with a hinge connection to the remainder of the beam as shown in Fig. 8c. It is also of critical importance to ensure that the connection (gusset plate and end section of BRB) has sufficient

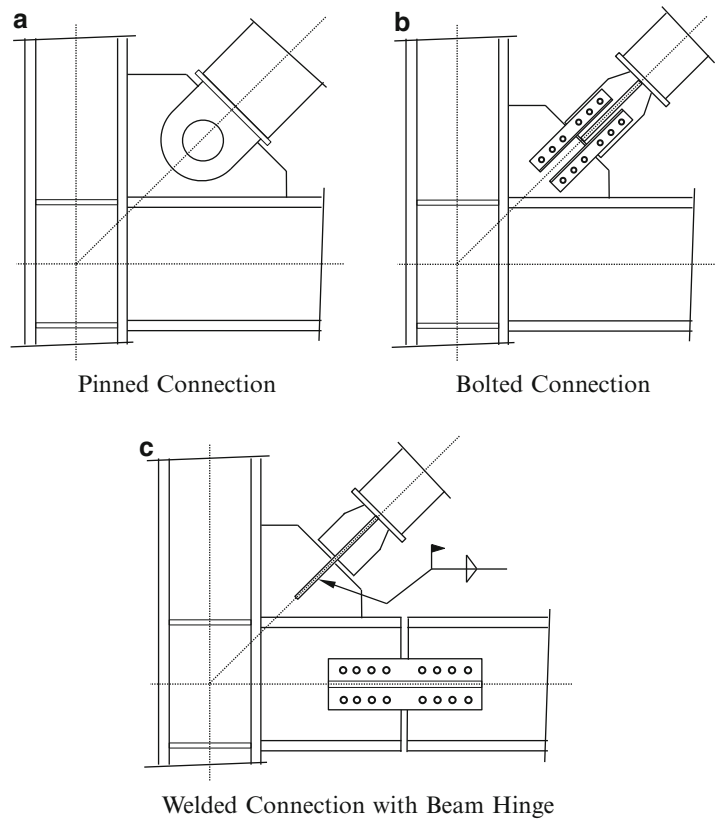
**Buckling-Restrained Braces and Their Implementation in Structural Design of Steel Buildings,**

**Fig. 7** Determination of adjusted brace strength from test data



**Buckling-Restrained Braces and Their Implementation in Structural Design of Steel Buildings,**

**Fig. 8** Typical gusset plate connection details





out-of-plane flexural resistance to resist buckling up to the full strength of the core section. Typical gussets for BRBFs are markedly smaller than those used in CBFs.

In addition to typical frame structures, BRBs can be used anywhere a ductile fuse element is required. Examples include bridges as ductile connections between the superstructure and the substructure, stadiums as part of the lateral resisting systems, and dam intake towers to prevent lateral motion while limiting the forces imparted to the dam. They have also been used more recently in the San Francisco Airport Air Traffic Control Tower which is a self-centering system where the BRBs provide hysteretic energy dissipation (Muthukumar and Sabelli 2013).

It is interesting to note that the design for BRBs in Japan is different from the USA. In Japan, braced frames are designed to higher force levels than moment frames (i.e., the equivalent of the R value penalizes braced frames) due to the potential for buckling. Because of this fact, most low-rise construction in Japan is designed with moment frames. However, for taller buildings, BRBs are used significantly due to the increased stiffness. In order to use BRBs for their stiffness and energy dissipation without the force penalty, they are used as hysteretic energy-dissipating devices as part of a dual system with moment-resisting frames (Xie 2005). The first reported use of a BRB in Europe was in 2006 at the University of Ancona in Italy. Use of BRBs in Europe is much less than in Japan and the USA (Della Corte et al. 2011).

### **Buckling-Restrained Brace Innovations**

Buckling-restrained braces are one of the more impactful developments in earthquake engineering. They are considered today a standard option for both new designs and retrofits of existing buildings in significant seismic hazards. However, as with any innovation, additional improvements are constantly explored to further improve

on the existing concept. One of the biggest weaknesses of BRBs that has been identified in analytical and experimental research is residual displacements following significant earthquakes. The modifications and/or additions to BRBs have primarily aimed to reduce residual deformations in BRBFs. This movement is also centered on a larger goal of providing a higher performance standard than life safety in buildings for major earthquakes. Since BRBs are an effective lateral system, additions and modifications to a high-performance seismic system represent an ideal way to move toward damage reduction in addition to life safety.

The first of these innovations is called the hybrid passive control device (HPCD). The HPCD consists of a BRB in series with a viscoelastic damping device. For small deformations, only the viscoelastic damper is active. After a specified displacement, the viscoelastic device locks out and the BRB becomes active. The device was tested in the laboratory and implemented in analytical models of a nine-story structure. Experimental testing showed the concept worked as designed. The building response to a suite of earthquakes was improved, and residual displacements were reduced when compared to a BRB frame (Marshall and Charney 2010a, b).

One of the ways that has been explored to improve building response and reduce damage is through the use of self-centering systems. The idea of these systems is to provide an element that remains elastic while a fuse element yields and dissipates energy. Analytical and experimental research was completed on a self-centering buckling-restrained brace (SC-BRB) using nickel-titanium-based shape memory alloys. The shape memory alloy's unique properties provide the capacity to self-center in addition to providing additional energy dissipation. The SC-BRB consists of typical BRB with two additional outer concentric tubes and free-floating end plates so the shape memory alloy rods were always loaded in tension. The experimental testing showed significant capacity for energy

dissipation, deformation ductility, and self-centering which would result in a lateral system with the ability to reduce structural response and limit residual damage in the event of a large earthquake (Miller et al. 2012).

An additional innovation associated with BRBs is the use of a multi-core BRB with different steel grades, called a hybrid BRB (HBRB). The idea of using a low yield stress steel core (100 MPa/14.5 ksi) in combination with a typical or higher yield stress steel presents a unique option. Since the modulus of elasticity is the same for the two steels, the low yield stress steel will yield earlier and begin to dissipate energy while the structure still has significant stiffness. The system can be optimized based on the ratio between the area of low yield point steel and the other steel in the BRB. The idea here is to dissipate significant energy before the structure reaches a state where the stiffness has decreased significantly. This concept has been shown to reduce residual displacement and decrease the number of simulated collapses when compared to typical BRBFs (Atlayan and Charney 2012).

## Summary

Buckling-restrained braced frames are a resilient lateral system for structural steel buildings. The ability to control both the stiffness and strength, nearly independently of each other, and the large, full hysteresis loops makes a BRBF an effective seismic system that can be designed for many different hazards. BRBs are versatile and can be used in many different types of structures including both new construction and seismic retrofits. This has been demonstrated by both the increase in usage for construction projects and the continued worldwide experimental research, both completed and ongoing. As with any lateral resisting system, there are weaknesses which need to be resolved. Continued improvement through research and development will continue to improve performance of this ductile lateral resistance system.

## Cross-References

- ▶ [Buildings and Bridges Equipped with Passive Dampers Under Seismic Actions: Modeling and Analysis](#)
- ▶ [Cast Fuse Braces: Design and Implementation](#)
- ▶ [Earthquake Protection of Essential Facilities](#)
- ▶ [Friction Dampers for Seismic Protections of Steel Buildings Subjected to Earthquakes: Emphasis on Structural Design](#)
- ▶ [Passive Control Techniques for Retrofitting of Existing Structures](#)
- ▶ [Seismic Analysis of Steel Buildings: Numerical Modeling](#)
- ▶ [Steel Structures](#)

## References

- AISC (2005) ANSI/AISC 341–05 Seismic Provisions for Structural Steel Buildings, American Institute of Steel Construction, Chicago, IL
- AISC (2010) ANSI/AISC 341–10 Seismic Provisions for Structural Steel Buildings, American Institute of Steel Construction, Chicago, IL
- Atlayan O, Charney FA (2012) Hybrid steel frames. In: 15th World conference on earthquake engineering. International Association for Earthquake Engineering, Lisbon, Sept 24–28
- Black CJ, Makris N, Aiken ID (2004) Component testing, seismic evaluation and characterization of buckling-restrained braces. *J Struct Eng* 130(6): 880–894
- Bruneau M, Uang C-M, Sabelli R (2011) Ductile design of steel structures, 2nd edn. McGraw Hill, New York
- Della Corte G, D’Aniello M, Landolfo R, Mazzoniani FM (2011) Review of steel buckling-restrained braces. *Steel Constr* 4(2):85–93
- Fahnestock LA, Ricles JM, Sause R (2006) Experimental study of a large-scale buckling restrained braced frame using the pseudo-dynamic testing method. In: 8th US National conference on earthquake engineering, Earthquake Engineering Research Institute, San Francisco
- Lopez WA, Sabelli R (2004) Seismic design of buckling-restrained braced frames. Structural Steel Educational Council, Moraga
- Mansour N, Christopoulos C, Tremblay R (2011) Experimental validation of replaceable shear links for eccentrically braced steel frames. *J Struct Eng* 137(10):1141–1152
- Marshall JD, Charney FA (2010a) A hybrid passive control device for steel structures I: development and analysis. *J Constr Steel Res* 66(10):1278–1286

- Marshall JD, Charney FA (2010b) A hybrid passive control device for steel structures II: physical testing. *J Constr Steel Res* 66(10):1287–1294
- Miller DJ, Fahnstock LA, Eatherton MR (2012) Development and experimental validation of a nickel-titanium shape memory alloy self-centering buckling-restrained brace. *Eng Struct* 40:288–298
- Muthukumar S, Sabelli R (2013) Nonlinear seismic analysis of a round concrete tower with a post-tensioned self-centering system. ASCE/SEI Structures Congress 2013, American Society of Civil Engineers, Pittsburgh, 2–4 May 2013
- UBB (2014) <http://www.unbondedbrace.com/facts.htm>. Accessed Jan 2014
- Wakabayashi M, Nakamura T, Kashibara A, Morizono T, Yokoyama H (1973) Experimental study of elastoplastic properties of precast concrete wall panels with built-in insulating braces. Summaries of technical papers of annual meeting, Architectural Institute of Japan, pp 1041–1044 (in Japanese)
- Xie Q (2005) State of the art of buckling-restrained braces in Asia. *J Constr Steel Res* 61(6):727–748

---

## "Build Back Better" Principles for Reconstruction

Sandeeka Mannakkara, Suzanne Wilkinson and Tinu Rose Francis  
 Department of Civil and Environmental Engineering, The University of Auckland, Auckland, New Zealand

### Synonyms

BBB; Reconstruction; Recovery

### Introduction

"Build Back Better" signifies an ideal reconstruction and recovery process that delivers resilient, sustainable, and efficient recovery solutions to disaster-affected communities. The motivation behind the Build Back Better concept is to make communities stronger and more resilient following a disaster event. Statistics from the United Nations Environment Programme in 2008 show an increase in the number of natural disasters over time attributing to growing populations,

urban growth in risk-prone areas due to scarcity of land, and global warming. Along with increasing frequency, recent disasters show an increase in magnitude and resulting destruction according to studies by the Red Cross. Both natural and technological/man-made disasters have seen nearly exponential rises in the number of disasters over time.

Despite the increasing number of disaster experiences, post-disaster activities remain inefficient and poorly managed and need to be improved according to Halvorson and Hamilton (2010). Traditionally, post-disaster reconstruction consisted of simply repairing the physical damage that has been induced by a disaster. However, Kennedy et al. (2008) pointed out that rebuilding the built environment and infrastructure exactly as they were prior to a disaster often re-creates the same vulnerabilities that existed earlier. If restored to pre-disaster standards, disaster-affected communities would face the same difficulties if exposed to another disaster event in the future. The reconstruction and recovery period following a disaster poses an opportunity to address and rectify vulnerability issues found in communities.

As a result of witnessing the ongoing impacts of disasters on communities, a concept started to emerge where post-disaster reconstruction was to be taken as an opportunity to not only reconstruct what was damaged and return the community to its pre-disaster state but to also seize the opportunity to improve its physical, social, environmental, and economic conditions to create a new state of normalcy that is more "resilient" (Boano 2009). This concept was termed "Build Back Better," suggesting that successful recovery of communities following disasters needs to amalgamate the rehabilitation and enhancement of the built environment along with the psychological, social, and economic climates in a holistic manner to improve overall community resilience. The phrase "Building Back Better" became popular during the large-scale reconstruction effort following the Indian Ocean Tsunami disaster in 2004 after which it became more officially embraced with the creation of sets of BBB Guidelines to steer recovery and

reconstruction activities toward achieving this goal (Clinton 2006).

This chapter reviews what BBB entails and presents the key elements required to improve post-disaster reconstruction and recovery practices to build back better. First, existing guidelines and reports providing recommendations for BBB are introduced. Key information from the guidelines and reports is used to then identify the key concepts which represent Building Back Better. Finally, each concept and its importance for building back better are reviewed.

### The Need for Building Back Better

The South Asia Disaster Report (DNS and PA 2005) states that disasters are produced due to the weaknesses and vulnerabilities of communities, countries, and structures to withstand encountered hazards. Wisner et al. (2004) defines vulnerability as the lack of capacity to anticipate, cope with, resist, and recover from the impact of a hazard. The destruction and loss of human lives from the 2005 Kashmir Earthquake in Pakistan was primarily due to the collapse of inappropriately built structures constructed on earthquake-prone land using substandard building materials and designed with little earthquake resistance. Poorly planned and sometimes illegal developments and their resulting impacts on the environment worsened the damage from the Mumbai Floods in 2005. A similar situation was seen in Sri Lanka after the Indian Ocean Tsunami.

Restoration of the damaged physical, social, economic, and environmental impacts of disasters is a complicated and drawn-out process. Reconstruction and recovery projects often focus on quick restoration of affected communities which can replicate and worsen existing vulnerabilities faced by the community. The Tsunami Evaluation Commission Synthesis Report in 2007 provided examples where escalated pressures and the need for fast rebuilding and recovery processes following a disaster can further increase the vulnerability of a community. Examples include: nonadherence to design and construction policies for buildings and

infrastructure, insufficient focus given to certain aspects of the recovery process such as livelihood development programs and small business support programs, overruling of local government agencies, and neglecting vulnerable groups of people in the community.

Complete recovery requires attention to many different elements. BBB was defined by Khasalamwa (2009) as a way to utilize the reconstruction process to improve a community’s physical, social, environmental, and economic conditions to create a more resilient community, where resilience is defined as “the capacity to recover or ‘bounce back’ after an event” (Twigg 2007). Therefore, what the concept of BBB proposes is a broad holistic approach to post-disaster reconstruction in order to address the wide range of prevalent issues including those mentioned above and ensure that affected communities are regenerated in a resilient manner for the future.

### Existing Guidelines for Building Back Better

Clinton’s (2006) “Key Propositions for Building Back Better” was the earliest known official document to be published which attempted to provide a comprehensive guideline for implementing BBB practices in post-disaster environments. The report was based on and aimed at the Indian Ocean Tsunami disaster. He introduced ten propositions for building back better.

Clinton’s propositions were:

- Proposition 1: Governments, donors and aid agencies must recognize that families and communities drive their own recovery.
- Proposition 2: Recovery must promote fairness and equity.
- Proposition 3: Governments must enhance preparedness for future disasters.
- Proposition 4: Local Governments must be empowered to manage recovery efforts, and donors must devote greater resources to strengthening Government recovery institutions, especially at the local level.

- Proposition 5: Good recovery planning and effective coordination depend on good information.
- Proposition 6: The UN, World Bank, and other multilateral agencies must clarify their roles and relationships, especially in addressing the early stages of a recovery process.
- Proposition 7: The expanding role of NGOs and the Red Cross/Red Crescent Movement carries greater responsibilities for quality in recovery efforts.
- Proposition 8: From the start of recovery operations, Governments and aid agencies must create the conditions for entrepreneurs to flourish.
- Proposition 9: Beneficiaries deserve the kind of agency partnerships that move beyond rivalry and unhealthy competition.
- Proposition 10: Good recovery must leave communities safer by reducing risks and building resilience.

Several other guidelines directly and indirectly proposing BBB-based recovery and reconstruction operations include:

- United Nations Disaster Relief Organization's "Principles for Settlement and Shelter" in 1982 which addresses stakeholder role allocation, needs-based provision of resources to the community, and risk reduction
- The Government of Sri Lanka's "Post-Tsunami Recovery and Reconstruction Strategy" and "Build Back Better Guiding Principles" in 2005 which include needs-based resource allocation and provision of locally appropriate solutions, community participation and consultation in recovery activities, equity, transparency between stakeholders, risk reduction and consideration of future sustainability, and livelihood support
- Federal Emergency Management Agency's "Rebuilding for a More Sustainable Future: An Operational Framework" in 2005 which mentions role allocation and coordination of stakeholders, community-centered recovery operations, and hazard-based sustainable risk reduction practices

- Monday's "Holistic Recovery Framework" in 2002 which addresses enhancing the quality of life in the community, economic vitality, and the quality of the environment, risk reduction, and participatory decision-making in recovery activities
- Bam's Reconstruction Supreme Supervisory and Policymaking Association's "Bam's Reconstruction Charter" in 2010 which includes policies for reconstruction management; community participation, employing suitable construction technology and materials; preserving cultural and architectural heritage; and ensuring stability of construction
- Victorian Bushfire Reconstruction and Recovery Authority's "Recovery and Reconstruction Framework" in 2011 which focuses on the safety and well-being of the community, needs-based resource allocation, community engagement, equity, and tailored solutions
- Canterbury Earthquake Recovery Authority's "Recovery Strategy" in 2013 which entails leadership and integration to manage recovery activities using a participatory approach, regenerating the economy, restoring and enhancing the community, reconstruction of the built environment, and restoring natural and healthy ecosystems

## Key Concepts

The concepts proposed to achieve BBB during reconstruction and recovery in the various guidelines in the previous section feature similarities. Aspects such as role allocation of stakeholders, community participation, and risk reduction appeared in most of the guidelines. The key concepts introduced in the guidelines for improving reconstruction and recovery efforts and building back better include: risk reduction, psychosocial recovery, economic recovery, effective implementation, and monitoring and evaluation. The next few subsections describe these key concepts in further detail.

## Risk Reduction

Risk reduction identifies all actions taken toward reducing disaster risks in communities to improve the physical resilience in the built environment. Previous post-disaster experiences have emphasized the need to identify prevalent hazards and determine solutions to be undertaken to reduce risks imposed on people. The Red Cross's World Disaster Report in 2010 disclosed that the risks seen in cities are due to a number of reasons such as: growth in informal or illegal settlements, inadequate infrastructure, and building on sites at risk from hazards. The report also stated that many past disasters could have been anticipated and avoided with proper planning, design, and construction methods. The Victorian Bushfires Royal Commission Final Report in 2010 recommended the amendment of the Australian Building Code following the Victorian Bushfires ensuring greater safety standards. The Royal Commission suggested identifying bushfire-prone areas and adopting suitable building and planning controls.

The National Mitigation Strategy produced in Turkey following the Kocaeli and Duzce earthquakes of 1999 also stated the need for site-specific hazard identification before reconstruction as well as retrofitting and updating structural codes and the use of tax incentives to encourage mitigation work (Bakir 2004). The 2008 South Asia Disaster Report by the nongovernmental organizations Duryog Nivaran and Practical Action recommended producing hazard and vulnerability maps and enforcing building codes to avoid development-related disasters in the future. The two primary ways of risk reduction are through improving structural designs and through better land-use planning.

The importance of reviewing and changing building designs and codes to improve the structural integrity of buildings and infrastructure following a disaster is widely understood but is however less frequently attained successfully in practice due to a range of common issues. Poor regulative powers and the lack of strict enforcement can lead to building code changes being disregarded resulting in substandard structures

in the rebuild. When the Indian Ocean Tsunami struck, enforcement of building codes was mainly restricted to urban and suburban areas in Sri Lanka. The rural and coastal areas were the main victims of the disaster, where the lack of strict structural standards resulted in magnified damage (Pathiraja and Tombesi 2009). Extra costs incurred by adopting new technologies and materials to improve structural resilience also discourage compliance of new building codes worldwide (Batteate 2006).

The experiences of post-disaster reconstruction efforts worldwide have provided lessons which can be adopted when implementing structural changes to avoid the above mentioned issues and build back better. BBB theory suggests that hazard-based building regulations should be created using multi-hazard assessments in areas chosen for redevelopment and reconstruction. Consistent regulations and a strong legal framework are necessary to assist the adoption of building codes and regulations and ensure that structural changes improve the built environment (Clinton 2006). As structural improvements are expensive and unaffordable especially in post-disaster settings, long-term funding needs to be made available to cover extra costs for structural improvements and promote adoption. Quality of reconstruction can be maintained by arranging inspections during construction by local governmental authorities. Stakeholders involved in the rebuild such as builders, engineers, and architects should be trained on revised building codes and other specific requirements to avoid inconsistencies and produce good quality results in order to build back better.

A land-use planning strategy was used in the post-disaster recovery efforts following the Indian Ocean Tsunami and the Samoan Tsunami, resulting in the relocation of coastal communities further inland to prevent future impacts of coastal hazards (Kennedy et al. 2008). The mandatory resettlement operations in Sri Lanka and Samoa were problematic due to the lack of consideration given to the lifestyles of the local people which led to the loss of their sea-dependent livelihoods,



dissatisfaction with their new settlements, and illegal return of people to the original coastal lands (Kennedy et al. 2008). A recurring issue with relocation is the focus given to moving communities away from a certain hazard resulting in exposing communities to new unanticipated hazards. Well-intended land-use planning measures can also fail due to the lack of knowledge and awareness of local people who do not conform to new regulations and the lack of experience and knowledge of local governing authorities who do not enforce new regulations (Kennedy et al. 2008).

Therefore, it was recommended by Baradan (2006) that hazard assessments of current land sites and possible new land sites should be carried out, after which risk zone maps are to be created which divide the land into zones based on the level of risk. Appropriate land uses and new planning and building regulations based on the risk zone maps are to be created. The risk zone maps should be legislated and included in council development plans and approval permit procedures to ensure compliance. Examples, such as Taiwan's Mitigation Plans, the Philippines Municipal Maps, and the Christchurch City Plan in New Zealand following the Canterbury earthquakes, display successful application of BBB measures to create safer developments. If resettlement to lower-risk lands is opted for, Mannakkara and Wilkinson (2012b) recommend that a comprehensive resettlement strategy should be created with community consent which takes into account risk levels of new lands, community preferences, and livelihood and lifestyle opportunities offered in the new locations for resettlement to be a success.

DN and PA (2008) encourage educating communities about risks and the importance of risk reduction measures and engaging them in collective risk reduction efforts. The Participatory Flood Risk Communication Support System (Pafrics) developed in Japan to educate locals and other stakeholders including NGOs and local governments on flood risks and risk management strategies is an example of a participatory tool.

### **Psychosocial Recovery**

Supporting psychosocial recovery of affected communities has been identified as essential for building back better (Davidson et al. 2007). Post-disaster recovery often focuses on providing fast solutions in an attempt to reestablish a sense of normality in affected communities as soon as possible (Khasalamwa 2009). The focus on speed results in overlooking the real needs of communities. The community is often not consulted to provide their input on reconstruction and recovery (Boano 2009). The lack of community consultation and participation leads to the provision of recovery solutions that are not suitable. For example, some of the new houses constructed in Sri Lanka by humanitarian agencies during the Indian Ocean Tsunami rebuild featured bathrooms made with half-heighted walls and shared bathrooms for males and females which were culturally unacceptable (Ruwapura 2009). Locals were unhappy with the reconstruction of homes following the 1999 Marmara Earthquake in Turkey as their local life, culture, and aesthetics were not considered. Khasalamwa (2009) stated that insufficient attention to social, cultural, and ethnic facets of communities during recovery can exacerbate preexisting vulnerabilities. Separation during disasters and resettlement operations disrupt community cohesion and psychological recovery (Florian 2007).

Social issues arising in post-disaster environments are primarily related to social/cultural/religious/ethnic factors, and psychological factors. Reconstruction is a chaotic and stressful time for individuals who are also experiencing trauma. These communities require various forms of assistance as part of building back better. Personalized advice and one-on-one support provided to families in Columbia during the 1999 earthquake recovery were a success. Similar forms of personal assistance were provided during the Victorian Bushfire recovery in Australia as well. James Lee Witt Associates (2005) recommended arranging specialized assistance for vulnerable communities. Providing psychological support and counseling are essential during recovery. The establishment of information centers which

offer easy access to recovery-related information for the community is also recommended. Upholding a sense of community spirit and improving community cohesion through organizing group activities are recommended for social recovery. The Canterbury Earthquake Recovery in Christchurch proposed sports, recreation, arts, and cultural programs to engage the community and provide a sense of normality.

One of the first steps to be taken in post-disaster recovery efforts in order to build back better is to understand the local context of the affected community through needs assessments and surveys in order to provide appropriate assistance to satisfy the community (Khasalamwa 2009). The reconstruction and recovery policies must then be developed based on local requirements to support and preserve the local culture and heritage. Batteate (2006) stated that maintaining community involvement throughout recovery is integral for BBB success. The importance of decentralization to empower disaster-affected communities by enabling them to take responsibility of the recovery effort and become involved in decision-making has been stressed by literature. The establishment of community consultation groups is an effective way to communicate with the community. Community consultation groups consisting of community leaders from preexisting community groups and reputed members of the community to liaise between the wider community and governmental authorities have been successful in Sri Lanka and India. Existing community groups can also be called upon to assist with recovery activities.

### **Economic Recovery**

Supporting economic recovery of the community and supporting livelihood regeneration and entrepreneurship are also an important part of recovery. Disasters cause damage to the economy of communities with the disruption of businesses and income-generating industries leading to issues such as high inflation rates and poverty. The adverse effects of disasters on the economy can also impede the overall recovery of a city. Hurricane Katrina displayed a disaster's long-term impacts on higher education and health

care in New Orleans, which were the foundations of the city's economy, eventually leading to a decline in population numbers as people moved away in search of better opportunities.

Post-disaster recovery efforts to date have shown support for economic recovery with strategies such as: "cash-for-work" programs, provision of business grants, "asset replacement" programs to provide industries with necessary resources, and training programs to up-skill locals and help them find work. In Aceh, Indonesia, tsunami-affected people were trained and employed in reconstruction to provide them with a source of income alongside the opportunity to become involved in their own recovery (Kennedy et al. 2008). In Japan following the 2011 earthquake and tsunami, the government decided to consolidate smaller fishing markets into large fishing centers to enable fishermen to support each other (Okuda et al. 2011). The Christchurch City Council's Central City Plan proposes fast-tracking of building consents for businesses to allow faster repair and construction work. Despite the implementation of such initiatives, post-disaster economic recovery is reportedly slow and below pre-disaster levels. The lack of success in economic recovery initiatives can be attributed to insufficient backing from policies and legislation for employment creation and lack of consideration given to the needs of affected communities.

Clinton (2006) said in his BBB propositions that "a sustainable recovery process depends on reviving and expanding private economic activity and employment and securing diverse livelihood opportunities for affected populations." Thus, the uniqueness of BBB comes from the integrated approach it proposes by giving economic recovery as much importance as reconstruction and aiming to provide solutions to suit local dynamics and preferences.

Monday (2002) stated that one of the first steps needed for effective economic recovery is to obtain accurate information about the local population through data collection and consultation with local governmental authorities, and a comprehensive economic recovery strategy must be created that is tailor-made to suit each

different community based on data obtained. Where applicable, attractive and flexible low-interest loan packages, business grants, and resources should be provided to support the livelihoods of the disaster-affected. Training programs should be held to support people in improving their existing livelihoods or acquire new skills. Mannakkara and Wilkinson (2012a) propose that business support and counseling services should be provided to assist with the economic recovery. Rebuilding of businesses must also be facilitated through special fast-tracked permit procedures. Incentives such as subsidized accommodation must be provided to attract builders from other areas to participate in rebuilding.

### Effective Implementation

A successful recovery effort requires effective and efficient recovery solutions as part of building back better. Two ways in which the efficiency and effectiveness of post-disaster recovery can be improved are through better management of stakeholders and through the use of appropriate post-disaster legislation and regulation.

One of the most common issues with post-disaster environments is the difficulty in coordinating between stakeholders to produce a unified outcome. Initially, there is often no organization in charge of the overall recovery effort. The lack of guidance leads different stakeholders to participate disjointedly promoting personal agendas which conflict with the interests of the local community (Batteate 2006). For example, nongovernmental organizations (NGOs) who operated in Sri Lanka following the Indian Ocean Tsunami constructed homes which were unsuitable for locals and were largely abandoned. The pressure for fast results during recovery also prevents well-intentioned stakeholders from considering community needs. Ambiguity about the roles of different stakeholders is another issue. The Victorian Bushfires Royal Commission report, 2010, stated that the roles of personnel involved in the recovery effort were unclear which led to the duplication of some activities. Many stakeholders involved in recovery have no previous experience in post-disaster

environments leading to ad hoc responses (Kennedy 2009). Often post-disaster interventions are governed by the national government without sufficient consultation or power given to local councils (Clinton 2006). Local-level organizations with useful local knowledge lack the capacity to operate to their full extent when impacted by disasters and are therefore excluded from recovery efforts. The lack of proper role allocation, coordination, and involvement of local-level stakeholders is a common issue found in post-disaster reconstruction environments.

A step taken to improve the management of large numbers of stakeholders in major disasters in order to build back better is the creation of a separate body to act as a recovery authority. Examples of recovery authorities created to manage reconstruction include: the Bureau of Rehabilitation and Reconstruction (BRR) in Indonesia following the Indian Ocean Tsunami, Bam's Reconstruction Supreme Supervisory and Policymaking Association (BRSSPA) in Iran following the 2003 Bam Earthquake, the Victorian Bushfire Reconstruction and Recovery Authority (VBRR) in Australia following the 2009 Victorian Bushfires, and the Canterbury Earthquake Recovery Authority (CERA) following the 2010 and 2011 Canterbury earthquakes in New Zealand. The recovery agencies contributed to the success of recovery to differing extents. Clinton (2006) said that stakeholders must operate with a common set of standards, approaches, and goals in order for recovery to be a success. Twigg (2007) proposes that the recovery authority should be responsible for establishing clear roles and responsibilities for the different stakeholders to divide recovery tasks based on resources and skills and avoid duplication.

Functional partnerships and linkages established between organizations can enhance reconstruction projects. Post-disaster recovery is a unique environment which requires deviation from normal procedures. Information sharing between organizations is one such deviation. The Federal Emergency Management Agency in the United States advocates the sharing of information, contacts, resources, and technical

knowledge between organizations to help recovery activities (FEMA 2000). Knowledge from past disasters should be retained and transferred to the government and other relevant organizations who will be involved in future post-disaster efforts. Twigg (2007) recommends that local government should be included as a key stakeholder in the recovery effort and also given the responsibility to manage local-level activities.

Another obstacle preventing successful BBB-centered recovery is the absence of proper controls to enforce BBB principles. Having BBB knowledge and producing recovery plans in-line with these principles are futile without proper legislation and regulations in place to ensure they are implemented. A common challenge in post-disaster environments is the sudden increased work load, especially in the building industry, along with a drop in the workforce across local organizations which slow down and impede recovery activities. Post-disaster reconstruction requires time-consuming activities such as hazard analysis, land selection, infrastructure development, and rebuilding to be done in a relatively short period of time. It is important to facilitate recovery-related activities by simplifying, fast-tracking, and exempting certain rules and regulations using special legislation.

Post-disaster legislation can be used to ensure compliance with BBB-based activities as well as to facilitate normal operations to improve the efficiency of recovery efforts. The lack of enforcement of hazard-related laws and adequate risk-based building controls contributed to the large-scale devastation caused by the 2004 Indian Ocean Tsunami (DNS and PA 2005). The same was seen in countries like Pakistan, Turkey, Samoa, and Haiti. Enforcing updated risk-based building design standards through the use of compulsory building codes and maintaining construction standards through careful inspections is an important regulatory requirement in reconstruction (James Lee Witt Associates 2005). Lack of awareness and understanding of new legislation can also lead to noncompliance. In the post-tsunami recovery effort in Sri Lanka, external nongovernmental organizations (NGOs) who took part did not comply with local standards

due to unawareness (Boano 2009). The National Post-Tsunami Lessons Learned and Best Practices Workshop held in Sri Lanka in 2005 highlighted the importance of training stakeholders (especially external NGOs) about existing and newly introduced legislation and regulations. The community's support can also be obtained by educating them about legislation and regulations that must be adhered to in reconstruction and recovery.

Post-disaster legislation can also be used to simplify and assist recovery activities to speed up the recovery process. Legislation that is customarily used to impose security and safety controls (such as building consents) can become an obstacle in high-pressure post-disaster environments. Time-consuming procedures, insufficient resources to process permits, and the lack of fast-tracked methods delay reconstruction. Delays in permits were a major reason for the holdup in housing repair and rebuilding following the 2005 Bay of Plenty storm in New Zealand (Middleton 2008). Fast-tracked consenting procedures, collaboration with other local councils, and open access to information between stakeholders can help speed up recovery.

Legislation can be used to remove unnecessary red tape to facilitate recovery activities. Meese III et al. (2005) reported a good example in the recovery following the 1994 Northridge Earthquake, USA, where legislative suspensions and emergency powers greatly reduced highway reconstruction time. The construction work provided employment and opening up the highways soon after the disaster helped boost the economy.

### Monitoring and Evaluation

The effectiveness and efficiency of post-disaster reconstruction and recovery activities is crucial to the success of a community's restoration following the impact of a disaster event. Having the knowledge of Build Back Better concepts in designing recovery programs is insufficient without systems in place to overlook and monitor implementation. The creation of a recovery strategy to assist in conducting post-disaster reconstruction and recovery activities is a common response following disaster events. Despite

having recovery strategies and revisions in legislation and regulation to improve recovery activities, the findings by Tas (2010) indicated that compliance was not monitored in the respective recovery efforts in Sri Lanka and Turkey, leading to poorly executed recovery projects. The lack of properly trained professionals who were competent in post-disaster environments and disaster management activities poorly affects the outcome of recovery efforts. The shortage of effective information and knowledge sharing and dissemination are also reasons for unsatisfactory disaster management practices. Findings from the Business Civic Leadership Center in 2012 on "What a Successful Recovery Looks Like" raised concerns that long-term recovery beyond reconstruction often does not take place due to the lack of mechanisms and expertise which prevents affected communities from satisfactorily "building back better" in the long run.

Recommendations to improve post-disaster recovery efforts through monitoring and evaluation have been provided in many sources of literature. The role of monitoring and evaluation is twofold: (1) to monitor and ensure compliance of recovery activities in accordance with the recovery strategy in place and relevant guidelines and regulations (Clinton 2006) and (2) to obtain lessons for the future and improve future disaster management and post-disaster reconstruction and recovery efforts (Monday 2002).

The 2003 Bam earthquake reconstruction provided a good example where rebuilding was monitored by providing construction supervision which assisted in assuring the quality of the rebuild. Clinton (2006) stated that the Tsunami Recovery Impact Assessment and Monitoring System (TRIAMS) was put in place during the Indian Ocean Tsunami recovery for the most affected countries. The recovery strategy in Christchurch, New Zealand, has also been equipped with monitoring mechanisms. Clinton (2006) suggested that long-term recovery should be monitored through continued data collection to ensure that recovery efforts do not leave communities with residual issues.

Monday (2002) pointed out that monitoring can be used to identify problems with post-

disaster interventions and establish lessons learnt. Lessons learnt should be incorporated into revising policy and procedures for future disaster management practices. Bakir (2004) recommends that public education campaigns should be run on lessons learnt, including the community in participatory disaster management. Public seminars have been held and advice notes have been distributed in Australia during the Victorian Bushfires recovery to keep the community informed about revised guidelines and standards. Workshops have been held in the Philippines, Japan, and California involving the community in vulnerability identification which have been successful (Batteate 2006).

## Summary

"Build Back Better" is an important concept for post-disaster reconstruction and recovery, signifying the need to use reconstruction as an opportunity to not only recover from the encountered disaster but to improve the resilience of communities to face and withstand future disaster events. BBB represents adopting a holistic approach toward recovery by addressing risk reduction of the built environment, psychosocial recovery of affected people, and rejuvenation of the economy in an effective and efficient manner. Risk reduction can be achieved primarily through the improvement of structural designs in buildings and infrastructure and through better risk-based land-use planning. BBB requires improved building codes and land-use plans to be enforced using a strong legal framework along with financial backing to encourage adoption. Quality assurance of the rebuild is also integral for building back better.

Psychosocial recovery needs to be addressed to assist communities with moving forward with their lives as an important part of overall community recovery. Psychosocial recovery of affected people needs to be assisted through the provision of support services such as personal case management, counseling, and social activities. Inclusion of community members in recovery activities is another way to support psychosocial

recovery and provide recovery solutions that are in-line with community needs as part of building back better.

Economic recovery is essential for the recovery of communities. An informed economic strategy to address and support community-specific issues is the first step toward BBB-based economic recovery. Financial assistance, training, and business rebuilding support need to be provided to assist with economic recovery.

Reconstruction and recovery requires effective management of stakeholders and the use of post-disaster legislation and regulation in order to build back better. The creation of a recovery authority to allocate roles and coordinate and manage stakeholders is recommended. Successful recovery requires local-level partnerships and contribution to provide locally viable recovery solutions. Compliance of BBB-based concepts in recovery needs to be ensured through the use of appropriate post-disaster legislation and regulation to enforce risk reduction and community recovery initiatives. Legislation and regulation can also be used to facilitate post-disaster recovery activities by fast-tracking and exempting normal procedures.

The effective implementation of risk reduction and community recovery initiatives concurrently will result in building back better. Recovery efforts also need to be monitored continuously through short-term and long-term recovery to ensure compliance with BBB concepts and to obtain lessons to improve future disaster management efforts.

### Build Back Better: The Way Forward

Understanding and implementing the concept of Building Back Better is integral to improving a community's resilience following a disaster event in order to achieve positive changes for affected communities. The elements required to build back better which are; risk reduction, psychosocial recovery, economic recovery, effective implementation and monitoring and evaluation, have been introduced and discussed in this chapter. This understanding can be used to create

practical guidelines to design future reconstruction and recovery efforts including all these key facets to effectively build back better. Further comprehension of how these strategies for building back better can be more successfully implemented in different environments can be gained by studying different disaster events in the future. It is also suggested that criteria for measuring levels of resilience should be established which can serve as indicators to measure progress and effectiveness of build back better practices.

The long-term sustainability of resilience in communities instilled by using BBB concepts depends on how they are linked with on-going developmental strategies. It is therefore important for the key concepts identified in this chapter to be incorporated into local and national government policies for community planning and development even during non-disaster periods.

### Cross-References

- ▶ [Building Codes and Standards](#)
- ▶ [Building Disaster Resiliency Through Disaster Risk Management Master Planning](#)
- ▶ [Community Recovery Following Earthquake Disasters](#)
- ▶ [Economic Recovery Following Earthquakes Disasters](#)
- ▶ [Land Use Planning Following an Earthquake Disaster](#)
- ▶ [Legislation Changes Following Earthquake Disasters](#)

### References

Bakir PG (2004) Proposal of a national mitigation strategy against earthquakes in Turkey. *Nat Hazards* 33(3):405–425

Baradan B (2006) Analysis of the post-disaster reconstruction process following the Turkish earthquakes, 1999. In: GROUP IR (ed) International conference on post-disaster reconstruction meeting stakeholder interests, University de Montreal, Florence

Batteate C (2006) Urban disaster risk reduction and regeneration planning: an overview. *Focus J City Reg Plan* Dep 3(1):11–17



- Boano C (2009) Housing anxiety and multiple geographies in post-tsunami Sri Lanka. *Disasters* 33(4):762–785
- Clinton WJ (2006) Lessons learned from tsunami recovery: key propositions for building back better. Office of the UN Secretary-General's Special Envoy for Tsunami Recovery, New York
- Davidson CH, Johnson C, Lizarralde G, Dikmen N, Sliwinski A (2007) Truths and myths about community participation in post-disaster housing projects. *Habitat Int* 31(1):100–115
- DN & PA (2008) Disaster and development in South Asia: connects and disconnects, South Asia disaster report. Duryog Nivaran & Practical Action, Colombo
- DNS & PA (2005) Tackling the tides and tremors: South Asia disaster report 2005. Duryog Nivaran Secretariat & Practical Action – South Asia Programme, Colombo
- FEMA (2000) Rebuilding for a more sustainable future: an operational framework. FEMA report. Federal Emergency Management Agency, Washington, DC
- Florian S (2007) Housing reconstruction and rehabilitation in Aceh and Nias, Indonesia – Rebuilding lives. *Habitat Int* 31(1):150–166
- Halvorson SJ, Hamilton JP (2010) In the aftermath of the Qa'yamat: the Kashmir earthquake disaster in northern Pakistan. *Disasters* 34(1):184–204
- James Lee Witt Associates (2005) Building back better and safer: private sector summit on post-tsunami reconstruction. James Lee Witt Associates, Washington, DC
- Kennedy J (2009) Disaster mitigation lessons from “build back better” following the 26 December 2004 Tsunami. In: Ashmore J, Babister E, Kelman I, Zarins J (eds) *Water and Urban Development Paradigms*, Taylor and Francis Group, London
- Kennedy J, Ashmore J, Babister E, Kelman I (2008) The meaning of ‘build back better’: evidence from post-tsunami Aceh and Sri Lanka. *J Conting Crisis Manag* 16(1):24–36
- Khasalamwa S (2009) Is ‘build back better’ a response to vulnerability? Analysis of the post-tsunami humanitarian interventions in Sri Lanka. *Nor J Geogr* 63(1):73–88
- Mannakkara S, Wilkinson S (2012a) Build back better principles for economic recovery: the Victorian bushfires case study. *J Bus Contin Emerg Plan* 6(2):164–173
- Mannakkara S, Wilkinson S (2012b) Build back better principles for land-use planning. *Urban Des Plan* 166(5):288–295
- Meese E III, Butler SM, Holmes KR (2005) From tragedy to triumph: principled solutions for rebuilding lives and communities, Heritage special report. The Heritage Foundation, Washington, DC
- Middleton D (2008) Habitability of homes after a disaster. In: 4th international i-REC conference on building resilience: achieving effective post-disaster reconstruction. International Council for Research and Innovation in Building and Construction, Christchurch
- Monday JL (2002) Building back better: creating a sustainable community after disaster. *Natural Hazards Informer* [Online], 3. Available <http://www.colorado.edu/hazards/publications/informer/infrmr3/informer3b.htm>. Accessed 27 Feb 2013
- Okuda K, Ohashi M, Hori M (2011) On the studies of the disaster recovery and the business continuity planning for private sector caused by Great East Japan earthquake. *Commun Comput Inf Sci* 219:14–21
- Pathiraja M, Tombesi P (2009) Towards a more “robust” technology? Capacity building in post-tsunami Sri Lanka. *Disaster Prev Manag* 18(1):55–65
- Ruwanpura KN (2009) Putting houses in place: rebuilding communities in post-tsunami Sri Lanka. *Disasters* 33(3):436–456
- Tas M (2010) Study on permanent housing production after 1999 earthquake in Kocaeli (Turkey). *Disaster Prev Manag* 19(1):6
- Twigg J (2007) Characteristics of a disaster-resilient community – a guidance note. DFID Disaster Risk Reduction Interagency Coordination Group, London
- Wisner B, Blaikie P, Cannon T, Davis I (2004) *At risk: natural hazards, people's vulnerability and disasters*. Routledge, New York

---

## Building Codes and Standards

P. Gülkan<sup>1</sup> and Robert K. Reitherman<sup>2</sup>

<sup>1</sup>Department of Civil Engineering, Çankaya University, Ankara, Turkey

<sup>2</sup>Consortium of Universities for Research in Earthquake Engineering, Richmond, CA, USA

### Synonyms

Codes of practice; Guidelines; Regulations

### Introduction

Selected key elements of modern seismic codes are reviewed here, along with a brief review of their historical development. What can be considered a single seismic code pertaining to a nation or a subdivision thereof consists of dozens of pages of provisions and by reference includes thousands of pages of standards that relate to loads, testing procedures, manufactured

building products, and materials. As used in this general discussion, “code” includes these other documents. Thus, it is far beyond the feasible scope here to provide an encyclopedic review of current seismic codes. Instead, this contribution is an attempt to delineate key features of most modern seismic codes and trace the development of their underlying concepts as they have evolved through the decades.

Preparing a global review of seismic codes runs the risk of turning out to be country specific and omitting other important references or milestones. This entry will attempt to avoid that. Instead the narrative will describe what a code should look like and what its important elements should contain. A building code places legal requirements on designers and constructors. Codes that fail to keep up with technological change and the advancement of knowledge become irrelevant. Building codes must be revised frequently, often at about 3-year increments. As more earthquakes occur and related building performance is observed, and as more research is conducted, the seismic provisions of a code often are one of the sections that change the most from one edition of a building code to the next.

The main purpose of building codes is to protect public health, safety, and general welfare as they relate to the construction and occupancy of buildings and structures. The building code becomes law of a particular jurisdiction when formally enacted by the appropriate governmental or private authority. The parts of a building code that relate to special requirements that must be fulfilled in order to inject a desired level of protection against the effects of ground shaking are called a seismic code. This broad description applies also to other types of construction, e.g., bridges, water tanks, towers, and port facilities. There are often additional codes or sections of a building code that have more specific requirements that apply to particular occupancies, for example, providing simplified requirements for the typical dwelling and more extensive requirements for the school, theater, or hospital.

## Overview of Model Codes

A model building code is a convenient resource that can be adopted by the appropriate jurisdiction as its legal requirement. This makes the cost of maintaining and updating a code more economical and also provides design and construction consistency from one city to the next than would be the case if each developed its own code. That multiplicity of codes in a country was the rule throughout the nineteenth century and in many cases has only gradually trended toward nationally uniform provisions in the twentieth century. Two important interests that have pushed for uniformity are the construction and building materials industries, which can operate more efficiently if they have one set of rules, and the insurance industry, which desires up-to-date code provisions that can be easily evaluated for rate-setting purposes.

The practice of developing, approving, and enforcing building codes varies considerably among nations. Several countries have adopted model codes, including earthquake regulations, on a national basis, such as Japan, New Zealand, and Italy. In such countries, building codes are developed by the government agencies or quasi-governmental standards organizations and then made to apply across the country by the central government. Until 2000, the United States had three major model codes and associated seismic regulations, and even after their integration into the International Building Code, the process of adopting and enforcing the regulations, sometimes with significant variations, is left to the states and local governments. Similarly, in India each municipality and urban development authority has its own building code, which is mandatory for all construction within its jurisdiction. In Europe, the Eurocode is a pan-European building code that has all but superseded the older national building codes. Each country must now develop its own “national country annex” to localize the contents of the Eurocode. The seismic component of the Eurocode is only one small part of that model code. While the consistency of the regulations across European national

boundaries provides a better technical basis for its seismic and other provisions, the more important motive for such a code of European scope is economic. The Euro economic block can compete more effectively against the nations outside it if its design, construction, and building materials industries are guided by consistent provisions.

### **Prescriptive and Performance-Based or Objective-Based Codes**

Building code requirements are usually a combination of prescriptive requirements that spell out exactly how something is to be done, on the one hand, and performance requirements that just outline what the required level of performance is and leave it up to the designer how this is achieved, on the other. An example of the former would be a rule of thumb for spacing of anchor bolts in house construction; an example of the latter would be to have the engineer calculate interstory drift and then design concrete cladding to accommodate that building-specific distortion. In recent years there has been a move among many building codes to move to more performance requirements and less prescriptive requirements. Performance-based code requirements still require tight definitions so that adequate performance can be evaluated by the building regulatory agency. The fire protection field has developed performance-based design approaches for many years, in which test or other data can be used to provide alternate means of fire protection instead of following the prescriptive requirements of a code.

In recent years, several countries, beginning with Australia, have moved to much shorter objective-based building codes. Rather than prescribing specific details, objective-based codes list a series of objectives all buildings must meet while leaving open how these objectives will be met. When applying for a building permit, the designers must demonstrate how they meet each objective. This makes it necessary for approving authorities to employ correspondingly qualified personnel so that a productive synergy can be

created between innovative designs and traditional safety concerns. It also requires a high degree of professionalism, because it gives the architect and engineer more leeway, as compared to more prescriptive requirements, and also requires a higher level of building code enforcement review. Seismic isolation, inclusion of damping devices, response history analyses, and displacement-based design are some of the innovative approaches currently in use in some places where this higher level of design and review capacity is present. Each of these represents challenges in analysis and design that require an intimate knowledge of the underlying mechanics-based mathematical theory and its limitations. As such, they are best performed by professionals with considerable experience because there are alternative approaches that require deep insight on the part of the engineer.

Seismic codes begin with the goal of providing safety, and many stop there in most respects, but some include requirements for protecting the functionality of essential buildings, such as fire stations, hospitals, and emergency communications centers or data processing centers. This is discussed in the separate chapter on Essential Facilities and is only mentioned in passing here. Some of the most stringent regulations of this type were passed in California after the 1971 San Fernando Earthquake, when the Hospital Seismic Safety Act of 1972 was passed. The Veterans Administration adopted its own regulations after that earthquake, regulations that seek to not provide not only safe hospitals but also more functional ones. Some voluntary above-code (“performance-based design”) approaches lead an owner to invest in the cost of greater seismic protection to achieve less property damage in earthquakes, but the most common seismic design criteria that go beyond the goal of providing safety are related to protecting essential functions.

### **Geologic and Geotechnical Topics**

Mentioned briefly here are geologic and geotechnical engineering aspects to the seismic

provisions of a building code. Construction regulations that deal effectively with earthquake vulnerabilities must include within their purview geologic hazards such as surface faulting and liquefaction. Geologic and geotechnical engineering provisions to deal with those hazards came later than structural provisions. In 1972, the state of California passed the Alquist-Priolo Fault Zoning Act (the current name, which has changed over the years), and slightly before that the city of Portola Valley, which is bisected by the San Andreas Fault, passed its own legislation. Surface fault zoning is the most clearly delineated of the earthquake ground failure hazards, and thus it was logically the first to be subject to regulations. Liquefaction was not a word that soils engineers (then the term for geotechnical engineers) used prior to the 1964 Alaska and the closely following 1964 Niigata Earthquake, but in the following decades, areas of a jurisdiction that were suspect in terms of poorly compacted granular soils and high water table were frequently zoned as requiring special geotechnical investigations. Geotechnical engineers now have at their disposal field and laboratory investigation techniques and a knowledge base about how soils behave in earthquakes that did not exist in the 1960s. Codes and standards of practice can now require geotechnical evaluations that would have been impossible to perform a few decades ago.

One tool that developed out of non-seismic slope stability concerns that later was seen to have a seismic benefit is the grading ordinance. The city of Los Angeles passed such a law in 1952 controlling how excavation and cut and fill could be performed. Such ordinances have become common, and the geotechnical engineering evaluations required in the design stage now typically include earthquake considerations in regions where a seismic code is enforced as well as non-seismic landslide hazards.

## Nonstructural Code Provisions

Coming later than structural regulations were provisions to protect the nonstructural features of a building. The first detailed report on

earthquake nonstructural damage was done for the 1964 Alaska Earthquake (Ayres et al. 1973), with a similar report on the 1971 San Fernando Earthquake (Ayres and Sun 1973). Nonstructural provisions are only briefly mentioned here but are an essential part of the modern seismic building code. Approximately three-quarters of the initial value of a modern building's construction, dwellings excepted, is composed of nonstructural components, such as enclosure systems, elevators, partitions, fire sprinklers, ceilings, and heating-ventilating-air-conditioning equipment. In general it can be said that the leading seismic codes of the world have increasingly included more and more detailed regulations for the calculations of loads that are used to design nonstructural bracing and anchorage, but a lack of coordination of the implementation of these rules still persists. Different design professionals work on their own systems – architects on partitions and ceilings, fire protection engineer on fire sprinkler system, mechanical engineer on the HVAC system, and so on – and yet it is the structural engineer with the most expertise for such work. And then different contractors and trades work on the implementation phase, often with little guidance or oversight. Recent earthquakes have demonstrated that simply having nonstructural damage protection rules on the building code's books is not sufficient to actually protect that myriad of components. A common example is that some codes for many years have contained a clause stating that nonstructural components must be designed for the motions and deformations that the structure imposes upon them, but in actual practice, partitions and other components were constructed without this engineering.

## Historic Context

Some accounts of historic building code evolution claim that the Code of Hammurabi (a Babylonian king of some 3,800 years ago who was considered by his subjects to be a god as well) engraved on stone is the first building code ever to have been put into effect. That notion needs to be dispelled because the Code

of Hammurabi is much more of a civil or penal code as it has only a few articles out of several hundreds that even mention buildings. It has harsh penalties for builders of shoddy buildings, but the rest of the provisions are divine orders that deal with the trade of commodities, sale of slaves, marriage unions, inheritance regulations, and the like. King Hammurabi informs a builder that if the house he builds should collapse and kill the person who owns it, then he too stands to lose his life, but there is no explanation for how one might build a house that does not collapse. Thus, it fails the test of belonging to the family of codes because it has no stipulations for how things should be done; only penalties are listed that must have been intended to discourage negligence of good building practices.

Tobriner (1984a) provides a historical survey of the development of building codes, noting that they originated primarily in the form of fire-resistant construction requirements, and then only much later in most countries had seismic regulations added to them. The first systematic national building standard was the London Building Act of 1844. Among the provisions, builders were required to give the district surveyor 2 days' notice before building, and they contained regulations regarding the thickness of walls, height of rooms, the materials used in repairs, and the dividing of existing buildings. The placing and design of chimneys, fireplaces, and drains were to be enforced, and streets had to be built to minimum requirements. The city of Baltimore passed its first building code in 1859. The Great Baltimore Fire occurred in February, 1904. Subsequent changes were made that matched the contemporary fire-resistant regulations of some other large American cities. In Paris, under the reconstruction of much of the city by Baron Haussmann during the Second Empire (1852–70), great blocks of apartments were erected, and the height of buildings was limited by law to six stories. Though height limits were instituted for city planning reasons, they later sometimes became part of seismic codes in determining allowable structural systems for various heights.

## Construction Regulations Preceded Engineering Regulations

A historic survey of prescriptive requirements on how to build for better seismic performance shows that these landmarks were always reached after cataclysmic experiences. These early regulations, such as were passed after the 1509 Istanbul Earthquake, 1755 Lisbon Earthquake, or the 1880 Luzon (Manila) Earthquakes, were limited to descriptions of allowable building materials and building heights. They predated the extensive use of reinforced concrete and steel. Unreinforced masonry was an allowable material in these early regulations, and no quantitative method was provided for calculating either demands or capacities. Thus, they are primitive seismic codes in today's light, regulating some features of construction but not employing the quantitative methods civil engineers would later develop. That notwithstanding, these efforts are impressive for making such early attempts to improve the building stock's earthquake resistance.

The major earthquake that shook Istanbul in the summer of 1509 led to the banning of stone masonry construction in the city, because most deaths had occurred when such buildings collapsed. This decision paved the way for the emergence of another form of disaster that plagued the city for the next four centuries: fires consumed not only timber construction but also much of the cultural heritage. Following the 1755 earthquake in Lisbon, which destroyed the city center area known as Baixa, the Marquis of Pombal gathered a group of builders to determine the best manner of earthquake-resistant construction to use for the rebuilding. The type of construction selected became known as the Pombalino wall. In its complete form, it is also referred to as "gaiola" or "cage" construction. Most, if not all, of the buildings reconstructed in the reconfigured planned Baixa area were constructed with Pombalino walls and sometimes (but not always) with complete "gaiola" timber frames (Tobriner 1984b; Langenbach 2003).

The Pombalino system was not based on what today would be known as rational methods of

analysis, applying engineering theory to a given case and calculating loads and resistances. It was an attempt at earthquake-resistant construction, not earthquake engineering per se, because the engineering techniques of the nineteenth and twentieth centuries were far off in the future. It was decreed in royal fashion for use in a city that had experienced one of the most destructive earthquakes in Europe and was based on the construction tradition in the Mediterranean basin and may have borrowed construction lore developed by shipbuilders. It was used on the interior of buildings that consisted of timber frames with vertical and horizontal timbers of approximately 10–12 cm square, with internal braces, forming an “X,” referred to in Italy and Portugal as the “Cross of St. Andrew.” The timbers for the cross were 9 cm by 11 cm in section. The frame was then “nogged” (i.e., filled with brick) in the triangular spaces formed by the crosses with a mixture of stone rubble, broken brick, and square pieces of Roman brick in different patterns in each panel. The interior walls were then covered with plaster, hiding the infill and the timber frame. The exterior facades of the Baixa buildings were reconstructed with load-bearing masonry walls of about 60 cm in thickness, some of which had a timber frame on the inside face (Gülkan and Langenbach 2004).

The 1906 San Francisco Earthquake was something of a nonevent in the history of seismic codes. Although the cause of the earthquake was accurately noted – the San Andreas Fault had been mapped in several areas before the earthquake and its surface rupture was well documented afterward – and although civil engineers trained in universities were in existence, no engineering consensus existed around provisions that would define how to calculate loads and then calculate the lateral resistance of a structure. Unreinforced masonry was not prohibited, and by the time the city took stock of its unreinforced masonry building seismic hazards in the 1980s, over 90 % of the 2,000 buildings that required retrofitting were dangers that were built after the earthquake, not before it. The San Francisco building code even reduced the wind load a few years after the earthquake. In that era, the wind

load was sometimes thought to be a surrogate for seismic load.

A few years later, after the 1910 Cartago Earthquake in Costa Rica, a national code was passed that phased out adobe and trapia (rammed earth) structures, substituting bahareque construction (sawn lumber or bamboo framing with plaster). This was a similar but more regulatory approach to the substitution of wood for masonry that occurred in construction styles after some other earthquakes, such as the 1855 Wairarapa (Wellington, New Zealand) Earthquake.

### The First Seismic Codes with Engineering Content

Soon after the 1906 California Earthquake, the 1908 Messina-Reggio Earthquake occurred in southern Italy, but it had a different and more beneficial impact on building codes. Sorrentino (2007, 2011) relates how a committee of engineers developed an equivalent lateral force analysis method that was adopted into the building code of the disaster region. It even had the refinement of applying a different lateral force coefficient (*rapport sismica*) to the ground story (1/12) than the story above (1/8), accounting for greater acceleration in the second or third stories. After the 1915 Avezzano (or L’Aquila) Earthquake, the code was changed to have factors of 1/8 for the ground story and 1/6 for the upper stories. These Italian seismic provisions applied only to the area affected by the earthquakes, a pattern that was common in early codes prior to the availability of national maps depicting the hazard of seismic ground shaking.

At the turn of the nineteenth to twentieth century, Riki Sano was getting his PhD from the University of Tokyo on “Seismic Design Concept for Building Structures,” along with Tachu Naito, his student; Sano was to be instrumental in the development of the Japanese equivalent lateral force method. Their work came to fruition after the 1923 Great Kanto or Tokyo Earthquake of 1923, when the 1924 Urban Building Law Enforcement Regulations were passed. It used a 10 % lateral force factor (*shindo*) applied



uniformly up the height of the building. As an example of how engineering practice in some cases is in advance of the codes, when the 1923 earthquake occurred, three large buildings designed by Tachu Naito had already been built (and performed well in the earthquake, giving the new equivalent lateral force method a boost into the code).

An important threshold was crossed in Japan toward the implementation of scientifically determined national seismic provisions (Otani 2008). The objectives of the Japanese Building Standard Law, proclaimed in May 1950, were “to safeguard the life, health, and properties of people by providing minimum standards concerning the site, structure, equipment, and use of buildings.” The law outlined the basic requirements, and the technical details were specified in the Building Standard Law Enforcement Order (Cabinet Order) and in a series of Notifications by the Minister of Construction.

The seismic design provisions of the Building Standard Law Enforcement Order were significantly revised in 1981, including the following three major changes:

1. Structural calculations are required to examine (a) maximum story drift under design earthquake forces, (b) lateral stiffness distribution along the height, (c) eccentricity of mass and stiffness in plan, and (d) story shear-resisting capacity at the formation of a collapse mechanism.
2. Earthquake resistance is specified (a) in terms of story shear rather than horizontal floor forces, (b) as a function of fundamental period of a building and soil type, and (c) separately for the allowable stress design and the examination of story shear-resisting capacity.
3. Required story shear-resisting capacity is varied for construction materials and with the deformation capacity of hinging members under earthquake forces.

The framework of the law was also significantly revised in 1998, (a) introducing performance-based regulations wherever feasible, (b) allowing private agencies to execute the

building confirmation and construction inspection works, (c) deregulating urban land use, and (d) allowing public survey of design and inspection documents. New technical specifications in the form of the Law Enforcement Order and a series of Notifications of the Minister of Construction were issued in June 2000, including the definition of performance objectives at design limit states and the specifications for verification methods.

California’s contribution to the development of the modern seismic code based on engineering calculations had a small start after the 1925 Santa Barbara Earthquake, and then after the 1933 Long Beach Earthquake, statewide regulations were passed that were derived from the Japanese code. The 1930s was the decade when the lineage of seismic codes in several countries began. Provisional earthquake regulations were enacted in Chile in 1930 after the Talca Earthquake and became more institutionalized after the 1939 Chillán Earthquake. In New Zealand, following the 1931 Hawke’s Bay Earthquake, the 1935 New Zealand Standard Model Building By-Law included earthquake regulations. India adopted its first seismic code in 1935 following destructive earthquakes in 1931 and 1935 in Quetta (now part of Pakistan), and the 1939 Erzincan Earthquake in Turkey led to its first engineering regulations for the earthquake hazard.

### **Equivalent Static Elastic Lateral Force Method**

A seismic load on a building is actually dozens of different significant seismic loads that occur during the 20–60 s during which the ground is strongly shaking. The earliest practical way to “put a number” on that bewildering set of loads, which are not well known in advance of the earthquake, was to represent the worst loading effect as a percentage of the weight of the structure, recognizing that seismic shaking causes inertial loads, and inertia is a product of mass and acceleration. The full descriptive name of the method is the equivalent static elastic seismic lateral force analysis method. It is intended to be

equivalent to or adequately represent the actual earthquake forces; the method computes a single static force to represent the changing dynamic forces; that force is applied to an analytical structural model that remains elastic, even though inelastic behavior obviously occurs; and it is an analysis method for determining only the design loads, not for distributing them through the structural components and connections that provide the resistance to the loads. And finally, the only design loads were lateral or horizontal, whereas strong motion records routinely measure some vertical motions as well. Each of these limitations was to be worked on in the following decades. From these first incarnations, the equivalent lateral force method was refined to include several necessary considerations.

Instead of applying seismic regulations to a region after it had an earthquake, earth scientists compiled maps showing where earthquakes should be expected. This was first done with a small number of large-scale zones for a country, each zone defining the force factor to be applied. Then beginning in the 1950s in Japan, a probabilistic basis to the maps was developed. Kawasumi (1951) developed three maps, depicting the shaking that should be expected to occur in exposure periods of 75, 100, and 200 years. The Applied Technology Council in its ATC-3 document (Applied Technology Council, 1978) included national maps produced by S.T. Algermissen that had a probabilistic basis. In China in 1977 a national seismic design map was based on shaking with 3 % and 10 % probabilities of being surpassed. Formats such as these for tying the probability of occurrence to the severity of shaking have become standard in seismic codes today. Another refinement has been microzonation: zoning small areas as having different ground shaking severities, or ground failure hazard (e.g., liquefaction), based on local soils. It became increasingly known that in general soft soils amplified ground shaking, though the large differential response between soft and hard grounds as measured in low-level shaking was not found to be linear up through high levels of ground motion: a column of soft soil 30 m high simply cannot move back and forth rapidly

enough to track rapid and severe motion of the underlying strata, and soil can behave nonlinearly just as structural materials do. The limiting case of microzonation is the site-specific evaluation, where the construction to be placed on a site is designed for a customized set of earthquake criteria, a more expensive approach usually reserved for major facilities.

On the structural side, knowledge of different structural systems and materials had to evolve for codes to seismically regulate them, and a growing body of structural laboratory research provided that information. The steel and concrete industries in particular were the settings for a large amount of research conducted in the 1950s and later. Research on reinforced concrete in great part conducted at the University of Illinois was the technical basis for an important document that advanced the use of that material in seismic codes (Blume et al. 1961). The other kind of research that provided this knowledge was actual earthquake performance. Earthquake reconnaissance or field surveys of the effects of earthquakes became increasingly common in the 1960s.

The early codes provided loads computed with a slide rule that were low enough to keep the structural model that was on the engineer's drawing board in the elastic range. (Computers did not become widespread in seismic design or other civil engineering practice until the 1970s.) Slowly, inelastic behavior was included in codes by including requirements for ductility. Classifying structural systems and materials was an approximate first approach. A structure thought to have greater ductility was designed for lower elastic-level forces, because there was confidence in how it would perform when pushed into the inelastic range. The ability of ductile connections and members to absorb punishment without failure, and also the softening effect (period lengthening) and its beneficial effect on response, became increasingly recognized in the 1960s, 1970s, and 1980s. Today, the choice of a structural system is heavily influenced by how the code defines its ductility. Seismic structural codes are all aware that ground motions are random and can be determined only approximately

in advance. For this reason they contain provisions to prevent unexpected surprises leading to catastrophic failures. Lessons that have been taught by past earthquakes for how building components behave under ground shaking are embedded in their verbiage. As theory and experiment combine to lead to more refined ways of seismic protection, this knowledge must be incorporated into the newer versions of codes for continuous improvement.

### The Response Spectrum Method

Yet another improvement in seismic codes was consideration of the dynamic properties of the structure, its period or periods of vibration, and the amount of damping. The tendency of the structure to respond at its natural frequency was only useful information if the frequency content of the ground shaking was also known: in structural dynamics, it takes two to tango. Because the first strong motion seismograph (accelerograph) was only deployed in 1932, it took years for records to accumulate to provide a statistical picture of earthquake severity in terms of frequency content. Trifunac (2006) traces the history of the response spectrum method of analyzing earthquake ground motions and producing design spectra that engineers could use to proportion required resistance of the structure. Two of the most influential developers of the method were Maurice Biot and George Housner, whose doctoral theses at the California Institute of Technology (1932 and 1941, respectively) were devoted to this topic. The theory became widely applied in engineering practice in the 1970s and 1980s when several conditions were favorable. First, there were more earthquake records. Second, engineers could afford to have the new, more powerful electronic computers on their desks that could do the extensive mathematical work. Housner (1997, p. 33) notes a third factor: "Because of the practicing engineers' reluctance to employ the design spectrum, I think it was essentially the nuclear power business that got the spectrum into widespread use."

Concerning the growing number of earthquake records, the city of Los Angeles played an important role when it passed a revision to its building code in 1965 requiring that three strong motion instruments be installed in buildings six stories or taller (one at the base, one at mid-height, one at the roof). This resulted in the large harvest of ground motion and structural motion records from the 1971 San Fernando Earthquake. The city of Los Angeles also was precocious in its 1943 adoption of a formula in its code that related period of vibration as represented by number of stories to the base shear coefficient calculation in its equivalent lateral force method: the taller the building, the lesser the base shear. In 1957, Los Angeles also had a strong effect on the development of earthquake codes, even though it was not an earthquake code revision: the zoning code was revised to allow buildings taller than 150 ft. Engineers in California thought that taller, more flexible (longer period) buildings could be designed for lower force coefficients, and they also knew that if the same coefficients as were used for low-rise buildings (typically 10 % to 13 %) were applied to every story in a tall building, the large amount of strength, and thus area taken up by shear walls and other structural material, would have very negative architectural and real estate implications.

When it seemed that engineers in the two large urban regions of California, centered on Los Angeles in the south and San Francisco in the north, could be diverging toward significantly different provisions for dealing with the tall building question and the modernization of seismic codes, the statewide structural engineering organization Structural Engineers Association of California (SEAOC) began its influential set of editions of the "Blue Book," the *Recommended Lateral Force Requirements and Commentary* (SEAOC 1959). Its requirements became the seismic provisions of the Uniform Building Code used in various editions and adaptations throughout California and the Western United States until the year 2000 when the UBC was folded into the IBC, as previously described.

## The Response History Method

The equivalent static lateral force method leads the engineer to calculate a single quantity, the total shear at the base of the building, the base shear, and then proportion that load up the height of the structure according to procedures that attempt to represent the dynamic response of the building in a simple way. While there is dynamic thinking underlying the method, it still represents the series of motions that occur during the earthquake with a static view or “snapshot” of the overall effect of those motions. The response spectrum method similarly is a way to give the engineer a base shear to use in design. A given overall representation of one record, for example, the peak ground acceleration, might exceed that of another record and yet that other record might be more damaging to a particular structure. A record with greater duration, more pulses above a threshold such as the elastic limit of a portion of the structure, can create more demand than a record of smaller duration, even if the latter has a greater peak value (Johnson 2013). The logical improvement was seen to be to calculate the various forces and deformations that occurred to a structural model split second by split second in response to the changing ground motion.

Three sources of research information that developed from the 1960s to the present day provided the basis for incorporating a fully dynamic method into seismic codes, subjecting the analytical model of the structure to the motions of several recorded earthquakes. One came from completely outside the earthquake engineering field, the development of the modern computer. A second prerequisite was a large library of earthquake records, conveniently supplied by growing coverage of highly seismic areas with strong motion instruments and, unfortunately, by Earth’s frequent earthquakes. The third was improved knowledge of structural behavior, in particular of how structures behaved in the inelastic range. While computers played a role in that research on structural behavior, it has also required the traditional approach of subjecting specimens to simulated seismic loading in the laboratory. Computer simulation is not

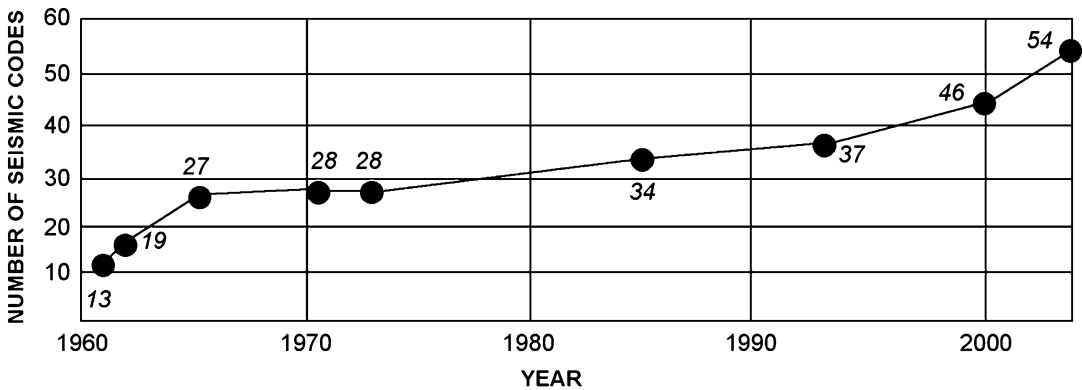
capable of substituting for the simulation of physical testing.

A 1973 benchmark for the development of the response history method is provided by the seismic design manual of the US military (Departments of the Army, the Navy, and the Air Force 1973, pp 3–3): “Since the mechanics of dynamic analysis requires that a separate solution must be obtained for each instant of time during the entire history of interest, computation by computers is necessary. This kind of analysis is generally beyond the kind of effort that can be afforded in the design of almost all but the most critical structures.” Today, the method is more frequently used, though it still is applied to a small minority of all the structures being seismically designed. Chopra (2005, p. 107) provides an assessment of the future of the method:

At the present time, nonlinear RHA [response history analysis] is an onerous task, for several reasons. First, an ensemble of site-specific ground motions compatible with the seismic hazard spectrum for the site must be simulated. Second, despite increasing computing power, inelastic modeling and nonlinear RHA remains computationally demanding, especially for un-symmetric-plan buildings—which require three-dimensional analysis to account for coupling between lateral and torsional motions—subjected to two horizontal components of motion. Third, such analyses must be repeated for several excitations because of the wide variability in demand due to plausible ground motions, and the statistics of response must be considered. Fourth, the structural model must be sophisticated enough to represent a building realistically, especially deterioration in strength at large displacements. Fifth, commercial software is so far not robust enough to predict response with high reliability. Sixth, an independent peer review of the results of nonlinear RHA is required by the FEMA-356 guidelines, adding to the project duration and cost. With additional research and software development, most of the preceding issues should be resolved, and nonlinear RHA may eventually become the dominant method in structural engineering practice.

## Growth in Adoption of Seismic Codes

Figure 1 provides a quick way to see how seismic codes have spread from an initially small number of countries. The numbers are drawn from the



**Building Codes and Standards, Fig. 1** Growth in the adoption of seismic codes (Reitherman 2012, p. 582)

various editions of *Regulations for Seismic Design: A World List*, published by the International Association for Earthquake Engineering (1960 and later editions).

One could argue that because seismic codes now cover most of the significantly seismic areas of the world, seismic safety has now been achieved on a global scale. This would be overly optimistic for two reasons. First, there are always older, pre-code buildings that did not benefit from a modern seismic code. Secondly, even today in countries with regulations “on the books,” legally binding laws that include the latest earthquake engineering thinking, those regulations are not always thoroughly carried out.

The seismic provisions in a code must be complemented with reliable implementation of the code, its effective enforcement. This remains one of the hardest issues to solve, especially in poorer countries but also in the most developed. Merely making seismic codes more sophisticated as each new edition is promulgated every few years is not a solution, unless comprehensive implementation also occurs. This includes the education and professional training of the engineers and other design professionals involved as well as the thoroughness of the quality control measures of building regulation agencies, such as in the plan review and construction inspection phases. In some instances, the comprehensive protection that the provisions in a building code seem to provide exists mostly on paper. Up until the 1990s, even the most advanced seismic codes

listed only a few specific nonstructural components that needed anchorage and then added a general phrase such as “all other equipment and machinery.” That sounds comprehensive, but in the absence of a well-defined definition of that all-encompassing phrase, it was not particularly meaningful. Another example is the accurate calculation of interstory drift, which in some codes was seemingly covered many decades ago but in practice was not well-implemented in standard practice. The engineer who diligently tried to meet that code requirement had inadequate analytical tools available because of the lack of underlying knowledge of the displacements that would actually occur. Conversely, some engineers incorporated design measures that were only required by the code much later. In the words of George Housner (1986, p. 25), “in some instances, earthquake requirements were adopted in building codes but were not used by architects and engineers. And in other instances earthquake design was done by some engineers before seismic requirements were put in the code.”

## Summary

Model building codes are common around the world, although the consistency with which they are applied throughout a jurisdiction can vary greatly. In New Zealand and Japan, there is a high degree of consistency in how a nationally

standardized set of seismic provisions are adopted and enforced at the local level. In India and the United States, there is greater variation. Seismic provisions in model building codes are usually a combination of prescriptive and performance-based procedures. Seismic provisions in building codes evolved from the earlier building codes that were typically motivated by concern over fire resistance and urban conflagrations. The first seismic regulations governed construction characteristics such as wall material or number of stories, but because they preceded civil engineering developments of the 1800s and 1900s, they lacked quantitative methods for calculating loads and capacities. In the early 1900s, the first seismic codes based on engineering methods were developed in Japan and Italy. The equivalent static elastic lateral force method originated in these codes. By the 1930s, seismic regulations based on the equivalent lateral force method were adopted in New Zealand, the United States, Turkey, India, and Chile. Later, as earthquake engineering research accumulated, as strong motion records were collected, and as powerful and inexpensive computers became available, the response spectrum and the response history methods were added to the modern building code's seismic provisions. A fundamental problem in reducing earthquake risks through adoption of up-to-date building code provisions is enforcement and implementation. While the problem is most prominent in poorer countries, it is also an issue in the most technologically advanced areas of the world. It is to be expected that displacement-based procedures will make further inroads into routine structural system analyses. Also, as seismic isolation technology becomes more mature, it will be accepted by more owners on account of observed benefits.

### Cross-References

- ▶ [Analytic Fragility and Limit States \[P\(EDPI IM\)\]: Nonlinear Dynamic Procedures](#)
- ▶ [Analytic Fragility and Limit States \[P\(EDPI IM\)\]: Nonlinear Static Procedures](#)

- ▶ [Assessment of Existing Structures Using Response History Analysis](#)
- ▶ [Behavior Factor and Ductility](#)
- ▶ [Code-Based Design: Seismic Isolation of Buildings](#)
- ▶ [European Structural Design Codes: Seismic Actions](#)
- ▶ [Global View of Seismic Code and Building Practice Factors](#)
- ▶ [Learning from Earthquake Disasters](#)
- ▶ [Masonry Modeling](#)
- ▶ [Masonry Structures: Overview](#)
- ▶ [Nonlinear Dynamic Seismic Analysis](#)
- ▶ [Performance-Based Design Procedure for Structures with Magneto-Rheological Dampers](#)
- ▶ [Probabilistic Seismic Hazard Models](#)
- ▶ [Reinforced Concrete Structures in Earthquake-Resistant Construction](#)
- ▶ [Response Spectrum Analysis of Structures Subjected to Seismic Actions](#)
- ▶ [School Seismic Safety and Risk Mitigation](#)
- ▶ [Seismic Analysis of Steel–Concrete Composite Buildings: Numerical Modeling](#)
- ▶ [Seismic Analysis of Steel Buildings: Numerical Modeling](#)
- ▶ [Seismic Risk Assessment, Cascading Effects](#)
- ▶ [Seismic Strengthening Strategies for Existing \(Code-Deficient\) Ordinary Structures](#)
- ▶ [Steel Structures](#)
- ▶ [Timber Structures](#)

### References

- Ayres JM, Sun TY (1973) Nonstructural damage. In: The San Fernando, California earthquake of February 9, 1971. National Oceanic and Atmospheric Administration, Washington, DC
- Ayres JM, Sun TY, Brown FR (1973) Nonstructural damage to buildings. In: The great Alaska earthquake of 1964: engineering. National Academy of Sciences, Washington, DC
- Blume JA, Newmark N, Corning LH (1961) Design of multistory reinforced concrete buildings for earthquake motions, Portland Cement Association, Chicago
- Chopra A (2005) Earthquake dynamics of structures: a primer. 2nd ed. Earthquake Engineering Research Institute, Oakland
- Departments of the Army, the Navy, and the Air Force (1973) Seismic design for buildings. Departments of the Army, Navy, and Air Force, Washington, DC



- Gülkan P, Langenbach R (2004) The earthquake resistance of traditional timber and masonry dwellings in Turkey. In: Proceedings, 13th World conference on earthquake engineering, Vancouver, Canada, (Paper no. 2297)
- Housner GW (1986) Historical view of earthquake engineering. In: Proceedings, 8th World conference on earthquake engineering, San Francisco. (The complete set of proceedings for all World Conferences on Earthquake Engineering is freely available at: <http://www.nicee.org/wcee/>)
- Housner GW (1997) George W. Housner, Connections: EERI Oral History Series. Stanley Scott, interviewer. Earthquake Engineering Research Institute, Oakland
- International Association for Earthquake Engineering (IAEE) (1960a, 1963, 1966, 1973, 1976, 1980a, 1980b, 1992, 1996, 2000, 2004). Regulations for seismic design: a world list. International Association for Earthquake Engineering, Tokyo
- Johnson J (2013) Energy methods: what does the future hold? *Structure* 2013:14–15
- Kawasumi H (1951) Measures of earthquake danger and expectancy of maximum intensity throughout Japan as inferred from the seismic activity in historical times. *Bulletin of the Earthquake Research Institute, University of Tokyo*, 21:469–481
- Langenbach R (2003) Crosswalls instead of Shearwalls: a proposed research project for the retrofit of vulnerable reinforced concrete buildings in earthquake areas based on the traditional “hımsı” construction. In: Proceedings of the fifth [Turkish] national conference on earthquake engineering, Istanbul. Available on [www.conservationtech.com](http://www.conservationtech.com)
- Otani S (2008) The dawn of structural earthquake engineering in Japan. In: Proceedings, 14th world conference on earthquake engineering, Beijing
- Reitherman R (2012) Earthquakes and engineers: an international history. ASCE Press, Reston
- SEAOC (1959) Recommended lateral force requirements. Structural Engineers Association of California, Sacramento
- Sorrentino L (2007) The early entrance of dynamics in earthquake engineering: Arturo Danusso’s contribution. *ISET J Earthq Technol* 44(1):1–24
- Sorrentino L (2011) Engineering solutions after the Messina 1908 earthquake. In: *Engineering history and heritage*. Institution of Civil Engineers, London
- Tobriner S (1984a) The history of building codes to the 1920s. In: Proceedings, SEAOC annual convention. Structural Engineers Association of California, Sacramento
- Tobriner S (1984b) A history of reinforced masonry construction designed to resist earthquakes: 1755–1907. *Earthq Spectra* 1(1):125–149
- Trifunac MD (2006) Biot response spectrum. *Soil Dyn Earthq Eng* 26(2006):491–500

---

## Building Damage from Multi-resolution, Object-Based, Classification Techniques

Marco Chini

Luxembourg Institute of Science and Technology (LIST), Environmental Research and Innovation Department (ERIN), Belvaux, Luxembourg

### Synonyms

Earthquake damage mapping; Object-oriented classification; Very high-resolution SAR and optical images

### Introduction

During a seismic event a fast and reliable damage map of the urban areas involved is very important to manage civil protection interventions. Satellite remote sensing data can provide valuable pieces of information in this respect, thanks to their capability to have an instantaneous synoptic view of the scene especially if the seismic event is located in remote regions or the main communication systems are damaged. The major limitation that could hamper the operational use of this source of information is the speed of data collection just after a disastrous event. This is a key point for civil protections that need a fast overview of the epicentral area, quick information on to the extension and distribution of damages and the evaluation of infrastructure conditions such as roads, bridges, focal and crucial buildings and so on. A single satellite can provide access time to a specific site in the order of days as a result the necessity to use any kind of available satellite image and making mandatory data integration approaches to increase the chance of collecting information in near real time (Chini 2009).

Since the end of the twentieth century satellite systems and image-analysis techniques have progressed a lot in the aspects where they can contribute significantly to support the

management of major natural disasters, as well as humanitarian crisis situations. Compared to 15 years ago the availability of satellite imagery, amount, timeliness and the capability to cover a certain crisis situation or disaster event with high degree of detail have all improved substantially. There are several factors which have led to this. First of all ground pixel spacing of civil Earth Observation (EO) systems has developed to the meter domain (or less) for optical and radar systems, such as synthetic aperture radar (SAR) (Voigt et al. 2007). Indeed on September 24 1999 the commercial EO satellite IKONOS was launched, the first able to collect openly available high-resolution imageries that were both panchromatic and multispectral with a spatial resolution of 1 and 4 m, respectively. Two years later, on October 18, 2001, another important step forward was made with the launch of one more high-resolution commercial EO satellite, QuickBird, with an increased spatial resolution up to 0.6 m for the panchromatic sensor and 2.4 m for the multispectral one. The first earthquake where this kind of data proved its usefulness in conjunction with automatic image-analysis techniques was the one that struck the city of Bam (Iran) in 2003, provoking a lot of damage to man-made structures and causing the death of many people (Yamazaki et al. 2005; Gusella et al. 2005; Stramondo et al. 2006; Gamba et al. 2007; Chini et al. 2008b; Chini et al. 2009; Bignami et al. 2011). Concerning SAR satellite sensors, the spatial resolution breakthrough arrived in 2007 with the launch of the first two satellites of the two X-band satellite constellations, COSMO-SkyMed and TerraSAR-X, on June 8 and on June 15, 2007, respectively, both having the capability to acquire images in the so-called SpotLight image mode with a spatial resolution of 1 m. TerraSAR-X mission is composed of two satellites, the second one was launched on June 21, 2010, while COSMO-SkyMed has four satellites, the fourth one launched on November 5, 2010. The fact that they are constellations has reduced the site access time down to two and a half days with TerraSAR-X and to 12 h with COSMO-SkyMed. This latter issue is the second

important factor that makes satellite data able to face and provide useful information during the crises phase soon after an earthquake.

Both optical and SAR data have characteristics to be used as a source of information to provide a damage map after an earthquake (Yonezawa and Takeuchi 2001; Matsuoka and Yamazaki 2004; Chini et al. 2008a; Chini et al. 2013), with particular attention to very high-resolution data, which has the potential to monitor wide areas, but at the same time giving information on single structures present in the scene (Stramondo et al. 2008; Turker and Sumer 2008; Brunner et al. 2010; Chini et al. 2011; Dell'Acqua et al. 2011; Ferro et al. 2013). The huge amount of information carried by these kinds of data can hamper the visual inspection, which is time consuming during a crisis phase, fostering the implementation of more automatic approaches.

## Methodology

The automatic or semiautomatic classification of remote sensing data is a tool to help understand and monitor a large variety of scenarios, converting them into tangible data, which can be utilized in conjunction with other data sources to provide crucial and accurate information. Even if metric or submetric resolution images provide new opportunities in the damage mapping field, new problems arise at the same time in automatic classification procedures. Indeed, the aim of image classification analysis is to extract information and display the results in a simple and effective way for possible further studies. In metric resolution images a single pixel represents a small area ( $0.5 \div 10 \text{ m}^2$ ) of the acquired scene and is usually smaller than the size of the objects of interest. Hence the information of a single pixel is strongly linked to the information carried by its neighbors, which are part of the same object, pointing out the necessity to perform an object-oriented analysis, although the measurable statistics typically exploited for classification purposes are necessarily pixel

based (Blaschke 2010). This aspect is very interesting, because it makes possible to focus on a single object, for example, a building or also other man-made structure, having the advantage of a valuable amount of pixels to characterize the object itself.

Object-based techniques recognize that important semantic information is not always represented in single pixels but in meaningful image objects and in their contextual relations. For example, it is more likely that a pixel adjacent to a private garden should be classified as a house, road, or private garden rather than as a forest. Usually, object-based classification comprises two steps: the image segmentation and the object classification. Image segmentation subdivides the image into groups of contiguous pixels called objects or segments that correspond to meaningful features or targets in the field (Blaschke 2010). The images are segmented into homogeneous objects based on the spectral information and local patterns or textural information that are included in groups of neighboring pixels. As a result, the object-based classifications can consider a wide range of variables such as mean reflectance, texture, shape and size of objects and can potentially produce more accurate and detailed maps than conventional classification strategies (Mathieu et al. 2007; Blaschke 2010; Chini et al. 2014).

All algorithms exploiting metric resolution data for damage mapping purposes have to deal with object-oriented approaches even if the final target is not the object itself, but maybe just a classification useful for restricting the analysis and the statistics to classes we are interested in. Such an example could be a change detection approach to identify a collapsed building using one pre-earthquake image and one post-earthquake image by a threshold approach. At this resolution many regions will be affected by changes even those not relevant for damage purposes. Thus to fix the threshold used to identify damaged buildings (pixels that have changed their radiometric values because of the earthquake) we should restrict the analysis to objects of interest such as buildings (Chini et al. 2009).

It is worth recalling the optical and SAR image properties that are usually used for damage detection purposes, highlighting characteristics that are relevant to damage mapping analysis such as the physical properties of the measured signal and the spatial resolution that can have an impact on the final products. Basically, the process for forming a SAR image is different from that used for an optical image for two main aspects: the physical properties of the imaged targets that contribute to the measured signal and the signal processing steps used to create the image. Optical sensors measure the radiometric properties of reflected sunlight in spectrally distinct regions of the visual and near-infrared spectrum or integrated in a single panchromatic band. The material properties of objects, the illumination conditions of the scene and the sensor perspective determine the radiometric and geometric appearance of distinct targets in optical imagery. The SAR system is an active sensor and measures the backscatter of a transmitted signal, typically in a narrow microwave frequency band and sampled in the range direction, i.e., the line of sight (LOS) from SAR sensor to target. Backscattering is primarily determined by the geometry and dielectric properties of an object and the transmit/receive configuration of the SAR sensor (Brunner et al. 2010).

Concerning optical images it is easier for the reader to grasp how different spatial resolutions make buildings appear and more in general, cities, where if the resolution is higher, the amount of detail composing land use classes of interest will be greater. Indeed, in high-resolution optical images the radiance of each pixel is not directly related nor can be considered representative of the class it belongs to. However, many studies are able to demonstrate that the advantage of being able to aggregate pixels to an object and then address object characteristics, is that it can discern between different kinds of buildings and different kinds of asphalted areas such as roads or parking lots, turning all of this augmented complexity of understanding into an information luxury (Pacifi et al. 2009). Such an example could be the shadow from a building, which has at this resolution a clear signature in the image,

giving us information about the building height, which could be also an important source of information for damage detection purposes. As a matter of fact, Turker and Sumer (2008) detected damaged buildings from the big earthquake in Turkey in 1999, applying a watershed segmentation on a post-event optical image utilizing the relationship between the buildings and their shadows, labeling 80 % of buildings correctly as either damaged or undamaged. Another example of how object-oriented approaches are useful is presented in Gusella et al. (2005) that quantified the number of collapsed buildings of the Bam earthquake in 2003, starting from the inventory of buildings as objects in QuickBird satellite imagery taken before the event.

Pertaining to SAR data an in depth description of how a building appears is necessary. For this purpose, it is useful to describe how radar returns from different parts of the building are mapped on the SAR image due to the fact that they reach the receiver at different times (Kropatsch and Strobl 1990; Franceschetti et al. 2002; Franceschetti et al. 2003; Guida et al. 2008; Guida et al. 2010). Given an isolated building on ground and proceeding in the SAR image with a constant azimuth from near to far range, we can identify four main singular contributions:

1. A bright stripe corresponding to a mixture between the backscattering from the ground, facade, and roof, which is a typical example of layover in a SAR image. Layover is called “radar mapping,” where different object points having the same time and same range are mapped into one image point, i.e., more than one point on the Earth’s surface are mapped into one image point (many to one mapping). SAR mapping is mainly an integration of reflected signals having the same Doppler frequency (azimuth or along-track measurement) and same distance (range or across-track measurement) (Kropatsch and Strobl 1990).
2. A very bright line corresponding to facade-ground and ground-facade double-bounce scattering, because double-bounce ray paths all have the same length, equal to

the distance between SAR sensor and the facade base (all different scattering points are positioned at a unique distance, corner reflector).

3. The contribution from the roof that could be of two types: (a) flat roof, a unique gray area corresponding to backscattering from the roof, and (b) gamble roof, the roof has a different scattering signature with respect to a flat one. Basically it is different due to the presence of a second bright scattering feature, which is closer to the sensor than to the double-bounce contribution (Brunner et al. 2010). This behavior concerns only the direct backscattering from the part of the roof that is oriented toward the sensor.
4. A dark area corresponding to the SAR building shadow which should be not confused with the shadow concept in an optical image. Shadow in radar imagery is called the region where an object point is not reached by any radar beam. Such object points produce a “zero” signal in the image. Therefore, shadow regions appear as dark areas corrupted by noise (Kropatsch and Strobl 1990)

Of course this is a simplistic schematization of the phenomenon; other parameters also play an important role in the backscattering values of the four building parts such as geometric parameters (height, length, and width of the building and the roughness of the ground) and the electromagnetic parameters (dielectric constants of facade, roof, and ground). The four types of building responses with a distinct backscattering values can be detected as separate objects if the resolution is higher than the dimension of a building itself, while this distinction is not possible if the SAR resolution is lower than the buildings being identified. As a matter of fact an urban area imaged by a SAR sensor with a resolution in the order of tens of meters appears uniformly brighter than other land cover classes since the double-bounce effects are the dominant scattering component in the SAR resolution cell (i.e., the image pixel), that one characterizing the backscattering for such scenario. Whilst in metric resolution SAR sensors such as COSMO-SkyMed and

TerraSAR-X, we still have very bright values in the city, principally double-bounce pixels, but we have gray and dark regions as well, roofs and shadows respectively, that are well identified and with a remarkable spatial extension. On the contrary big uniform surfaces, such as bare soil or asphalted industrial areas, appear the same in both high- and low-resolution SAR since their extension is bigger than both sensor resolutions. Change detection approaches with lower-resolution SAR stem from the concept that the double-bounce effect fails when a building collapses (which is the dominating scattering mechanism in the resolution cell); thus in the comparison between two images, one acquired before and one after the seismic event, a decrease in the backscattering value is expected (Yonezawa and Takeuchi 2001; Matsuoka and Yamazaki 2004; Stramondo et al. 2006). It is a different case with the high-resolution SAR data because we can see a decrease of the backscattering for the pixel where the double-bounce is located, but also an increase in the roof part, since rubble can cause an increase of the backscattering as compared to a smooth roof. Furthermore, where the shadow is present in the pre-event image, some changes are expected in the post-event image, depending on the structures shadowed before the collapse.

As it appears from the aforementioned description of the optical and SAR data, the high resolution has drastically changed the semantic of objects as they were known so far. Indeed the lower resolution caused them to appear differently than the metric or submetric spatial resolution, thus the necessity to introduce new characteristic features and a new vocabulary. For this reason the object-oriented approach seems more promising than per pixel, since with submetric resolution image without having a well-defined semantic for identifying classes of interest we can just identify primitive objects, which are different from objects of interest. Indeed only objects of interest match real-world objects, e.g., the building footprints. Primitive objects are usually the necessary intermediate step before objects of interest can be found by a segmentation and classification process, having

as a smallest image object the pixel. Of course an object can be defined in different ways, depending on our scope and at which scale of detail we want to provide the information. An object can be a building or a neighborhood in a city with a particular type of structure and both of them can give us important information in terms of damage mapping. The following are some examples of applied object-oriented methodologies in real scenario, where very high-resolution optical and SAR data have been used for the seismic events that occurred in Bam (Iran) in 2003 and in the city of L'Aquila (Italy) in 2009.

### Case Studies

On December 26, 2003, the southeastern region of Iran was hit by a 6.5 moment magnitude (Mw) earthquake whose epicenter was located very close to the city of Bam. The event had a tremendous impact all over the world, due to a heavy loss of lives, injuries, and destruction; the earthquake caused the death of more than 26,000 residents and injured another 30,000. Additionally, the city of Bam was a UNESCO World Heritage Site and as such it plays an important historical role. The Bam earthquake was the worst seismic event in recent Iranian history. The damage was concentrated in a relatively small area around Bam. Ninety percent of the structures in the city of Bam were left more or less heavily damaged or totally collapsed. In particular, the main historical and traditional adobe buildings collapsed. Contemporary houses demonstrated better resistance to earthquake shake, even though many collapsed due to poor construction practices and the presence of weak stories in the buildings (EERI 2004; Chini et al. 2009). As already highlighted this event was the first one to be imaged by an optical sensor with a submetric spatial resolution (60 cm) such as QuickBird, so for this event we have many papers where the damage mapping was treated making use of these new satellite sensors. Within these, three publications have been selected to show the different scales of products that can be provided and the synergy between the optical and



SAR sensors, but not only and also the impact that the very high resolution can have in the lower-resolution products.

In Chini et al. (2008b) pre- and post-earthquake QuickBird panchromatic images have been used to show the capability of this data to map damage at building scale by means of segmentation approach based on the application of mathematical morphology operators (Pesaresi and Benediktsson 2001; Soille 2003). In this article, a classification procedure was applied to the two panchromatic available data, one taken before (September 30, 2003) and one after (January 3, 2004) the seismic event. The buildings' extraction from one single panchromatic image is not an easy task. Many objects in the imaged scene can be confused because they have very close radiance values: cars with some buildings, shadow with some asphalt roads, soil with some kinds of roofs and so on. Due to the lack of multispectral data with a resolution of 60 cm, a contextual analysis is needed to extract geometric information of objects/classes within the images. Morphological profiles from the original panchromatic images taken before and after the earthquake have been carried out in order to classify all the buildings in the scene. The classification was done so as to avoid false alarms in the change detection process caused by shadow or other temporary objects like cars or recovery tents. For this purpose, the open and close morphological operators have been applied and the derived profiles have been used as inputs to an unsupervised classifier in order to extract the entire map of buildings before and after the earthquake. Hence, after the classification process, each single building has been recognized and then labeled. Finally, the damage estimation can be computed, by comparing the pixel belonging to the same building before and after the seismic event. The percentage of the damaged pixels with respect to the total for each building is an estimation of the damage level (ratio between the number of pixels after and before the earthquake forming the single object). The higher the number of damage pixels, the higher damage level of the buildings. The map deals with a classification criteria where each building of Bam city has

been labeled as belonging to one of three possible damage levels: light or no damage, medium and heavy. Two thresholds have been set in order to identify the three classes. The satellite-based damage map has been compared with a map derived from ground survey, provided by Geological Survey of Iran, which reports the map of collapse ratio. This latter concerns the percentage of completely collapsed buildings with respect to the total number of buildings within a city block. It is worth noting that the information about damage from field survey was given at district scale, while the results from object-oriented approach provided information at building scale. Although the different scales of the maps did not allow a direct comparison, a qualitative accuracy evaluation was done counting the percentage of the three classes from remote sensing data in each regional class obtained from ground survey. It is interesting to highlight that the percentage of heavy damaged buildings (from the object-oriented analysis) increased with the increase of ground survey damage degree.

In Chini et al. (2008b) the semiautomatic classification approach aimed to identify completely or partially collapsed buildings based on the optical satellite images vocabulary; it was basically a change detection approach at building scale, which evaluated how much the radiance value for all pixels of each building changed as an effect of the earthquake. A step forward was attempted in the next article we will describe (Bignami et al. 2011) where an analysis was performed on the sensitivity of textural features at object scale with respect to the damage levels according to the European Macroseismic Scale 1998 (EMS98). Textural features were clearly demonstrated to be a method to overcome the lack of spectral resolution for classification purposes. Indeed texture analysis plays an increasingly important role in digital image processing and interpretation, especially for very high-resolution data (Haralick et al. 1973; Haralick 1979; Pacifici et al. 2009). This is mainly due to supplementary information about image properties it can provide. Such information can be fruitfully exploited for change detection applications as well. In Bignami et al. (2011), the analysis was



focused on the sensitivity of some textural features for change detection purposes; in particular it was focused on earthquake damage mapping. This approach was preferred in order to give information strictly related to each building and to mitigate false alarms weighting per-pixel classification error. Instead of the usual textural features extraction by considering the co-occurrence matrix on a moving window, the proposed method was based on the calculation of textural parameters at object scale. Indeed, the co-occurrence matrix is evaluated by taking into account all the pixels belonging to a single object, i.e., the building, and considering a shift of one pixel in the horizontal and vertical directions. In this way for each building a co-occurrence matrix was obtained. The algorithm makes use of the same dataset as Chini et al. (2008b) and also of some outcomes of the algorithm such as the buildings map, where each building/object was singled out. Stemming from this building map, the textural parameters for each specific object is derived, overcoming the dependency from the window size, which makes the analysis test case dependent. Following the formulation of the textural parameters described in Haralick et al. (1973) and Haralick (1979), for each one of the selected building in the two images, pre- and post-earthquake, four different object textural parameters have been calculated, such as contrast, dissimilarity, homogeneity and entropy. In order to investigate the sensitivity of these parameters to damage degree from EMS98 damage scale, some buildings were selected by the ground truth map described in Hisada and Shibaya (2004), where some buildings, located around eight strong motion stations, were surveyed and classified. The EMS98 classifies five damage levels: G1 (negligible to slight), G2 (moderate), G3 (substantial to heavy), G4 (very heavy) and G5 (destruction). The G1 level can also include the non-damage class, because the difference between G1 and no damaged building cannot be appreciated using this kind of satellite data. Once the four object textural parameters have been derived on both pre-seismic and post-seismic data, the difference between post- and

pre-seismic at object scale has been computed in order to analyze their sensitivity to the damage levels for those building labeled by ground survey. A total of 367 buildings were accounted for in the sensitivity analysis. For each object textural feature the mean value within a damage class from the ground survey was evaluated and the difference between post-seismic and pre-seismic features was calculated. These values have been plotted in respect to the five ground survey damage grade. By observing the plots, some evidence of sensitivity with respect to damage levels are observed. A positive trend in the difference of textural features has been obtained for the contrast, the dissimilarity and the entropy, while a negative trend is visible for the homogeneity. The trends reflect the expected behavior of these textural parameters. In fact, as the damage level of an object increases, the numbers of pixels within the object, which appear scattered, increase. From a textural point of view, the homogeneity of the object should decrease, i.e., the more scattered pixels are, the less homogeneous is the object. On the contrary, the contrast, the dissimilarity, and the entropy increase with the increasing number of scattered pixels. A comparison with textural parameter extracted by using a moving window with a fixed size has also been carried out, highlighting that the trends were not as expected. This work showed that to better understand some discrepancies present between satellite information and ground survey damage grade, an object-by-object analysis is needed. It was stated that the damage level assigned to an object should be validated also from the remote sensing point of view because sometimes the damage level cannot be identified from satellite data. A typical false alarm case is the pancake effect which occurs when severe damage affects a building (G3 and G4 levels), or sometimes it collapses (G5 level), but the roof remains almost undamaged, preventing its identification from space images.

The Bam earthquake was also studied in Chini et al. (2009), where the integration between medium resolution SAR data was analyzed, from 20 m resolution C-band sensor onboard of

Envisat satellite mission and very high-resolution optical data, with the aim of producing damage maps at district scale with three different levels of damage. In this article additional parameters, namely, the InSAR complex coherence and the intensity (or backscattering) correlation, have been computed, since couples of pre- and post-seismic interferometric images were available (two images before and one or two after the event). Both parameters can be derived by combining the pre-seismic pair, the post-seismic, and the coseismic (i.e., one pre-seismic and one post-seismic image) ones. Note that these two features contain slightly different information concerning changes in the scene. The complex coherence is primarily influenced by the phase difference between radar returns, which is a distinctive parameter measured by a coherent sensor like SAR. It is particularly related to the spatial arrangement of the scatterers within the pixel and, thus, to their possible displacements. Conversely, the intensity correlation is more related to changes in the magnitude of the radar return. Unfortunately, for this event, SAR interferometric image pairs have very high values of the perpendicular baseline, around 500 m for both pairs and the resulting high spatial decorrelation prevents their employment from detecting damage levels through the InSAR phase coherence, which has almost the same values both in damaged and undamaged areas when the baseline is too large (Zebker and Villasenor 1992). Concerning the use of the backscattering correlation as an indicator of surface changes, the approach is founded on the idea that the correlation coefficient is high when two images are similar, while it becomes low when changes have occurred in the surface target. Thus, in the latter case, a decrease of correlation of coseismic images is expected to be relative to pre-seismic ones and this phenomenon is expected to increase with the increase of damaged buildings on the ground. The difference between the pre- and coseismic intensity correlations has been averaged within areas of homogeneous damage levels provided from a ground survey map, and it is clearly shown how this difference increases

with the increase of damage level (Yonezawa and Takeuchi 2001; Stramondo et al. 2006). In addition to Envisat SAR data, the information extracted from a high-resolution optical QuickBird image has been used, by extracting the building maps before the earthquake carried out with the adoption of object classification approaches. The building map was used as a mask to restrict the SAR intensity correlation change detection only to built-up areas, in order to reduce possible false alarms. Indeed, in Bam City, there were a lot of vegetated areas, which could affect the value of the correlation. The intensity correlation difference showed an increase of the dynamic range of about 25 % with respect to the non-masked data, using the information on buildings from optical data.

On April 6, 2009, a  $M_w = 6.3$  earthquake hit a wide portion of the Abruzzi region in Italy, with the epicenter located 4 km southwest of the city of L'Aquila, whereas the highest damages occurred about 8 km to the southeast. In L'Aquila and in the neighboring villages, the earthquake caused the collapse or irreparable damage to over 15,000 buildings, killing 308 people and causing the relocation of over 65,000 (Stramondo et al. 2011). For this event very high-resolution SAR images, acquired in SpotLight mode (1 m per pixel on ground) from the X-band COSMO-SkyMed satellite mission, were available. The very high resolution images from optical sensors such as QuickBird and IKONOS were available as well. It is interesting to see how information has been exploited in the work of Dell'Acqua et al. (2011), for estimating the damage at districts levels from a post-event SAR image and the fusion with optical images for increasing the accuracy. It is commonly acknowledged that due to speckle effects, single-pixel classification of SAR images leads to unsatisfactory results, and this seems to hold true also when damage assessment is concerned. Satisfying results may be achieved if the damage is assessed at a block level, somehow averaging the unreliable results of pixel-wise comparing pre- and post-event images due to speckle noise. In the Dell'Acqua et al. (2011) article, damage was considered at

pixel scale, in optical data and at block scale, in SAR data, separately. Indeed, the pixel-based approach by using optical data provided useful information on the discrimination between damaged or non-damaged areas. Even though no further classification with respect to damage levels can be retrieved, the information derived from optical imagery can be effective where apparently very high-resolution SAR data is least with the proposed method, and it could be probably the reason why fusion of optical and SAR data in this method is promising. Indeed in this work the SAR textures, which were the features used as damage indicator, were somehow correlated to low damage levels (or affected by other factors than damage), whereas optical data were more suitable to distinguish between damage and non-damage classes. Definitely, the SAR texture was more effective to distinguish between two different levels of damage, in the regions that were identified as damaged by optical data. Some important issues remained still open; such an example could be finding suitable threshold levels for classification in future cases, although significant links between satellite-derived indicators and damage levels have been discovered. It seems that some texture maps computed on SAR data can provide an estimate of damage levels, only if independent information concerning presence or absence of damage in a given block would be available. It is evident from the results that further studies are required and they should be aimed at finding sufficiently independent statistics, extracted from SAR data, which may possibly be linked to presence or absence of damage.

## Summary

This entry highlights the characteristics of very high-resolution optical and SAR images that are pertinent for earthquake damage mapping purposes. Automatic or semiautomatic classification algorithms, which make use of this kind of data, have been described as well. Particular attention has been paid to object-based classification approaches, which are more suitable to deal with metric or submetric resolution data.

Relevant case studies, where object-based damage mapping approaches have been considered, are here presented.

**Acknowledgment** The author would like to thank R. De Meo for reviewing this manuscript.

## Cross-References

- ▶ [Building Disaster Resiliency Through Disaster Risk Management Master Planning](#)
- ▶ [Building Monitoring Using a Ground-Based Radar](#)
- ▶ [Damage to Ancient Buildings from Earthquakes](#)
- ▶ [Damage to Buildings: Modeling](#)
- ▶ [Damage to Infrastructure: Modeling](#)
- ▶ [Earthquake Damage Assessment from VHR Data: Case Studies](#)
- ▶ [Earthquake Disaster Recovery: Leadership and Governance](#)
- ▶ [Estimation of Potential Seismic Damage in Urban Areas](#)
- ▶ [Features Extraction from Satellite Data](#)
- ▶ [Hyperspectral Data in Urban Areas](#)
- ▶ [Remote Sensing in Seismology: An Overview](#)
- ▶ [Resilience to Earthquake Disasters](#)
- ▶ [SAR Images, Interpretation of](#)
- ▶ [Seismic Collapse Assessment](#)
- ▶ [Seismic Loss Assessment](#)
- ▶ [System and Damage Identification of Civil Structures](#)
- ▶ [Urban Change Monitoring: Multi-temporal SAR Images](#)

## References

- Bignami C, Chini M, Stramondo S, Pierdicca N, Emery WJ (2011) Objects textural features sensitivity for earthquake damage mapping. In: IEEE GRSS and ISPRS Joint Urban Remote Sensing Event – JURSE 2011 proceedings, pp 333–336
- Blaschke T (2010) Object based image analysis for remote sensing. *ISPRS J Photogramm* 65:2–16
- Brunner D, Lemoine G, Bruzzone L (2010) Earthquake damage assessment of buildings using VHR optical and SAR imagery. *IEEE Trans Geosci Remote* 48:2403–2420

- Chini M (2009) Earthquake damage mapping techniques using SAR and optical remote sensing satellite data. In: Jedlovec G (ed) *Advances in geoscience and remote sensing*. InTech, Vukovar, pp 269–278
- Chini M, Bignami C, Stramondo S, Pierdicca N (2008a) Uplift and subsidence due to the December 26th, 2004, Indonesian earthquake and tsunami detected by SAR data. *Int J Remote Sens* 29:3891–3910
- Chini M, Bignami C, Emery WJ, Pierdicca N, Stramondo S (2008b) QuickBird panchromatic images for mapping damages at building scale caused by the 2003 Bam earthquake. In: 2008 I.E. International Geoscience and Remote Sensing Symposium (IGARSS) – proceedings, vol 2, Issue 1, II1029–II1031
- Chini M, Pierdicca N, Emery WJ (2009) Exploiting SAR and VHR optical images to quantify damage caused by the 2003 Bam earthquake. *IEEE Trans Geosci* 47:145–152
- Chini M, Cinti FR, Stramondo S (2011) Co-seismic surface effects from very high resolution panchromatic images: the case of the 2005 Kashmir (Pakistan) earthquake. *Nat Hazard Earth Syst Sci* 11:931–943
- Chini M, Piscini A, Cinti FR, Amici S, Nappi R, De Martini PM (2013) The 2011 Tohoku-Oki (Japan) tsunami inundation and liquefaction investigated by optical, thermal and SAR data. *IEEE Geosci Remote Sens Lett* 10:347–351
- Chini M, Chiancone A, Stramondo S (2014) Scale object selection (SOS) through a hierarchical segmentation by a multi-spectral per-pixel classification. *Pattern Recognit Lett* 49:214–223
- Dell'Acqua F, Bignami C, Chini M, Lisini G, Polli D, Stramondo S (2011) Earthquake rapid mapping by satellite remote sensing data: L'Aquila April 6th, 2009 event. *IEEE J Selected Top Appl Earth Observations Remote Sens* 4:935–943
- Earthquake Engineering Research Institute – EERI (2004) Preliminary observations on the Bam, Iran, earthquake of December 26, 2003. EERI Special Earthquake Report, [Online]. Available at [http://www.eeri.org/lfe/pdf/iran\\_bam\\_eeri\\_preliminary\\_report.pdf](http://www.eeri.org/lfe/pdf/iran_bam_eeri_preliminary_report.pdf)
- Ferro A, Brunner D, Bruzzone L (2013) Automatic detection and reconstruction of building radar footprints from single VHR SAR images. *IEEE Tran Geosci Remote Sens* 51:935–952
- Franceschetti G, Iodice A, Riccio D (2002) A canonical problem in electromagnetic backscattering from buildings. *IEEE Trans Geosci Remote Sens* 40:1787–1801
- Franceschetti G, Iodice A, Riccio D, Ruello G (2003) SAR raw signal simulation for urban structures. *IEEE Trans Geosci Remote Sens* 41:1986–1995
- Gamba P, Dell'Acqua F, Trianni G (2007) Rapid damage detection in the Bam area using multitemporal SAR and exploiting ancillary data. *IEEE Trans Geosci Remote Sens* 45:1582–1589
- Guida R, Iodice A, Riccio D, Stilla U (2008) Model-based interpretation of high-resolution SAR images of buildings. *IEEE J Selected Top Appl Earth Observations Remote Sens* 1:107–119
- Guida R, Iodice A, Riccio D (2010) Height retrieval of isolated buildings from single high-resolution SAR images. *IEEE Trans Geosci Remote Sens* 48:2967–2979
- Gusella L, Adams BJ, Bitelli G, Huyck CK, Mognol A (2005) Object-oriented image understanding and post-earthquake damage assessment for the 2003 Bam, Iran, earthquake. *Earthq Spectra* 21(S1):225–238
- Haralick RM (1979) Statistical and structural approaches to texture. *Proc IEEE* 67:786–804
- Haralick RM, Shanmuga K, Dinstein IH (1973) Textural features for image classification. *IEEE Trans Syst Man Cybern* 3:610–621
- Hisada Y, Shibaya A (2004) Building damage and seismic intensity in Bam city from the 2003 Iran, Bam, earthquake. *Bull Earthquake Res Inst Univ Tokyo* 79:81–93
- Kropatsch WG, Strobl D (1990) The generation of SAR layover and shadow maps from digital elevation models. *IEEE Trans Geosci Remote Sens* 28:98–107
- Mathieu R, Aryal J, Chong AK (2007) Object-based classification of Ikonos imagery for mapping large-scale vegetation communities in urban areas. *Sensors* 7:2860–2880
- Matsuoka M, Yamazaki F (2004) Use of satellite SAR intensity imagery for detecting building areas damaged due to earthquakes. *Earthq Spectra* 20(975):994
- Pacifici C, Chini M, Emery WJ (2009) A neural network approach using multi-scale textural metrics from very high resolution panchromatic imagery for urban land-use classification. *Remote Sens Environ* 113:1276–1292
- Pesaresi M, Benediktsson JA (2001) A new approach for the morphological segmentation of high-resolution satellite imagery. *Trans Geosci Remote Sens* 39:309–320
- Soille P (2003) *Morphological image analysis – principles and applications*. 2nd edn. Springer, Berlin
- Stramondo S, Bignami C, Chini M, Pierdicca N, Tertulliani A (2006) Satellite radar and optical remote sensing for earthquake damage detection: results from different case studies. *Int J Remote Sens* 27:4433–4447
- Stramondo S, Chini M, Salvi S, Bignami C, Zoffoli S, Boschi E (2008) Ground deformation imagery of the may Sichuan earthquake. *EOS Trans Am Geophys Union* 89:341–342
- Stramondo S, Chini M, Bignami C, Salvi S, Atzori S (2011) X- C- L-Band DInSAR investigation of the April 6th, 2009, Abruzzi earthquake. *IEEE Geosci Remote Sens Lett* 8:49–53
- Turker M, Sumer E (2008) Building-based damage detection due to earthquake using the watershed segmentation of the post-event aerial images. *Int J Remote Sens* 29(11):3073–3089
- Voigt S, Kemper T, Riedlinger T, Kiefl R, Scholte K, Mehl H (2007) Satellite image analysis for disaster

- and crisis-management support. *IEEE Trans Geosci Remote Sens* 45:1520–1528
- Yamazaki F, Yano Y, Matsuoka M (2005) Visual damage interpretation of buildings in Bam city using QuickBird images following the 2003 Bam, Iran, earthquake. *Earthq Spectra* 21(S1):329–336
- Yonezawa C, Takeuchi S (2001) Decorrelation of SAR data by urban damage caused by the 1995 Hoyooken-Nanbu earthquake. *Int J Remote Sens* 22:1585–1600
- Zebker HA, Villasenor J (1992) Decorrelation in interferometric radar echoes. *IEEE Trans Geosci Remote Sens* 30:950–959

## Building Disaster Resiliency Through Disaster Risk Management Master Planning

Fouad Bendimerad<sup>1</sup>, Jerome Zayas<sup>1</sup>,  
Bijan Khazai<sup>2</sup> and Moses Kent Borinaga<sup>1</sup>  
<sup>1</sup>Earthquakes and Megacities Initiative, Quezon City, Philippines  
<sup>2</sup>Karlsruhe Institute of Technology, Center for Disaster Management and Risk Reduction Technology (CEDIM), Karlsruhe, Germany

### Introduction

Since impacts of disasters are most felt at the local level, they require proactive action and intervention directly from local authorities and affected communities. However, the extent of impacts varies from one area to another. Highly urbanized areas are typically more vulnerable to natural hazards as a result of environmental and socioeconomic stresses brought about by rapid and often unplanned urbanization. Because of the concentration of population, infrastructure, and resources in urban areas, they stand to lose more in the event of actual disaster. Thus, it is becoming increasingly imperative for city government authorities and local actors in urban areas to develop and enhance their capacity to manage disaster risks in order to protect their development.

Cities have largely and chronically been neglected by national governments and international organizations in terms of dealing with risk

and its contributory factors such as poverty and rapid urbanization (Khazai and Bendimerad 2008). Contrary to popular misconception of local authorities in urban areas having the requisite capacity to address risk on their own, most cities, particularly in the developing world, have actually been ineffective in managing their risk, which remains high and is continuously rising. The relative negligence of disaster risk management as a local responsibility is also exacerbated by the fact that many local authorities are already overburdened by their presently mandated responsibilities.

Disaster risk management (DRM) is defined by the United Nations International Strategy for Disaster Reduction (UN-ISDR) as “*the systematic process of using administrative directives, organizations, and operational skills and capacities to implement strategies, policies and improved coping capacities in order to lessen the adverse impacts of hazards and the possibility of disaster*” (UN-ISDR 2009). Current approaches to managing disaster risk are often characterized by (a) the prevalence of a response or humanitarian perspective rather than a development perspective, (b) the lack of cross-disciplinary and cross-sectoral processes demanded by a more integrated mainstreaming approach that captures the parameters of risk that are relevant to each sector, and (c) the absence of policymaking processes based on consensus building and effective engagement of the concerned stakeholders. These factors are correlated, calling for a holistic approach to urban resilience, one that integrates disaster risk reduction (DRR) with developmental policy and planning, delivery of core services, natural and environmental resource management, and poverty reduction. A methodology that could define needs to be met and why and how to do it is necessary to generate support for allocating resources to disaster risk reduction, especially in view of overwhelming demands from citizens for vital services and to meet day-to-day needs.

The key to manage disaster risks in urban areas without draining the resources of local authorities is to mainstream DRM in the daily functions and services of the city. By integrating



risk reduction parameters in planning processes, such as land use and urban planning, public works, delivery of core services, and emergency response planning, among others, the task of managing disaster risks becomes more attainable. However, mainstreaming DRM in the operations of urban local authorities is easier said than done. Disaster risk management in general is a new field of practice for most city officials and personnel, not to mention that disaster risk reduction implementation itself is complex. It takes time, effort, training, and, most importantly, scientifically designed methods and tools in order to effectively and fully assimilate disaster risk reduction in city functions and ongoing operations. DRM mainstreaming is also closely in line with the commitment of countries to several international conventions and agreements such as the Hyogo Framework for Action for 2005–2015 (HFA) and the UN Millennium Development Goals (MDG), to name a few.

This entry further elaborates the concept of DRM mainstreaming, shows examples of tools that are used for mainstreaming, and provides a case study of an actual application of DRM mainstreaming using the Disaster Risk Management Master Planning (DRMMP) process developed by the Earthquake and Megacities Initiative (EMI).

## The Concept of DRM Mainstreaming

Mainstreaming is a core concept of DRM but is seldom understood. Mainstreaming is essential to achieving effectiveness in a DRM structure. It is about defining and distributing roles and responsibilities between national and local authorities and civil society in a way that would result in greater outcome for lower amount of resources. It is about determining the parameters of risk that are most relevant to each sector and function of government and making these parameters an integral part of the governance and management of urban life. An organization that has accomplished mainstreaming has effectively integrated the practice of risk management within its governance, its functions, and operations.

Mainstreaming requires a deliberate and well-founded strategy and consistent applications of policies that strive to pinpoint and enforce roles and responsibilities. Inherent in this process is a policy of decentralization of authority and accountability. The current practice shows an overemphasis on centralization at the national level of all DRM functions. The reasons are twofold:

- (a) Lack of decentralization and coordination structures. The DRM practice is an emerging function of government; sublevel government institutional structure and coordination mechanisms have yet to be devised and put in place.
- (b) Lack of capacity of local authorities. The central authorities of the government are reluctant to provide local government with the authority for DRM out of prudence.

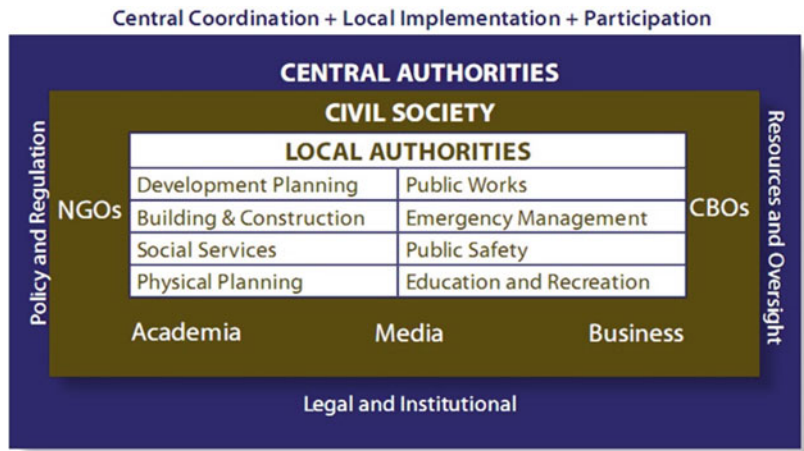
Despite these limitations, a distribution of roles and responsibilities between the various levels of government is critical to achieve mainstreaming. One approach to establish a mainstreaming strategy is to follow the scheme shown in Fig. 1 (EMI 2009). The three encompassing boxes provide a descriptive assignment of roles and responsibilities. Fundamentally, the model represented in the figure indicates that, following other more conventional functions of government, DRM implementation has three principles of mainstreaming: central coordination, local implementation, and participation (Bendimerad and Zayas 2015).

- *Local implementation:* Implementation should as much as possible be delegated to local authorities and local actors. Local authorities cannot mainstream DRM without a clear authority and resources.
- *Central coordination:* The role of the central authorities should focus on establishing policy, enacting regulation, putting in place control processes, allocating resources, and exercising oversight.
- *Participation:* Government (central and local) must open the door to the participation of civil



**Building Disaster Resiliency Through Disaster Risk Management Master Planning,**

**Fig. 1** Framework for mainstreaming disaster risk reduction. Functions are indicative (Source: EMI. State of the practice report on urban disaster: open file report. June 2009)



society, which collectively groups all the active agents of society.

The central government delegates aspects of policy, regulatory powers, and other functions and allocates additional resources to local government. It should in turn monitor the performance of local authorities based on sanctioned guidelines and criteria. The boxes do indicate a strict division between the various entities. In fact, flexibility and coordination are keys to success. Within this mainstreaming framework, an optimization of resources and outcome is accomplished when local authorities are strategically establishing internal policies and process where planning, programming, and action for risk reduction is integral to each of their jurisdictional responsibilities either as a service provider or as a regulator. This process is sometimes referred to as “integrated” or “holistic” approach to DRM.

This framework also suggests that risk reduction can be mainstreamed in local governance by harnessing existing legal mechanisms (e.g., local government acts, environmental management acts, DRM acts and related laws and regulatory mechanisms), processes (e.g., licensing, land use, etc.), and service delivery systems (e.g., health, education, transport, utilities, revenue generation) and making use of such resources. For local authorities, this would translate into having processes and practices that inherently incorporate urban risk reduction in these core functions

that they undertake such as construction and building licensing, land use and urban development planning, environmental management, and social welfare as well as in the services that they provide or regulate. To provide necessary authority, additional reforms are often needed, particularly in aligning DRM laws and policies with other acts that regulate local government functions. The point is that wherever responsibility is located, authority and resources should also be provided.

**Review of Tools for DRM Mainstreaming**

In line with global efforts to reduce disaster risks by focusing on local-level action through mainstreaming, several disaster risk management models have been developed that integrate disaster risk in local development. A review has been conducted of 76 tools, 10 of which were shortlisted for detailed assessment because of their applicability for local application in urban settings (Berse et al. 2009). “Tools” are used interchangeably with models and instruments and in this context refer to a framework that lays out the methodology for undertaking DRM including the mechanism for implementing the elements in the methodology.

Each tool’s relevance to disaster risk reduction and their applicability or feasibility to the local government’s capacity to institutionalize disaster

risk reduction efforts within its functions and operations were carefully considered and weighed in the assessment. Each tool has its own strengths and weaknesses that local authorities in urban areas can learn from in mainstreaming DRM. Evaluation of DRM tools were based on a set of criteria indicators representing the three principles of mainstreaming, i.e., central coordination, local implementation, and participation. The criteria indicators are meant to assess effectiveness and relevance to DRR processes, feasibility requirements, and applicability to the urban setting especially of developing countries. Through this study (which is not exhaustive), a set DRM instruments have been developed—or at least have the potential—for replication in areas outside of their respective origins and were rated for local adoption in the urban context. A summary of the results of this study is provided here.

## Effectiveness

### Local Implementation

The paradigm shift in the disaster management policies has elicited the participation and commitment of local governments to a more proactive disaster risk management. It is argued that since local stakeholders are the ones greatly affected in the events of disasters, it is critical for local governments to play a major role in the DRM. This is the very reason for giving emphasis on the local implementation of DRM mainstreaming models.

Of the frameworks reviewed, the following have evolved around the concept of DRM mainstreaming: Comprehensive Hazard and Risk Management (CHARM) Programming Approach (SOPAC 2002), Total Disaster Risk Management (TDRM) (ADRC 2005), Central United States Earthquake Consortium's (CUSEC'S) Disaster Resistant Community (DRC) Model (CUSEC 1997), and the Bangladesh DRR Mainstreaming model (Siddiqui 2007). CUSEC's DRC Model was developed by a consortium that includes both the local community and business sectors and not surprisingly gives the most emphasis on the involvement of

these constituencies in the DRM processes. Although designed to be implemented at the national level, Emergency Management Australia's (EMA) Emergency Risk Management Process (Commonwealth of Australia 2004) can also be developed for local government DRM mainstreaming implementation.

### Central Coordination

The reviewed DRM mainstreaming models are consistently aligned with the disaster risk reduction strategies formulated by the DRM authorities of their respective countries. The TDRM as in a few other cases was developed by nongovernmental organizations for application in different cities and countries. The Total Disaster Risk Management implementation strongly encourages endorsement from the central DRM authority and adaptation to the DRM institutional framework of the country of application. The Total Disaster Risk Management developed by the Asian Disaster Reduction Center- Office for the Coordination of Humanitarian Affairs (ADRC-OCHA) was endorsed by the government of Thailand and its central DRM authority and adapted for implementation in the country (ADRC 2005).

### Participation

The need for stakeholder participation is a well-established approach used in development work. Its main tenet is that stakeholders are collaborators in a development project at every stage of the process. Through this approach, stakeholders influence and share control over the decisions that affect them and their resources. In essence, the stakeholders drive the development process. They are the ones who decide in the planning, design, implementation, monitoring, and evaluation of the project. In this process, they are guided by experts and specialists who also processed the outcome in a scientifically rigorous output. With this, participation does not only ensure stakeholders' ownership but also encourage commitment. In general, the reviewed models emphasize multistakeholder participation at every stage of the DRM planning process. They also recognize the relevance of the participatory process as

enabling communication mechanisms. Models provide more relevance to particular stakeholders: national authorities (e.g., Comprehensive Hazard and Risk Management and Total Disaster Risk Management), local authorities (e.g., Central United States Earthquake Consortium), business sector (e.g., Central United States Earthquake Consortium's Disaster Resistant Community), or community (e.g., BDRRM, Central United States Earthquake Consortium). At the same time, other tools such as the BDRRM provide specific indications of the targeted stakeholders.

## Applicability

### Relevance

The reviewed DRM mainstreaming models generally adhere to the main goal of integrating risk management in the development and governance processes in order to reduce risks and mitigate the impact of disasters, albeit employing distinct strategies and aiming at varied focus.

The CUSEC model, for example, prioritizes achieving disaster-resistant communities. With this, the model aims to reduce community vulnerability to natural hazards in order to minimize losses and accelerate recovery (CUSEC 1997). The Emergency Management Australia's Emergency Risk Management Process, on the other hand, focuses on reducing risk by making modifications in the causes of risks (Commonwealth of Australia 2004). Similarly, South Pacific Applied Geoscience Commission Disaster Management Unit's Comprehensive Hazard and Risk Management Programming Approach aspires to develop preparedness and reduce vulnerabilities while increasing resilience of the community (SOPAC 2002). The added value of this particular model is that it engages the implementing institution in hazard and risk management in a more holistic manner as it intrinsically links DRR to national development (South Pacific Applied Geoscience Commission SOPAC 2002). Food and Agricultural Organization's DRM Framework (Baas et al. 2008) follows the same line and aims to reduce underlying factors of risk and to prepare for and initiate an immediate response should

disaster hit (Berse et al. 2009). The Asian Disaster Reduction Center- Office for the Coordination of Humanitarian Affairs' Total Disaster Risk Management model, like the Comprehensive Hazard and Risk Management model, is anchored on risk management. However, the TDRM also focuses on "total" approach of balancing the ability to respond to the consequences of disaster with predisaster actions that lessen the need for response (ADRC 2005).

### Feasibility/Resource Requirements

Financial and resource requirement are crucial factors for assessing the implementation potential of a particular DRM mainstreaming model. Oftentimes, the availability of resource dictates the scope of DRM mainstreaming implementation and the strategies or tools that will be utilized. Acknowledging this, most of the shortlisted DRM models signified the use of available resources and the development or enhancement of existing resources whether it be financial/material or human resources. While some DRM mainstreaming models identified low-cost tools and strategies for their implementation, others opted for more sophisticated and high-cost tools or mechanisms.

Apart from relying on the engagement of different stakeholders and the local government for human resources, interestingly Central United States Earthquake Consortium uses the strategy of providing incentives to promote steps and measures to reduce the vulnerability of communities to natural hazards (CUSEC 1997). The Food and Agricultural Organization's DRM Mainstreaming model, South Pacific Applied Geoscience Commission-DMU's Comprehensive Hazard and Risk Management, and the Bangladesh DRM Mainstreaming model all give importance on strengthening the capacities of local stakeholders in disaster management and risk reduction and improving advocacy and awareness (SOPAC 2002). They do not specify what would be the required resources for implementation.

Emergency Management Australia's Emergency Risk Management did more than this by identifying a package of special tools for risk

management (i.e., Unique Identifier System, the Risk Register Database, and the Geographic Information Systems) and at the same time by carrying out emergency risk management training for local stakeholders (Commonwealth of Australia 2004).

### Disaster Risk Management Master Plan (DRMMP)

The Disaster Risk Management Master Plan was developed by Earthquake and Megacities Initiative (EMI) to support local-level long-term planning and programming of disaster risk reduction activities. It follows the approach set out in Australian/New Zealand Standard 4360-2004, a standard in risk management developed jointly by Australia and New Zealand and recently adopted by the International Standards Organization as ISO31000 for risk management. The DRMMP is based on EMI's mainstreaming framework that optimizes resources by defining and distributing roles and responsibilities across various stakeholders at all levels of government.

The DRMMP provides opportunity for local authorities to systematically and rigorously identify programs, projects, and activities (PPA) aimed at reducing risk caused by natural and man-made hazards and to define processes for implementing these projects and activities. Local authorities are familiar with the master planning process as it is an integral part of their planning activities in particular for land use planning and transport. These plans constitute the basis for budgeting and investments.

Embedding the three principles of mainstreaming (i.e., local implementation, central coordination, and participation), the DRMMP process is designed to align along core planning processes of local governments and is strategically developed for local government DRM implementation. It is anchored on the regulatory framework that defines mandate and authority of government. It is a methodology for integrating risk parameters into various local government functions. EMI's DRMMP

implementation also strongly encourages formal endorsement from the central DRM authority and adaptation to the DRM institutional framework of the country of application. Finally, the DRMMP process has been designed as an approach for organizing the stakeholders in thematic Focus Groups to ensure efficiency and sustainability using a participatory process with targeted stakeholders.

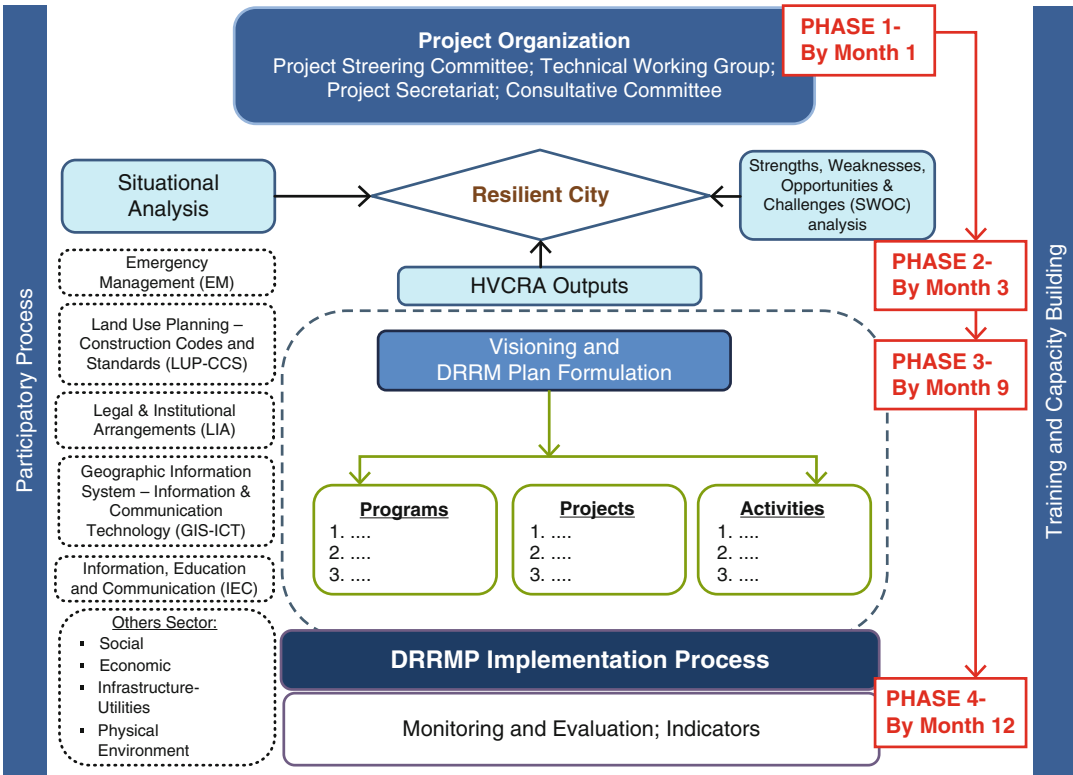
The DRMMP methodology follows similar principles and processes as other more conventional planning processes, e.g., land use planning, namely,

- It is structured and systematic and follows a consistent step-by-step methodology.
- It is science based and data driven.
- It is multisectoral and multidisciplinary.
- It applies to all hazards.
- It is participatory and consensus driven.

By anchoring on mainstreaming, the DRMMP puts in place a structured approach for setting up a DRM system that is based on science, understood by all, and provides the rationale for investments in DRR programs and projects. As of 2014, the DRMMP has already been applied to eight (8) local authorities, namely, Istanbul (Turkey), Kathmandu (Nepal), Metro Manila (Philippines), Amman (Jordan), Mumbai (India), Pasig City (Philippines), Quezon City (Philippines), and Dhaka (Bangladesh).

### Process to Implement the DRMMP

The Disaster Risk Management Master Plan provides a *road map* for a proactive DRM approach, which recognizes that disasters are not just “set-backs” or “roadblocks” to development but result from the paths that development is pursuing. Thus, by changing planning processes, and incorporating disaster risk parameters explicitly in the planning of processes and projects, it can be ensured that in future natural hazards will encounter resilient communities that are capable of withstanding their impact, reduce their losses, cope, and recover normal life faster. Ultimately,



**Building Disaster Resiliency Through Disaster Risk Management Master Planning, Fig. 2** The DRMP workflow (Source: Urban Resilience Master Planning: A Guidebook for Practitioners and Policy Makers, March 2015)

impacts of hazards become mere emergencies rather than disasters.

The undertaking of a DRMP follows a series of analyses along each of four phases, namely,

- Phase 1: Organization and Preparation
- Phase 2: Diagnosis and Analysis
- Phase 3: Plan Development
- Phase 4: Plan Implementation, Monitoring, and Evaluation

Figure 2 provides the workflow process for developing the DRMP, which can be completed in 12–24 months, depending on the elements that need to be covered. First, the elements that need to be included in the master planning process have to be identified. Some components are core to the DRMP methodology because they provide the essential scientific information on the DRM practice. These include

- Legal and Institutional Arrangements (LIA)
- Land Use Planning (LUP) and development controls
- DRM Database and Geographic Information System (GIS)
- Hazard, Vulnerability, and Risk Assessments (HVRA)
- Emergency Management (EM)

Further elements/sectors (e.g., housing, transport, sanitation, health, education, social services, and others) can be added depending on the jurisdictional responsibility of the city. This also depends on what is most relevant to local authorities in terms of priority, access to data, and availability of resources and expertise. For example, in the application of the DRMP in Greater Mumbai Project, there were additional elements that were included such as Water, Wastewater

and Storm Drainage Systems, and Transportation. This is due to the fact that the Municipal Corporation of Greater Mumbai regulates the delivery of these services. It is important to note that not all sectoral elements fall under the authority of the city or of other agencies of the government. Many could be provided by the private sector or utility companies (e.g., water, power). Others would be a mix of public and private entities (e.g., transport). Other elements may also have to be addressed because of the local context and conditions particular to a city. For example, in the Mumbai application, elements such as Slums, Shelter, and Housing, were likewise addressed because of the unique characteristics of the city that has more than 60 % of its population living in the slum areas.

A listing of additional elements included in the DRMMP includes

- Shelter and Housing (including slums and informal settlements) (S&H)
- Health
- Education
- Construction Codes and Standards (CCS)
- Water Systems
- Waste Water and Storm Drainage Systems (WWSD)
- Power Systems (PS)
- Transportation Systems (TS)
- Solid Waste Management (SWM)
- Telecommunications
- Possibly other relevant sectors

There are other elements that support the whole planning process and are crosscutting in nature. These include

- Training and Capacity Building (TCB)
- Information Education and Communication (IEC)

Training and Capacity Building and Information Education and Communication components facilitate the meaningful participation of stakeholders since their aim is to bring the gap in understanding of DRM concepts and principles between the EMI experts and practitioners and

the stakeholders. Throughout the DRMMP process, the stakeholders are made to understand and take ownership of the types of risks that their city faces as they acquire the competency and tools to be able to manage those risks on their own.

### **Participatory Approach to Develop the DRMMP**

The DRMMP allows for the meaningful participation of stakeholders. By design, the DRMMP provides stakeholders with an opportunity for learning the concepts of hazard, vulnerability, and risk and to understand their relevance to planning. It develops consensus among them on the trade-offs and the rationales for investment in urban resilience. With their engagement in the development of the plan, the stakeholders not only provide essential knowledge to the plan but acknowledge their roles and responsibilities in the implementation of the plan, thus taking ownership. The underlying principle to EMI's participatory approach is that urban DRR can only be made meaningful if stakeholders understand their risks. They should be well informed in order to meaningfully contribute. In most cases, there is a gap in how risk is understood and interpreted by various stakeholders with diverse backgrounds and oftentimes competing interests. Once there is shared understanding of risk, stakeholders can contribute to the work at hand in terms of data collection and validating findings and interpretations of risk assessments that are fundamental to any risk reduction program.

EMI's version of participatory approach was first applied in 2008 in the *Makati Urban Redevelopment Planning Project: Mainstreaming Disaster Risk Reduction in Megacities, A Pilot Application in Metro Manila and Kathmandu*. It was then further tested and applied in various cities and has become EMI's cornerstone strategy to stakeholder engagement in urban DRR. Using this approach, the participation by stakeholders is organized along key sectors that allow for generating inputs across a broad range of stakeholders with different agenda and interests but at the same time facilitate decision and action.



**Building Disaster Resiliency Through Disaster Risk Management Master Planning, Fig. 3**

Project organization structure of the disaster risk reduction in Greater Mumbai project which shows an example of a flat non-hierarchical structure that is composed of stakeholders from different sectors that are working together in a participatory approach



Typically, implementing the DRMMP requires organizing the stakeholders along the following:

- Creation of a **Project Management Team** (PMT) composed of the project managers and technical experts and specialists who make up the main workforce that will develop the DRMMP. It is multidisciplinary and structured as a single unit incorporating EMI’s experts and counterpart from the host local authority.
- Creation of the **Advisory Committee** which is composed of policy-/decision-making officials who are endorsed as representatives to the project by their respective institutions. It provides the platform to receive input and guidance from the stakeholders and share the project issues, findings, and accomplishments that the members can take back to their respective institutions.
- Creation of the **Scientific Consortium** which is composed of local experts in relevant fields

addressed by the project. The members of the Scientific Consortium are selected on the basis of their credentials. They advise on the validity of the scientific data and approach and help reach scientific consensus.

- Creation of the **Focus Groups** which are composed of local practitioners, researchers, and community leaders. These include midlevel managers and specialists from the various departments and offices of the city. They are organized along each of the sectors that are being analyzed in the DRMMP. Through the Focus Groups, relevant stakeholders get engaged in the development of the project by providing inputs and tackling issues, as well as validating the assumptions, findings, and recommendations relevant to the project.

Figure 3 below shows an example of the project organization structure of the DRMMP that was put in place in Mumbai. It reveals a flat nonhierarchical structure that puts emphasis on

teamwork and consensus building but at the same time assigns responsibility and accountability to the project team. It requires experts, practitioners, policymakers, community leaders, and private sector working together to provide inputs to develop the elements of the DRMMP. In the Disaster Risk Reduction in Greater Mumbai Project, there were more than 100 members of the Advisory Committee representing various organizations of government, civil society, technical agencies, and the private sector. In the Building a Disaster Resilient Quezon City Project, the various Focus Groups were organized under a Technical Working Group (TWG). They are composed of technical specialists from the different departments of the Quezon City Government officially assigned by the Office of the Mayor to work with EMI to develop the various elements of the DRMMP.

**Strong Emphasis on Data and Science**

The development of the DRMMP requires a strong emphasis on data and science. It includes collecting evidence to understand the DRM context and situation, assessing the inherent risks of the city, developing an information database on disaster risk management, and identifying the gaps and needs. The following sections describe several key activities that are conducted to produce the required assessments to develop the DRMMP.

**Development of the DRM Database and City Risk Profile**

A significant part of the effort goes into data collection, review, and structuring all data into a single DRM database. Data must be collected from several city departments as well as from relevant government agencies and other service providers. This is the most challenging task in the process as not all departments willingly share data. The data is typically organized at the resolution of the lowest geopolitical boundary of the city. This will enable an effective use and management of the data by the local and sublocal authorities. A list of the data that needs to be

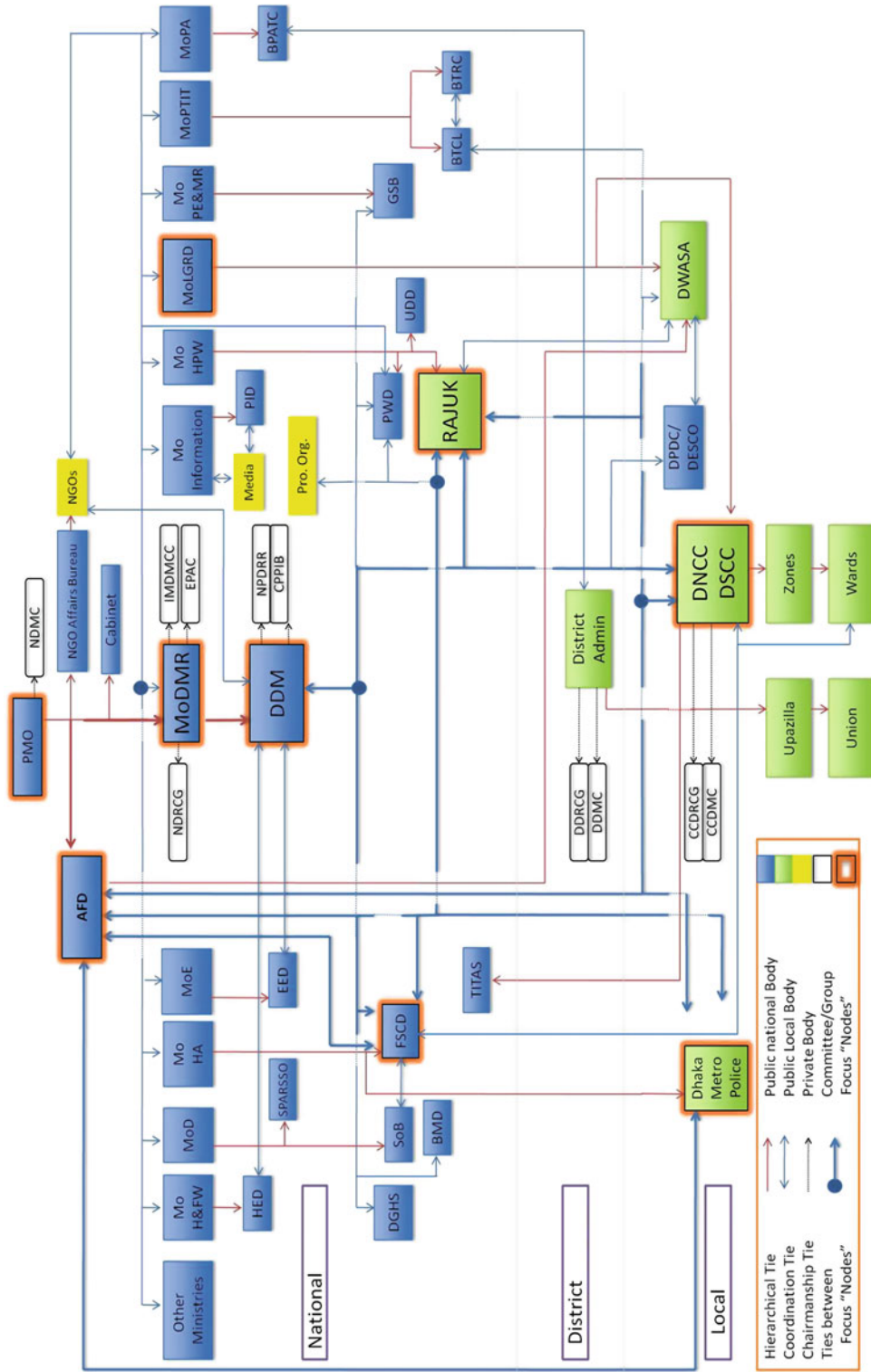
**Building Disaster Resiliency Through Disaster Risk Management Master Planning, Table 1** Data typically collected in the development of the DRMMP

Administrative and institutional	Build environment, including:
Demographic and socio economic	Buildings
Physical profiles including:	Critical and essential facilities
Topology; geology; hydrology; soil, climate	Infrastructure: transport, water, drainage, sanitation, power, communication, health
Land use	High loss facilities

collected is indicated in Table 1 below. The data is compiled in a City Risk Profile shared and validated with all the stakeholders. Knowledge-sharing mechanism is defined and endorsed to ensure the data is kept current and is benefiting other planning functions of the city. In addition to facilitating DRM planning, tax mapping provides another motivation for cities to have a centralized database in uniform format.

**Analysis of the Legal and Institutional Arrangements for DRM**

The DRMMP process is anchored on the legal and institutional arrangements that define the geopolitical boundaries of the concerned planning authority (i.e., the local government), its jurisdictional responsibility, and the potential elements of the plan. An in-depth analysis of the legal and institutional context is essential in providing legitimacy and credibility to the plan and in avoiding potential jurisdictional conflicts. Several outputs are generated such as a network analysis that shows the organizational chart of the DRM undertaking in the city with key agencies and their relationships. A functional mapping is also completed to indicate functions, roles, and responsibilities of each organization in the DRM process. The results are shared and validated with the stakeholders through focus group exercises to ensure that the DRM organization is understood by all concerned agencies and officials. An example of network analysis is shown in Fig. 4.



**Building Disaster Resiliency Through Disaster Risk Management Master Planning, Fig. 4** Network representation indicating relationship of DRM stakeholders in Dhaka (Source: EMI 2014)

### Hazard, Vulnerability, and Risk Assessment (HVRA)

The DRMMMP is informed by the hazard, vulnerability, and risk parameters which provide the scientific basis for the plan and ensures that the plan is responding to the objectives of risk reduction and resilience enhancement. The parameters defining the current practice of the elements of the plan (i.e., sectors) are checked against the risk parameters to define the gaps and the strategies for improving urban resilience. The hazard, vulnerability, and risk parameters are developed using scientific methodologies (e.g., scenario analysis or probabilistic risk assessment) that provide information on the distribution of damage and the social, economic, and material losses to the city considering both physical vulnerability and socioeconomic vulnerabilities. The risk assessment should be done at the highest resolution possible to provide an accurate and reliable understanding of the risks. The results are presented, discussed, and validated by the stakeholders. The greater the understanding of the risks, the more relevance is given to the master plan.

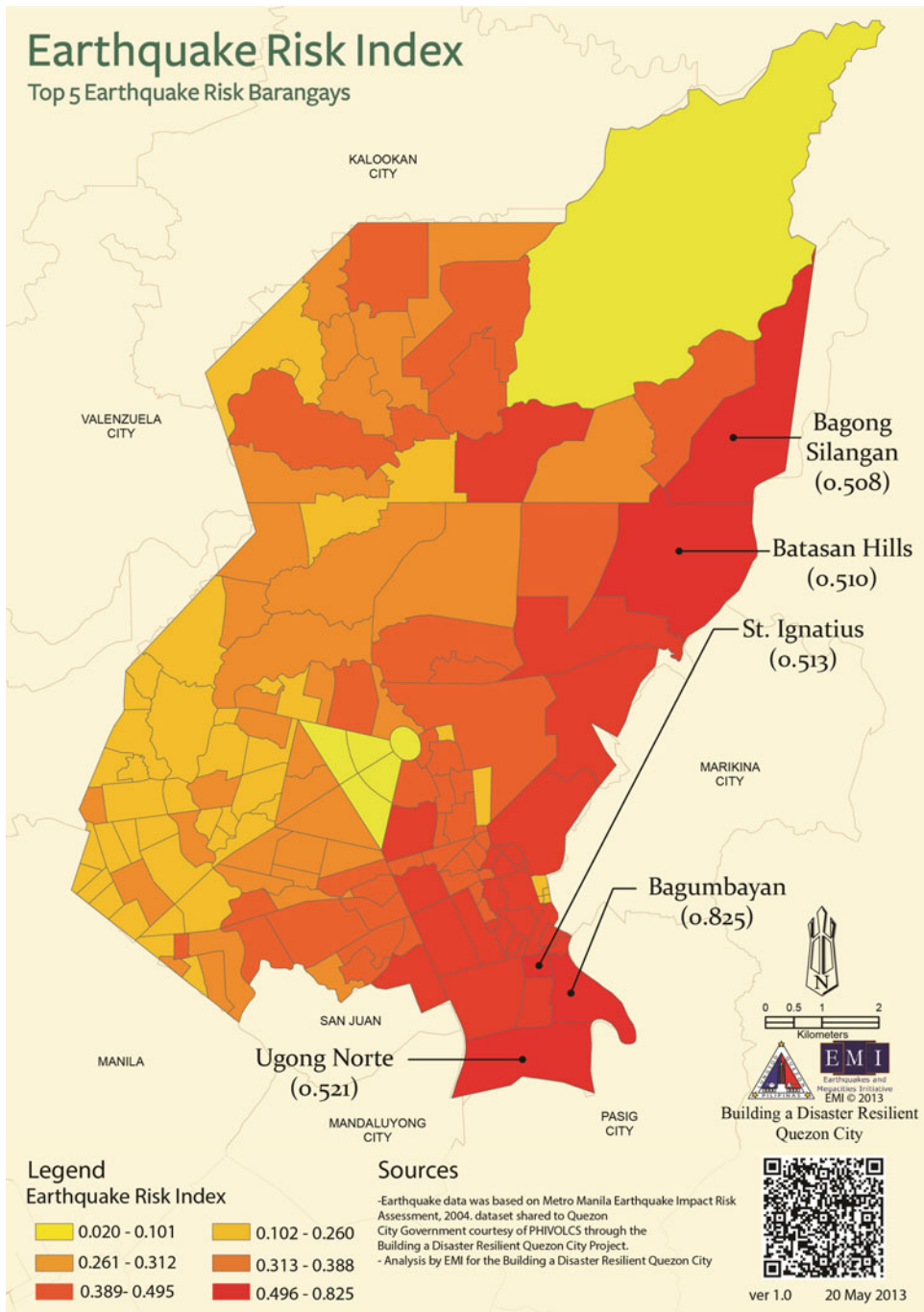
The Hazard, Vulnerability, and Risk Assessment also provides information on “hotspots” which are areas that have the highest risk for the considered hazards. The scientific approach to defining “hotspots” relies on developing dimensional indicators by which parameters of physical risk (e.g., number of heavily damaged buildings in a certain locality) are combined with parameters that represent the capacity of that particular locality to sustain and recover from the impact of an event (Nardo et al. 2005). Through the hotspots, local authorities will know where they should prioritize the DRR projects. Maps are produced to provide illustrations where the potential problems are highest. They indicate priorities for planning in terms of where the investments should be for reducing risk and building resilience that address area-specific issues. An example of hazard mapping and hotspot analysis is provided in Fig. 5.

### Situational Analyses of Urban Resilience Elements

Situational analyses on key urban resilience elements are conducted to provide the baseline for understanding the state-of-the-practice urban DRR. With the support of the experts, the stakeholders are guided through workshop-type exercises where they can determine the gaps relative to standards for urban resilience. Essentially, the stakeholders are presented with the risk parameters which are contrasted with their current practices. In small group exercises, they look at how the current systems and practices for particular development sectors are responding to the risk parameters and the requirements for disaster risk management. In the *Building a Disaster Resilient Quezon City Project*, the development sectors that were considered include population, economic activity, social services, emergency management, institutional and land use administration, and physical resources (EMI and QCG 2014). Figure 6 provides an example of framework for analyzing the resilience of lifeline systems in Greater Mumbai. It provides the work that needs to be done in the assessment process starting from the mapping of the exposure (i.e., the asset at risk) into a geographic information system (GIS), then superimposing the hazard information, then understanding the impact both in terms of direct damage and secondary damages, then assessing the impact on the system serviceability taking into consideration measures of resilience of the system including physical resilience and community resilience.

### Putting the Elements of the Plan Together

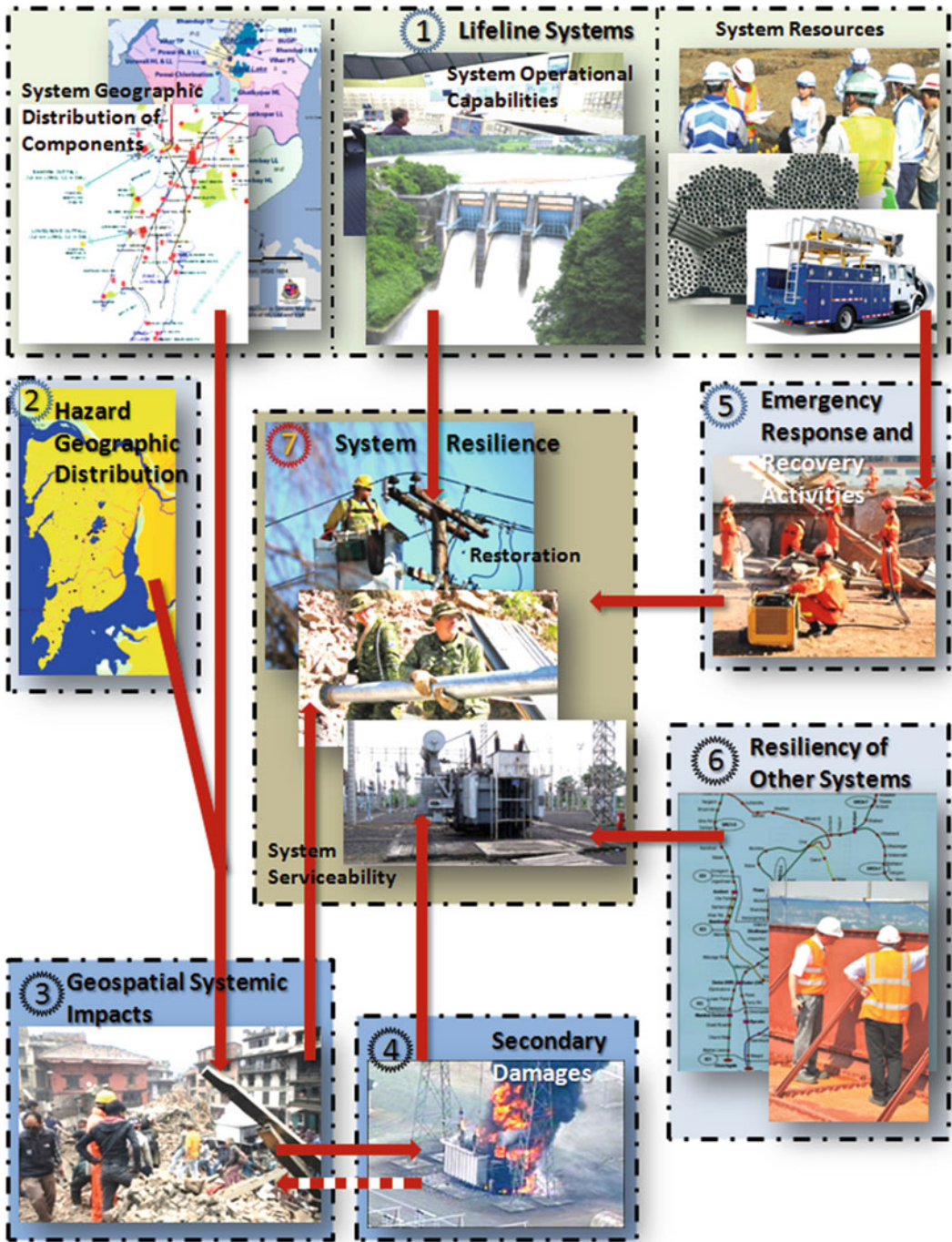
For each of the development sectors, programs, projects, and activities are identified as concrete actions to reduce risks and improve resilience. Stakeholders undertake the consequential analysis together with the experts. The consequential analysis is an interactive exercise which builds on the situational analysis but looking at “what-if” scenarios aimed at developing options to improve



**Building Disaster Resiliency Through Disaster Risk Management Master Planning, Fig. 5** Earthquake risk profile for Quezon City, Philippines, showing the hotspot counties. The map and corresponding information

was generated through the conduct of a hazard, vulnerability and risk assessment, which is a vital component of the DRMMMP





**Building Disaster Resiliency Through Disaster Risk Management Master Planning, Fig. 6** The diagram, as an example of a situational analysis exercise, shows the lifeline system and resiliencies and how they influence community resiliency. The elements of resiliency are numbered from ① to ⑦, each with visual representations. The arrows identify prerequisite elements; for example in

order to assess the geospatial systemic impacts ③ from an earthquake, one must first understand the geographic distribution of the system ① being analyzed and the geographic distribution of the hazard ②, in this case earthquake ground motions and permanent ground deformation. Taken from the *Disaster Risk Reduction in Greater Mumbai Project*. 2011



**Building Disaster Resiliency Through Disaster Risk Management Master Planning, Table 2** Results of consequential analysis of a magnitude 7.2 earthquake to physical resources of Quezon City

Primary hazards faulting, shaking, liquefaction, landsliding	Primary damage: building/ structural non-structural/ equipment	Primary loss: life/ injury, repair costs, function, communication/ control	Secondary hazard/ damage: liquefaction. landsliding fire, hazmat, flooding. . .	Secondary loss: business/operations interruptions, market share, reputation
<b>Collapse of water sam Extreme flood Loss of lives, physical injuries Damages to main roads, infrastructure</b>	Damage to water reservoir	Trauma (Stampede)	Possible trash slide in dumpsites	Loss of jobs
	Building collapse (Eastwood, Libis area)	Isolation of victims due to no road/ highways access	Loss of property, lives	Loss of income
	Loss of water supply	Operation interruptions in hospitals	Physical injuries	Loss of opportunities
	Loss of lives		Fire	Eastwood, malls
	Trapped inside the building		Houses made from light materials	Loss of livelihood
	Damage to equipment		Biogas plant explosion	Production halts
	Stranded people		Informal settlers	Businesses, offices
	Chaos/stampede (inside buildings)		Food shortage	No classes
Contamination of waterways				

the current practice. Through the consequential analysis, the stakeholders achieve an understanding of the impacts of the current practices and define strategies and rationales for reducing these impacts. They also identify the “entry points” for mainstreaming DRR in each particular development sector. Table 2 shows an example of the result of a consequential analysis for a magnitude 7.2 to the Physical Resources Sector of Quezon City.

Next is the establishment of a vision for resilience and a mission to reduce risk through a visioning exercise. In the Disaster Risk Reduction and Management Plan (DRRMP) process in Quezon City, the stakeholders took some time to establish consensus around developing the vision for the city. There was a long gridlock in identifying a common descriptor for the natural environment around descriptors such as habitable, sustainable, resilient, “clean and green.” This is followed by the development of resilience strategies through the conduct of Strengths-Weaknesses-Opportunities-Challenges (SWOC) exercise to formulate and prioritize strategies by

taking into account key internal and external elements that may affect the attainment of the resilience vision and mission.

After reaching consensus on the resilience strategies, programs, projects, and activities are then formulated. Apart from listing down and discussing potential investments, stakeholders also prioritize projects and activities. This **prioritization process** is based on a set of criteria that helps stakeholders focus their attention to interventions that will have the greatest impact in terms of reducing their risk while taking into account their inherent limitations such as budget capacity or resource constraints. The final form of the DRMMP is then validated. An example of a DRMMP program and its related projects are shown in Table 3.

**Ensuring Implementation of the DRMMP**

The time frame for a DRMMP can span anywhere from 6 to 15 years, depending on the planning cycles of cities. For the DRMMP to be fully

**Building Disaster Resiliency Through Disaster Risk Management Master Planning, Table 3** Example of DRMMP program, related projects, and priority ranking of each project

Program 2: Mainstreaming DRR in land use planning and land use management	
Mitigation and prevention projects	Priority
Formulating a communications plan to institutionalize HVRA within Quezon City (with focus on hotspot areas)	Immediate
Mainstreaming DRR in the 2010–2030 comprehensive land use plan	Medium-term
Consultation workshops for pilot project identification and feasibility of selected land use management methods for flood and earthquake risk reduction	Short-term
Program for improving Quezon City Government’s capacity and expertise in building and infrastructure construction project development permitting, monitoring and evaluation	Medium-term
Restructuring existing M and E program for stakeholder response(s) to and development impacts of Quezon City Government’s projects on disaster risk reduction and management	Short-term
Pilot projects on preferred land use management methods (e.g., development regulations, zoning earthquake hazard areas, floodway zoning and set-backs, fire zones)	Short-term

B

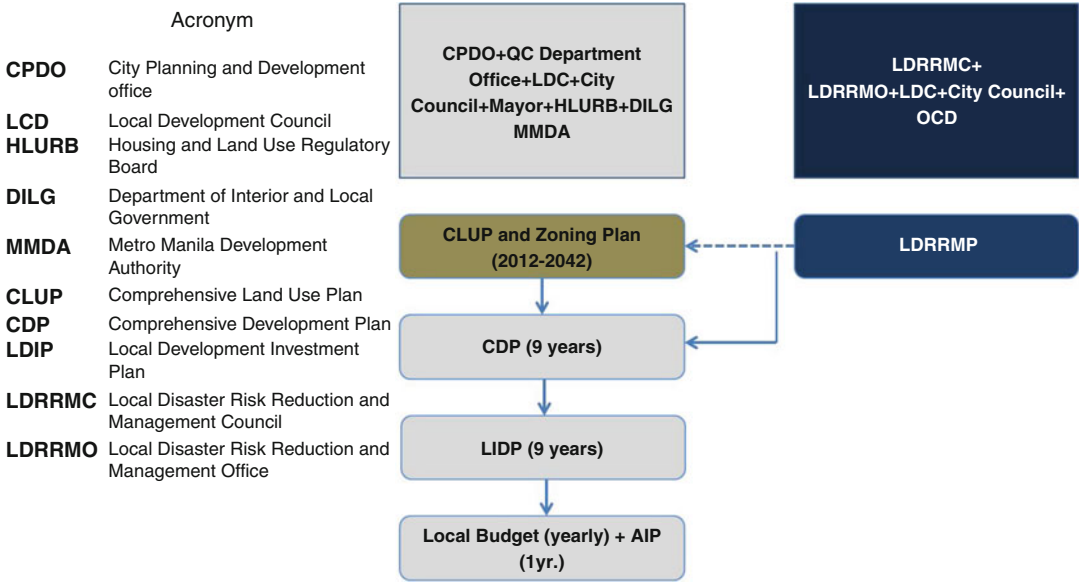
implementable, there has to be a clear understanding of the legal and administrative processes of a city that concerns with approval of mandated plans. This requires knowing who approves, when, and through which step in the approval process should the DRMMP be incorporated so that it becomes integrated in the budgeting cycle. This way, it is ensured that budget for priority projects identified in the DRMMP gets allocated in the overall budget of the city. Figure 7 below provides an example of the budget approval process of Quezon City indicating how the Local Disaster Risk Reduction and Management Plan (LDRRMP) gets integrated in the Annual Investment Plan (AIP). The Annual Investment Plan refers to the indicative yearly expenditure requirements of cities that will be integrated into their annual budget.

Understanding who approves, when, and through which steps in the approval process of cities helps ensure that DRMMP projects and activities are incorporated in the budget and, as such, get funded.

**Monitoring, Evaluation, and Communication**

To track the progress (or lack of progress) of implementation, monitoring and evaluation tools are developed. One of these tools is to develop a set of Indicators that set initial

benchmarks and can be used to measure progress. The first is the quantitatively derived **Urban Disaster Risk Indicators (UDRI)** which provide a holistic view of disaster risk in a local authority by capturing the direct physical damages and the aggravating social conditions contributing to total risk. The model and methodology referred to here as the Urban Disaster Risk Indicators was originally developed for the Inter-American Development Bank through the IDB-IDEA Indicators Program by the Institute of Environmental Studies (IDEA) of the National University of Colombia, Manizales (NUCM) (Cardona 2003; Carreno et al. 2006). In the context of EMI’s DRMMP methodology and approach, the indicators were used as an innovative risk communication tool to engage stakeholders in understanding their involvement and taking ownership of the risk factors in the city. Besides the initial EMI implementation in Metro Manila (Fernandez et al. 2006), the risk indicators have also been successfully implemented with stakeholders in Istanbul (Khazai et al. 2009), Amman (Bendimerad et al. 2009), Mumbai (EMI and Municipal Corporation of Greater Mumbai 2011a), and Quezon City (Bendimeard et al. 2013). The application of the Urban Disaster Risk Indicators in a city will prove its value if it is “mainstreamed” within the DRM practices and other planning processes that impact DRM in the city. To reach this objective, the indicators have been linked to the quantitative outputs and



**Building Disaster Resiliency Through Disaster Risk Management Master Planning, Fig. 7** Example of a budget approval process in Quezon City, Philippines

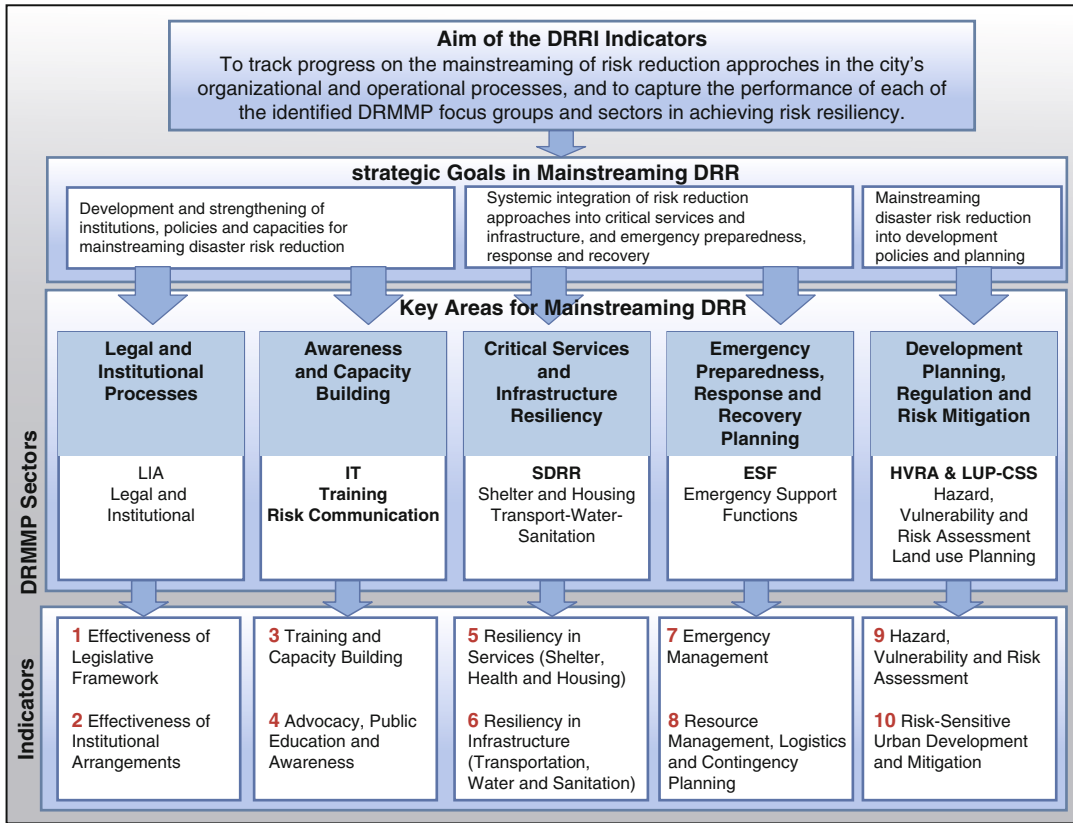
highlighting how the local disaster risk reduction and management plan gets integrated into the annual investment plan

analyses of the DRMMP. Guided by recommendations following implementation of the risk indicators by EMI in different cities, the current methodology encompasses the following three broad areas:

- To develop the system of indicators in close collaboration with the technical staff and officials in a city, to engage them in the development of the data and the understanding of the conceptual framework and methodology, and to ensure ownership over the indicator system and its periodic updating and upgrading
- To work closely with the Focus Group, in evaluating the indicators, such that they are relevant to the megacity scale of analysis, represent the conditions and reality of socio-economic vulnerability in the city, and reflect the outcomes of the various studies undertaken as part of the DRMMP (e.g., earthquake risk assessment, transportation study, housing and shelter, land use planning, construction codes and standards, water supply and water treatment analysis, etc.)
- To implement the system of indicators through a process of engaging a wider group

of stakeholders in the city, such that they are used as an effective risk communication tool that inherently relates to the city-level DRM practices; as a planning tool that aids in correcting, reviewing, and deciding on where to invest resources; and as Disaster Risk Management benchmarks which assist in policy decision-making and monitoring of different risk reduction practices implemented at the local level.

The second group of indicators is the qualitative **Disaster Risk and Resiliency Indicators** (DRRI) that is a set of ten (10) indicators that establishes initial benchmarks to measure to what extent risk reduction approaches have been mainstreamed in the organizational, functional, operational, and development systems and processes of local governments (EMI and MCGM 2011b). The Disaster Risk and Resiliency Indicators are linked to the priorities of the *Hyogo Framework for Action 2015–2015*. The aim of these indicators is to understand how well the local authority is performing in mainstreaming DRR into different sectors based on predefined benchmarks and performance



**Building Disaster Resiliency Through Disaster Risk Management Master Planning, Fig. 8** Disaster risk and resiliency indicators (DRRI) (Source: EMI and MCGM (2011b))

targets. The rationale for selecting the 10 DRRRI indicators can be traced in Fig. 8 by following the information from top to bottom of the chart. The main aim of the DRRRI indicators is to track progress on the **mainstreaming** of risk reduction approaches in the city’s organizational, functional, operational, and development systems and processes. The mainstreaming goal is further divided into three **strategic goals** shown in the chart. Each of the strategic goals corresponds to one or more **key areas** analyzed in the DRMP where these goals are to be implemented. Finally, two indicators corresponding to each of the five key areas of mainstreaming are shown. Mainstreaming risk reduction and achieving risk resiliency cuts across all the key areas and all the 10 indicators shown below. Thus, the stakeholders using and scoring the indicators should look at *all 10 indicators* together from the

perspective of their institutions and not only the indicators that relate most closely to their activities.

The scores for the DRRI are derived from a self-assessment along key functional activities/policies undertaken by the DRMP Focus Groups. A handbook is developed to describe the organization of the indicators, a rationale for their selection, and provide guidelines for their implementation and scoring that is contextualized to the city for which it is implemented by providing “guiding questions” and “evidence for discussion” derived from in-depth interviews with stakeholders along each indicator (EMI and MCGM 2011b). With five Performance Target Levels of attainment: little or no awareness, awareness of needs, engagement and commitment, policy engagement and solution development, and full integration, the DRRI allocates a

ranking for the 10 indicators that fall under the main 5 areas of mainstreaming, resulting in a graphic visualization of the mainstreaming disaster risk reduction at the Municipality at a point in time.

The Indicator System is also used as a risk communication and planning tool to assist in policy development, decision-making, and in monitoring the effectiveness of programs, projects, and activities. In actual practice, however, there is no clear motivation for cities to monitor performance and outcome of DRR investments beyond accounting for the number of projects and activities conducted. This is also because there are no existing tools as yet for monitoring and evaluating performance of DRR programs, projects, and activities that have been developed for cities.

## Lessons Learned

Building resilience, especially within the context of urban areas, requires not just raising awareness on risk reduction but actual investments on programs, projects, and activities that reduce risk. For the plan to be fully understood, accepted, and supported, it has to engage a broad range of stakeholders at all stages of the planning process. However, they have to be equipped with the knowledge and tools to be able to participate meaningfully and contribute to resilience building. Stakeholders have to understand what types of risk they face, what are the implications of these risks to their own mandated responsibilities, what options are available to them to reduce their risk, and what possible trade-offs they need to make in order to prioritize limited resources and address inherent constraints.

Full implementation of the DRMMP, however, requires continued technical assistance. Even if funding is available from cities to implement DRR projects, oftentimes, they lack the resources to manage and undertake DRR projects. It is a resource-intensive approach. The DRMMP only provides the roadmap for change in practice from a reactive to a more proactive approach. For the actual change to take place, the

city has to make continued investments in the medium to long term to make sure that it continues on the path toward risk reduction.

## Summary

Local authorities have difficulty in dealing with the risks from disasters due to the fact that they are overburdened by their development aspirations and mandated responsibilities. Mainstreaming DRM in the daily functions and services of the city is the key to manage disaster risks in urban areas without exacerbating cost for local authorities. By incorporating disaster risk parameters explicitly in the planning of processes and projects, it can be ensured that in future, natural hazards will encounter resilient cities that are capable of withstanding their impact, reduce their losses, cope, and recover faster. Ultimately, impacts of hazards become mere emergencies rather than disasters.

Mainstreaming necessitates the distribution of roles and responsibilities between the various levels of government and with the society. It gives emphasis to the local authority's implementation role, central government's coordination function (manifested in the control processes, allocation of resources, and exercising oversight on the performance of the local authority), and the participation of the civil society which is crucial in all facets of the process. Thus, it optimizes resources from these stakeholder institutions to reduce the risks.

Following the mainstreaming tenet, the DRMMP provides a road map for a proactive DRM approach to support local-level long-term planning and programming of disaster risk reduction activities. It follows a series of analyses in four phases, namely, (1) Organization and Preparation, (2) Diagnosis and Analysis, (3) Plan Development and Plan Implementation, (4) Monitoring and Evaluation. The DRMMP process is designed to align along core planning processes of local authorities. Furthermore, it provides stakeholders with an opportunity for learning the concepts of hazard, vulnerability, and risk and to understand their relevance to planning.

The DRMMP was developed taking into consideration other related DRM models that focus on local-level action through mainstreaming.

With DRMMP's strong emphasis on data and science, evidences are collected to understand the DRM context and situation, assessing the inherent risks of the city, developing information database on DRM, and identifying the gaps and needs. These tasks are achievable through a participatory approach involving a broad range of stakeholders. Implementing the DRMMP requires organizing these stakeholders into (1) Advisory Committee, (2) Scientific Consortium, and (3) Focus Groups. Guiding these groups is the Project Management Team.

The DRMMP provides opportunity for these stakeholders to understand the parameters of vulnerability and risk in the context of their own responsibilities and functions. With this knowledge, they can systematically and rigorously identify and prioritize programs, projects, and activities to implement in managing and eventually reducing their risk. These projects and activities are institutionalized by integrating these in the budgeting cycle. This way, it is ensured that budget for priority projects identified in the DRMMP gets allocated in the overall budget of the city. Monitoring and evaluation tools are then developed to track the progress (or lack of progress) of implementation.

With their engagement in the development of the plan, the stakeholders not only provide essential knowledge to the plan but acknowledge their roles and responsibilities in the implementation of the plan, thus taking ownership. By anchoring on mainstreaming, the DRMMP puts in place a structured approach for setting up a DRM system that is based on science, understood by all, and provides the rationale for investments in DRR programs and projects.

### Cross-References

- ▶ [Community Recovery Following Earthquake Disasters](#)
- ▶ [Earthquake Disaster Recovery: Leadership and Governance](#)

- ▶ [Earthquake Protection of Essential Facilities](#)
- ▶ [Earthquakes and Their Socio-economic Consequences](#)
- ▶ [Economic Recovery Following Earthquake Disasters](#)
- ▶ [Emergency Response Coordination Within Earthquake Disasters](#)
- ▶ [Land Use Planning Following an Earthquake Disaster](#)
- ▶ [Resilience to Earthquake Disasters](#)

### References

- Asian Disaster Reduction Center (ADRC) (2005) Total disaster risk management: good practices. ADRC, Kobe
- Baas S, Ramasamy S, De Pryck J, Battista F (2008) Disaster risk management systems analysis. FAO, Rome
- Bendimerad F (2009) State-of-the-Practice Report on Urban Disaster Risk Management. EMI internal report. <http://emi-megacities.org/?emi-publication=state-of-the-practice-report-on-urban-disaster-risk-management>. Quezon City
- Bendimerad F, Zayas J (2015) Urban Resilience Master Planning: A Guidebook for Practitioners and Policy Makers. EMI, Quezon City
- Bendimerad F, Mattingly S, Seva V, Kustu O, Khazai B, Reyes M, Berse K, Al-Soub W, Quran S, Al-Sous G, Khalili H, Dabaseh A (2009) Amman – disaster risk management master plan, support to building national capacities for earthquake risk reduction in Amman. volume 1, Earthquake and Megacities Initiative (EMI), main report. UNDP Jordan – 00051485, 31 Mar 2009, p 130
- Bendimerad F, Khazai B, Zayas J, Daniell JE, Salunat J, Perez B, Lingad L, Dakis K, Bergonia L, Magtaas B, Barba B, Pado I, Pino L, Lanuya E, Valera A, Villa P, Hisanan T (2013) Building a disaster resilient Quezon City project: hazard, vulnerability and risk assessment report. Earthquake and Megacities Initiative, Quezon City
- Bendimerad F, Zayas J, Pado I (2015) Legal and institutional arrangements guidebook, Urban resilience guidebook series. EMI, Quezon City
- Berse K, Bendimerad F, Cruz J, Dagli W, Deocariza M, Khazai B, Lopez IG, Pulmano N, Seva V (2009) Desk review of international disaster risk management models and tools intended for local institutional application. GFDRR, p 118, Makati City, Philippines
- Cardona OD (2003) The need for rethinking the concepts of vulnerability and risk from a holistic perspective: a necessary review and criticism for effective risk management. In: Bankoff G, Frerks G, Hilhorst D (eds) Mapping vulnerability: disasters, development and people. Earthscan Publishers, London



- Carreno L, Cardona O, Barbat A (2006) Urban seismic risk evaluation: a holistic approach. *Nat Hazards* 40(1):137–172
- Central United States Earthquake Consortium (CUSEC) (1997) Disaster resistant communities: a community-based approach to hazard mitigation. *CUSEC J* 4(1):2–4
- Commonwealth of Australia (2004) Emergency risk management application guide. Emergency Management Australia, Canberra
- EMI (2009) State-of-the-practice report on urban disaster risk management. Quezon City. Retrieved Mar 2014, from [http://emi-megacities.org/home/components/com\\_booklibrary/ebooks/StateofPractice\\_UrbanDRM.pdf](http://emi-megacities.org/home/components/com_booklibrary/ebooks/StateofPractice_UrbanDRM.pdf)
- EMI (2014) Legal and Institutional Arrangements Framework Guidebook. EMI, Quezon City
- EMI, Municipal Corporation of Greater Mumbai (MCGM) (2011a) Mumbai DRMMP framework report and implementation work outputs. EMI, Quezon City
- EMI, MCGM (2011b) Final technical report supplement. EMI, Quezon City
- EMI, Quezon City Government (QCG) (2014) Disaster risk reduction and management plan 2014–2020. EMI, Quezon City
- Fernandez J, Mattingly S, Bendimerad F, Cardona O (2006) Application of indicators in urban and megacities disaster risk management: a case study of Metro Manila. EMI topical report TR-07-01. p 30. A report for this application is available from the earthquakes and megacities Initiative website. [http://emi-megacities.org/upload/3cd\\_2007\\_MISReport\\_TR0701.pdf](http://emi-megacities.org/upload/3cd_2007_MISReport_TR0701.pdf). Cited Mar 2014
- Khazai B, Bendimerad F (2011a) Megacity Indicator Systems (MIS) for DRM in Greater Mumbai. In: Bendimerad F, Daclan JM, Dagli W, Zayas J (eds) *Mumbai Disaster Risk Management Master Plan (DRMMP)*. Earthquake and megacities initiative final technical report No CR-1 1-0, 31, MCGM
- Khazai B, Bendimerad F (2011b) Risk and resiliency indicators. Earthquake and megacities report No. TR-1 1-03. MCGM, p 103
- Khazai B, Wenzel F, Kilic O, Basmaci A, Konukcu B, Mentese EY, Sungay B (2009) Megacity indicator systems (MIS) for disaster risk management in Istanbul. International conference on megacities: risk, vulnerability and sustainable development, 7–9 Sept 2009. Helmholtz Centre for Environmental Research – UFZ, Leipzig
- Nardo M, Saisana M, Saltelli A, Tarantola S, Hoffman A, Giovannini E (2005) Handbook on constructing composite indicators. OECD Statistics working paper. OECD, Paris
- Siddiqui KM (2007) National institute of disaster management: 2nd Asian ministerial conference on DRR high level round table 1. Available at the National Institute of Disaster Management in India. [http://www.nidm.gov.in/amcd\\_presentations/HighLevel\\_Table1/BanglaDesh.pdf](http://www.nidm.gov.in/amcd_presentations/HighLevel_Table1/BanglaDesh.pdf). Cited Mar 2014
- South Pacific Applied Geoscience Commission (SOPAC) (2002) Comprehensive Hazard and Risk Management (CHARM): guidelines for pacific Island countries. SOPAC report DM0044, Suva, 32 pp
- UNISDR (2009) 2009 UNISDR terminology on disaster risk reduction. Available at: <http://www.unisdr.org/we/inform/terminology>. Cited Mar 2014

---

## Building Monitoring Using a Ground-Based Radar

Guido Luzi and Michele Crosetto  
CTTC Division of Geomatics, Av. C.F. Gauss,  
Castelldefels, Spain

### Synonyms

Displacements; Measurement; Natural frequencies; Real aperture radar; Structural health monitoring

### Introduction

This entry is focused on a terrestrial remote sensing technique that can provide a valuable input to earthquake engineering: the real aperture radar interferometry. In the last decades non-contacting measurement techniques based on optical sensors that can be employed for vibration monitoring have been largely described in the literature (Passia et al. 2008; Nassif et al. 2005; Gueguen et al. 2010). As an example, techniques like the Scanning Laser Doppler Vibrometry (SLDV) appear to be an appropriate non-contacting alternative to accelerometers, offering wide frequency bandwidths (0–200 kHz for the most common models) and extreme sensitivity to velocity and displacement (down to 2 pm). On the other hand, they suffer important limitations, due to constraints in the maximum observation angle and the maximum working range. In addition, they might need external acoustic stimulation to carry out measurements with adequate sensitivity, as described

in Esposito et al. (2004). Finally, they measure velocity, not displacements. Although less frequently, the use of microwave sensors to evaluate the vibration state of structures as buildings, bridges, and wind turbine towers has been investigated (Tarchi et al. 1997; Farrar et al. 1999; Pieraccini et al. 2003; Pieraccini et al. 2006; Bartoli et al. 2008; Pieraccini et al. 2008; Luzi et al. 2012a). Microwave techniques measure directly the displacement and have demonstrated to be an effective tool when the monitored displacements are down to tens of microns. Its capability to provide input data that can be used in a modal testing has been assessed, and the obtained results finally encouraged the production of radar instrumentation aimed at this application (Coppi et al. 2010). A coherent Real-Aperture Radar (RAR) is able to measure and monitor the natural vibrations of buildings, structures, and infrastructures. The main observations provided by the sensor are the displacements between the radar sensor and the observed target. The displacements can be observed at relatively high frequencies, up to 100 or 200 Hz with currently available sensors, thus providing a dense sampling of the displacements over time and space. For this reason, the technique is able to measure and monitor the vibrations of the observed objects. It is possible to derive key information of the observed objects as the main vibration frequencies, the main vibration modes, etc. from the displacement time series. There are two main potential applications of the described technique. The first and more consolidated is structural health monitoring, where RAR can provide input for the characterization of engineering structures, especially of their structural systems. This input can be provided periodically to determine the current state of system health and, in particular, to monitor its aging and degradation. In addition, the RAR can provide a valuable input after extreme events, such as earthquakes or blast loading, for rapid condition screening and assessment of the integrity of the structures at hand. The second potential application is the seismic risk evaluation of populated and industrialized areas that are seismically

active. This can be achieved through the measurement of dynamic parameters of buildings and structures, which can be done using a RAR system, and the dynamic parameters of the underlying soil in order to assess possible resonance phenomena.

This entry is organized in four main sections. The first one explains the RAR working principle and the main characteristics of the RAR measurements. The second to fourth sections describe three examples of vibration measurement: a tall tower, a building, and a bridge.

### Working Principle

Radar is a well-known instrument able to detect and range objects. It sends a modulated electromagnetic signal, the transmitted pulse, along the line of sight (LOS), and receives the portion of the signal reflected by the illuminated area. Different objects or parts of the illuminated area will reflect the microwave radiation with different intensities: the basic signal provided by a radar is a profile of the intensity backscattered from the scene as a function of the distance, usually referred as “range profile.” The radar acquires simultaneously the contributions from the different parts of the structure included in its antenna field of view (FOV), and different amplitude peaks correspond to contributions from parts of the observed structure located at different distances. The FOV of the radar is dictated by the pulse width and the antenna characteristics. The elementary sampling volume of a radar measurement is usually called radar bin and different bins are used to isolate different parts of the monitored structure. Such vision of the radar prevents to see details as optical systems do, but at the same time, this averaging allows to enhance the general behavior of the structure. In addition, the radar acquires all the bins simultaneously (with respect to the observed phenomenon) thus allowing to achieve a spatial sampling useful to estimate modal shapes. Reflecting properties of a given structure are strongly related to its geometry and the dielectric characteristics of the medium: for

example, metal objects, corners, and plane surface perpendicularly oriented with respect to the radar LOS display high values of reflectivity. If the reduction of the signal strength during propagation is not dramatic, that is to say in radar nomenclature if a good signal-to-noise ratio (SNR) is preserved, the received radar signal permits to retrieve the distance of the objects. The starting point is to achieve a good acquisition, consisting in selecting an observation geometry providing a valuable range profile, i.e., a signal where the bins of interest show a strong response. The RAR is only sensible to displacements along the LOS. For this reason, another important point is the selection of geometry where the LOS and the displacement are as much parallel as possible.

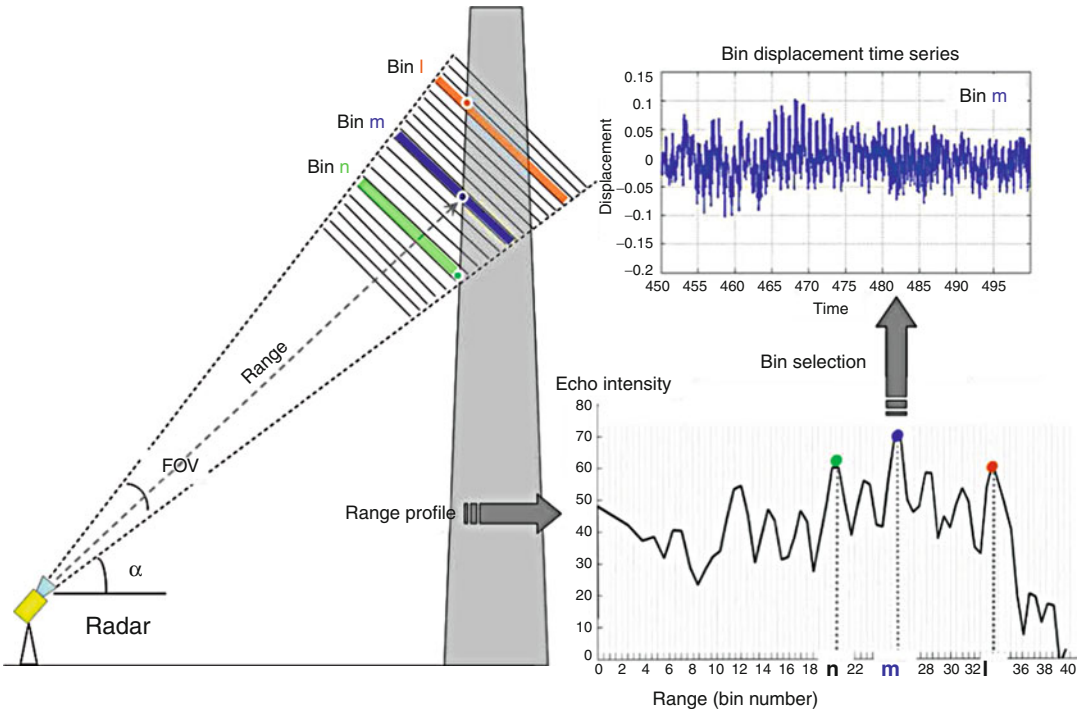
The minimum displacement detectable for conventional radar is dictated by the range resolution, i.e., the capability to distinguish different targets along the LOS, and this is usually not better than some tens of centimeters. Conventional techniques based on amplitude processing are not sufficient to measure the vibration displacements expected from building, which can reach values down to a few microns. On the other hand, interferometric techniques can be exploited to evaluate range variation along the LOS. Interferometric processing can be used only when the radar is coherent, i.e., able to measure not only the amplitude but also the phase of the received echoes. In this way, distance variations of the order of small fractions of the transmitted wavelength, which occurred between two or more acquisitions, can be estimated by comparing the phase of signals acquired at different times. A radar system designed to acquire periodically a set of received echoes, amplitude and phase values, of an entire range profile can provide a phase variation signal of each bin at the corresponding sampling frequency. Now, using the basic formula of differential interferometry, here below drawn as Eq. 1, these phase variations,  $\Delta\phi(t)$ , can be translated to displacement along the LOS time series,  $d_{\text{LOS}}(t)$ , for each bin:

$$d_{\text{LOS}}(t) = \frac{\lambda}{4\pi} \cdot \Delta\phi(t) \quad (1)$$

According to Eq. 1, the shorter the wavelength, the higher the sensitivity of the measurement: for a Ku radar, with wavelength  $\lambda = 1.76$  cm (operating frequency = 17 GHz), a phase variation of  $1^\circ$ , typically achievable using a state-of-the-art sensor, corresponds to a displacement of  $\approx 20$   $\mu\text{m}$ .

Equation 1 is a first approximation because it does not take into account some potential sources of error in phase estimation, but it is usually valid in the application here described; for a detailed discussion on this topic, see Luzi et al. (2012b). The standard deviation of the estimated displacements is related to the standard deviation of the measured phase, which in turn depends on the SNR of the radar measurement (Coppi et al. 2010). Vibrations with very small amplitudes, down to ten microns, can be detected when a good range profile with SNR peaks of up to 70 dB is acquired. The SNR must be statistically estimated when secondary undesirable vibrating targets (clutter) are included in the radar bin: its value decreases and the error in phase estimate increases. For this reason, and due to the high variability of the experimental conditions, it is very important to optimize the measuring conditions to acquire a good range profile.

A typical geometry used to monitor buildings is when the radar is positioned close to the base of the building, observing it along a LOS with an angle of inclination  $\alpha$  with respect to the horizon. According to the radar equation, the operating distance and the surface characteristics of the backscattering surface strongly affect the radar response. The strength of the received echo must be maximized, case by case, selecting the best observational position. This can be achieved by choosing a distance and an angle of observation able to assure a good range profile and a radar LOS close to the main direction of the observed displacements. Then, the displacement time series can be retrieved from a range profile. The measurement procedure is graphically resumed in Fig. 1 and consists in: (1) collecting an



**Building Monitoring Using a Ground-Based Radar, Fig. 1** Scheme of a standard procedure aimed at retrieving displacement time series from a radar acquisition. The radar collects an amplitude profile as a function of the

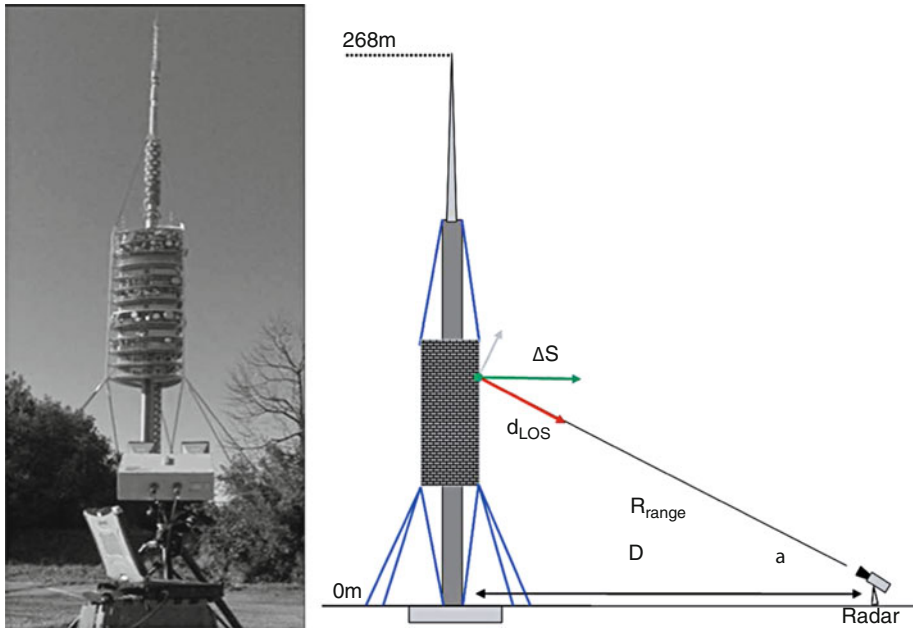
range, sampled at regular spatial steps, the radar bins. A displacement time signal is obtained from the interferometric phase of the echo of the selected bin using Eq. 1

amplitude profile as a function of the range, sampled at regular spatial steps (radar bins); (2) obtaining the interferometric phase of the echo of the selected bin; and, finally, (3) transforming the phase temporal variations into displacement time signal for analysis and processing using Eq. 1, as, for example, to calculate the spectral content of the signal.

The acquired data can be processed through conventional signal processing tools. Due to the statistical characteristics of the sampled phenomena, random and stationary, a typical approach consists in calculating the Power Spectral Density (PSD) using the Welch method (Welch 1967).

Nowadays only a few companies market radars for vibration monitoring; as a reference, the main characteristics of one of the interferometric radar most frequently cited in the literature and available at the CTTC, the IBIS-S,

manufactured and marketed by IDS (Ingegneria dei Sistemi SpA), are summarized. It is important to note that the results here discussed do not basically depend on the radar system used. IBIS-S is designed to monitor large structures as bridges and wind turbine towers. The system consists of a sensor module, a control PC, and a power supply unit. The maximum acquisition rate is currently 200 Hz. This parameter depends on the selected maximum range and decreases as the distance increases. The sensor is installed on a tripod equipped with a rotating head used to adjust the bearing of the sensor towards the investigated structure. The radar equipment is a continuous-wave (CW) step-frequency (SF) transceiver, which transmits continuous waves at discrete frequency values, sampling a bandwidth B at a constant interval. The transceiver transmits an electromagnetic signal at a central frequency of 17.2 GHz with a maximum



**Building Monitoring Using a Ground-Based Radar, Fig. 2** Photography of the tower and the radar sensor (left) and a simple scheme of the measurement geometry

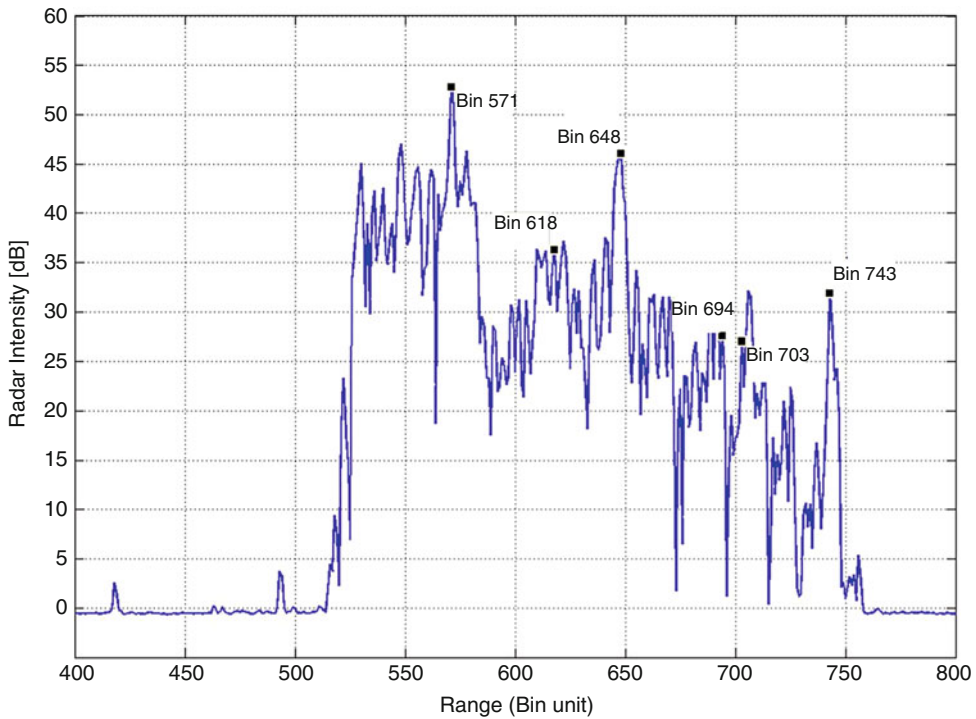
indicating the fraction of the displacement (*bold arrow*),  $d_{LOS}$ , detected by the radar (*right*)

bandwidth of 300 MHz, necessary to perform a range resolution of 0.5 m; details on the functioning principle can be found in Gentile (2011). The location and the dimension of the measured radar bins are dictated by the range resolution and the transmitting and receiving antennas. Antennas with different gain and aperture can be exchangeable; the most frequently used are pyramidal horns whose FOV is about 0.18 rad. At 10 m distance from the target, a  $3 \text{ m}^2$  area is approximately illuminated, and this value increases as the observation angle with respect to the horizontal increases. The sensor unit is managed by a control PC, through a standard USB communication, which is provided with system management software used to configure the acquisition parameters, store the measurement data, and show the displacements in real time. The power supply unit provides about 5 h of autonomy. The equipment is quick and easy to install and can be used both day and night, and in almost any weather conditions.

### Vibration Measurement of a Tall Tower

The first example here discussed is the monitoring of a tall tower, the Collserola communications tower, designed by the architect Norman Foster, which serves as a telecommunications tower for Barcelona and its neighborhood. The tower stands from an altitude of 445 m a.s.l., reaching a maximum 266 m height above the ground and 286 m above its base, see Fig. 2. It is made up of five main elements: a concrete shaft, a metal mast, block of platforms, pre-tensed metal guys, and fiber guys. The lower guys are steel cables anchored to concrete blocks; the remaining ones are Kevlar fiber guys. This structure represents an ultimate case from the measurement point of view for different reasons. Firstly, the tower is very high; thus, the magnitude of the amplitude of oscillation of its top, in normal wind conditions, is typically of several millimeters. Secondly, this assures a high number of bins available for data





**Building Monitoring Using a Ground-Based Radar, Fig. 3** Range profile, intensity of the radar echoes as a function of the range expressed in bins, obtained from

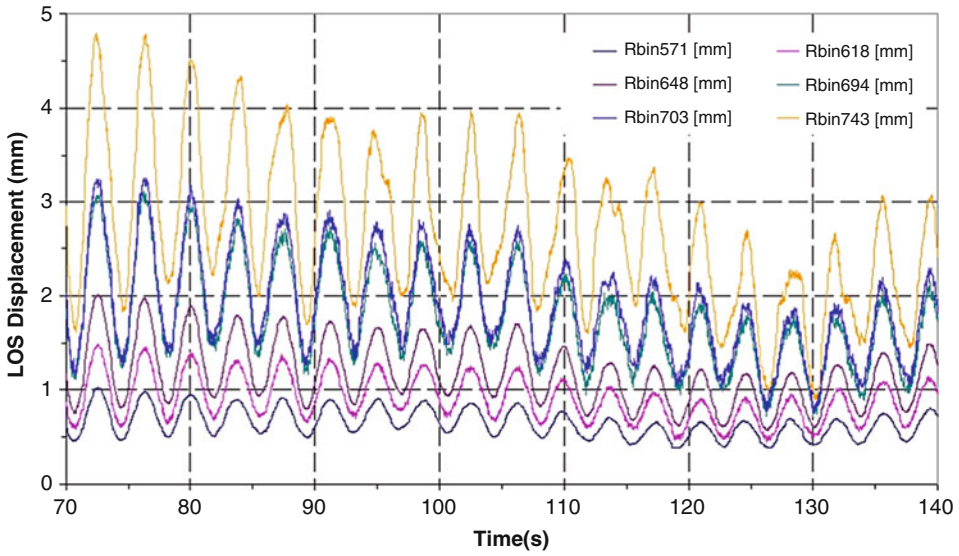
a tower monitoring. A selection of bins, to be processed and analyzed, is marked

interpretation. Finally, its geometry and composing materials, metal and concrete, offer a strong radar reflectivity and this allows acquiring data from ranges up to hundreds of meters. It is worth noting that an analogous monitoring carried out with conventional point-wise sensors, e.g., accelerometers, would be unadvisable due to its high costs and the strong electromagnetic noise of this environment.

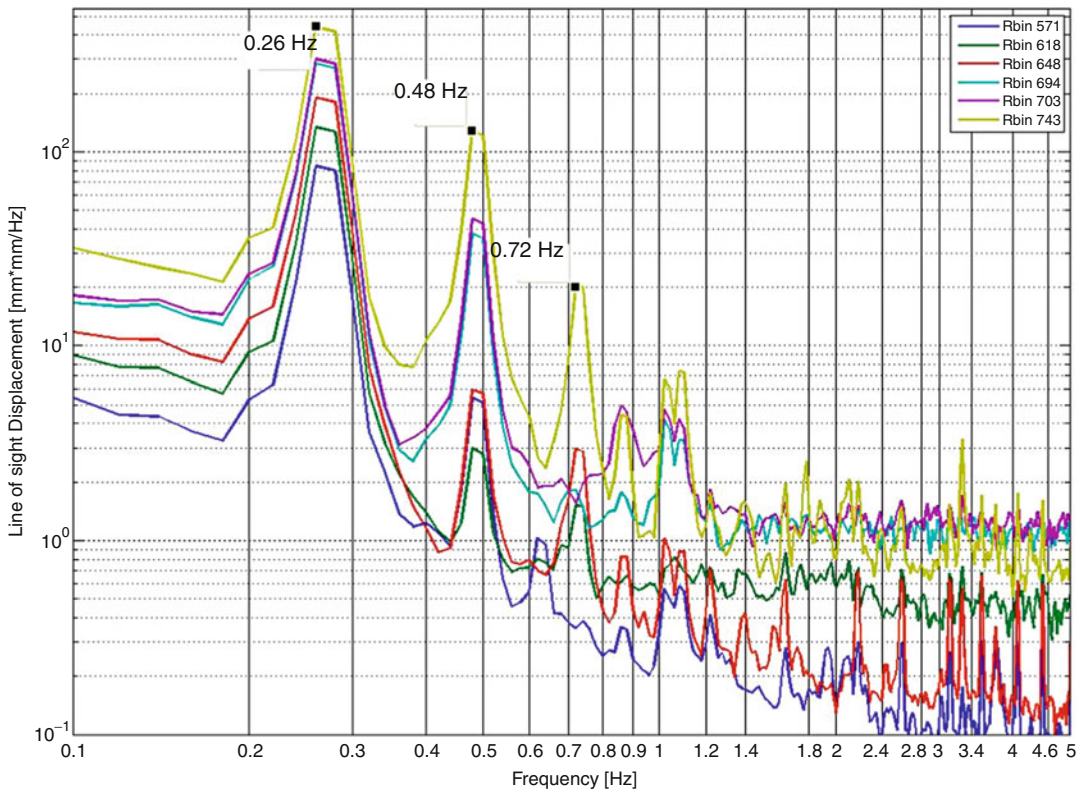
Different contributions from parts located at different heights can be clearly identified and selected for processing and observing a range profile acquired at a distance of 266 m from the tower and with an observation angle of  $37^\circ$  (Fig. 3). A typical approach consists in selecting a set of bins sampling the entire height of the structure and drawing the variation of the measured displacement as a function of the time. Figure 4 represents the starting point of the

analysis of the vibration behavior of the monitored structure. The curves retrieved from this plot indicate that the amplitudes of the displacement increase with the height; this trend fits the main mode of vibration of the tower, similar to the first mode expected from a clamped beam. The period of oscillation is also easily calculable in approximately 3.7 s (frequency 0.27 Hz). A spectral analysis has been carried out through the estimation of the PSD calculated using the Welch method (Welch 1967) to look for further vibration modes and deepen the analysis of the vibrating characteristics of the tower. The PSD calculated with the following configuration is plotted in Fig. 5: window duration = 50 s, type = Hamming, overlapping between windows: 66 % for different bins. The results obtained indicate the presence not only of the 0.27 Hz peak but also further peaks at 0.49 and





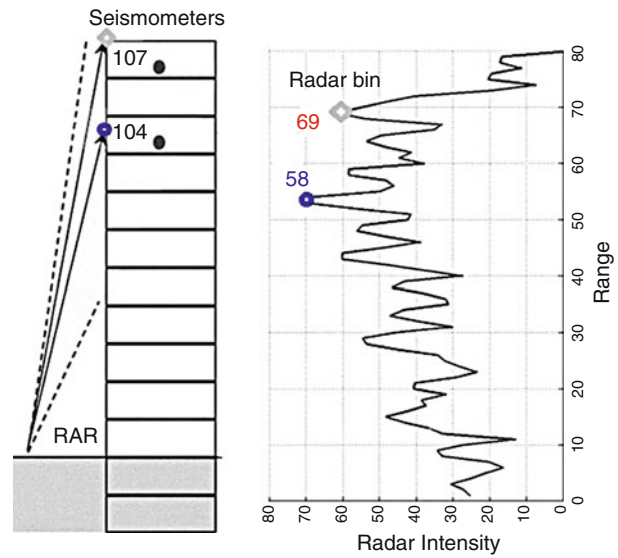
**Building Monitoring Using a Ground-Based Radar, Fig. 4** Example of a 70 s sample of the displacement of different bins retrieved from radar measurements as a function of the time



**Building Monitoring Using a Ground-Based Radar, Fig. 5** PSD calculated for the bins shown in Fig. 4. Different colors refer to different bins. The three peaks related to tower vibration are marked

### Building Monitoring Using a Ground-Based Radar, Fig. 6

Location of the seismometers (#104 and #107) with respect to the building, and radar bins (#53 and #69) selected from the range profile, to perform a radar data validation



0.72 Hz. Some minor peaks, probably caused by the cables and its interaction with the tower, are also present.

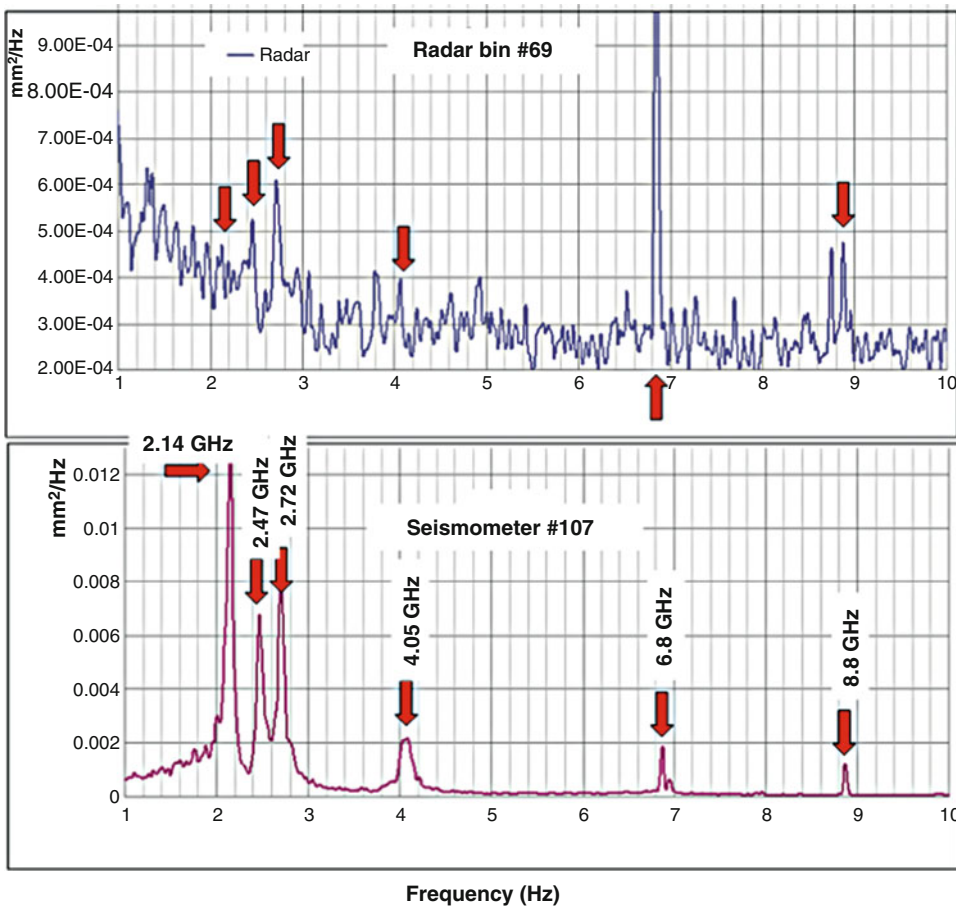
Case studies aimed at estimating vibration characteristics of towers of different shapes and heights, selected among architectural heritages, have been carried out by different authors (Pieraccini et al. 2005; Atzeni et al. 2010; Gentile and Saisi 2011).

### Comparison of Radar Observations and Conventional Measurements: The Case of a Building

Radar observations can be integrated with some standard point-wise measurements as a support to model calculation of the modal shapes of the investigated structures. This is the case described in Negulescu et al. (2013), where a building, part of a sportive complex located in Font Romeu (France), was monitored by means of radar and several accelerometers, and the results obtained were compared with a model calculation. The building has a reinforced concrete structure, with double basement, ground floor, 10 storeys, and a total height of 33 m (not including the basement). In this study, several sensors were

placed, in two different configurations, on the roof and at different heights of the structure. The experiment was carried out with the aim of comparing seismometer data with the displacement retrieved from several radar bins. In particular, a direct comparison was carried out between the data obtained using two radar bins and the closest sensors installed in the building, whose position is shown in Fig. 6, where the geometry of the measurement is also depicted. The seismometer acquisition set includes eight sensors and a wireless networking connection was used during the measurements. The normalized PSD calculated for the displacement signal retrieved from the radar measurements and that obtained from microtremor signal are compared in Fig. 7.

The location of the main peaks is almost coincident and the radar signal shows some minor peaks too. The amplitude is a little different; this can be imputed to the fact that the radar only measures the LOS component of the displacement and the two sensors are not exactly positioned in the same point. The agreement between radar observations and seismometer measurements was also confirmed by numerical model calculation and modal shape estimation (Negulescu et al. 2013).



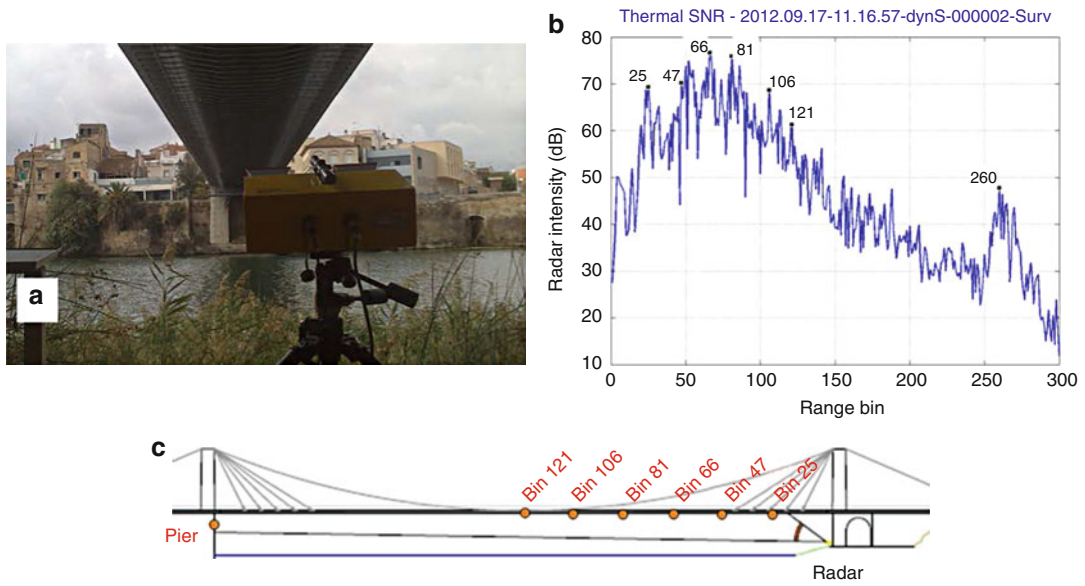
**Building Monitoring Using a Ground-Based Radar, Fig. 7** Comparison of the normalized Power Spectral Density (PSD) functions from the records obtained using the radar technique, bin #69 (*top*) and the seismometer #107 (*down*)

## Vibration Measurement of a Bridge

Bridge monitoring is an application where the technique has been thoughtfully studied and validated (Gentile 2010). Radar can be used for both static (Pieraccini et al. 2007) and dynamical studies (Stabile et al. 2013). Cable-stayed bridges can especially benefit from radar monitoring, with moderate time and cost recourses with respect to the use of conventional sensors. In this case, the radar monitoring is usually carried out with two different geometries. The first one aims at detecting the main features of the deck vibration, with the radar positioned below the bridge deck acquiring a range profile where the different bins provide a spatial profile of deflection which can occur both due to the wind and the ambient

solicitation as microtremor. The second position is carefully selected to detect the behavior of the stay cables avoiding the direct influence of the deck vibration. In this second case, the main objective is to acquire a range profile where the different stay cables are clearly identified. Figures 8 and 9 show the two geometries used during the monitoring of a cable-stayed bridge in Amposta (Spain), over the Ebro River.

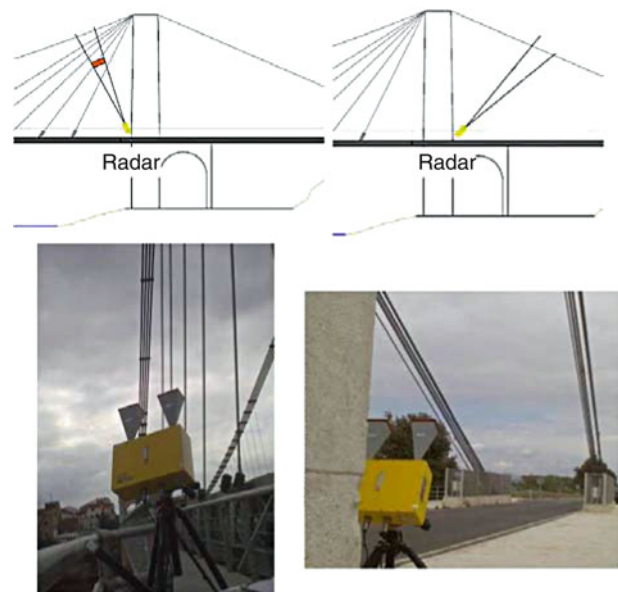
A typical signal acquired during the transit of a vehicle using the geometry depicted in Fig. 8 is shown in Fig. 10. The displacement responses of different bins of the bridge, corresponding to a sampling of half of the bridge deck, are jointly plotted. From Fig. 10 the difference in the deflection for the different bins is noticeable: the central part of the bridge (bin #81) lowers down to 4 mm,



**Building Monitoring Using a Ground-Based Radar, Fig. 8** Photography of the radar pointing towards the deck (a); range profile acquired (b); scheme of the

geometry of acquisition indicating the selected bins: bin 25, 47, 66, 81, 106, and 121 belong to the bridge deck, while bin 260 corresponds to the pier (c)

**Building Monitoring Using a Ground-Based Radar, Fig. 9** Photos and geometry of the acquisitions with the radar pointing towards the inner stay cables positioned within the two pillars (left) and watching the set of guys tied to the soil (right)

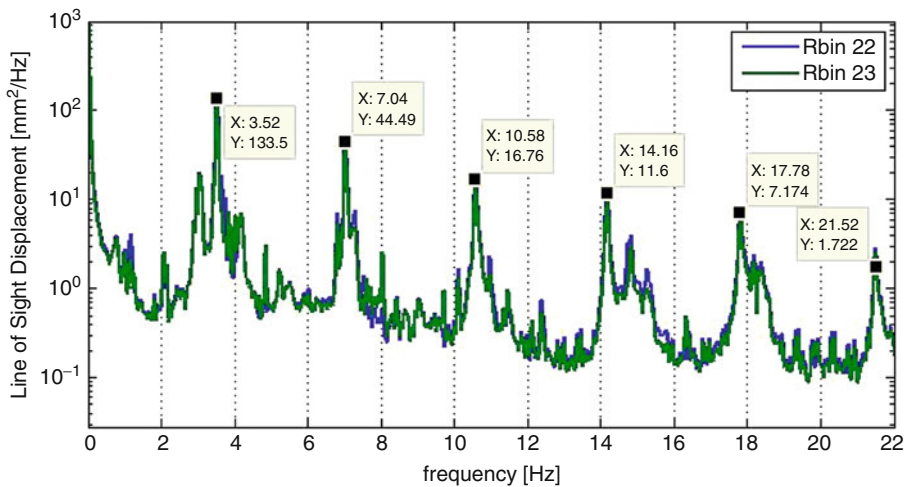
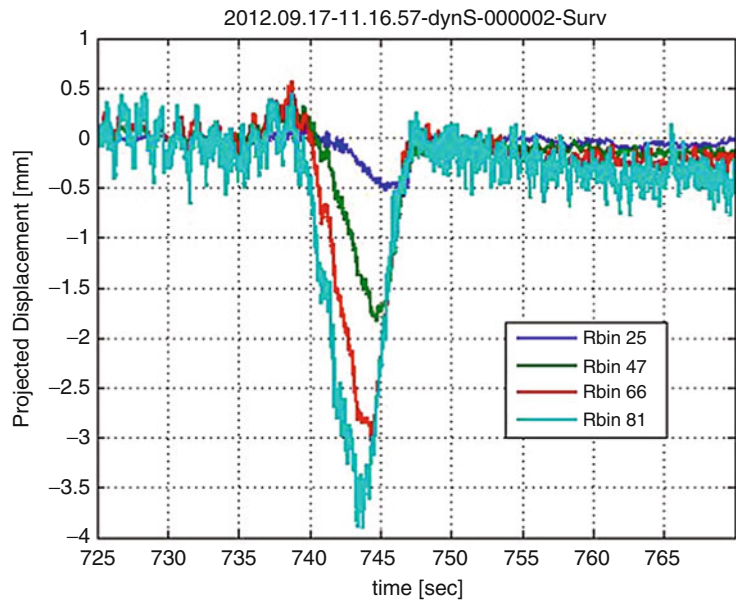


while the part close to the pier (bin#25) experiences a 500  $\mu\text{m}$  lowering. Using the second geometrical configuration (Fig. 9), the radar observation is focused towards the cables. In this case, the measurement of the natural frequency of the cable can be used to estimate the

tension force of the cable (applying a formula based on the tau string model; see Caetano and Cunha 2011; Gentile and Ubertini 2012; Luzi et al. 2014). The calculation of the PSD of the displacement signal allows detecting the main vibrating frequencies of the cables. Figure 11



**Building Monitoring Using a Ground-Based Radar, Fig. 10** Temporal displacement signal for four bins, retrieved from radar measurements carried out according to geometry shown in Fig. 8. Different colors refer to different bins



**Building Monitoring Using a Ground-Based Radar, Fig. 11** PSD calculated for two bins corresponding to two stay cables. Different colors refer to different bins

shows the results obtained from the simultaneous measurement of the displacements of two bins corresponding to two cables.

The values of the main peaks displayed in Fig. 11, 3.52, 7.04, 10.58, 14.16, 17.78, and 21.52, show that they are related to each other by a linear relationship. In fact, they are natural multiples of the fundamental frequency, 3.52 Hz, although the higher values gradually deviate. The first frequencies are in agreement with the values

expected from the tau string model, thus allowing the application of the model and the estimation of the tension force of the cables. It is worth noting that obtaining the same information using standard local sensors as accelerometer should be unfeasible. Besides, the knowledge of the spectral behavior of all the stay cables can also be used for evaluating the health state of the structure or comparing these experimental results with model analysis provided by structural engineering analysis.

## Summary

In this entry a radar technique applied to the monitoring of vibrations of structures as tower, buildings, and bridges has been introduced. After presenting the working principle and briefly describing a commercial radar system, a measurement procedure underlying the main critical aspects has been summarized. Experimental results from three case studies are then commented. The first is the monitoring of a tall tower which, thanks to the strength of the radar response and the millimeter amplitude of oscillation of its top, allows achieving abundant information. This monitoring also demonstrated that, in the best conditions, the technique is capable of acquiring data at ranges up to hundreds of meters. The second example shows a case where radar data has been validated using a network of standard point-wise measurements (seismometers). The last case study concerns the monitoring of a cable-stayed bridge, an application thoughtfully studied and validated by several authors. In this last case, the technique also allows detecting the vibration characteristics of the cables with moderate time and cost resources.

## Cross-References

- ▶ [Ambient Vibration Testing of Cultural Heritage Structures](#)
- ▶ [Geotechnical Earthquake Engineering: Damage Mechanism Observed](#)
- ▶ [Modal Analysis](#)
- ▶ [Remote Sensing in Seismology: An Overview](#)

## References

- Atzeni C, Bicci A, Dei D, Fratini M, Pieraccini M (2010) Remote survey of the leaning tower of Pisa by interferometric sensing. *IEEE Trans Geosci Remote Sens Lett* 7(1):185–189
- Bartoli G, Facchini L, Pieraccini M, Fratini M, Atzeni C (2008) Experimental utilization of interferometric radar techniques for structural monitoring. *Struct Control Health Monit* 15(3):283–298
- Caetano E, Cunha Á (2011) On the observation and identification of cable-supported structures. In: *Proceedings of the 8th international conference on structural dynamics EURO-DYN 2011*. Leuven, Belgium, 4–6 July 2011
- Coppi F, Gentile C, Ricci P (2010) A software tool for processing the displacement time series extracted from raw radar data. In: *Tomasini EP (ed) Proceedings of the 9th international conference on vibration measurements by laser and non-contact techniques and short course*, Ancona, Italy; 22–25 AIP conference proceedings 1253, June 2010
- Eposito E, Copparoni S, Naticchia B (2004) Recent progress in diagnostics of civil structures by laser vibrometry. In: *Proceedings of the 16th World conference on nondestructive testing*, on CD, Montreal, Canada, August 30–September 3, 2004
- Farrar C, Darling TW, Migliorini A, Baker WE (1999) Microwave interferometer for non-contact vibration measurements on large structures. *Mech Syst Signal Process* 13(2):241–253
- Gentile C (2010) Deflection measurement on vibrating stay cables by non-contact microwave interferometer. *NDT & E Int* 43:231–240
- Gentile C (2011) Vibration measurement by radar techniques. In: *De Roeck G, Degrande G, Lombaert G, Müller G (eds) Proceedings of the 8th international conference on structural dynamics, EURO-DYN 2011* Leuven, Belgium, 4–6 July 2011 ISBN 978-90-760-1931-4
- Gentile C, Saisi A (2011) Dynamic measurement on historic masonry towers by microwave remote sensing. In: *Gentile C, Benedettini F (eds) Proceeding of the international conference on experimental vibration analysis for civil engineering structures*, vol II, pp 524–530, 3–5 October 2011 Varenna, Italy. ISBN 978-88-96225-39-4
- Gentile C, Ubertini F (2012) Radar-based dynamic testing and system identification of a Guyed Mast. In: *10th international conference on vibration measurements by laser and noncontact techniques – AIVELA 2012* Ancona, Italy 27–29 June 2012, ISBN 978-0-7354-1059-6 ISSN 0094-243X, pp 318–325
- Gueguen P, Jolivet V, Clotaire M, Schweitzer AS (2010) Comparison of velocimeter and coherent lidar measurements for building frequency assessment. *Bull Earthquake Eng* 8:327–338. doi:10.1007/s10518-009-09137-2
- Luzi G, Monserrat O, Crosetto M (2012a) The potential of coherent radar to support the monitoring of the health state of buildings. *Research in Non-destructive Evaluation* 23(3):125–145 <http://dx.doi.org/10.1080/09349847.2012.660241>
- Luzi G, Monserrat O, Crosetto M (2012b) Real aperture radar interferometry as a tool for buildings vibration monitoring: limits and potentials from an experimental study. In: *10th international conference on vibration measurements by laser and noncontact techniques – AIVELA 2012* Ancona, Italy 27–29 June 2012, ISBN 978-0-7354-1059-6 ISSN 0094-243X, pp 309–317



- Luzi G, Crosetto M, Cuevas-González M (2014) A radar-based monitoring of the Collserola tower (Barcelona). *Mech Syst Signal Process* 49:234–248
- Nassif H, Gindy M, Davis J (2005) Comparison of laser Doppler vibrometer with contact sensors for monitoring bridge deflection and vibration. *NDT & Int* 38(3):213–218
- Negulescu C, Luzi G, Crosetto M, Raucoules D, Roullé A, Monfort D, Pujades L, Colas B, Dewez T (2013) Comparison of seismometer and radar measurements for the modal identification of civil engineering structures. *Eng Struct* 51:10–22
- Passia H, Staniek A, Szade A, Motyka Z, Bochenek W, Bartmański C (2008) Comparative studies of principal vibration parameters of a building using an LDV, laser tilt and vibration sensors and piezoelectric accelerometers. In: Tomasini EP (ed) 8th international conference on vibration measurements by laser techniques: advances and applications, Proc. of SPIE vol 7098, 70980J, (2008) 0277-786X/08/\$18 doi: 10.1117/12.803001
- Pieraccini M, Luzi G, Mecatti D, Noferini L, Atzeni C (2003) A microwave radar technique for dynamic testing of large structure. *IEEE Trans Microwave Theory Tech* 51(5):1603–1609
- Pieraccini M, Fratini M, Parrini F, Pinelli G, Atzeni C (2005) Dynamic survey of architectural heritage by high-speed microwave interferometry. *IEEE GRSL* 2(1):28–30
- Pieraccini M, Fratini M, Parrini F, Atzeni C (2006) Dynamic monitoring of bridges using a high-speed coherent radar. *IEEE Trans Geosci Remote Sens* 40(11):3284–3288
- Pieraccini M, Parrini F, Fratini M, Atzeni C, Spinelli P, Micheloni M (2007) Static and dynamic testing of bridges through microwave interferometry. *NDT & E Int* 40(3):208–214. doi:10.1016/j.ndteint.2006.10.007
- Pieraccini M, Fratini M, Parrini F, Atzeni C, Bartoli G (2008) Interferometric radar vs. accelerometer for dynamic monitoring of large structures: an experimental comparison. *NDT& E Int* 41(4):258–264
- Stabile TA, Perrone A, Gallipoli MR, Ditommaso R, Ponzo FC (2013) Dynamic survey of the Musmeci bridge by joint application of ground-based microwave radar interferometry and ambient noise standard spectral ratio techniques. *IEEE GRSL* 10(4):870–874. doi:10.1109/LGRS.2012.2226428
- Tarchi D, Ohlmer E, Sieber A (1997) Monitoring of structural changes by radar interferometry. *Res Nondestruct Eval* 9(4):213–225
- Welch PD (1967) The use of fast Fourier transform for the estimation of power spectra: a method based on time averaging over short, modified periodograms. *IEEE Trans Audio Electroacoust* 15(2):70–73

---

## Buildings and Bridges Equipped with Passive Dampers Under Seismic Actions: Modeling and Analysis

Theodore L. Karavasilis, George S. Kamaris and Angelos S. Tzimas  
School of Engineering, University of Warwick,  
Coventry, UK

### Synonyms

Bridges; Numerical simulation; Passive dampers; Steel buildings; Structural design

### Introduction

The scope of this contribution is the presentation of numerical models and analysis methods for structures equipped with passive dampers. The principal function of passive dampers and their application in buildings and bridges will be discussed. The most common types of passive dampers and the constitutive models used to simulate their hysteretic behavior will be presented. Finally, the analysis methods for seismic design and assessment of structures with passive dampers are covered.

Passive dampers include a variety of materials and devices that can enhance the damping, stiffness, and strength characteristics of structures. Passive dampers are suitable both for retrofitting existing vulnerable structures and for designing new ones and have been developed for a number of years with a rapid increase in applications in the mid-1990s. Passive dampers can significantly reduce plastic deformation demands on the primary lateral load-resisting system in addition to decreasing velocity and acceleration demands on non-structural components (Soong and Spencer 2002; Symans et al. 2008). Different types of passive dampers have been developed for seismic protection of structures such as viscous fluid dampers, viscoelastic solid dampers, elastomeric dampers, friction dampers, and metallic dampers.

Other devices that could be classified as passive dampers include tuned mass and tuned liquid dampers.

Passive dampers are typically used within conventional lateral load resisting systems to dissipate a significant portion of the seismic input energy (Christopoulos and Filiatrault 2006). The degree to which a passive damper is able to achieve this goal depends on the inherent properties of the lateral load resisting system, the properties of the passive damper and its connecting elements, the characteristics of the ground motion, and the limit state being investigated (Symans et al. 2008). Over the past decades, passive dampers have been specified for application to buildings and bridges with a wide variety of structural configurations. The growth in application of passive dampers has been steady to the extent that there are now numerous applications (Soong and Spencer 2002).

The first design/analysis procedure for buildings with passive dampers was published in SEAONC (Whittaker et al. 1993). The intent of these guidelines was to direct engineers in locating dampers in the lateral load resisting system to reduce repair costs and business interruption due to a severe earthquake. In the mid-1990s, the Federal Emergency Management Agency (FEMA) funded the development of guidelines for the seismic rehabilitation of buildings proposing, among others, basic principles for the seismic design with passive dampers. The outcome of this effort was the *NEHRP Guidelines for the Seismic Rehabilitation of Buildings*, FEMA Reports 273 and 274 (ATC 1997a, b). Later on, the 2003 *NEHRP Recommended Provisions* (BSSC 2004) included a chapter on design and analysis methods for buildings with passive dampers. These methods were reformatted and included in the 2005 edition of the ASCE/SEI 7-05 standard *Minimum Design Loads for Buildings and Other Structures* (ASCE 2005). The 2003 *NEHRP Recommended Provisions* (and the current 2010 ASCE/SEI 7 standard (ASCE 2010)) allow a reduced design base shear force for the seismic design of buildings with passive

damping systems where the expected performance is similar or higher than that of buildings with a conventional lateral load resisting system.

Recent analytical and experimental research showed that steel moment-resisting frames (MRFs) with elastomeric dampers can be designed to be lighter and perform better than conventional steel MRFs under the design basis earthquake (DBE; 475-year return period) (Karavasilis et al. 2011a, 2012a). However, it was shown that it is generally not feasible to design steel MRFs with passive dampers at a practical size to eliminate inelastic deformations in main structural members under the DBE (Karavasilis et al. 2011a). To address this issue, a seismic design strategy for steel MRFs that isolates damage in removable steel dampers and uses in parallel viscous fluid dampers to reduce drifts has been proposed by Karavasilis et al. (2012b). A study shows that supplemental viscous damping does not always ensure adequate reduction of residual drifts (Karavasilis and Seo 2011). A recent work evaluates the seismic collapse resistance of steel MRFs with viscous fluid dampers and shows that supplemental viscous damping does not always guarantee a better seismic collapse resistance when the strength of the steel MRF with dampers is lower or equal to 75 % of the strength of a conventional steel MRF (Seo et al. 2014).

In the following section, two major real-world applications of passive dampers in a tall building and a bridge are briefly discussed. The most common types of passive dampers and the models used to simulate their hysteretic behavior are then presented. Finally, the analysis methods that can be utilized to predict the response of structures with passive dampers are discussed.

### **Application of Passive Dampers in Buildings and Bridges**

Two relatively recent applications of passive dampers in a building and a bridge are discussed below.



**Buildings and Bridges Equipped with Passive Dampers Under Seismic Actions: Modeling and Analysis, Fig. 1** (a) Torre Mayor Tower under

construction showing partial view of megabraces; (b) view of installed viscous fluid dampers (Symans et al. 2008)

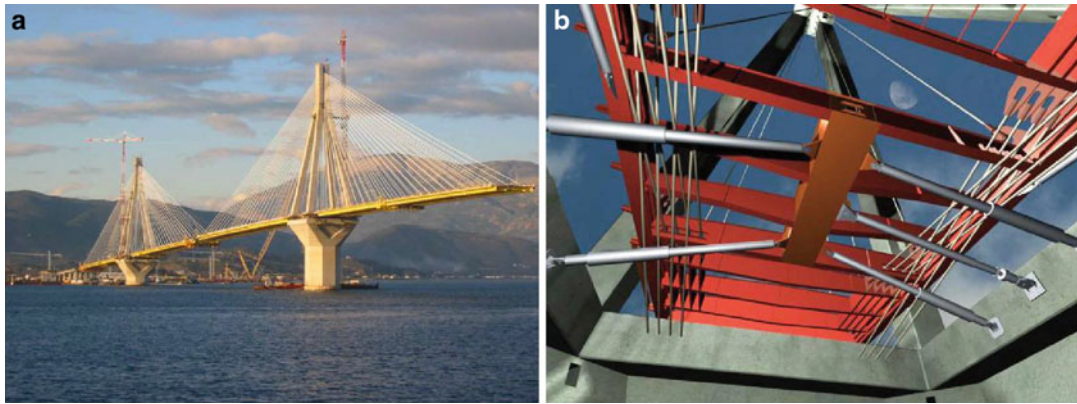
### Torre Mayor Tower, Mexico

The Torre Mayor Tower is a 77,000 m<sup>2</sup>, 57-story steel and reinforced concrete office/hotel tower in Mexico City. Its construction was completed in 2003 and its height is 225 m. The lower half of the superstructure is a rectangular tower which consists of steel framing encased in concrete, while the upper half consists of steel framing (Fig. 1a). The seismic design of the structure had the challenging objective of achieving “operational” performance for an expected 8.2 magnitude seismic event (Rahimian and Romero 2003). The seismic design employs 96 large nonlinear viscous fluid dampers with 2,670 and 5,340-kN force output capacities (Fig. 1b). The dampers on the faces of the building are installed in megabraces, which are diagonal braces that span over more than one story, as shown in Fig. 1a. Note that, a first design of the building without dampers resulted in weight of the building that was excessive for the soil capacity. The addition of the dampers resulted in less steel weight and acceptable soil bearing pressure. The structure experienced no damage during a seismic event with 7.8

magnitude and epicenter 500 km from the building site (Rahimian and Romero 2003).

### Rion-Antirion Bridge, Greece

The Rion-Antirion Bridge (Fig. 2), that crosses the homonymous strait in Greece, is located in the very active seismic region of the Gulf of Corinth. The deck of this multi-span cable-stayed bridge is continuous and fully suspended from four pylons (total length of 2,252 m). Its approach viaducts comprise 228 m of concrete deck on the Antirion side and 986 m of steel composite deck on the Rion side. Said structures are designed to withstand seismic events generating ground accelerations of up to 0.48 g through the use of viscous fluid dampers and other seismic devices. The Main Bridge seismic protection system consists of fuse restraints and viscous fluid dampers that act in parallel, connecting the deck to the pylons (Fig. 2b). The fuse restraints are designed as a rigid link intended to withstand high wind loads up to a predetermined force. Under the action of the design earthquake, the fuse restraints will fail and leave the dampers free to dissipate the semi



**Buildings and Bridges Equipped with Passive Dampers Under Seismic Actions: Modeling and Analysis, Fig. 2** Rion-Antirion Bridge: (a) main bridge

under construction; (b) arrangement of viscous fluid dampers and fuse restraints on the main piers (Infanti et al. 2004)

induced energy. The approach viaducts are seismically isolated utilizing elastomeric isolators and viscous dampers.

### Passive Dampers and Constitutive Models

Passive dampers can be classified in three main categories: (1) velocity-activated or rate-dependent, (2) displacement-activated or rate-independent, and (3) motion-activated (Symans et al. 2008; Christopoulos and Filiatrault 2006).

Velocity-activated or rate-dependent dampers have force output that depends on the relative velocity across the damper. Therefore, their efficiency to dissipate energy depends on the frequency of the input ground motion. The behavior of such dampers is commonly described using various models of linear viscoelasticity. Typical dampers falling in this category include viscous fluid dampers and viscoelastic dampers (Symans et al. 2008; Christopoulos and Filiatrault 2006).

Displacement-activated or rate-independent dampers have force output that does not depend on the relative velocity across the damper but on the magnitude of the displacement and possibly the direction of motion. Their behavior is



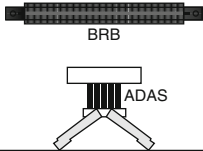
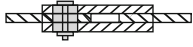
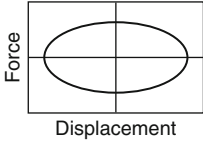
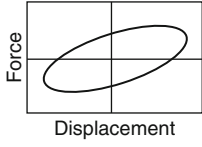
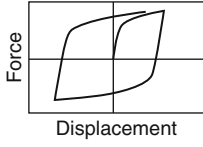
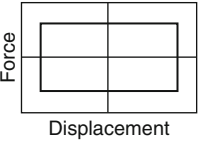
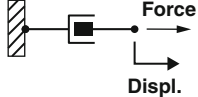
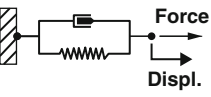
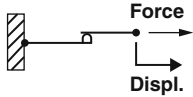
commonly described using various nonlinear hysteretic models. Typical dampers falling in this category include metallic dampers and friction dampers (Symans et al. 2008; Christopoulos and Filiatrault 2006).

Motion-activated passive dampers consist of secondary systems that disturb the flow of energy in the structure. These systems have the same resonance period with the main structure. Tuned-mass dampers (TMDs) are an example of motion-activated dampers. This last category is not discussed further in this contribution, but the reader is referred to documents such as the one by Soong and Spencer (2002) for more details.

A summary of velocity-activated and displacement-activated passive dampers is provided in Fig. 3 (reproduced from Symans et al. (2008)). Figure 3 lists the basic construction, the idealized hysteretic response and the associated physical model, and the major advantages and disadvantages of each passive damper.

### Viscous Fluid Dampers

Viscous fluid dampers consist of a hollow cylinder filled with fluid (Fig. 3), the fluid typically being silicone based. As the damper piston rod and piston head are stroked, fluid is forced to flow through orifices either around or through the piston head. The resulting differential in pressure

	Viscous Fluid Damper	Viscoelastic Solid Damper	Metallic Damper	Friction Damper
<b>Basic Construction</b>				
<b>Idealized Hysteretic Behavior</b>				
<b>Idealized physical Model</b>			Idealized Model Not Available	
<b>Advantages</b>	<ul style="list-style-type: none"> <li>- Activated at low displacements</li> <li>- Minimal restoring force</li> <li>- For linear damper, modeling of damper is simplified</li> <li>- Properties largely frequency and temperature-independent</li> <li>- Proven record of performance in military applications</li> </ul>	<ul style="list-style-type: none"> <li>- Activated at low displacements</li> <li>- Provides restoring force</li> <li>- Linear behavior, therefore simplified modeling of damper</li> </ul>	<ul style="list-style-type: none"> <li>- Stable hysteretic behavior</li> <li>- Long-term reliability</li> <li>- Insensitivity to ambient temperature</li> <li>- Materials and behavior familiar to practicing engineers</li> </ul>	<ul style="list-style-type: none"> <li>- Large energy dissipation per cycle</li> <li>- Insensitivity to ambient temperature</li> </ul>
<b>Disadvantages</b>	<ul style="list-style-type: none"> <li>- Possible fluid seal leakage (reliability concern)</li> </ul>	<ul style="list-style-type: none"> <li>- Limited deformation capacity</li> <li>- Properties are frequency and temperature-dependent</li> <li>- Possible debonding and tearing of VE material (reliability concern)</li> </ul>	<ul style="list-style-type: none"> <li>- Device damaged after earthquake; may require replacement</li> <li>- Nonlinear behavior; may require nonlinear analysis</li> </ul>	<ul style="list-style-type: none"> <li>- Sliding interface conditions may change with time (reliability concern)</li> <li>- Strongly nonlinear behavior; may excite higher modes and require nonlinear analysis</li> <li>- Permanent displacements if no restoring force mechanism provided</li> </ul>

**Buildings and Bridges Equipped with Passive Dampers Under Seismic Actions: Modeling and Analysis, Fig. 3** Summary of basic construction,

hysteretic behavior, physical models, advantages, and disadvantages of passive dampers for seismic protection applications (Symans et al. 2008)

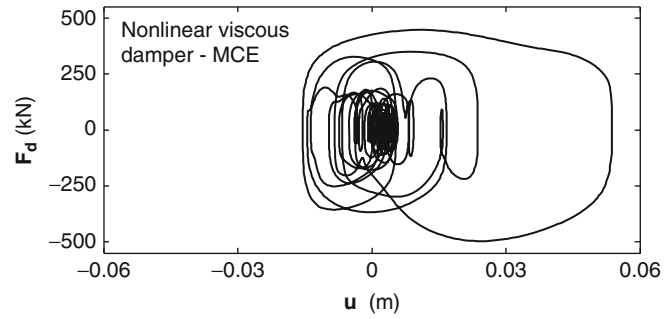
across the piston head can produce very large forces that resist the relative motion of the damper. The fluid flows at high velocities, resulting in the development of friction between

fluid particles and the piston head, which leads to energy dissipation in the form of heat. Interestingly, although the damper is called a *viscous fluid damper*, the fluid typically has a relatively



### Buildings and Bridges Equipped with Passive Dampers Under Seismic Actions: Modeling and Analysis,

**Fig. 4** Hysteretic behavior of a nonlinear viscous damper from nonlinear dynamic analysis (Karavasilis et al. 2012b)



B

low viscosity, e.g., silicone oil with a kinematic viscosity in the order of  $0.001 \text{ m}^2/\text{s}$  at  $20 \text{ }^\circ\text{C}$ . The term *viscous fluid damper* is associated with the macroscopic behavior of the damper, which is essentially the same as that of an ideal linear or nonlinear viscous dashpot, i.e., the resisting force is directly related to the velocity (Symans et al. 2008).

Experimental testing (Seleemah and Constantinou 1997) has shown that the behavior of viscous fluid dampers corresponds to a nonlinear viscous dashpot and can be modeled by the following nonlinear force-velocity relation:

$$P(t) = C|\dot{u}(t)|^a \text{sgn}[\dot{u}(t)] \quad (1)$$

where  $P(t)$  is the force developed by the damper,  $u(t)$  is the displacement across the damper,  $C$  is damping coefficient,  $a$  is an exponent whose value is determined by the piston head orifice design,  $\text{sgn}[\cdot]$  is the signum function, and the overdot indicates differentiation with respect to time,  $t$ . For earthquake protection applications, the exponent  $a$  typically has a value ranging from about 0.3 to 1.0. For  $a$  equal to unity, the damper can be described as an ideal linear viscous dashpot (Symans et al. 2008). Figure 4 shows the behavior of a nonlinear viscous damper installed in a prototype steel building subjected to a strong earthquake ground motion from nonlinear dynamic analysis conducted in Karavasilis et al. (2012b).

### Viscoelastic Solid Dampers

Viscoelastic solid dampers generally consist of solid elastomeric pads (viscoelastic material)

bonded to steel plates, which are attached to the structure within chevron or diagonal bracing (Fig. 3). As one end of the damper displaces with respect to the other, the viscoelastic material is sheared resulting in the development of heat, which is dissipated to the environment. Viscoelastic dampers provide both a velocity-dependent force, which provides supplemental viscous damping to the system (similar to viscous dampers), and a displacement-dependent elastic restoring force (Symans et al. 2008).

Experimental testing (Bergman and Hanson 1993) has shown that, under certain conditions, a suitable mathematical model for simulating the mechanical behavior of viscoelastic dampers is the Kelvin model of viscoelasticity. This model is described by the following equation:

$$P(t) = Ku(t) + C\dot{u}(t) \quad (2)$$

where  $K$  is the storage stiffness of the damper and  $C$  is the damping coefficient which is equal to the ratio of the loss stiffness to the frequency of loading. The physical model corresponding to Eq. 2 is a linear spring in parallel with a linear viscous dashpot.

A constitutive model that can be used to describe with more accuracy the behavior of viscoelastic dampers is the generalized Maxwell (GM) model. The GM model consists of a parallel combination of a linear spring, a dashpot and multiple in-series combinations of springs and dashpots as shown in Fig. 5 (Karavasilis et al. 2011b). Figure 5 shows the GM model in terms of shear stress,  $\tau$ , and shear strain,  $\gamma$ , of the viscoelastic material. Under harmonic loading of



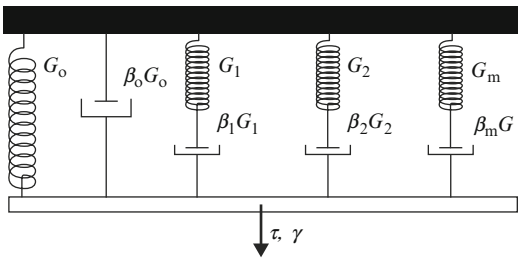
cyclic frequency  $\omega$ , the GM model provides storage shear modulus equal to

$$G'(\omega) = G_0 + \sum_{m=1}^n \frac{(\omega\beta_m)^2}{1 + (\omega\beta_m)^2} \cdot G_m \quad (3)$$

and loss factor equal to

$$\eta(\omega) = \frac{(\omega\beta_0)G_0 + \sum_{m=1}^n \frac{(\omega\beta_m)}{1 + (\omega\beta_m)^2} \cdot G_m}{G_0 + \sum_{m=1}^n \frac{(\omega\beta_m)^2}{1 + (\omega\beta_m)^2} \cdot G_m} \quad (4)$$

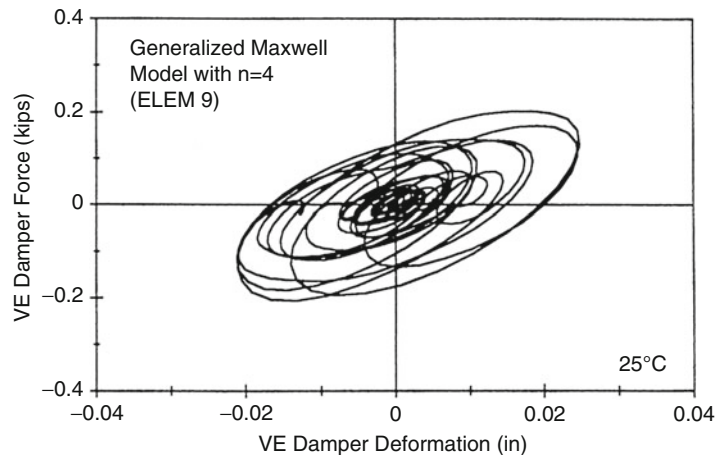
These equations can be used to calibrate the GM model against experimentally obtained values of  $G'$  and  $\eta$  for different cyclic frequencies. To use the GM model as a combination of linear springs and dashpots within a structural analysis



**Buildings and Bridges Equipped with Passive Dampers Under Seismic Actions: Modeling and Analysis, Fig. 5** Generalized Maxwell model for viscoelastic dampers

**Buildings and Bridges Equipped with Passive Dampers Under Seismic Actions: Modeling and Analysis,**

**Fig. 6** Hysteretic behavior of viscoelastic damper from nonlinear dynamic analysis (Fan 1998)



software, simply multiply  $G_0$  and  $G_m$  in Fig. 5 with the ratio  $A_d/t_d$  ( $A_d$ : horizontal area of the viscoelastic material;  $t_d$ : thickness of the viscoelastic material) to transform  $\tau$ - $\gamma$  behavior to force ( $F = \tau \cdot A_d$ ) – deformation ( $d = \gamma \cdot t_d$ ) behavior.

Figure 6 shows the hysteretic behavior of a typical viscoelastic damper from nonlinear dynamic analysis conducted in Fan (1998).

**Metallic Dampers**

Metallic dampers are designed to yield, based on the ability of steel to dissipate energy. Two major types of metallic dampers are the buckling-restrained brace (BRB) and the added damping and stiffness (ADAS) device.

A BRB consists of a steel brace with a cruciform cross section that is surrounded by a stiff steel tube. The region between the tube and brace is filled with a concrete-like material and a special coating is applied to the brace to prevent it from bonding to the concrete. Thus, the brace can slide with respect to the concrete-filled tube. The confinement provided by the concrete-filled tube allows the brace to be subjected to compressive loads without buckling. Under compressive loads, the BRB behavior is essentially identical to its behavior in tension. Since buckling is prevented, significant energy dissipation can occur over a cycle of motion (Symans et al. 2008).

The ADAS damper (Whittaker et al. 1991) consists of a series of steel plates wherein the

bottom of the plates are attached to the top of a chevron bracing arrangement and the top of the plates are attached to the floor level above the bracing. As the floor level above deforms laterally with respect to the chevron bracing, the steel plates are subjected to a shear force. The shear force induces bending moments over the height of the plates, with bending occurring about the weak axis of the plate cross section. The geometrical configuration of the plates is such that bending moments produce a uniform flexural stress distribution over the height of the plates so that inelastic action occurs uniformly over the full height of the plates. For example, in the case that the plates are fixed-pinned, the geometry is triangular; however, if the plates are fixed-fixed, the geometry is an hourglass shape.

Other types of metallic dampers have been developed for beam-column connections, braces and base isolation systems. Early developments include the U-strip hysteretic dampers and the T-ADAS damper. Other examples include the honeycomb damper used as seismic isolation system in bridges, C-shaped and E-shaped hysteretic dampers for bridges, slit-type dampers applied to beam-column connections or brace members, yielding shear panels, cast-iron yielding fuses installed in braces and hourglass shape pins installed in beam-column connections. A complete reference list for the aforementioned metallic dampers is provided in Vasdravellis et al. (2014).

Various mathematical models that describe yielding behavior of metals can represent the hysteretic behavior of metallic dampers such as the standard Bouc-Wen model (Wen 1976). The standard Bouc-Wen model results from the parallel combination of an elastic component and an

elastic-perfectly plastic component. The force output  $F$  of the model is

$$F = pku + (1 - p)F_y z \quad (5)$$

where  $u$  is the deformation across the model,  $F_y$  the yield force,  $k$  the elastic stiffness,  $p$  the post-yield stiffness ratio, and  $z$  a dimensionless hysteretic parameter governed by

$$\dot{z} = \frac{k}{F_y} \dot{u} [1 - |z|^n (\beta \text{sgn}[\dot{u}z] + \gamma)] \quad (6)$$

where  $\beta$  and  $\gamma$  are parameters controlling the shape of the hysteresis,  $n$  is a parameter that controls the sharpness of the smooth transition from the elastic to the inelastic region of the hysteresis,  $\text{sgn}[\cdot]$  is the signum function, and the overdot denotes derivative with respect to time.

Equation 5 shows that the Bouc-Wen model accounts for kinematic hardening (i.e., post-yield force increases with increasing deformation) due to the post-yield stiffness ratio  $p$ . However, the model does not account for the isotropic hardening (i.e., yield force  $F_y$  increases due to cyclic inelastic deformation) in the hysteresis of steel energy dissipation devices.

To account for isotropic hardening in the Bouc-Wen model, the mathematical formulation developed by Karavasilis et al. (2012b) is described below:

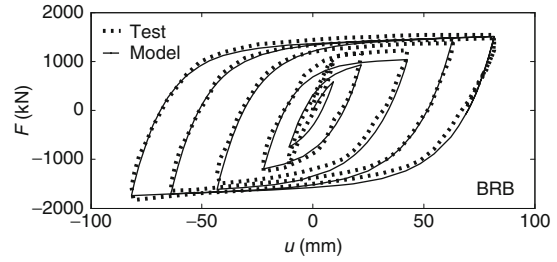
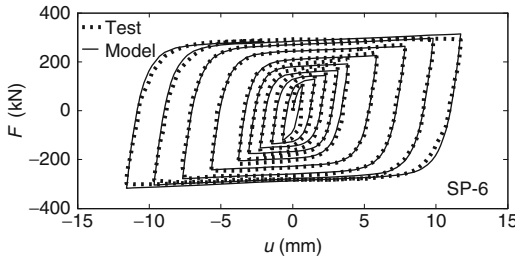
The yield force  $F_y$  needs to be updated by considering the history of the imposed cyclic deformation  $u$ . Examination of the constitutive Eqs. 5 and 6 reveals that a change in the yield force  $F_y$  can be achieved by appropriately including a third shape control parameter  $\Phi$  in Eq. 6:

$$\dot{z} = \frac{k}{F_y} \dot{u} \left[ 1 - |z|^n \left( \beta \text{sgn}(\dot{u}z) + \gamma - \frac{\Phi \text{sgn}(\dot{u}) (\text{sgn}(z) + \text{sgn}(\dot{u}))}{F_y} \right) \right] \quad (7)$$

The parameter  $\Phi$  quantifies isotropic hardening and is calculated using functions that cause  $\Phi$  to increase exponentially with increasing cumulative plastic deformation  $u_{pl,c}$ , i.e.,

$$\Phi_p = \Phi_{\max,p} \left[ 1 - \exp \left( -p_{\Phi,p} \left| \frac{u_{pl,c}}{u_y} \right| \right) \right] \quad (8a)$$

or



**Buildings and Bridges Equipped with Passive Dampers Under Seismic Actions: Modeling and Analysis, Fig. 7** Results from the modified Bouc-Wen

model proposed in Karavasilis et al. (2012b) and experimental results for a low-yield-strength shear panel and a BRB

$$\Phi_n = \Phi_{\max, n} \left[ 1 - \exp\left(-p_{\Phi, n} \left| \frac{u_{pl, c}}{u_y} \right| \right) \right] \quad (8b)$$

where  $u_y (= F_y/k)$  is the yield deformation,  $p_{\Phi, p}$  and  $p_{\Phi, n}$  are parameters that control the isotropic hardening rate due to cumulative plastic deformation, and  $\Phi_{\max, p}$  and  $\Phi_{\max, n}$  are the maximum possible values of  $\Phi$  for the fully saturated isotropic hardening condition, i.e., for  $u_{pl, c} \rightarrow \infty$ ,  $\Phi_p \rightarrow \Phi_{\max, p}$  and  $\Phi_n \rightarrow \Phi_{\max, n}$ . On the other hand, when  $u_{pl, c} = 0.0$ ,  $\Phi_p = 0.0$  and  $\Phi_n = 0.0$ .

$\Phi_p$  and  $\Phi_n$  are used to independently capture isotropic hardening in different loading directions (positive and negative). Typically, yielding devices exhibit the same isotropic hardening in different loading directions, and therefore,  $\Phi_{\max, p} = \Phi_{\max, n}$  and  $p_{\Phi, p} = p_{\Phi, n}$ . However, the model can simulate different isotropic hardening in different loading directions (e.g., compressive and tensile loading in BRB hysteresis) by using different parameter values in Eqs. 8a and 8b.

To understand the effect of  $\Phi$ , consider the proposed Bouc-Wen model with  $p = 0.0$  (i.e., without kinematic hardening),  $n = 1$  and  $\beta + \gamma = 1$ , under a positive deformation increment, i.e.,  $\text{sgn}[\dot{u}] = 1$ . Assume that in the previous deformation increment,  $z$  has reached its positive ultimate value  $z_u$ , and therefore,  $\text{sgn}[z] = 1$  and  $\dot{z} = 0.0$ . For this case, Eq. 7 yields  $z_u = 1/(1 - 2 \cdot \Phi)$  and Eq. 5 yields  $F = F_y \cdot z_u = F_y/(1 - 2 \cdot \Phi)$ . When  $\Phi = 0.0$  (i.e., without isotropic hardening),  $F$  is equal to  $F_y/(1 - 0.0) = F_y$ . When  $\Phi \neq 0.0$  (e.g.,  $\Phi = 0.1$ ),  $F$  is equal to  $F_y/(1 - 2 \cdot \Phi) = F_y/(1 - 2 \cdot 0.1) = 1.25 \cdot F_y$ . In that case,  $\Phi$

reflects a 25 % increase in the initial yield strength  $F_y$  due to isotropic hardening. The term  $\text{sgn}[\dot{u}]$  after the parameter  $\Phi$  in Eq. 7 ensures that the above calculations apply to the case of a negative deformation increment and a negative ultimate value of  $z$ .

The state determination procedure requires as an input the previous force and deformation, the previous  $z$  value, and the current deformation. The current value of the parameter  $\Phi$  is then calculated based on the following rules: Eq. 8a is used to update  $\Phi_p$  when the deformation increment changes from negative to positive within the plastic region of the hysteresis; Eq. 8b is used to update  $\Phi_n$  when the deformation increment changes from positive to negative within the plastic region of the hysteresis;  $\Phi$  equals to  $\Phi_p$  when a positive deformation increment occurs; and  $\Phi$  equals to  $\Phi_n$  when a negative deformation increment occurs. With the current  $\Phi$  value known, Eq. 7 is numerically integrated to obtain the current value of  $z$  which is simply used in Eq. 5 to provide the current force output  $F$  of the model.

Figure 7 shows how the aforementioned modified Bouc-Wen model captures the behavior of low yield strength shear panels showing significant isotropic hardening in their hysteresis as well as the behavior of BRBs showing different isotropic hardening in tension and compression.

### Friction Dampers

Friction dampers dissipate seismic energy by friction that develops between two solid bodies sliding relative to one another. Typical friction

dampers are slotted-bolted (Grigorian et al. 1993), where a series of steel plates are bolted together with a specified clamping force. The clamping force is such that slip occurs at a pre-specified friction force. Another configuration is the Pall friction damper, which consists of cross bracing that connects in the center to a rectangular damper (Pall and Marsh 1982). The damper is bolted to the cross bracing and, under lateral load, the structural frame distorts such that two of the braces are subjected to tension and the other two to compression. This force system causes the rectangular damper to deform into a parallelogram, dissipating energy at the bolted joints via sliding friction (Symans et al. 2008).

Experimental testing (Pall and Marsh 1982) has shown that the idealized Coulomb friction model can model the behavior of friction dampers, i.e., the force output of friction dampers is given by

$$P(t) = \mu N \text{sgn}[\dot{u}(t)] \quad (9)$$

where  $\mu$  is the coefficient of dynamic friction and  $N$  is the normal force at the sliding interface.

## Analysis Methods for Buildings and Bridges with Passive Dampers

The analysis methods used to predict the response of buildings and bridges equipped with passive dampers are classified in two categories: (1) linear analysis methods and (2) nonlinear analysis methods.

### Linear Analysis Methods

All linear analysis methods for structures equipped with rate-dependent passive dampers involve a simplified calculation of the supplemental (equivalent) damping ratio,  $\xi_{\text{eq}}$ . For example, given the damping coefficients  $C_i$  at each story  $i$  of a building and by assuming linear fluid viscous dampers ( $a = 1$  in Eq. 1) positioned in a horizontal configuration,  $\xi_{\text{eq}}$  at the fundamental period of vibration  $T_1$  under elastic conditions can be estimated as (Whittaker et al. 2003):

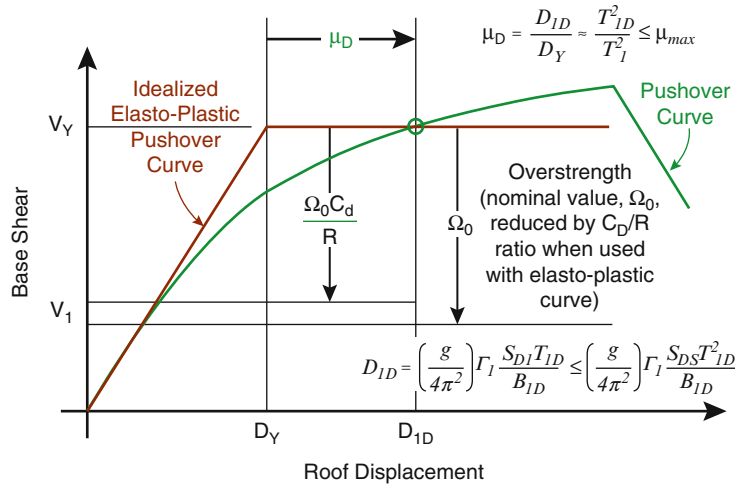
$$\xi_{\text{eq}} = \frac{T_1}{4\pi} \times \frac{\sum_i C_i (\phi_i - \phi_{i-1})^2}{\sum_i m_i \times \phi_i^2} \quad (10)$$

where  $\phi_i$  and  $\phi_{i-1}$  are the first modal displacements of stories  $i$  and  $i - 1$ , respectively, and  $m_i$  is the mass of story  $i$ . Equation 10 assumes that the braces supporting the dampers are stiff enough (essentially rigid) so that story deformation results in damper deformation rather than brace deformation. Alternative equations that take into account the effect of the brace flexibility on  $\xi_{\text{eq}}$  are provided for various brace-damper configurations in Hwang et al. (2008).

$\xi_{\text{eq}}$  is used to calculate the damping reduction factor, which is then utilized to appropriately reduce the ordinates of the elastic response spectrum. This reduced highly damped spectrum is used to estimate the response of the structure with dampers. Lin and Chopra (2003) have evaluated the premise that the peak displacement of an elastic SDOF system with a natural period  $T_n$  and equipped with a viscous damper (damping coefficient  $C$ ) in series with a brace of stiffness  $K_b$ , can be estimated by a linear viscous SDOF system with the same period  $T_n$  along with a simplified calculation of the added damping ratio (see Eq. 10). This premise was found valid for SDOF systems with  $\tau/T_n < 0.02$ , where  $\tau$  is the relaxation time, i.e.,  $\tau = C/K_b$ . As discussed by Lin and Chopra (2003), the relation  $\tau/T_n < 0.02$  is satisfied for the practical range of values for the bracing axial stiffness  $K_b$  and the damping coefficient  $C$ . Therefore, the damper and brace properties necessary to ensure that elastic drift demands do not exceed a prescribed design limit can be determined using the reduced elastic design spectrum associated with the equivalent damping ratio.

In the 2003 *NEHRP Recommended Provisions* (BSSC 2004) for buildings with passive dampers, and for the equivalent lateral force (ELF) analysis (linear static analysis) specifically, the response is defined by two modes: the fundamental mode and the residual mode, which is used to approximate the combined effects of higher modes. For response spectrum analysis, higher modes are

**Buildings and Bridges Equipped with Passive Dampers Under Seismic Actions: Modeling and Analysis, Fig. 8** Idealized elastoplastic pushover curve used for linear analysis (Symans et al. 2008)



explicitly evaluated. For both the ELF and the response spectrum analysis procedures, the shape of the fundamental-mode pushover capacity curve is not known and an idealized elastoplastic pushover curve is assumed, as shown in Fig. 8. Note that, in Fig. 8, the parameters  $\Gamma_1$  and  $S_{DS}$ , which are used to compute the design earthquake displacement,  $D_{1D}$ , represent the modal participation factor for the fundamental mode and the 5 % damped design spectral response acceleration at short periods, respectively. The idealized pushover curve permits defining the effective global ductility demand due to the design earthquake,  $\mu_D$ , as the ratio of design roof displacement,  $D_{1D}$ , to the yield displacement,  $D_Y$ . This ductility factor is used to calculate various design factors and to limit the maximum ductility demand,  $\mu_{max}$ , in a manner that is consistent with conventional building response limits. Passive dampers should be designed for actual fundamental-mode design earthquake forces corresponding to a base shear value of  $V_Y$ , while the elements of the seismic-force-resisting system be designed for a reduced fundamental-mode base shear,  $V_1$ , where the force reduction is based on system overstrength,  $\Omega_0$  (Symans et al. 2008).

A simplified linear method of analysis for building frames with elastomeric or viscoelastic dampers has been proposed by Lee et al. (2009) and has been recently extended to the case of fluid viscous dampers by Seo et al. (2014). This method is fully compatible with linear methods

of analysis used for conventional lateral load resisting systems in seismic codes and adopts the use of the strength reduction factor to calculate the required design base shear and the displacement amplification factor to estimate drifts.

**Nonlinear Analysis Methods**

The 2003 NEHRP Recommended Provisions (BSSC 2004) specify procedures for nonlinear static analysis and nonlinear dynamic (response-history) analysis. The nonlinear static analysis procedure is similar to the ELF procedure, in that the pushover capacity curve is used to define the nonlinear behavior of the structure. However, in the nonlinear static analysis procedure, the actual nonlinear force-displacement relation is used, rather than an idealized elastoplastic curve. In addition, since actual pushover strength is known from the nonlinear pushover analysis, the force reduction for design of the seismic-force-resisting system is based on overstrength alone with no additional reduction (Symans et al. 2008).

In general, the nonlinear dynamic analysis procedure is the most robust procedure available for evaluating the behavior of structures with passive dampers. It allows explicit modeling of individual devices, the elements connecting the devices to the structure, and the structure itself. If the connecting elements or the structural framing yields during the response, this behavior must be incorporated into the analytical model.

It is noted that accurate modeling of the flexibility of the floor diaphragm and of the connecting elements (braces) is essential since a loss of effective damping may occur if these elements are overly flexible.

Nonlinear dynamic analysis may be performed using a variety of commercially available software. In addition, there are several *academic* programs available, such as DRAIN-2DX (Prakash et al. 1993) and OpenSees (Mazzoni et al. 2006). Most of these programs can readily be used to model the behavior of linear fluid viscous dampers, viscoelastic dampers, friction dampers, or metallic yielding dampers. However, modeling of some damping devices (e.g., nonlinear viscous dampers and dampers with temperature-dependent or frequency-dependent mechanical properties) can be more challenging or, in some cases, not possible with a given program.

When nonlinear dynamic analysis is used, it is often beneficial to investigate the sensitivity of the structure response to one or more systemic parameters. Examples of parameters to vary include ground motion scaling parameters and parameters of the passive dampers (Symans et al. 2008).

## Summary

The scope of this contribution was the presentation of numerical models and analysis methods used for structures equipped with passive dampers. The principal function of passive dampers and their application in buildings and bridges were discussed. The most common types of passive dampers and the constitutive models used to simulate their hysteretic behavior were presented. Finally, the analysis methods used for seismic design and assessment of structures with passive dampers were covered.

## Cross-References

- ▶ [Assessment of Existing Structures Using Response History Analysis](#)

- ▶ [Behavior Factor and Ductility](#)
- ▶ [Buckling-Restrained Braces and Their Implementation in Structural Design of Steel Buildings](#)
- ▶ [Earthquake Response Spectra and Design Spectra](#)
- ▶ [Earthquake Return Period and Its Incorporation into Seismic Actions](#)
- ▶ [Equivalent Static Analysis of Structures Subjected to Seismic Actions](#)
- ▶ [European Structural Design Codes: Seismic Actions](#)
- ▶ [Mixed In-Height Concrete-Steel Buildings Under Seismic Actions: Modeling and Analysis](#)
- ▶ [Modal Analysis](#)
- ▶ [Plastic Hinge and Plastic Zone Seismic Analysis of Frames](#)
- ▶ [Response Spectrum Analysis of Structures Subjected to Seismic Actions](#)
- ▶ [Seismic Analysis of Masonry Buildings: Numerical Modeling](#)
- ▶ [Seismic Analysis of Steel and Composite Bridges: Numerical Modeling](#)
- ▶ [Seismic Analysis of Steel–Concrete Composite Buildings: Numerical Modeling](#)
- ▶ [Soil-Structure Interaction](#)
- ▶ [Steel Structures](#)
- ▶ [Strengthening Techniques: Code-Deficient Steel Buildings](#)
- ▶ [Structural Design Codes of Australia and New Zealand: Seismic Actions](#)
- ▶ [Time History Seismic Analysis](#)

## References

- American Society of Civil Engineers [ASCE] (2005) Minimum design loads for buildings and other structures. ASCE/SEI, Reston, pp 7–05
- American Society of Civil Engineers [ASCE] (2010) Minimum design loads for buildings and other structures. ASCE/SEI 7–10. ASCE, Reston
- Applied Technology Council [ATC] (1997a) NEHRP commentary on the guidelines for the seismic rehabilitation of buildings. 1997 ed, report no FEMA-274, prepared for the Building Seismic Safety Council (BSSC) by the Applied Technology Council (ATC). Federal Emergency Management Agency (FEMA), Washington, DC



- Applied Technology Council [ATC] (1997b) NEHRP guidelines for the seismic rehabilitation of buildings. 1997 ed, report no FEMA-273, prepared for the Building Seismic Safety Council (BSSC) by the Applied Technology Council (ATC). Federal Emergency Management Agency (FEMA), Washington, DC
- Bergman DM, Hanson RD (1993) Viscoelastic mechanical damping devices tested at real earthquake displacements. *Earthq Spectra* 9(3):389–418
- Building Seismic Safety Council [BSSC] (2004) NEHRP recommended provisions for seismic regulations for new buildings and other structures. 2003 ed, report no FEMA-450/1 and FEMA-450/2, prepared by the Building Seismic Safety Council (BSSC) for the Federal Emergency Management Agency (FEMA), Washington, DC
- Christopoulos C, Filiatrault A (2006) Principles of supplemental damping and seismic isolation. IUSS Press, Milan
- Fan C-P (1998) Seismic analysis, behavior, and retrofit of non-ductile reinforced concrete frame buildings with viscoelastic dampers. Phd Lehigh University, Bethlehem
- Grigorian CE, Yang TS, Popov EP (1993) Slotted bolted connection energy dissipators. *Earthq Spectra* 9(3):491–504
- Hwang J-S, Huang Y-N, Yi S-L, Ho S-Y (2008) Design formulations for supplemental viscous dampers to building structures. *J Struct Eng ASCE* 134(1):22–31
- Infanti S, Papanikolas P, Benzoni G, Castellano MG (2004) 13th world conference on earthquake engineering, paper no 2174, Vancouver
- Karavasilis TL, Seo C-Y (2011) Seismic structural and non-structural performance evaluation of highly damped self-centering and conventional systems. *Eng Struct* 33:2248–2258
- Karavasilis TL, Ricles JM, Sause R, Chen C (2011a) Experimental evaluation of the seismic performance of steel MRFs with compressed elastomer dampers using large-scale real-time hybrid simulation. *Eng Struct* 33(6):1859–1869
- Karavasilis TL, Blakeborough T, Williams MS (2011b) Development of nonlinear analytical model and seismic analyses of a steel frame with self-centering devices and viscoelastic dampers. *Comput Struct* 89(11–12):1232–1240
- Karavasilis TL, Sause R, Ricles JM (2012a) Seismic design and evaluation of steel MRFs with compressed elastomer dampers. *Earthq Eng Struct Dyn* 41(3):411–429
- Karavasilis TL, Krawala S, Hale E (2012b) Model for hysteretic behaviour of steel energy dissipation devices and evaluation of a minimal-damage seismic design approach for steel frames. *J Constr Steel Res* 70:358–367
- Lee KS, Ricles J, Sause R (2009) Performance based seismic design of steel MRFs with elastomeric dampers. *J Struct Eng ASCE* 135(5):489–498
- Lin W-H, Chopra AK (2003) Earthquake response of elastic single-degree-of-freedom systems with nonlinear viscoelastic dampers. *J Eng Mech ASCE* 129(6):597–606
- Mazzoni S, McKenna F, Scott MH, Fenves GL (2006) Open system for earthquake engineering simulation: user command language manual. University of California at Berkeley, Pacific Earthquake Engineering Research Center, Berkeley
- Pall AS, Marsh C (1982) Seismic response of friction damped braced frames. *J Struct Div* 108(6):1313–1323
- Prakash V, Powell GH, Campbell S (1993) DRAIN-2DX base program description and users guide. Department of Civil Engineering, University of California at Berkeley, Berkeley
- Rahimian A, Romero EM (2003) Super structure. *Civ Eng NY* 73(6):21–69
- Seleemah A, Constantinou MC (1997) Investigation of seismic response of buildings with linear and nonlinear fluid viscous dampers. Report no NCEER 97-0004. State University of New York at Buffalo, National Center for Earthquake Engineering Research, Buffalo
- Seo C-Y, Karavasilis TL, Ricles JM, Sause R (2014) Seismic performance and probabilistic collapse resistance assessment of steel moment resisting frames with fluid viscous dampers. *Earthq Eng Struct Dyn* 43(14):2135–2154
- Soong TT, Spencer BF Jr (2002) Supplemental energy dissipation: state-of-the-art and state-of-the-practice. *Eng Struct* 24(3):243–259
- Symans MD, Charney FA, Whittaker AS, Constantinou MC, Kircher CA, Johnson MW, McNamara RJ (2008) Energy dissipation systems for seismic applications: current practice and recent developments. *J Struct Eng ASCE* 134(1):3–21
- Vasdravellis G, Karavasilis T, Uy B (2014) Design rules, experimental evaluation, and fracture models for high-strength and stainless-steel hourglass shape energy dissipation devices. *J Struct Eng* 140(11):04014087. doi: 10.1061/(ASCE)ST.1943-541X.0001014
- Wen YK (1976) Method for random vibration of hysteretic systems. *J Eng Mech Div* 102(2):249–263
- Whittaker AS, Bertero VV, Thompson CL, Alonso LJ (1991) Seismic testing of steel-plate energy dissipating devices. *Earthq Spectra* 7(4):563–604
- Whittaker AS, Aiken ID, Bergman D, Clark PW, Cohen J, Kelly JM, Scholl RE (1993) Code requirements for design and implementation of passive energy dissipation systems. In: Proceedings of ATC-17-1 seminar on seismic isolation, passive energy dissipation, and active control, vol 2. ATC, Redwood City, pp 497–508
- Whittaker AS, Constantinou MC, Oscar MR, Johnson MW, Chrysostomou CZ (2003) Equivalent lateral force and modal analysis procedures of the 2000 NEHRP provisions for buildings with damping systems. *Earthq Spectra* 19(4):959–980